Occupancy-driven intelligent control of HVAC based on thermal comfort

By

Mehdi Pazhoohesh

A DISSERTATION

Submitted to

The University of Liverpool

Supervisors: Dr. Cheng Zhang

Dr. Steve Jones

30 March 2017

ABSTRACT

Occupancy-driven intelligent control of HVAC based on thermal comfort

Nowadays, the building sector is a substantial consumer of world's energy. The dominant energy share of Heating, Ventilation and Air-Conditioning (HVAC) systems, makes it the focus of research for saving energy. Current air conditioning systems often rely on maximum occupancy assumptions and fixed schedules to maintain sufficient comfort level. Having information regarding occupancy situation may lead to significant energy-savings. On the other hand, focusing on the reduction of energy only, may lead to sacrificing the thermal comfort of the occupants in a building. Moreover, due to the difference of preference of thermal comfort of individuals, particularly in a shared space, a fixed set point for HVAC systems, can cause discomfort. Therefore, a comprehensive technique is required to save energy while maintaining thermal comfort.

The present research proposes an occupancy-driven HVAC control system based on thermal comfort analysis. A ZigBee-based indoor localization system is developed to monitor the location of occupants inside the buildings. Algorithms are used to improve the accuracy of positioning system, which include Near Neighbour Area (NNA), Principle Component Analysis (PCA) and Exponential Moving Average algorithms (EMA). Computational Fluid Dynamics (CFD) is used to simulate the thermal comfort through modelling the indoor air distribution and flows. Wind velocity and temperature are simulated in several scenarios and the Predicted Mean Vote (PMV) and the Predicted Percentage Dissatisfied (PPD) are computed. The simulation results are verified through

a survey asking for occupants' real feelings and consequently thermal comfort zones are identified with associated occupants, which are used for possible energy saving while providing satisfied level to all the occupants.

To investigate different satisfaction feeling of occupants, a personalized thermal profile is created for individuals inside the test bed area. A fuzzy based approach is used to develop a fuzzy map of each occupant and as a result, a personal thermal preference profile is created. Based on the present occupants in the room, the minimum and maximum preferred temperatures are estimated and used for controlling the HVAC system.

The Semi-hidden Markov chain method is used to create the occupants' behavioural pattern which can reduce the frequencies of turning ON or OFF the HVAC systems. The real-time locations of the persons, estimated based on the NNA and MA localization method, are combined with their behavioural patterns and thermal preference profiles and their comfort zones to control the corresponding HVACs.

The proposed method has been implemented to a shared office occupied by nine users and equipped with two individual air conditioners. The comparison of different control strategies show that the proposed intelligent control has a significant potential of saving energy and at the same time maintaining occupants in a reasonable thermal comfort range.

DECLARATION

I hereby certify that this dissertation constitutes my own product, that where the language of others is set forth, quotation marks so indicate, and that appropriate credit is given where I have used the language, ideas, expressions or writings of another.

I declare that the dissertation describes original work that has not previously been presented for the award of any other degree of any institution.

Signed,

Mehdi Pazhoohesh

ACKNOWLEDGEMENTS

Thanks to Almighty God for giving me strength and ability to understand, learn and complete this thesis.

I would like to express my sincere gratitude to my supervisor, Dr. Cheng Zhang for her consistent guidance, support and patience in last three years. She always trusted and encouraged me during the ups and downs of my research duration.

I also admire the help and guidance of Prof. Dr. Sai Gu, my previous supervisor.

I owe an enormous debt of gratitude to my wife, Elaheh. Through the struggles and trials of this thesis, she has been a constant source of energy. Thank you.

Last but not least, my parents, Robab and Hossein, receive my deepest gratitude and love for their dedication and the many years of support during my education career.

TABLE OF CONTENT

Page

LIST OF TABLES

Page

LIST OF FIGURES

Page

LIST OF PUBLICATIONS

- M. Pazhoohesh and C. Zhang, " *Investigating Occupancy-driven Air Conditioning Control based on Thermal Comfort Level*," (In Press)
  Journal of Architectural Engineering, American Society of Civil Engineers (ASCE)
- C. Zhang**,** M. Pazhoohesh**,** R. Shahmir Nazim, A. Hammad, *"Quick construction progress monitoring for concrete structure using thermal imaging techniques,"*
  Submitted to Journal of Construction engineering and management, American Society of Civil Engineers (ASCE), Second round revision
- C. Zhang and M. Pazhoohesh, "Construction progress monitoring based on thermal-image analysis," *in ICCBEI & CCACHE,* Taipei, Accepted
- C. Zhang and M. Pazhoohesh, "Thermal Comfort based Occupancy-driven Building Energy Saving Control Strategies," *in WSBE17,* Hong Kong, Accepted
- M. Pazhoohesh, C. Zhang, R. Shahmir Nazim, "Investigating thermal comfort and occupants position impacts on building sustainability using CFD and BIM," in *49th International Conference of the Architectural Science Association(ANZAScA),* Australia, 2015
- M. Pazhoohesh and C. Zhang, "A Practical Localization System Based on principal component analysis," in *2nd World Congress on Computer Applications and Information Systems*, Hammamet, Tunisia, 2015.
- M. Pazhoohesh and C. Zhang, "Building Energy Management based on occupant location," in *Sustainable Buildings and Structures: Proceedings of the 1st International Conference on Sustainable Buildings and Structures*, Suzhou, P.R. China, 2015.
- M. Pazhoohesh and C. Zhang, "Automated construction progress monitoring using thermal images and wireless sensor networks," in *CSCE 2015, Building on Our Growth Opportunities*, Regina, Canada, 2015.

Chapter 1: Introduction

1 Introduction

Heating, Ventilation, and Air-Conditioning (HVAC) systems are widely used to control the indoor environment to provide comfortable conditions in homes, offices, and commercial buildings. While there are many arguments in the favour of HVAC systems such as having healthier life and a more productive environment, there are some critical issues. For example, HVAC systems use a large portion of energy and occupants in a shared space will experience different levels of satisfaction. Hence, the challenge of saving energy while maintaining comfort motivates further research to find a solution to these problems.

1.1 Energy demand and buildings

The global market energy usage is increasing continuously and is predicted to keep an almost 50% upward trend from 2009 to 2035. Developing economies outside the Organization for Cooperation and Development (OECD), non-OECD Asia in particular, is where this growth mostly occurs. Over the predicted period, the energy use by developed OECD nations rises by 14%, while entire non-OECD energy consumption rises by 84%. Figure 1(a) illustrates the trend of world primary energy consumption from 1990 to 2014. A sharp rise in the energy consumption of the Asia and Oceania can be observed which is due to the rapid economic growth of these regions. As

Figure 1(b) indicates, in 2014 China and USA were leading countries of global energy use with 23% and 18% energy usage, respectively [1].

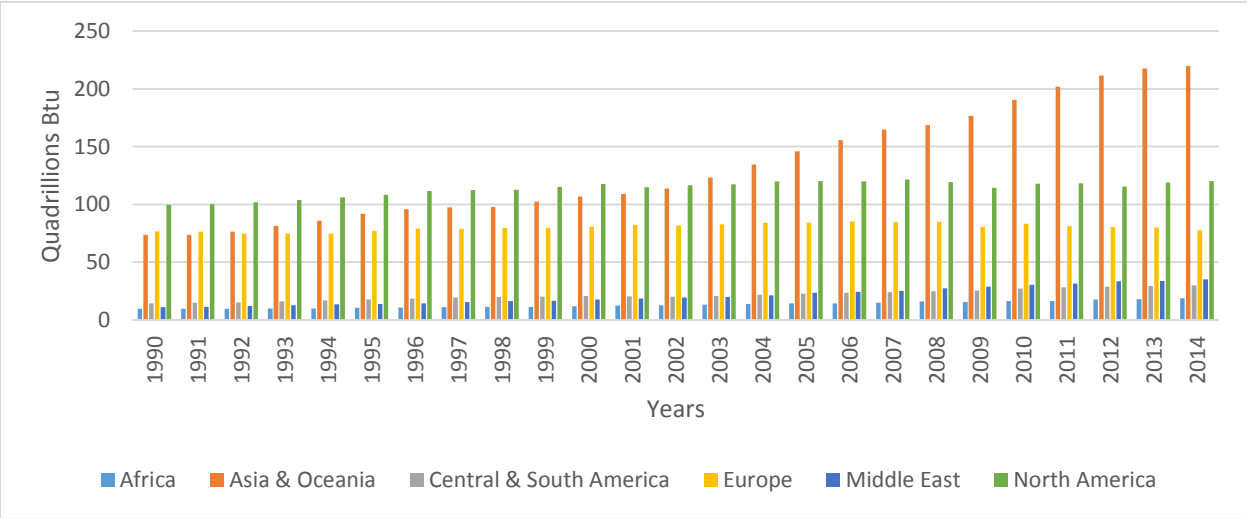

(a) Total Primary Energy Consumption

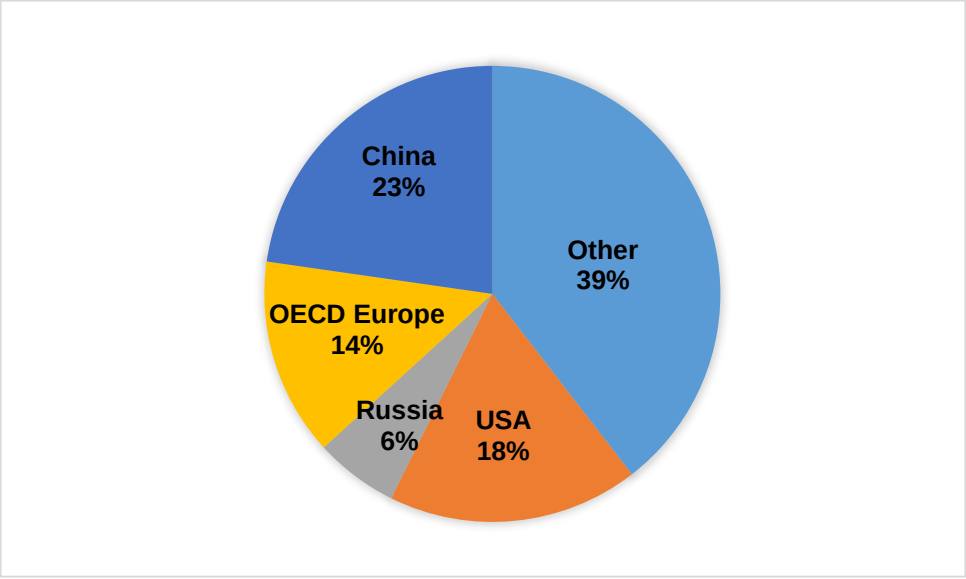

(b) Total Primary Energy Consumption for selected countries

Figure 1: : World primary energy consumption in 2014

To investigate where the most energy is consumed, energy consumption can be divided into four principle categories: commercial, transportation, industrial, and buildings. Energy consumption in buildings has the greatest share and is a remarkable contribution in most regions based on pay levels, climate, and resources.

In 2014, the entire energy usage of residential and non- buildings in Europe was approximately 40% of total energy consumed [2]. Considering all end-use divisions, buildings are the leading division, and transportation follows it with 33% as Figure 2 represents.

In building sectors, European households consumed 38% more electricity in the last 20 years. In addition, during the same duration, non-residential buildings were responsible for 74% more electricity consumption in the last 20 years.

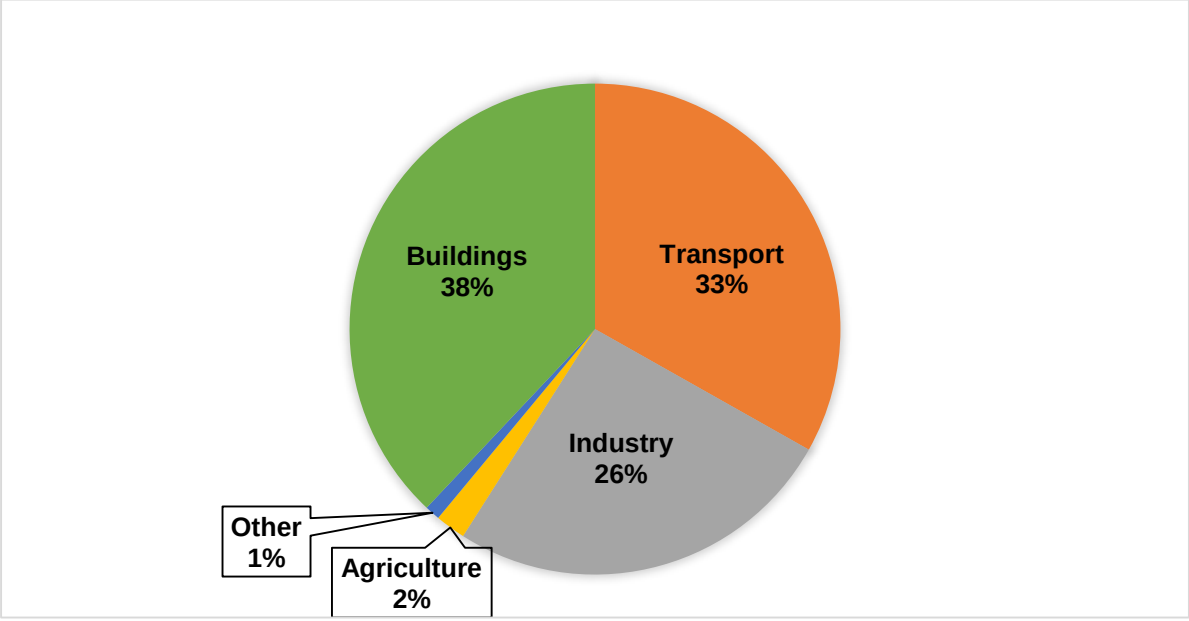

Figure 2: Energy consumption by sectors in EU

From Figure 3, in the USA, 41% of energy consumption is in building sectors, 36% more than in transportation and industrial sectors [3].

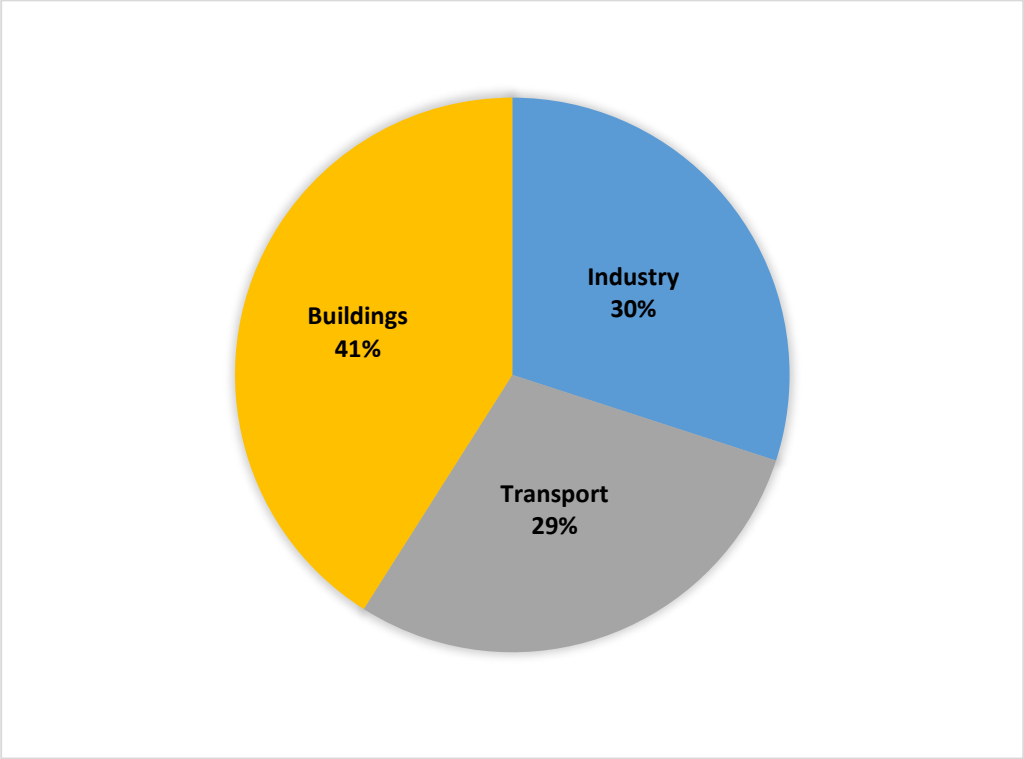

Figure 3: Energy consumption by sectors in USA in 2016

As a result of global climate change, population increase, and an average of 90% time spent inside buildings, an upward trend of energy consumption is expected in the building sector. Referring to [4], an increase of 1.1% per year for residential energy usage and a growth of 1.5% per year for commercial sectors from 2008 to 2035 is expected which leads to increasing energy demands. Therefore, investigators focus more on building sectors where the greatest potential of energy saving is expected [5].

1.1.1 Energy Demand of HVAC systems

HVAC systems have the greatest end use energy consumption in buildings. Investigations indicate that 10% to 60% of the total building energy consumption is due to air-conditioning systems [6]. From Figure 4, it can be concluded that HVAC systems in buildings are responsible for 50% of the on-site energy consumption in the USA [7]. The share of HVAC energy use in residential and non-residential buildings is 54% and 43% of on-site energy consumption, respectively. (Figure 5 and Figure 6).

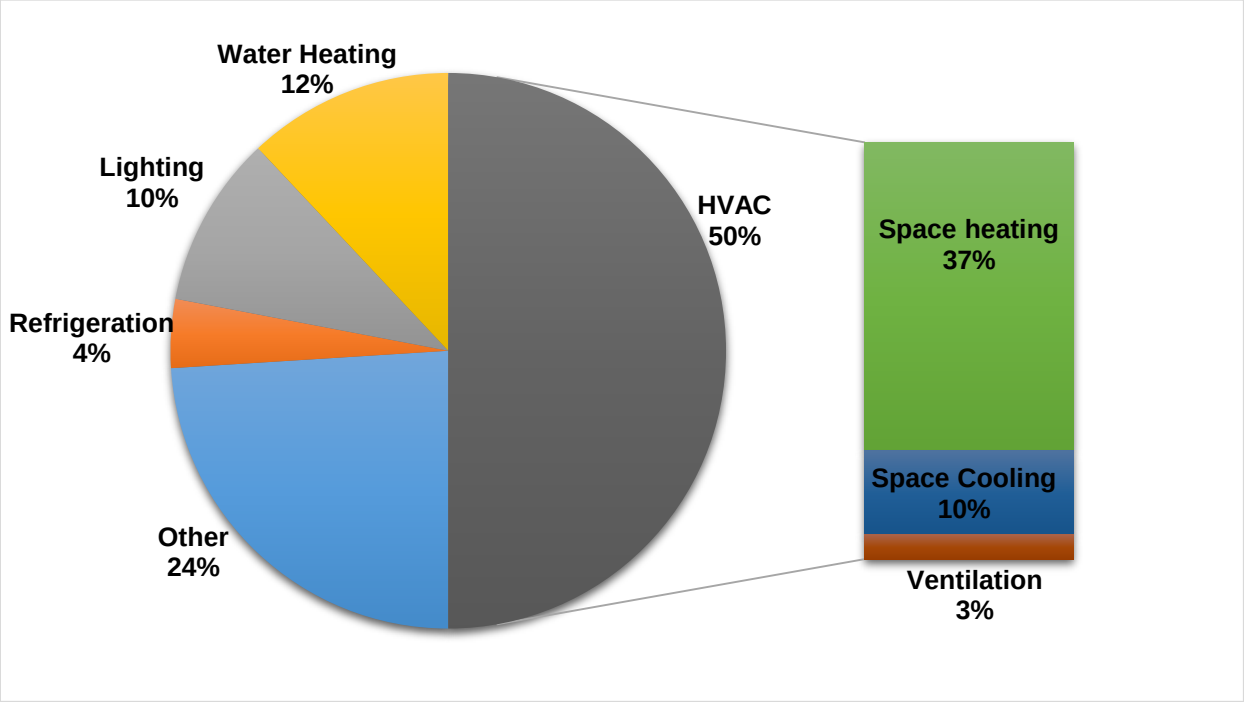

Figure 4: Building site energy consumption by end use in the USA

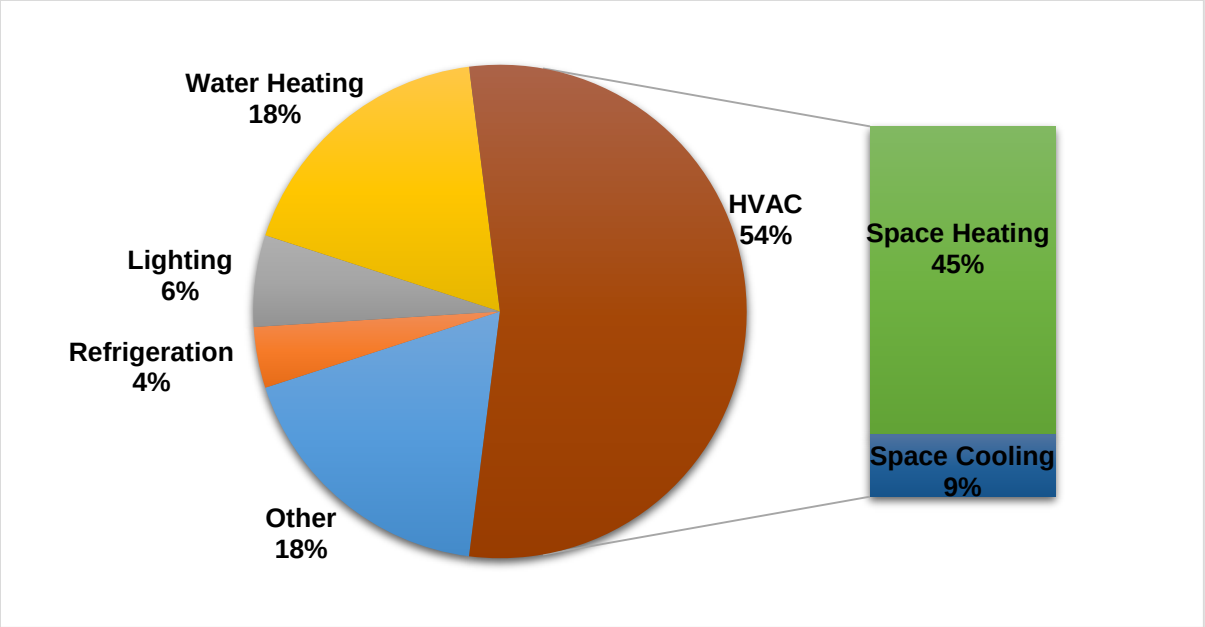

Figure 5: Residential site energy consumption by end use in the USA

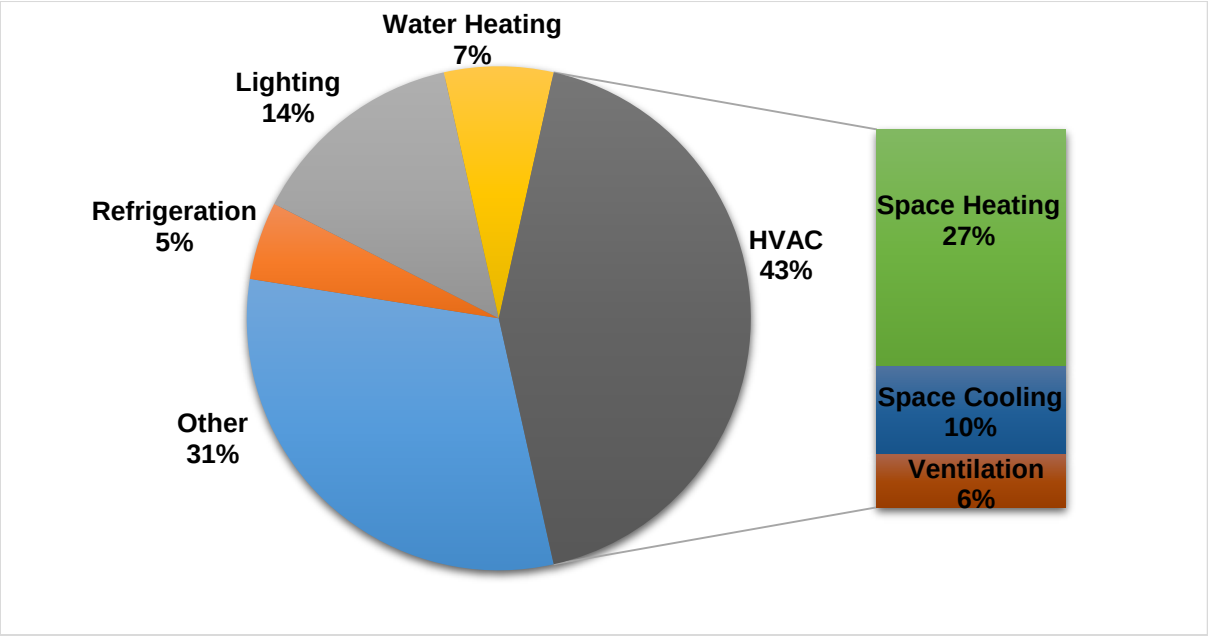

Figure 6: Non-residential site energy consumption by end use in the USA

Despite various energy efficiency guidelines and programs in the EU, electricity usage has continued to increase in recent decades. In the period of 1999-2004, the total electricity usage in building sector increased by 10.8% [8].

The demand of air conditioning in UK buildings also increased dramatically to respond to the increased demands of comfort by occupants in the buildings. It is expected that about 40% of commercial floor-space will be covered by air conditioners by 2020 compared with 10% coverage in 1994. In a typical office, over 30% of the annual electricity usage is referred to the air conditioning systems [9].

Presented statistic data from different regions of the world indicates the importance and potential for energy savings in building sectors. In addition, the role of HVAC systems in buildings' energy consumptions makes it a key factor in the world energy savings.

1.1.2 HVAC systems and thermal comfort

Well-designed building ventilation systems not only lead to a reduction in energy consumption, but should also provide satisfaction for building occupants. A good indoor environment is essential for good productivity, less vacancy, and better health [10]. The assessment of thermal comfort in offices showed that good thermal comfort level delivered more satisfaction for the occupants, and also improved their performance [11].

Thermal comfort is an important factor that is considered to evaluate the indoor environment quality [11]. The American Society of Heating, Refrigeration and Air-Conditioning Engineers (ASHRAE) defines *Thermal Comfort* as the condition of the mind which expresses satisfaction with the thermal environment. Thermal comfort is determined by several factors: temperature (air, radiant, and surface), humidity, air speed, outdoor temperature design conditions, outdoor

humidity design conditions, clothing, and expected activity [12]. According to Kan et al., bad indoor environments may lead to upper-respiratory symptoms, headaches, fatigue and rashes, known collectively as Sick-Building syndrome [13].

The scientific community has been gathering knowledge on comfort level in indoor environments and the significant findings are now in the form of international and national standards and solutions. For example, results of a study in Germany on workplace occupants' satisfaction in 16 office buildings showed that the effect of occupants' intervention and control may influence their thermal satisfaction and productivity [14]. Cena and Dearhave analysed the thermal comfort in 22 air-conditioned office buildings in different climates. They concluded that job satisfaction has a relationship with thermal comfort level [15]. Huizenga et al. provided a survey in 215 buildings in the US, Canada and Finland and concluded that 61% of occupants were not satisfied with the adjusted temperature in their office [16]. Above research observes the importance of thermal comfort and the difficulties in satisfying all persons in the same workspace. However, performing a survey is not accurate enough to evaluate the thermal comfort in a building.

Meanwhile, simulations based on relevant parameters are used to analyse and improve thermal comfort. Computational Fluid Dynamics (CFD) is known as the most reliable method for simulation and evaluation in industry sectors, especially for indoor environment. The main advantage of CFD is in dealing with complex flows within built environments where it can provide safe, healthy and comfortable conditions, test energy-efficient designs, or employ specific environmental requirements. On the other hand, the accuracy of its predictions is a main challenge as the simulation is based on the highest capacity of thermal loads in each environment and some other variables such as occupied areas during a working day are also needed to be considered [10] [17] [18] [19].

Furthermore, the CFD simulation results can be used to draw a guideline for an automated control system to meet the requirements of both thermal comfort satisfaction and energy saving. For example, Kan et al., proposed a computational intelligence approach to reduce power consumption while providing occupants' comfort satisfaction [13].

1.2 Problem Statement

Despite various attempts at energy consumption reduction, the HVAC system remains a very large portion of the total energy usage in building sectors.

In addition, the location of occupants is a significant parameter to be considered to provide a better thermal comfort and reduce unnecessary energy. Current air conditioning systems often rely on maximum occupancy assumptions and fixed schedules to maintain sufficient comfort level. Having knowledge regarding the occupancy situation may lead to significant energy-savings in a building. However, due to unpredictable locations of the occupants during the design stage, the fixed locations of ventilation systems, outlets, doors, and windows give little options to the occupants during operation stage. Therefore, more focus should be put on methods that can maintain the comfort level to occupants with minimum energy usage.

In addition, the ‘feeling comfortable’ range was very personal and could not be characterized objectively due to the differences, both physiological and psychological, of individuals. Hence, providing satisfaction for share rooms is still challenging.

Although the Predicted Mean Vote (PMV) model has extensively utilized for thermal comfort modelling, this model has some drawbacks including its limitation to consider behavioural and thermal variations.

An automated occupancy-driven HVAC system may lead to reduction of energy in buildings. However, it is essential to consider the occupants' comfort level for such systems.

The overview of problems and related approach is depicted in Figure 7.

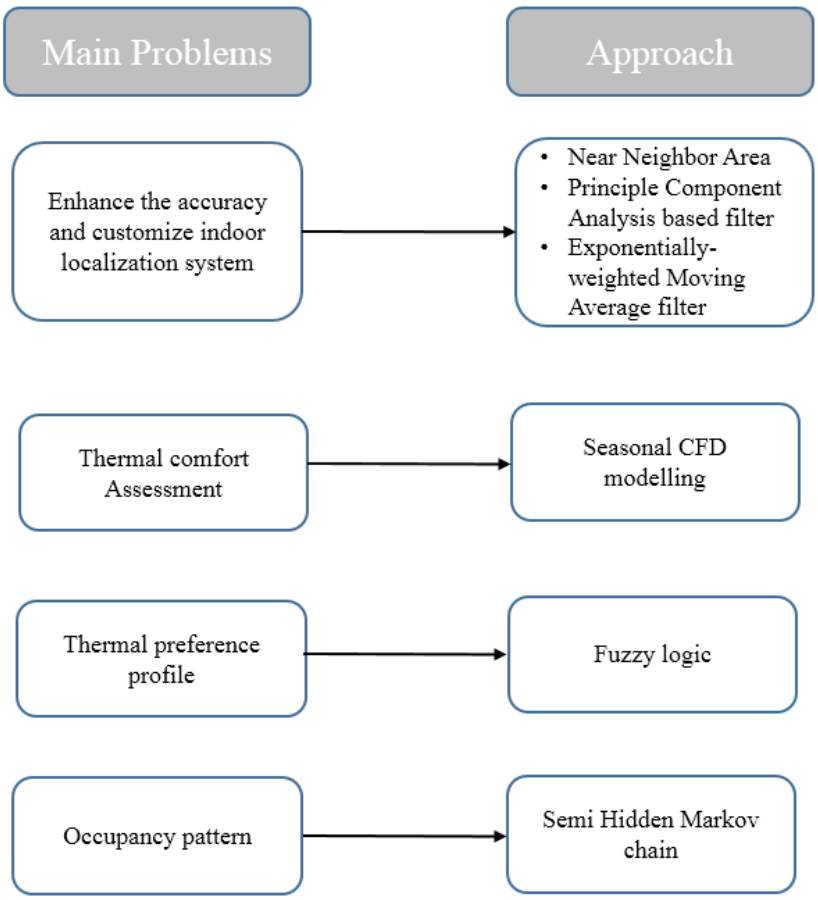

Figure 7: Schematic overview of the main problems, the approaches followed to find the solutions

1.3 Objectives

The aim of this research is to propose an innovative approach of intelligent control of HVAC system to meet both energy saving and providing satisfaction for the occupants in a shared space.

The main objectives are as follows

- To customize and enhance the accuracy of an indoor localization system for the goal of real-time tracking of occupants and identification of the unoccupied areas and providing data to create occupants' behavioural patterns;
- To define thermal zones in the share space based on thermal comfort level assessments and create an individual thermal profile for occupants;
- To develop an algorithm that optimizes energy consumption while maintaining comfort level with knowledge about current temperature, thermal zones, real-time and historical occupancy data, and thermal preference profiles of users; and
- To investigate the performance of the proposed approach through practical testing and show that the method can achieve valuable energy savings while attaining occupants' satisfactions.

This work is structured as follows.

Chapter 2: Literature review: a comprehensive description of the various areas that are relevant to this project is presented in this chapter.

Chapter 3: Methodology: This section outlines the problems presented in Figure 7 and the approach taken to find the solution.

Chapter 4: Implementation: This section presents the developed approach and corresponding results and validation of the proposed approach.

Chapter 5: Conclusion: This section summarizes this research and discusses the implications for future research and development.

Chapter 2: Literature review

In this chapter, a comprehensive description of the various areas that are relevant to this project work are introduced. An overview of localization systems and different technologies are presented. The Received Signal Strength Indicator (RSSI) based technique and trilateration model are explained. Indoor spatial modelling techniques are discussed. Next, the general description of HVAC systems is presented. Finally, a review of relevant related works carried out by other researchers in the thermal comfort areas is provided.

2 Indoor Localization systems

After the success of the satellite-based localization services for outdoor environment, location services for indoor environments have become a focus of research. As the GNSS (Global Navigation Satellite System) cannot perform well within buildings, indoor localization systems have become more attractive topic of research. However, locating people and objects in the indoor environment is a significant challenge. This has left indoor positioning applications waiting for a feasible technical solution. Enhancing the performance of indoor localization systems, has the potential to create unprecedented new commercial and scientific opportunities.

Most positioning systems should theoretically work in both environments. However, practically, system performances differ significantly because indoor environments are challenging for position finding for several reasons such as: Non-Line-of-Sight (NLoS) conditions, Signal reflection from walls and furniture which creates a multipath problem, Signal scattering and attenuation due to greater density of obstacles and high demand for precision and accuracy in

indoor environment. However, indoor environments facilitate positioning in other ways such as: Small coverage areas, low weather impact, infrastructure such as electricity, internet access, walls suitable for target mounting, lower dynamics and fixed geometric constraints from planar surfaces and orthogonality of walls.

There are various applications for indoor positioning system. For example, in indoor environment, Location-Based Service (LBS) can provide information to find a specific store in a large mall or a specific office in a public building. LBS applications include navigation to the right terminal at the airport or train station. Home applications of indoor positioning systems include physical gesture games, lost object search, and all location based services. For instance, Ambient Assisted Living (AAL) systems focus on IT support for elderly people in their homes and indoor positioning functionality is an essential part of the system. As an example, Lin et al. [20] provided a wireless health care service system for elderly with dementia and family members can identify the real-time positions of missing elderly using mobile phone through the service platform. Indoor positioning systems have become increasingly important for medical applications in hospital. For example, it is essential to track the location of medical personnel in emergency situations or fall detection of patients. Jihong [21] utilized a ZigBee based network to facilitate the monitoring and managing patient in the hospital. He considered the RSSI value to develop positioning system on the platform of G2455 module. To check some phenomenon such as temperature, pressure, humidity, and deformation of objects and structures, environmental monitoring is used. A group of nodes are designed as Wireless Sensor Network (WSN) to observe such parameters. Deshmukh and Shinde [22] discussed an environmental monitoring system using open source hardware raspberry pi and ZigBee to gather the data of different environmental parameters. One of the applications of indoor localization system can be defined as the smart parking. For this purpose, it

is essential to detect the parking space occupation and provide navigation data. Yuan et al. [23] utilized a WIFI system for navigation and geomagnetic sensors as a wireless sensor network to provide a smart parking system. There are various applications of localization systems in construction sites such as tracking workers for safety purposes or monitoring the progress of constructions. We introduced an automated progress monitoring system in construction sites using a ZigBee network and infrared camera [24] .

2.1 Overview of Technologies

High-level sensor technologies are characterized in Table 1. Specific accuracy and coverage values are given in interval form wherein most approaches reside, though there are many exceptions. The table only mentions the main measuring principles and applications.

Table 1: Overview of indoor positioning technologies

Technology	Typical Accuracy	Typical Coverage(m)	Typical Measuring Principle	Typical Application
Cameras	0.1mm-dm	1-10	Angle measurements from images	Metrology, robot navigation
Infrared	cm-m	1-5	Thermal imaging, active beacons	People detection, tracking
Tactile & Polar Systems	µm-mm	3-2000	Mechanical, interferometry	Automotive, metrology
Sound	cm	2-10	Distances from time of arrival	Hospitals, tracking
WLAN/WiFi	M	20-50	Fingerprinting	Pedestrian navigation, LBS
RFID	dm-m	1-50	Proximity detection, fingerprinting	Pedestrian navigation
Ultra-wideband	cm-m	1-50	Body reflection, time of arrival	Robotics, automation
High Sensitive GNSS	10m	‘global’	Parallel correlation, assistant GPS	Location based services
Pseudolites	cm-dm	10-1000	Carrier phase ranging	GNSS challenged pit mines
Other Radio Frequencies	m	10-1000	Fingerprinting, proximity	Person tracking

Inertial Navigation	1%	10-100	Dead reckoning	Pedestrian navigation
Magnetic Systems	mm-cm	1-20	Fingerprinting and ranging	Hospitals, mines
Infrastructure Systems	cm-m	building	Fingerprinting, capacitance	Ambient assisted living

The description of some popular technologies is provided in the following sections.

2.1.1 Infrared sensor

The infrared (IR) spectral region has been commonly used for detecting or tracking objects or persons. IR wavelengths are longer than visible light wavelengths, but shorter than those of terahertz radiation. IR light is invisible to the human, so this technology is less intrusive compared to visible light positioning. Exploiting infrared signals has three general methods: a) use of active beacons [25], b) infrared imaging using natural (i.e. thermal) radiation or c) artificial light sources [26].

Artificial IR light sources can be detected by systems using high resolution infrared sensors at sub-mm accuracy. However, systems that contain active beacons or natural radiation are used to detect the presence of an individual in a room or for rough position estimation.

2.1.2 Laser Scanners

Terrestrial laser scanners use a non-contact ranging technology for 3D point measurement and 3D point cloud acquisition. Combining readings at a horizontal and a vertical circle, Cartesian coordinates are developed from the polar coordinates of measured points, generating a so-called point cloud of the scene. Optical triangulation, phase and pulse measurements are the major

methods of distance estimation. Close range scanning captures an area of less than 100 m or up to 3 km. Registration can be used to combine scans from multiple stations, making laser scanning a scalable technique. An example of laser scanner for indoor localization can be mentioned as Khoshelham [27] in which during multiple scans, he matched planar objects such as walls. If two scans exhibit at least 3 correspondences of intersecting planes, it is possible to determine relative scanner positions with an accuracy of a few centimetres. Due to the long acquisition times for capturing large 3D point clouds, this method is not viable as a real-time method for indoor positioning.

2.1.3 ZigBee sensors

ZigBee is a standard of wireless technology, which can be regarded as a low rate Wireless Personal Area Network (WPAN). It is most useful in applications with demanding low-power consumption without large data throughput. A ZigBee node has a signal range of up to 100 m in free space, but only 20 m to 30 m indoors. RSSI values are used to calculate distance between two ZigBee nodes. Unfortunately, radio communication can be disrupted using ZigBee since it operates in the unlicensed ISM (Industrial, Scientific and Medical) bands and affect by interference from a wide range of signal types of the same frequency. Two types of nodes are used in a ZigBee-based localization network; reference nodes and blind nodes. Reference nodes are installed in places with known coordinates. Blind nodes are carried with targets whose locations need to be tracked. The position of the target can be estimated from the RSS value and Trilateration or Triangulation methods. Larrañaga et al. [28] installed a ZigBee network using 8 reference nodes in an office space, where a mobile ZigBee node was located. They reported an average accuracy of 3 m for positioning the target.

2.2 Positioning Methods

The RF localization techniques can be categorized in three major groups: proximity, sense analysis, and Trilateration. In the proximity method, sensors detect and measure reflected infrared, visible light, or RF waves to recognize the presence of an object or person in certain areas [29]. Sense analysis (fingerprinting) consists of two phases; offline and online. During the offline phase, a radio map database is created based on the radio signal behaviours. In the online phase, the location of the target is estimated according to the similarity between the received signal strength and the database. Trilateration is a method based on measuring the distance between a mobile target and reference nodes. For this method, at least three reference nodes are required. Different techniques can be utilized to estimate the position of the mobile target: Time of Arrival (ToA) [30], Phase of Arrival (PoA) [31], Time Difference of Arrival (TDoA) [32], Received Signal Strength (RSS-based) [33], hop-based and Reverse Time of Flight (RTOF) [34].

The main concept of indoor and outdoor positioning can be summarized as follows. Signal packets are sent from reference nodes (fixed anchor) to mobile nodes. Afterward, the characteristic of the received signal based on the Resieved Signal Strength Indicator (RSSI), the time of arrival (ToA), the link quality indicator (LQI) [35], or the angle of arrival (AoA) [36], is analysed. By utilizing any position detection algorithms, the location of the mobile target is estimated. Due to the simplicity of measuring RSSI or its relative LQI, RSSI-based localizations have attracted considerable attention. In RSSI-based systems, the distance between the transmitter and the

receiver is computed utilizing the received signal strength by considering the signal propagation model.

Equation (1), represents the most popular form of propagation model proposed by Rappaport [37].

$$P_r(d)[dBm] = P_r(d_0)[dBm] - 10n\log_{10}\left(\frac{d}{d_0}\right) + x_\sigma[dBm] \qquad \textbf{(1)}$$

where d denotes the distance between transmitter and receiver, d_0 is the reference distance, $P_r(d)$ is the received power, $P_r(d_0)$ the received power of the point with a reference distance d_0, n is path loss exponent factor which is environment dependence, x_σ is Guassian random variable which shows the change of power when distance is fixed. To simplify the computation, the Guassian random variable is ignored and 1 meter distance is replaced as d_0 as

$$RSS\ [dBm] = P_r(d)[dBm] = A - 10n\log d \qquad \textbf{(2)}$$

where A is the received signal power of receiver for one meter.

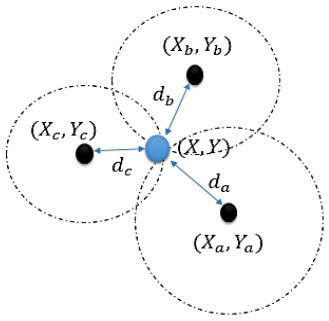

Figure 8: Intersection of three spheres in 2D

By the use of trilateration model, the position of target will be calculated. Figure 8 illustrated the three reference nodes (a, b and c) that have three distances (d_a, d_b, d_c) to the blind point. The formula for all spheres equals to:

$$\begin{aligned} &SphereA: d_a{}^2 = (x - x_a)^2 + (y - y_a)^2 \\ &SphereB: d_b{}^2 = (x - x_b)^2 + (y - y_b)^2 \\ &SphereB: d_c{}^2 = (x - x_c)^2 + (y - y_c)^2 \end{aligned} \quad \textbf{(3)}$$

Applying Dixon method results in achieving the radical plane for sphere intersection.

$$\begin{aligned} &x(x_c - x_b) + y.(y_c - y_b) = ((d_b{}^2 - d_c{}^2) - (x_b^2 - x_c^2) - (y_b^2 - y_c^2))/2 = k_a \\ &x(x_a - x_b) + y.(y_a - y_b) = ((d_b{}^2 - d_a{}^2) - (x_b^2 - x_a^2) - (y_b^2 - y_a^2))/2 = k_b \end{aligned} \quad \textbf{(4)}$$

Therefore, the position based on X-Y can be found from

$$Y = \frac{k_b(x_c - x_b) - k_a(x_a - x_b)}{(y_a - y_b)(x_c - x_b) - (y_c - y_b)(x_a - x_b)}$$

$$X = \frac{k_a - Y(y_c - y_b)}{(x_c - x_b)} \quad \textbf{(5)}$$

For n reference nodes, equations can be written in the form of matrix;

$$\begin{bmatrix} 2(x_2 - x_1) & 2(y_2 - y_1) \\ \vdots & \vdots \\ 2(x_n - x_1) & 2(y_n - y_1) \end{bmatrix} \begin{bmatrix} X \\ Y \end{bmatrix} = \quad \textbf{(6)}$$

$$\begin{bmatrix} (d_1^2 - d_n^2) - (x_1^2 - x_n^2) - (y_1^2 - y_n^2) \\ \vdots \\ (d_{n-1}^2 - d_n^2) - (x_{n-1}^2 - x_n^2) - (y_{n-1}^2 - y_n^2) \end{bmatrix}$$

Or

$$A\begin{bmatrix} X \\ Y \end{bmatrix} = B \quad \textbf{(7)}$$

And,

$$\begin{bmatrix} X \\ Y \end{bmatrix} = \left(\bar{A}^T \bar{A}\right)^{-1} * \left(\bar{A}\,\bar{B}\right) \quad \textbf{(8)}$$

The diversity of various technological solutions for indoor positioning indicates how significantly interdisciplinary the field is. Despite the abundance of approaches, it is important to choose the most suitable technology for a given application. For this research, ZigBee technology has been selected due to factors such as availability, minimal costs, coverage range and simplicity of installation and programming. In addition, the importance of user identification in this project is another reason to utilize the ZigBee technology.

2.3 HVAC systems and thermal comfort

Energy efficiency can be evaluated from different perspectives, such as that of an HVAC-system, a building, or human behaviour. Investigating the energy efficiency of HVAC systems can either concentrate on the performance of the system in total or the efficiency of sub components. For instance, the target can be focused on the electrical efficiency of components such as the pump

or fans, or settle on an arrangement of how to schedule the overall workloads of the components. If the objective is to focus on the building, minimizing thermal losses should be the target.

Another type of analysis is to focus on the demand side where the occupants' behaviours play an important role in the study. Occupancy is amongst the most critical elements affecting energy efficiency of HVAC systems as it determines loads on the demand side.

2.3.1 Description of general HVAC systems

A Heating, Venting and Air Conditioning (HVAC) system is used to control the temperature, humidity and CO_2 level. Typically, the capacity of an HVAC system is designed based on the space that needs to be conditioned and controlled. In most cases, the designed capacity is greater than the actual load [38]. Therefore, the lack of a well-designed control system may result in overheat or overcool spaces.

The main classification of HVAC systems can be defined as central systems and self-contained unit packages. The central systems utilize the primary energy source (electricity or fuel), which is placed in a central location. A combination of the central subsystem and multiple end-use subsystems provide heating or cooling and distribute this throughout the building [38].

The combination of central hot and chilled water and fan systems or terminal units can be labelled as a frequently used system. A VAV box is used as a mixing box where the multiple end-use spaces are considered. A single unit that utilizes a primary energy source (electricity or gas) and generates heating or cooling to the space can be defined as the unit package. The rooftop HVAC systems and air-to-air heat pumps are referred to as the self-contained unit packages.

The starting, regulation and stopping, HVAC systems can be defined as the term control. These controls also measure variables and collect data, processing data and inducing a control action are distinct functions which are needed to be controlled [38]. The sensor, controller, controlled device, and source of energy are the essential elements needed from the simplest room thermostat to the most complicated computerized control. Sensors measure the controlled variables such as humidity, temperature, or airflow and transfer this data to the controller. The controller processes the data and provides output for the controlled device. The controlled device minimizes the error of controlled variables to keep the controlled variable (air temperature) to some predefined value, defined as the set point. The source of energy provides power for the control system.

2.3.2 Self-Tuning and Artificial Intelligence

As tuning is known to be a time consuming and complicated process in HVAC systems, many investigators have focused on this area. The basic classification of tuning methods can be defined as follows:

1) Auto-tuning – modern buildings are equipped with computer software to control and monitor mechanical and electrical equipment such as HVAC systems. The software is known as Building Management Systems (BMS) or Building Automation systems (BAS). The software can be adjusted to control air conditioners based on different schedules.
2) Adaptive Techniques – The capability of BMS software to monitor the changing conditions and choose different settings based on new sensed conditions.
3) Artificial Intelligence- This type of control is designed to make a decision based on the various inputs or previous data. The intelligent control can generate the output signal using fuzzy logic, neural networks or machine learning algorithms.

2.3.3 Energy Management Techniques

There are various strategies can be used to save energy in HVAC systems such as Timed Programmed Commands, Duty Cycle and Optimum Start / Stop. Following is the explanation of most popular techniques.

Time-Programmed Commands

Despite the high potential for energy savings using this strategy, this method is only effective for buildings with long unoccupied periods. For instance, when the building had a certain occupancy schedule, the heating or cooling setpoint adjusted to a specific temperature. At night, lights and HVAC components such as fans, chillers, and other mechanical components are deactivated. There are various temperature setpoints for this strategy.

On the other hand, for the occupants who enter the building outside the scheduled time, the comfort level will be insufficient.

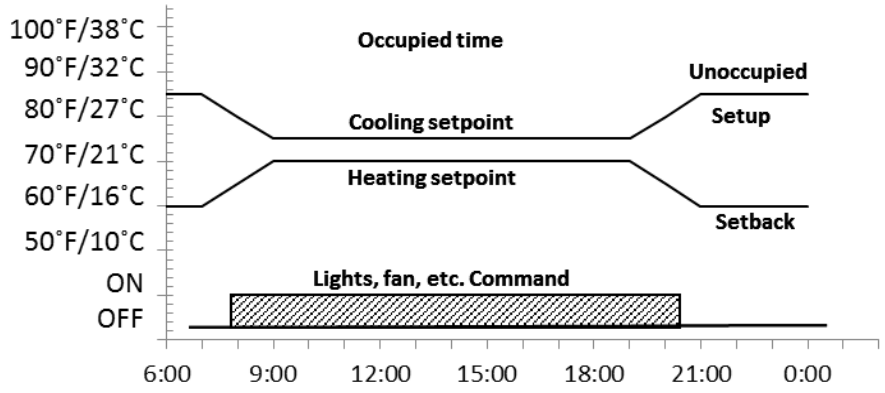

Figure 9: Time-Programmed Commands

Duty Cycling

Duty cycling (Figure 10) is a strategy that performs based on cycles of specific loads [39]. For example, each component may be cycled “On” for 20 minutes and then “Off” for a period of 10 minutes. A different cycling schedule can be implemented for occupied and unoccupied periods. Despite the simplicity of the method, cost effectiveness and a lower thermal level are the main differences in this strategy.

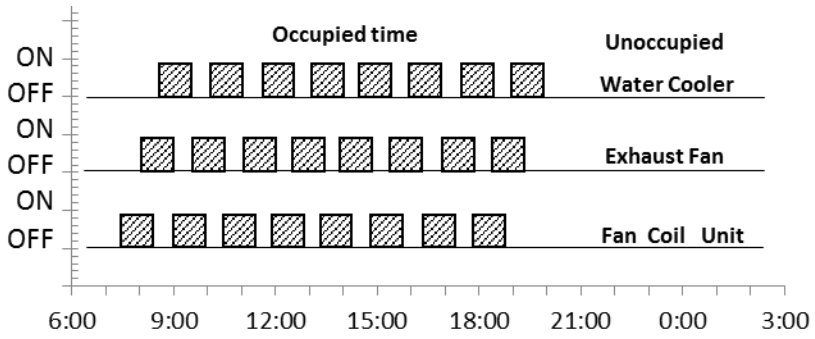

Figure 10: Duty cycling method

Optimum Start / Stop

Optimum start/stop are the main feature of Time-Programmed Commands. In this method, the computer calculates the best or optimum time to start or stop HVAC systems based on the occupants’ regular schedules [40]. However, this strategy can be useful if there is a long unoccupied period in the building.

2.3.4 Thermal comfort

The Predicted Mean Vote (PMV) and the Predicted Percentage Dissatisfied (PPD) models are widely used to measure and assess occupants' thermal comfort. Several strategies have been used to integrate the PMV and PPD models with HVAC systems to obtain optimized energy consumption. Some of these methods focus on the setpoint adjustment based on the existing HVAC control logics [41], while others act as a go-between for existing HVAC control logics. For instance, fuzzy controllers [42] [43], genetic algorithm [44], and neural network based controllers [45] are utilized as different approaches.

Kan et al. proposed a computational intelligence approach to reduce power consumption while providing occupants' comfort satisfaction [13] .Intelligent control on an HVAC system was applied to improve the thermal comfort, visual comfort, and air quality comfort. Yu and Lin also proposed an intelligent control system based on wireless sensing technology, prediction models, and fuzzy theory [46]. That system was able to analyse and forecast the indoor working environment and efficiently provide comfortable air while optimizing energy consumption. The dynamic matrix control (DMC) and generalized predictive control strategies were compared by Nowak et al. by utilizing a simulation to optimize energy consumption and maintain PMV values between -0.5 and 0.5 on the PMV index [47].

Freire et al. [48] investigate the possibility of saving energy while maintaining thermal comfort by considering two strategies; one based only on comfort level and the other based on both energy use and comfort assessment. They used simulation-based predictive control laws to minimize energy consumption and maintain the comfort level in an acceptable range. In other work, Ferreira

et al. [49] create an actual building model and evaluate a neural network based control strategy results. They report the potential of 50% energy savings while maintaining thermal comfort.

In spite of the fact that researchers have broadly utilized the PMV model for thermal comfort assessment, there are some arguments against the PMV model. Some arguments include the inability of PMV to account for the dynamic behaviour of occupants or the difficultly for occupants to adapt to the thermal environment [50]. Additionally, several parameters have to be monitored in real-time from the environment and from occupants, which make this a complex and expensive process [51]. Researchers recently used personalized and real-time comfort sensing approaches to address these challenges. [52] [53] [54] [55].

These methodologies focus on occupant's comfort levels, which are modelled individually in order to develop comfort driven HVAC systems. A participatory approach for adjusting room temperature is used by Erickson and Cerpa, [55]. Results show a reduction of 10.1% in comparison with existing HVAC controls while all occupants were satisfied. Murakami et al., [56] proposed a method to collect votes by a group of 50 occupants and estimate the daily HVAC set points. They report a 20% reduction of energy usage when compared with a constant set point of 26 °C.

Occupancy is another significant factor impacting the energy efficiency of HVAC systems. Occupancy data will reshape the energy demands of HVAC systems, which can minimize the difference between actual consumptions and demands. Numerous studies have focused on energy savings based on occupants' locations. Varick et al [57] show the potential of 42% saving energy based on sensor network occupancy model prediction. Marshall et al. investigated different occupancy patterns and calculated energy savings based on these patterns in residential buildings [58]. Their research revealed the importance of occupancy data for saving energy in buildings but ignored the occupant's comfort levels. A real-time occupancy measurement system was integrated

with an intelligent control of HVAC systems. Klein et al. introduced a multi-agent based system which also considers the location of users by using RFID tags [59]. They modelled the energy consumption based on thermal zones, temperature, and occupants' preferences and schedules. They concluded that a 12% reduction in buildings' energy use was reached by taking the occupant's position data into consideration. However, the above mentioned research did not evaluate the thermal comfort level of individual occupants.

2.3.5 Summary

Based on the literature review, it can be observed that most of existing HVAC systems only work based on the maximum scheduled loads which may lead to huge waste of energy during unoccupied periods. Real-time occupancy data is a suitable solution for this problem. However, control HVAC systems only based on pure real-time occupancy information may not be efficient and economical due to the increase of maintenance costs.

Developing the occupancy pattern based on historical data has the potential to solve this issue. However, unpredictable locations of the occupants need a suitable and feasible pattern to be used by HVAC controllers.

Although PMV model has extensively utilized for thermal comfort modelling in many research, this model has some drawbacks including its limitation to consider behavioural and thermal variations. In addition, several parameters are required to be collected using different type of sensors to implement PMV model which could be complex and costly to be deployed in buildings. Consequently, purely simulation based methods cannot answer the problem of comfort level assessment. Hence, the combination of occupant's thermal profile including feedback from

users and simulation results has a great potential to solve such problems and make the comfort level accountable.

Chapter 3: Methodology

This section outlines the main research processes, including localization, CFD modelling, and energy savings. The proposed methodology is based on simulations and qualitative design methods that include surveys of occupants and real-time experiments. The purpose is to collect qualifying data from occupants' thermal preferences and historical behavioural patterns of their presence. The overall process of the methodology is depicted in Figure 11.

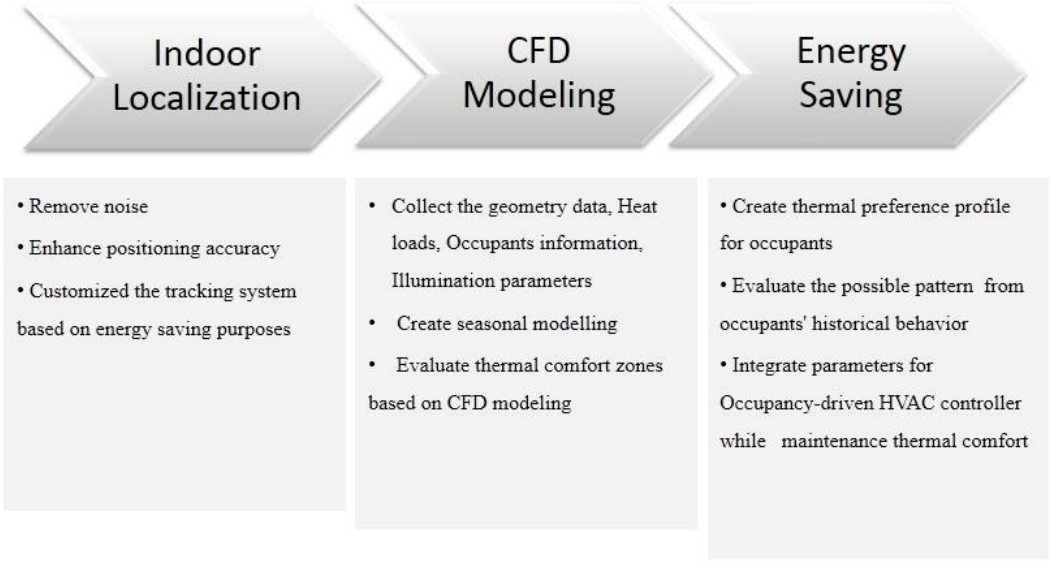

Figure 11: : Overview of Methodology

In the first step, two techniques for removing the unwanted signals and noise, and consequently improving the technological accuracy are introduced: Principle Component Analysis and Moving Average. Afterward, to customize the technology for energy saving purposes, the Near Neighbour Area technique is used to show the location of occupants. Details are provided in Section 3.1.

In the second step, the process of creating the CFD model and extracting the corresponding thermal zones are explained in detail in Section 3.2.

For the final stage of this chapter it is explained how to collect thermal sensation votes and organize them to provide the thermal preference profile of building occupants. Next, the description of the Markov chain and the method of extracting the possible pattern from occupants' historical behaviours were discussed. Finally, the complementary control approach based on all parameters is explained. Section 3.3 provides details regarding thermal comfort approach.

3.1 Indoor localizations

Estimating the position of a target in the indoor environment with high accuracy is the main challenge for investigators. Interference and attenuation from multi-path, reflection, deflection and diffraction are the main sources of error. In this research, the author customized the indoor positioning technique for the specific objective of saving energy. Therefore, the location of an occupant in a specific room is an important parameter used to find out the exact area with the corresponding HVAC outlet. Three methods are utilized to achieve the targets, which are explained below.

3.1.1 PCA

Moving the mobile nodes can cause rapid changes in the RSSI values which leads to significant reduction in the accuracy of estimating the position of the target. Therefore, factor analytic

technique is utilized to increase the accuracy of the position. We have clustered the received signals (packets) from mobile node into 10 signals to introduce one representative signal for each cluster using PCA. This gives us an approximation signal for each cluster, and hence we obtain a 'noise-free' coordinates of the target. For each cluster we are able to identify the representative signal in the order of importance, i.e. the received signals are ranked and weighted by the relative change in their cluster at the specific time point.

The main applications of factor analytic techniques are: (1) to reduce the number of variables and (2) to detect structure in the relationships between variables, that is, to classify variables. Therefore, factor analysis is applied as a data reduction or structure detection tool [60] . Principal component analysis (PCA) is a widely used method for factor extraction, which is the first phase of exploratory factor analysis. PCA reduces the number of variables of the data, by maintaining as much variance as possible. PCA technique transforms a d-dimensional sample vector into a lower dimensional vector i.e. x=$(x_1, x_2, \dots, x_d)$T into y=$(y_1, y_2, \dots, y_k)$T , where d represents the number of variables (signals) and k is the number of selected components. Therefore, the k x d matrix V provides the PCA transformation, such that

$$y = Vx \qquad \textbf{(9)}$$

with population variance-covariance matrix:

$$\text{var (X)}=\begin{pmatrix} \sigma_1^2 \sigma_{12} \cdots \sigma_{1p} \\ \sigma_{21} \sigma_2^2 \cdots \sigma_{2p} \\ \vdots \quad \vdots \quad \ddots \\ \sigma_{p1} \sigma_{p2} \cdots \sigma_p^2 \end{pmatrix} \qquad \textbf{(10)}$$

Consider the linear combinations

$$\begin{aligned} Y_1 &= e_{11}X_1 + e_{12}X_2 + \cdots e_{1p}X_p \\ Y_2 &= e_{21}X_1 + e_{22}X_2 + \cdots e_{2p}X_p \\ &\vdots \\ Y_p &= e_{p1}X_1 + e_{p2}X_2 + \cdots e_{pp}X_p \end{aligned} \qquad \textbf{(11)}$$

Each of these can be thought as a linear regression, predicting Y_i from $X_1, X_2, \cdots, X_p$. There is no intercept, but $e_{i1}, e_{i2}, \cdots e_{ip}$ can be defined as the regression coefficients. In order to draw out the maximum possible variance, with successive factoring continuing, factor weights are calculated until no meaningful variance remains.

PCA is used to develop a filter to reduce unwanted signals that may result in a higher accuracy of the tracking system. The process of this filter is depicted in Figure 12. According to the number of received packets, the first 10 packets are considered the initial input data. By utilizing PCA, the number of packets is reduced to a single packet representative of the 10 initial packets [61]. The target location is estimated based on the representative packet instead of all received packets. Therefore, unwanted signals will be removed from the position calculation. The PCA and estimating the position codes are provided in Appendix E.

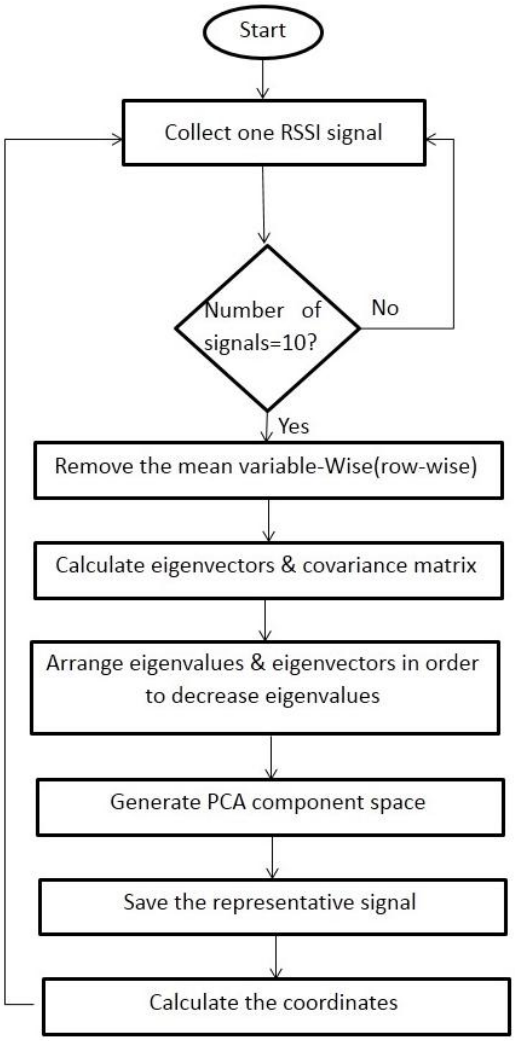

Figure 12:Principal Component Analysis flowchart for RSSI signals

Based on the experimental results described in Section 4.1.2, this filter is suitable for targets with low speed and provides high accuracy. However, as the walking speed is usually normal or high, another filter is used for monitoring occupants inside buildings, explained in Section 3.1.2.

3.1.2 Exponentially-weighted moving average (EWMA)

The principle challenge in the RSSI-based localization system is its high affectability to the environmental progressions. For instance, different signal strengths can be obtained even if the mobile target does not move. Therefore, the Moving Average algorithm is utilized to reduce the dynamic fluctuation of radio signals received so as to obtain essential patterns in the data, while ignoring noise or other rapid phenomena.

In statistics, the Simple Moving Average (SMA) is known as a mathematical method to analyse a data point by exploiting a series of averages from different subsets of the data. By applying more weight to recent data, the lag can be reduced which this method is known as Exponential Moving Average(EMA) or Exponentially Weighted Moving Average (EWMA).

In this section, the EMA has been utilized to predict the next location of the user. Also it is used to smooth the RSS values and remove the unwanted signals according to a logical pattern. This method is based on the fact that there is a relationship between present positions and past locations. By using this method, it is possible to extrapolate the future position of the users. If the estimated and calculated positions are far from each other, the system will consider the result as a noise and try to smooth these differences. Following is the mathematical definition of MA algorithm. The notations are as follows:

Notations:

$\widehat{P}_{t+1}$= Forecast position for period (t+1) made by time t

P_t = Actual position in period t

$\widehat{P}_t$ = Forecast position for period t made by $(t-1)$

α = Constant $(0 < \alpha < 1)$

The mathematical relationship between the past, present and future positions can be explained as:

$$\widehat{P}_{t+1} = \widehat{P}_t + \alpha(P_t - \widehat{P}_t) \quad \textbf{(12)}$$

On the other hand,

$$\widehat{P}_{t+1} = \alpha P_t + (1-\alpha)\widehat{P}_t \quad \textbf{(13)}$$

By substituting past forecasting values we have

$$\widehat{P}_{(t+1)} = \alpha P_t + (1-\alpha)\left[\alpha P_{(t-1)} + (1-\alpha)\widehat{P}_{(t-1)}\right] = \alpha P_t + \alpha(1-\alpha)P_{(t-1)} + (1-\alpha)^2\widehat{P}_{(t-1)} \quad \textbf{(14)}$$

By keeping on substituting past forecasting values we have:

$$\widehat{P}_{(t+1)} = \alpha P_t + \alpha(1-\alpha)\widehat{P}_t + \alpha(1-\alpha)^2\widehat{P}_{(t-1)} + \cdots + \alpha(1-\alpha)^{(t-1)}P_1 + (1-\alpha)^t P_0 \quad \textbf{(15)}$$

Which can be written in the more compact sigma notation as

$$\widehat{P}_{(t+1)} = \alpha \sum_{k=0}^{t-1}(1-\alpha)^k \widehat{P}_{(t-k)} + (1-\alpha)^t P_0 \quad \textbf{(16)}$$

It is clear that there are exponentially declining values; $\alpha(1-\alpha)$, $\alpha(1-\alpha)^2$ on P_t, P_{t-1}, …. .

Before the algorithm process to create our forecasting, we need to consider

- The initial value of P_0
- Determine the value of α

The coefficient α is a constant smoothing factor between 0 and 1 that represents the degree of weighting decrease.

To find the best value, the notation N needs to be explained. N can be considered the un-weighted mean of the previous n data points. On the other hand, N represents the number of past predictions

that we want to use to smooth and predict the future point. One of the recommended relationships between α and N is as follows [62]

$$\alpha = \frac{2}{(N+1)} \quad \textbf{(17)}$$

Moreover, P_0 represents the initial position of the user which can be assumed to be a specific point by the operator or researcher. This algorithm is extended for both prediction of future distance and prediction of next received RSSI. Therefore, for RSSI values we have

$$\widehat{\boldsymbol{R}}_{(\boldsymbol{t+1})} = \boldsymbol{\alpha R_t} + (\mathbf{1}-\boldsymbol{\alpha})\widehat{\boldsymbol{R}}_{\boldsymbol{t}} \quad \textbf{(18)}$$

where $\widehat{R}_{(t+1)}$ represents the forecast RSSI value for t+1 and R_t represents the actual RSSI value with period t.

To calculate the exponential moving average (EMA), three steps are required.

First, The SMA which is used for the initial EMA value as the previous period's EMA in the first calculation. Second, the weighting multiplier. Finally, the exponential moving average is calculated for each data (i.e. RSSI value) between the initial EMA value and the current data, using current value, the multiplier, and the previous period's EMA value. For instance, the formula below is for a 10-period EMA.

1) *Initial SMA 10-period sum/10*
2) *Multiplier: (2/Time periods+1)) = (2/ (10+1) =0.1818 (18.18%)*
3) *EMA: {current value - EMA(previous value)} x multiplier + EMA(previous value)*

The value of 18.18% means that a 10-period exponential moving average applies an 18.18% weighting to the most recent data.

The localization error of this algorithm is calculated by

$$\text{Localization Error (LE)} = \sqrt{(x_{pred-}x_{actual})^2 + (y_{pred-}y_{actual})^2} \quad \textbf{(19)}$$

After calculating the estimated points, LMS fitting was applied to reduce the final estimation error. If we consider coordinates (x_s, y_s) as the initial estimation of the mobile node, then d_i represents the distance between the blind node and the reference node according to the following model

$$d_i = \sqrt{(x_{s-}x_i)^2 + (y_{s-}y_i)^2} \quad \textbf{(20)}$$

It is possible to calculate the difference between the measured and estimated distance by

$$|f_i(x, y)| = \left| d_i - \sqrt{(x\_x_i)^2 + (y\_y_i)^2} \right| \quad \textbf{(21)}$$

It should be mentioned that d_i can be considered the measured distance without implementing the algorithm. Consequently, we obtain a system of N nonlinear equations, which can be solved with the LMS fitting method. However, if an initial estimation(x_s, y_s), is close to(x, y), a linear system can be find from (20) and calculated, obtaining the Best Linear Unbiased Estimator (BLUE) for these type of problems [63].

Applying the LMS method by considering (x_s, y_s) as our initial values providing as algorithm starting point. Then we have

$$\Delta x = x - x_s$$
$$\Delta y = y - y_s \quad \textbf{(22)}$$

and

$$\frac{\partial f_i(x, y)}{\partial x}\Big|_{\substack{x = x_s \\ y = y_s}} = \frac{(x_{s-}x_i)}{\sqrt{(x_{s-}x_i)^2 - (y_{s-}y_i)^2}} \quad \textbf{(23)}$$

$$\frac{\partial f_i(x,y)}{\partial y}\Big|_{\substack{x=x_s\\y=y_s}} = \frac{(y_s - y_i)}{\sqrt{(x_s - x_i)^2 - (y_s - y_i)^2}} \quad \textbf{(25)}$$

Then, to calculate the positions we can rearrange into the following linear model

$$H\theta = B + W \quad \textbf{(24)}$$

where

$$\theta = [\Delta x, \Delta y]^r$$
$$H = [H_1^T, H_2^T] \quad \textbf{(26)}$$

and

$$H_1 = \left[H_{1,0}, \dots, H_{1,N-1}\right],\ H_2 = \left[H_{2,0}, \dots, H_{2,N-1}\right]$$

$$H_{1,i} = \frac{\partial f_i(x,y)}{\partial x}\Big|_{\substack{x=x_s\\y=y_s}},\ H_{2,i} = \frac{\partial f_i(x,y)}{\partial y}\Big|_{\substack{x=x_s\\y=y_s}}, i = 0, \dots, N-1 \quad \textbf{(27)}$$

$$B = [b_0, b_{N-1}],\quad b_i = f_i,\quad W = [w_0, \dots, w_{N-1}]$$

and

$$\widehat{\theta} = H^{-1}B \quad \textbf{(28)}$$

$$[\hat{x}, \hat{y}] = [x_s, y_s] + \widehat{\theta}^T \quad \textbf{(29)}$$

$\widehat{\theta}^T$ may be computed by doing iterative and this calculation continues to obtain an acceptable error.

Finally, the new position can be found by

$$x_s = x_s + \Delta x$$
$$y_s = y_s + \Delta y \quad \textbf{(30)}$$

3.1.3 Near Neighbour Area (NNA)

The Near Neighbour Area (NNA) method is also known as a clustering technique. NAA considers the cases where nodes are deployed in more than one room. The concept of this method is to ignore drifting effects. As the signals can pass through the wall, the accuracy for estimating the user's position inside the buildings would be decreased. This method is based on the fact that every reference node sends its RSSI and X and Y coordinates to the mobile node where they can communicate with each other. Figure 13 shows the concept of this method.

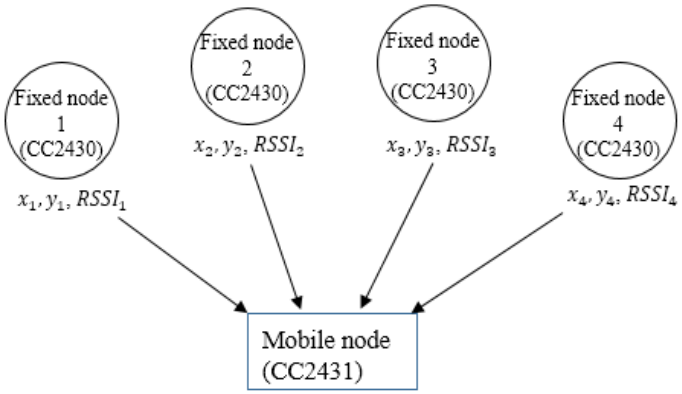

Figure 13: Mobile node input data from reference nodes

To implement this technique, two principles are considered. First, it is essential to describe the architecture of signals to implement NNA in a network. Z-Stack is TI's ZigBee-compliant protocol stack for a growing portfolio of IEEE 802.15.4 products and platforms. Z-Stack supports CC2430/CC2431, which is the hardware utilized in this research. The architecture of received sample signals is depicted in Table 2. The packet start point and command ID is denoted by SOP and CMD, respectively. The number of bytes in data field and data information is introduced by

LEN and Data as well. FCS refers to the frame check sequence. From the received signal, it is possible to extract information regarding the address and RSSI value of the nearest reference node to the mobile node. Hex numbers for example, in parenthesis of Table 2, show the values of X and Y, while the RSSI values correspond to the nearest reference node with coordinates (0, 0). This information is utilized for the proposed NNA algorithm. The predefined zones are introduced based on the X and Y values. Each specific zone can be defined according to the fixed nodes with known coordinates in that area. By the confirmation of the RSSI value from the nearest reference node in any predefined zone, other signals received from outside the zone nodes can be ignored in further calculations.

Table 2: Z-stack message format

SOP	CMD	LEN	DATA	FCS
1 BYTE	2 BYTES	1 BYTE	VARIES IN SIZE	1 BYTE
02	1018	14	CB F550 D3 1400 0D 0009 0005 0004 7B 28 (0000 0000 28)	CB

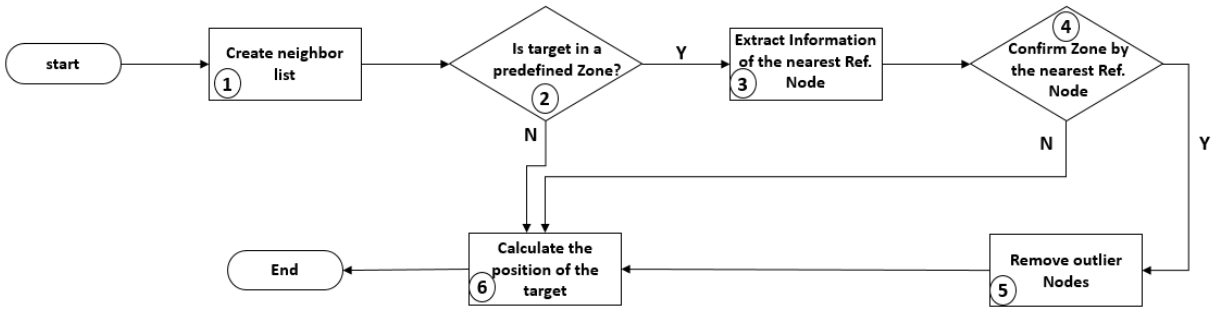

Figure 14: Process flowchart of NNA localization

Figure 14 shows a flowchart of the proposed algorithm bringing out the process clearly: (1) A neighbour list from reference nodes, within the communication range, in accordance with their coordinates is created; (2) Any similar aspects between the created list and any other predefined

list is identified. (3) When a predefined zone is recognized, the coordinates of the nearest reference node will be extracted from the received packets (i.e. refer to parenthesis of Table 2).

(4) The algorithm makes a confirmation if that particular node has its location in the zone. (5) The outlier nodes (nodes not located in the zone but that had communication with mobile node) are removed from the calculation. (6) For the final stage, the position of the target will be computed and if the total nodes are not listed in the neighbouring areas (stage 2 or 4), the system continues calculating the regular position. In the presence of moving objects, stages 3 and 4 significantly reduce the drifting error and therefore increase the accuracy of the user's location estimation.

3.2 Occupancy-driven and thermal comfort

Figure 15 illustrates the overview of the process of intelligent control. The overall procedure takes two major aspect for consideration which are comfort and energy parts.

As mentioned in the literature review section, different persons have different thermal perceptions and it is difficult to make all of them satisfied in a shared space. Therefore, a survey should be done to collect persons' thermal preference. The feedback data are used to develop a thermal preference profile for each user. A boundary of temperature preference can be addressed based on minimum and maximum thermal preferences of all persons present in a room.

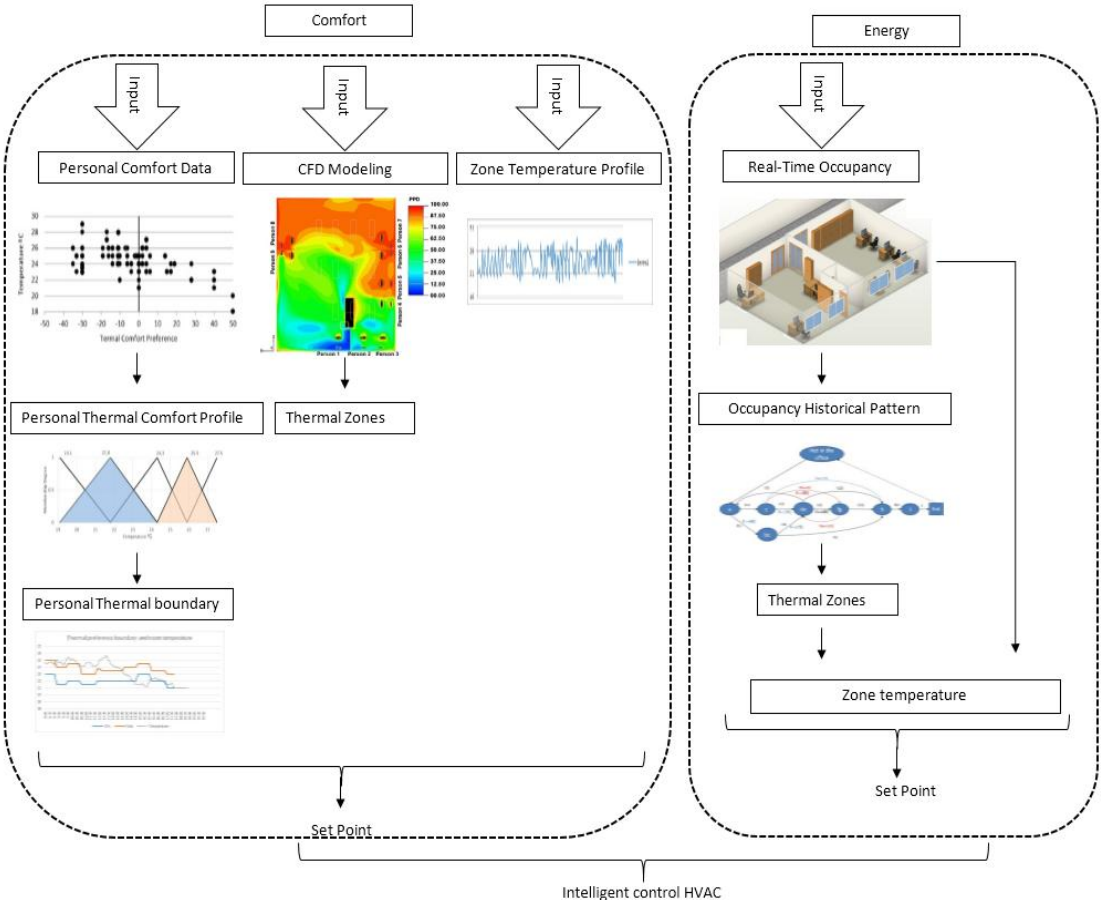

Figure 15: Diagram of intelligent control

The second step is to create the thermal model of the room. Thermal zones can be defined after investigation of the satisfied and dissatisfied areas. Commonly, a thermal zone is the space where all heat loads will be served by the same HVAC system or by the same kind of HVAC system and mostly users located in the comfort area. However, in this research, the thermal zone is redefined as the group of occupants located in similar comfort areas during different thermal conditions.

In another word, the thermal zones introduces in this research is not only based on the space and location of users and their distances to the HVAC outlets. But also considering the satisfied and dissatisfied areas during different scenarios extracted from modelling. Therefore, each user is

associated with one or more thermal zone and each thermal zone is associated with a corresponding HVAC outlet.

In reality, thermal zones may change seasonally due to changing weather conditions. Therefore, the seasonal thermal modelling combined with users' thermal preference profile is used to provide a reasonable input to control the HVAC systems accordingly.

For the energy part, the positions of occupants inside a building will be monitored in real-time. Such data can provide historical occupancy data, which is then used to create historical behaviour patterns for each person. In addition, the real-time data is utilized to identify the location of occupants inside buildings and their presence in the corresponding thermal zones define from previous step. All the information are used to develop rules to control HVAC systems for the purpose of achieving efficient energy consumption while maintaining occupants comfort level. Details of each step are explained as following sections.

3.2.1 Creating CFD model

CFD has a history back to the 1930s as a computer modelling technology, which compounds computer sciences, numerical techniques and physical sciences. At present, CFD modelling has been applied in various fields. It can evaluate the original and continuous physical quantity fields in space and time by adopting a series of finite discrete points and a set of variable data. Solving the algebraic equation sets provides a field variable approximation. In reality, thermal zones can be a dynamic or static area. On the other hand, the modelling and calculating of a thermal zone is a time consuming process. Hence, it is difficult to model a dynamic thermal zone specifically for

a real-time control purpose. Therefore, in this research, seasonal modelling is applied to evaluate satisfied and dissatisfied areas for each season of the year and this method consequently defines thermal zones in the test bed area.

To develop the model and identify thermal zones, the geometry data of the area were retrieved from an as-built BIM model, which is explained in Section 3.2. Indoor and outdoor temperatures are collected and all the data are imported to the CFD model. A simulation is then performed to analyse the comfort level at different areas in the room. Based on the HVAC performances, the most common scenarios and corresponding controls can be modelled.

3.2.2 Detecting occupants location

One of the most popular approaches to estimate the locations of mobile targets in both indoor and outdoor environments is RSS. Among them, the ZigBee-based wireless sensor network is a technology that can be utilized for this project, which is explained in detail in the literature review.

The X and Y coordinates of the targets are recorded in real time while they are inside the building. Furthermore, it is possible to identify each person and the place where they are located by identifying the unique ID associated with each tag and the BIM model. This information will be used not only for real-time monitoring, but also for creating a historical behaviour pattern for individual occupants to predict their positions.

3.2.3 Predicting behavioural based on historical pattern

The proposed data acquisition system in Section 3.1 can collect the occupancy data from a single or multiple occupant environment. The PhD research office occupied with nine users in the

environment building at Xian Jiaotong-Liverpool University is an example of a multiple occupancy situation in which the proposed indoor localization system was installed.

Although the occupancy data collection during a long period is not impossible, it is subject to some restrictions. For example, suitable office with enough number of occupants, the number of volunteers who accept to carry the mobile nodes during the experiment's period, the restrictions in the number of hardware equipment such as ZigBee nodes and the required resources for the maintenance of sensor network. All the restrictions can make the occupancy data collection fairly limited.

The nature of identifying the occupancy behavioral pattern and make it in a mathematical format is somewhat complicated. However, it is possible to simplify the occupants' behaviour and mainly focus on a particular places which can reduce the computational process.

Therefore, in this research, each occupant has a routine work life which includes five unique locations: 1) The office, which is considered the fixed working place for the occupants. 2) Short temporary locations such as the coffee room. 3) Long-stay locations outside of the office room. For example, classrooms and meeting rooms. 4) The elevator, where occupants leave the current floor and is denoted *Lift*. 5) Outside the building [64].

In the current stage of this research, the focus is only on the fifth floor of the building. When the occupants use the lift and the exit/entrance sensor out of the building does not identify them, this can be assumed as a long-term leave of the office without considering the position of occupants in the other floors. In the future, this will be considered. These different situations are considered in to predict the periods of time when each person leaves the office.

For one occupant in a typical day, the number of movements between different predefined areas is called *transition* and the time spent in each area is introduced as *duration*.

A typical example of one occupant is depicted in the form of a signal-graph in Figure 16.

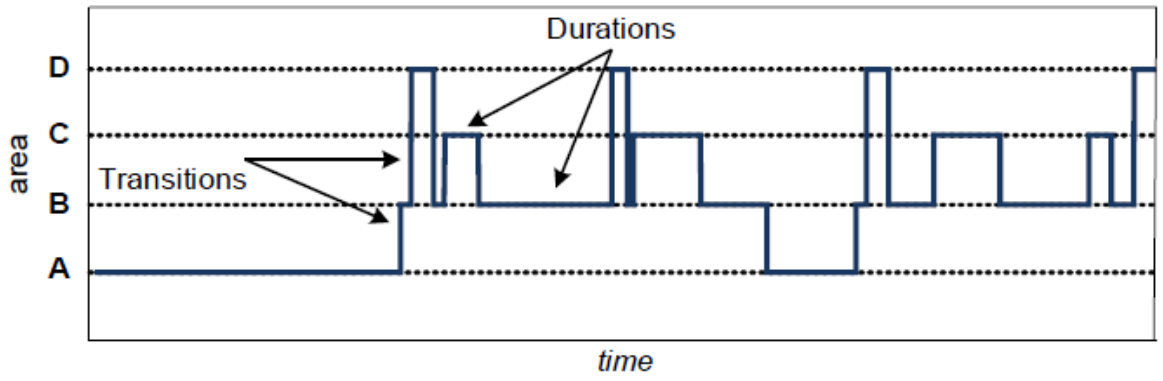

Figure 16: A signal model of an occupant in different areas

Figure 17 shows an overview approach of the occupancy pattern detection. Following is the description of proposed approach.

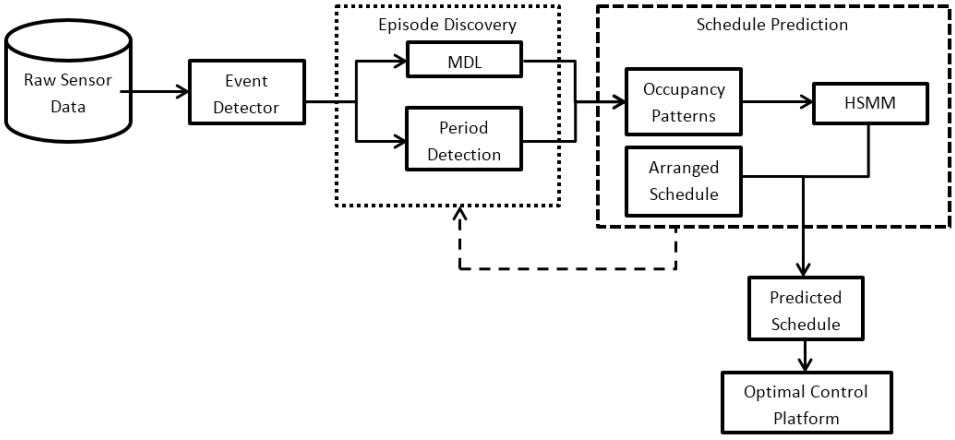

Figure 17: An overview of the occupancy pattern detection approach

Event Detector

A symbol denotes the significant position of occupants and called "the event" and the sequence of symbols are considered as an "episode". Table 3 represents symbol assignments based on different situations.

Table 3: Event codes

Place of sensors	State Transitions	Code
Office	1. Enter	a
	2. Stay	b
	3. Left	c
Coffee room (short-term stay place)	1. Enter	d
	2. Left	e
Meeting room/Classroom (long stay place)	1. Enter	f
	2. Left	g
Lift/Elevator	Detect	h
Outside	Detec	i

Episode Discovery

The more frequently repeated an episode, the more likely it is that the episode is a regular behaviour pattern. Hence, based on the method introduced in [65], the important patterns are discovered. First, the candidate sequences are generated and the important sequences are purified.

Using the sliding time window, the time series position event sequences are created. Afterward, the minimum description length (MDL) criteria and periodicity detection (PD) are applied to determine the most significant behavioral mode.

Minimum description length (MDL) method

In the MDL method, the dataset are encoded alphabetically to reduce the description length and constraints are applied to discover event models with the shortest description lengths [66].

Frequent pattern $\Phi=\{\varphi_1, \varphi_2, \varphi_3 \ldots \varphi_n\}$,
Where φ_n is the n^{th} episode.

1. Ordering Φ based on
   I. Frequency
   II. Length

2. Compress (Φ)

CodeTable = *allsingletonpatterns;*
*minDBsize = computeSize(*CodeTable*)*
Foreach φ_i *in* Φ; (in order)
CodeTable.add (φ_i)
newsDBsize =computesize (CodeTable);
IF (newDBsize < minDBsize)
minDPsize=newDBsize;
else
CodeTable.remove (φ_i);
Return CodeTable;

Algorithm 1: MDL Method

Periodicity detection (PD)

Often, occupants' behaviour can be detected in the form of a pattern exhibiting periodicity. For instance,

> *At 10:00Am on Monday, Wednesday, and Friday of every week, User 3 left the work office and went to the classroom.*

In a time series T, both the symbol and the periodic episode can be detected. For example, if a symbol, "s", with a period, "p", exists *almost* every p time-stamps can be considered as a periodic event.

To filter out short-stay occupants and temporary behaviour of occupants in different areas, the occupancy resolution t_R was set as 5 min and 15 min were chosen as the length of time window, since this duration is sufficient to smooth the fluctuation. However, for selecting the proper time window further investigation is required in future.

As shown as Figure 18 when one user is detected in the office, short-term stay places or long-term stay places, the number of times that user stays in one window is calculated as

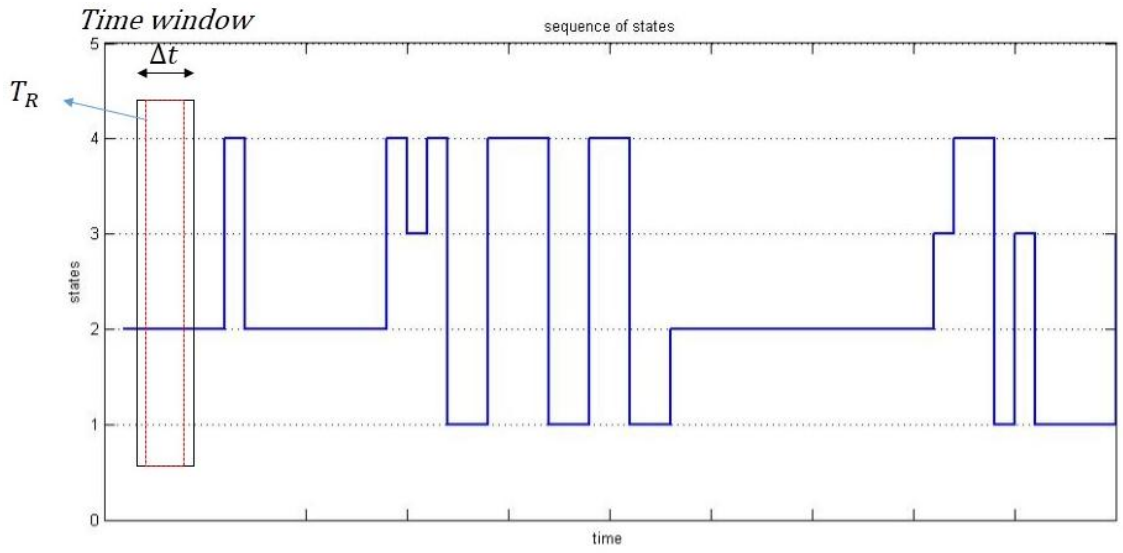

Figure 18: Periodicity detection using time window

$$l_{\Delta t}^{j} = l_{(n+1)}^{j} \Big|_{t=tn+\Delta t} - l_{n}^{j} \Big|_{t=tn} \quad \textbf{(31)}$$

In one window

$$l_{\Delta t}^{j} \rightarrow n_{\Delta t} = 1 \quad \textbf{(32)}$$

$$N_{\Delta t} = \sum n_{\Delta t} \quad \textbf{(33)}$$

where

j shows the particular areas (office =1,short-stay place=2,long-stay place=3)

tn represents the star time in the new area;

Δt is the length of a time window;

$l_n^j \; and \; l_{(n+1)}^j$ show the number of times that user is detected from T=0 to tn and tn+Δt in the specific area of j;

$l_{\Delta t}$ is the number of times the user is detected in one time window;

$n_{\Delta t} = 1$ means at least one occupant is in the time window;

$N_{\Delta t}$ counts the total number of occupants in the time window;

$$\Delta T = \left(l_{\Delta t}^{j} - 1\right) * t_R \quad \textbf{(34)}$$

where ΔT shows the duration of staying an occupant in the area within a time window

The duration time function f_p^j (t) in one day for a specific area (j) for one user (p)can be defined as

$$f_p^j \text{ (t)} = \sum_{i=1}^{k=\frac{24*60}{\Delta T}} \Delta T = \sum_{i=1}^{k} \left(l_{(n+1)}^{j} \Big|_{t=tn+\Delta t} - l_n^j \Big|_{t=tn} - 1 \right) * t_R \quad \textbf{(35)}$$

The hidden semi-Markov model (HSMM)

In the occupancy-driven based applications, it is important to investigate the duration of occupancy in the room. Therefore, it is essential to predict the current state's duration for each user in order to find the daily occupancy pattern. Hence, from the event patterns, the occupancy behaviour of all users in the room is modelled.

To model the stochastic processes the Markov chain is a popular technique in which through analysing the transitions from one state to another the process can be modelled. The transition is measured by two input parameters: the initial status and transfer probability. In this research, when the occupant detected in a room, the model introduces he/she as "Enter" status and when he/she identified in another place, the model consider the person as "Left" status as shown in Figure 19.

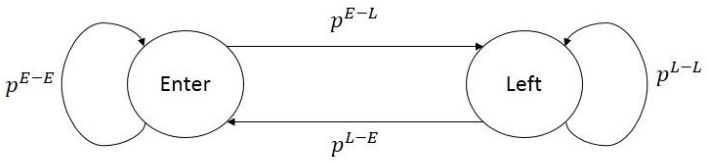

Figure 19: General Markov chain model

A hidden semi-Markov model is utilized to determine the duration of each state before transition to the next state. For instance, Duong et al. investigated human activity patterns using the HSMM [67]. In the present research the proposed algorithm for the occupancy pattern recognition is trained by a forward-backward algorithm [68].

To develop a historical pattern for the attendances of each person of a specific day in a week, it is essential to record two types of data: their entrance/exit time to the test-bed area and their corresponding destinations. Moreover, the fixed schedule of each person is also useful to develop the pattern. Therefore, the probabilistic of short-term and long-term leave is calculated based on the historical pattern by using the Markov Chain method [69].

For the two initial statuses of "Enter" and " Left" , the transition probability matrix at the time t of one occupant can be defined as

$$TPM_t^i = \begin{bmatrix} p_t^{E-L} & p_t^{E-E} \\ p_t^{L-L} & p_t^{L-E} \end{bmatrix} \quad \textbf{(36)}$$

where

TPM_t^i means the transition probability matrix for user i at the current time t;

p_t^{E-L} presents the observed probability that this user change his/her status from "Enter" to "Left" in the next time window;

p_t^{E-E} denotes the probability of status staying in "Enter";

p_t^{L-E} and p_t^{L-L} show the possibility of changing from " Left" to "Enter" and remaining "Left" at the current time t.

Using the identified conditional probability from historical data, the probabilities are computed. For instance, p_t^{L-E} is calculated as

$$p_t^{L-E} = P\left(identified\ state = \text{Enter} \,\middle|\, identified\ state\ = 0\right)\ (t > 1) \qquad \textbf{(37)}$$

The pattern is developed based on the probability of existence of users in the room at a specific time and on a specific day of the week. In other words, locations of users for one month are used to calculate the probability of presence and absence for each 15 minutes.

The developed pattern of each person's historical behaviour is combined with that person's real-time location and corresponding thermal zones for energy saving analysis.

3.2.4 Creating thermal preference profile

Upon the development of a thermal-comfort-based HVAC controller, acquiring personal thermal preference profiles is essential. By analysing the feedback from persons in the room about their perception of the environment in different seasons, a satisfactory thermal condition can be obtained for individual occupants. To assess the occupants' perceptions of the environment,

different thermal comfort sensation scales, such as the ASHRAE thermal sensation scale, the Bedford comfort scale, the McIntyre 3-point preference scale, and the acceptability scale can be used. Although the combination of these scales will provide an accurately representative occupant comfort, it requires a multi-thread interface, which may complicate data analysis [70]. Therefore, a user-led decentralized thermal comfort method, introduced by Jazizadeh et al. [52], was utilized in this research, where both the functionality of the thermal sensation scale and the preference scale were integrated into one scale with a range of intensity.

The process of thermal preference profile is depicted in Figure 20. The whole process is divided into the offline and online phases. During the offline period, occupants submitted their votes regarding their preferences based on the current zone temperature. The setpoints of HVACs were changed at different values so that the occupants could react in different temperature ranges. Afterward, the personal comfort data of occupants are utilized to create the individual comfort pattern based on the fuzzy map.

During the online phase, occupancy data included the personal identifications and corresponding thermal zones where identified. Consequently, from the combination of preference votes of presented occupants, the associated fuzzy pattern was extracted. Finally, the range of satisfied temperatures were computed and applied to the HVAC system. Details of each part are provided as follows.

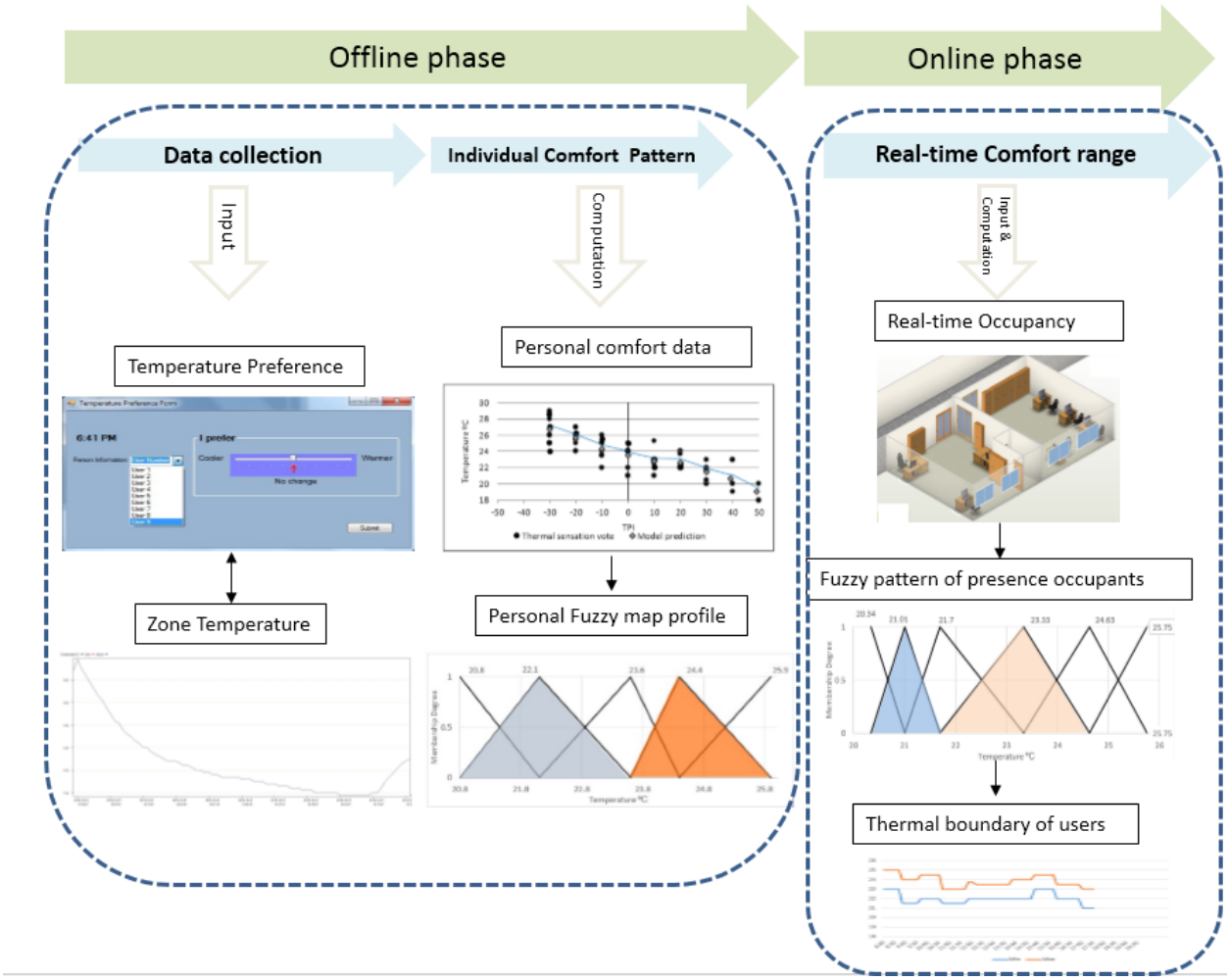

Figure 20: The process of thermal preference profile and room's temperature calculation

Data collection

A data collector is designated in the present research to collect thermal preference scales from the occupants. As shown in Figure 21, the slider contains three major points: cooler, neutral and warmer. The range of the slider varies between -50 to +50 from the cooler side to warmer side. When a user moves the slider to -25, it means that his/her perception of the current ambient condition is hot/warm and he/she prefers colder conditions. Simultaneously, his/her perception of the thermal environment, time, and his/her location are stored in a database for further analysis, as

described in Section 3.1. The feedback values associated with the slider are called thermal perception index (TPI), which indicates the intensity related to a person's vote.

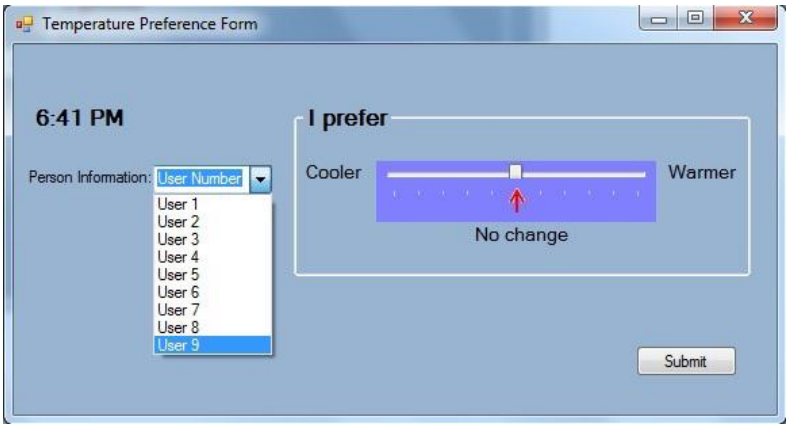

Figure 21: Temperature preference form

Fuzzy map profile

In the fuzzy classification methods, the grid positioning technique is used for different applications such as pattern recognition, decision making and data mining. In this method, it is assumed that a small number of fuzzy sets can be considered as representatives of all variables [71]. To automatically generate the fuzzy rules with the low complexity and with good classification rates and no redundant rules, the Wang-Mendel (VM) fuzzy pattern recognition is a well-known technique which produces relatively small rule bases [72]. In this method, the number of training pairs is utilized to limit the number of generated rules.

Consider x_i as input with (i=1, 2,…,n) and y as output, given a set of input-output pairs:

$(x_1^{(1)}, x_2^{(1)}, \dots, x_n^{(1)}; y^{(1)}), (x_1^{(2)}, x_2^{(2)}, \dots, x_n^{(2)}; y^{(2)}), \dots$

the VM method provides a mapping as

$$f: (x_1, x_2, \dots, x_n) \rightarrow y \qquad \textbf{(38)}$$

The region of occurrence of the variable is defined by each input and output in the 'domain intervals' and included a number of fuzzy sets with triangular membership functions. To interpret the fuzzy sets, they may have labeled like cold (C_1, C_2, C_3), $Netural\ (N) and\ warm(W_1, W_2, W_3)$ as shown in Figure 22.

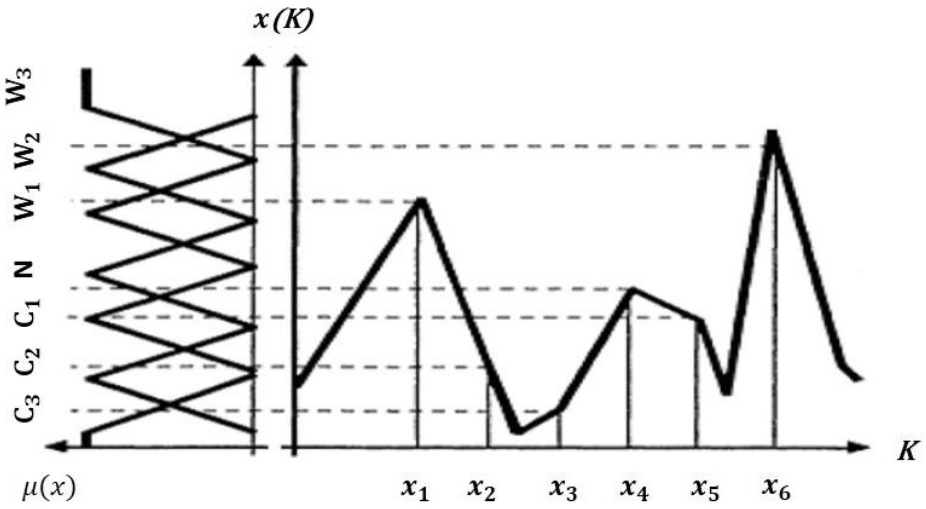

Figure 22: Mapping time series data to fuzzy sets

By mapping from the time series to the pre-specific fuzzy sets, membership functions are specified to individual variables. Considering the (x_1, x_2) as inputs and (x_3) as the output in Figure 22, a sample rule is

If x_1 is W_1 $|W_2$ and x_2 is C_1 $|C_2$ then $x_3$is C_2 $|C_3$

i.e. x_1, x_2 and x_3 are relating to fuzzy sets $W_1$and W_2 ; C_1 andC_2; C_2 and C_3 , respectively.

Consequently, each variable belongs to the fuzzy set with the maximum membership function.

If x_1 is W_1 and x_2 is C_2 THEN $x_3$is C_1

To remove the rules with similar antecedents and different consequents, each rule is assigned by a degree D based on their membership functions$\mu(x)$.

$$D_{Rule} = \mu_{A1}(x_1) \ldots\ldots \mu_{Am}(x_m)\ \mu_B(y) \quad \textbf{(39)}$$

The selected rules with the highest degree are then used to populate the fuzzy rule base.

In this research, to identify the temperature ranges, fuzzy sets are assigned to the preference votes collected from occupants using Wang–Mendel fuzzy pattern recognition approach and the code is provided in Appendix G.

Figure 23 shows scatter graphs extracted from collected data of one person located in a thermal zone. The horizontal axis represents the value of the thermal preference index (TPI values) and the vertical axis illustrates the associated temperature. Each vote is associated with a range of temperatures and those data have a fuzzy pattern, which is used to develop a fuzzy map. The fuzzy map includes hundreds of fuzzy rules represented by a function of (f:tp→ t) to create the thermal preference profile for all users.

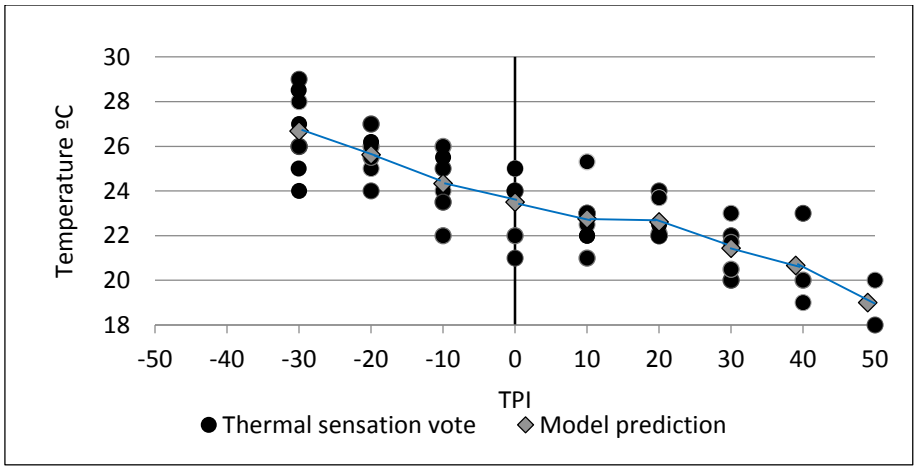

Figure 23: Thermal preference of an occupant and associated temperature

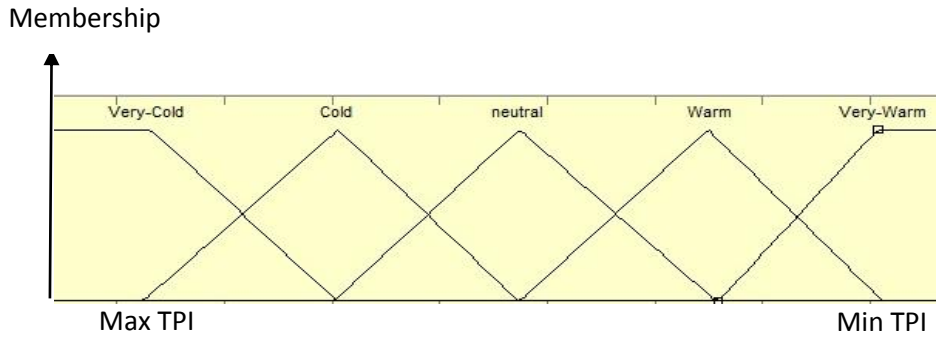

Figure 24: Fuzzy sets membership function for thermal preference profile

The thermal perception index (TPI) and associated temperature are categorized as (tp_i, t_i) ,where tp_i represents the thermal perception index, and t_i is the associated temperature.

Figure 24 illustrates five fuzzy sets, which are very cold, cold, neutral, warm and very warm, based on collected data points. The fuzzy sets are introduced between minimum and maximum tp_i. Zero value, which represents the neutral feeling of occupants, is considered the center of the fuzzy

set and equal intervals are defined for the right and left side of the neutral fuzzy set. For each (tp_i, t_i), by selecting the maximum membership function for tp_i, an IF-THEN rule is generated.

Next, t_{av} is defined as the canter of the THEN part. There is a high possibility that the same condition (IF part) will result in different events (THEN part). A weight w_i is considered for each fuzzy rule, which represents the membership value of tp_i. The rule weights combined the similar IF part rules with THEN parts entered at average weights of the t_i^k. Here, k represents the group of rules in which

$$t_{av}^k = \frac{\sum_{i=1}^{l} w_i^k . t_i^k}{\sum_{i=1}^{l} w_i^k} \quad \textbf{(40)}$$

t_{av}^k denotes the weighted average of t_i for each combined rule k, and l equals the number of rules with the same IF parts. Finally, the combined rules create a predictive model for the fuzzy map, utilizing the singleton fuzzifier and centre-average defuzzifier [73].

$$f(tp) = \frac{\sum_{k=1}^{L} t_{av}^k . M^k(tp)}{\sum_{k=1}^{L} M^k(tp)} \quad \textbf{(41)}$$

where L is the total combined rules and M^k represents the membership value of each combined fuzzy rules. The fuzzy sets and corresponding predictive model lead to the thermal preference profiles.

For instance, considering the neutral temperature to be the middle of the thermal preference profile (Figure 25), 23.5ºC is the neutral temperature with the minimum and maximum temperatures of 22.7 ºC and 24.3 ºC respectively.

The temperatures for the lower and upper preference boundaries in specific thermal zones are calculated based on the thermal profile of the occupants who are present in that zone. If the occupants are from different zones, there is no need for combination of their thermal profiles. Figure 25 shows and example of the case which two persons in the same zone are attended in the office. The individual profile of user 3 shows the prefer temperature range between 23.1 ºC with 25.2 ºC, and for user 7 this range is between 21.5 ºC with 22.7 ºC. The fuzzy map extracted from the combination of their thermal preference profile shows the accepted range between 22.8 ºC with 23.8 ºC for both occupants. As the estimated boundary is less than 1.5 ºC which is the minimum acceptable range for boundaries, system will extend the boundary to the minimum and maximum range of the combination fuzzy map which is between 22.17 ºC with 24.23 ºC.

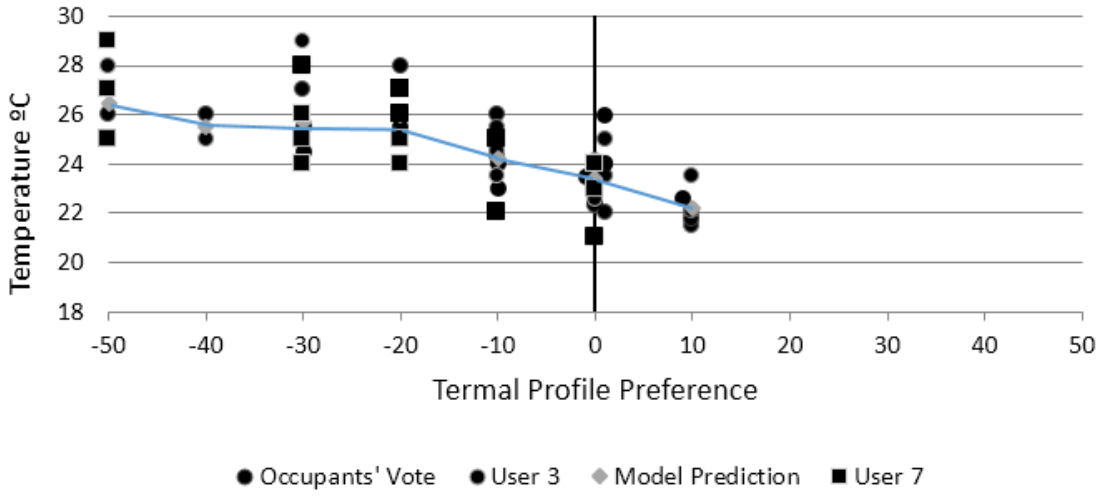

(a) Thermal preference profile for two occupants in the same thermal zone

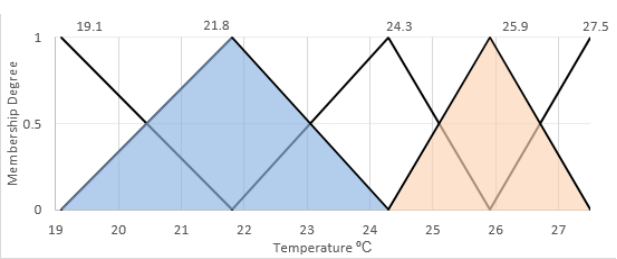

(b)Fuzzy map for user 3

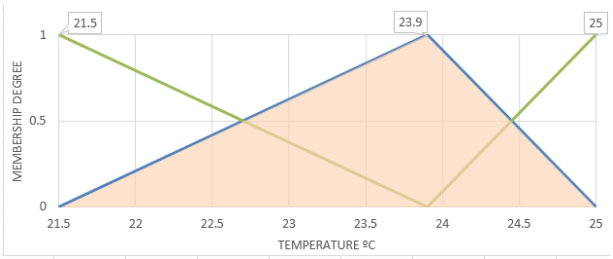

(c) Fuzzy map for user 7

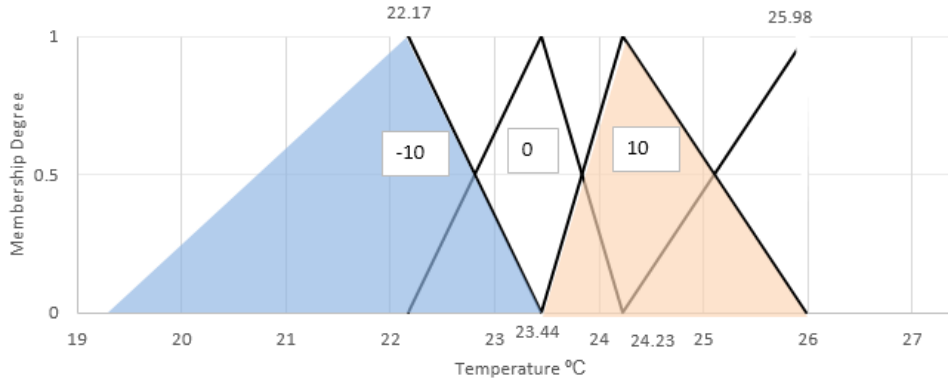

(d) Fuzzy map from the combination of thermal profiles of user 3 and 7

Figure 25: Fuzzy map for two persons in the same thermal zone

3.2.5 Complementary control approach

Based on the occupancy behaviour pattern, thermal preference profiles, the real-time location of users, and current zone temperatures the intelligent control approach is proposed. The existence of users in specific thermal zones is identified and the temperature of that zone is kept as close as possible to the user's preferred temperature. If the room temperature is within the boundaries, no action is needed to control the HAVC based on his or her movement. Otherwise, specific rules will be triggered to turn on/off the corresponding HAVC which will be explained in details in section 4.2.5.

In summary, Any exit/entrance from/to the room will be monitored. When one person enters or leaves the room, the information of that person and related thermal zone is identified. Afterwards, the corresponding behavioural patterns are considered to predict the duration of these changes. Thermal preferences of occupants and current temperature will be evaluated. Sensors are installed in each zone and the zone temperature is calculated based on the average of those sensors (t_z). Once the users are recognized in a specific thermal zone, their thermal preference profiles (tp_i, t_i) are taken into account and (tp_i, t_i) from all existing users are utilized to create the boundary of their thermal preference and make all the users as comfortable as possible. The preference boundaries will be updated based on occupants' attendances in real-time. All the information about the zones' temperature, thermal preference profiles, historical behaviour of occupants, and their real-time locations are used to develop rules to control HVAC systems for the purpose of achieving efficient energy consumption while maintaining occupants' comfort levels. Details of each step are explained in following Section.

Chapter 4: Implementation

The implementation process based on the introduced methodology is presented in this section. Section 4.1, presents the implementation of localization algorithms to customize the indoor localization system for the energy saving purposes. In Section 4.2, thermal comfort of the test bed area during different scenarios based on CFD modelling is investigated. Seasonal PMV and PPD models are developed and the satisfied and dissatisfied areas are identified. Furthermore, the fuzzy-based thermal preference profile of occupants and the extracted occupancy data and patterns are presented. For this section, data recorded for six months and consequently the last month of winter are considered for the test based on the patterns extracted from collected data. The performance of the proposed method is evaluated in section 4.3. For the energy saving part of the method, different strategies are compared with the intelligent technique. The second survey conducted to verify the computed personal thermal preference profiles and subsequently the comfort level of occupants.

4.1 Indoor Localization system development

The CC2431 is TI's system-on-a-chip (SoC) equipment included in a hardware-based positioning engine to address the issues of low-power ZigBee/IEEE 802.15.4 wireless sensor networks. The chip's positioning engine has the capability to calculate and estimate the location of relevant nodes with unknown locations based on the received signal strength indicator (RSSI) from nodes with known positions. It then transfers the position information to the server. RSSI function has the potential to decrease the network communication delay and traffic. Under standard

conditions, it can accomplish a location precision of 3 ~ 5 m with 0.25 m resolution. CC2431 offers 128 KB flash memory, 8 KB Ram, ultra low-power utilization, and other powerful features. The CC2430 is also SoC solution for IEEE 802.15.4 and ZigBee projects which have a low cost, 128 KB flash memory, and 8 KB Ram. It has outstanding sensitivity and vigour to interferers (Figure 26). The main difference of CC2431 with CC2430 is that CC2431 module equipped with a positioning engine which can calculate the position of target and can demonstrate the position on their framework which is called the Z-engine.

Figure 26: CC2430 covered by a box

The experiments were conducted in the realistic ZigBee (2.4 GHz RF communication system) sensor networks located on the fifth floor of the environment building at Xian Jiaotong-Liverpool University, (Figure 27). The highlighted area represents the experimental zones (Figure 27(a)). The Texas Instrument CC2431 nodes are adopted as the mobile target and CC2430 nodes are implemented as reference nodes. In addition, to analyse the proposed algorithms, mobile nodes are programmed to obtain the raw RSSI values, which are then sent to the server for further computations. According to our architecture, all reference nodes (CC2430) in the office transmit

their coordinates and RSSI values to the mobile tag. Note that CC2431 was used as a bench mark for the comparative experimental study and CC2430 was utilized as a mobile node for the proposed algorithms. The Trilateration method is used to calculate the estimated position during the experiment. The code is provided is Appendix F.

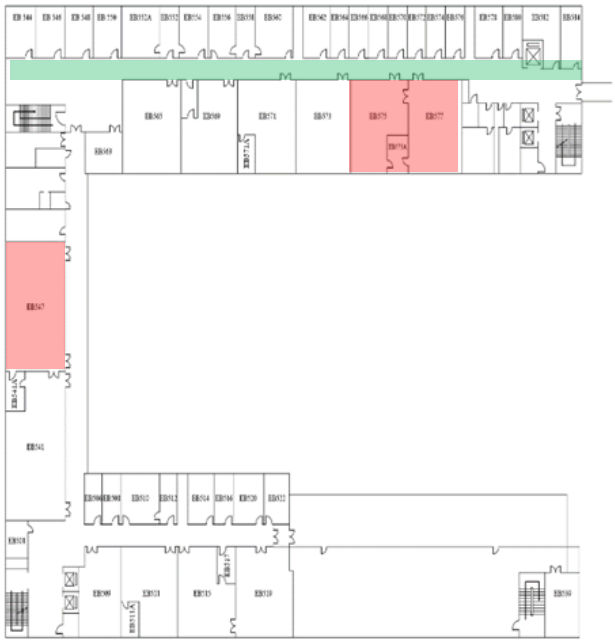

(a) The fifth floor of Xian Jiaotong-Liverpool University

(b) Fixed reference nodes installed in an office

(c) Fixed reference nodes installed in the room EB547

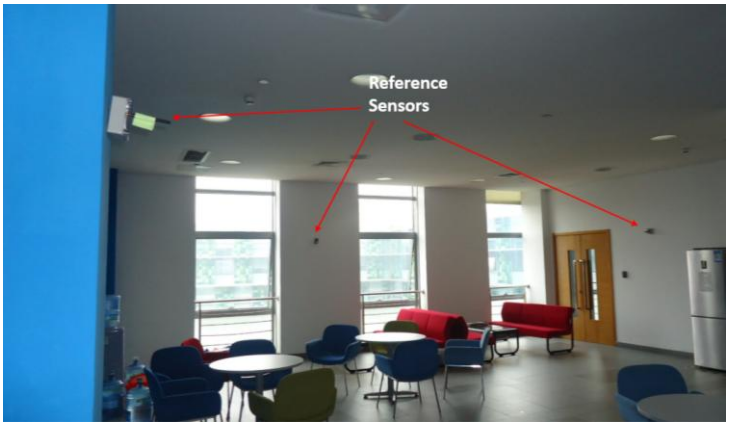

(d) Fixed reference nodes installed in the coffee room

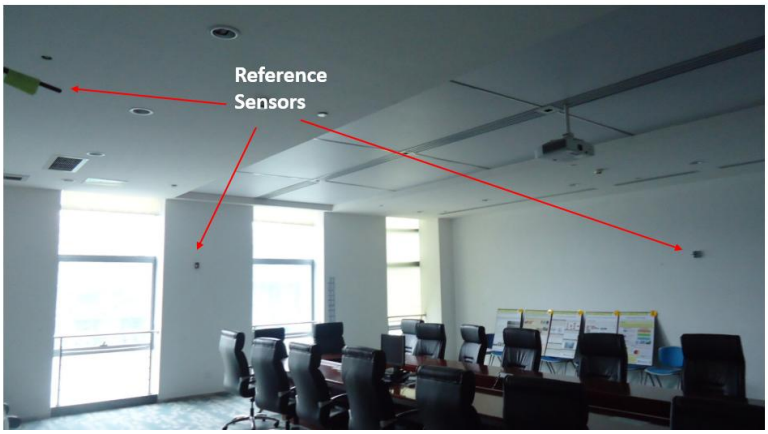

(e) Fixed reference nodes installed in the meeting room

(f) Fixed reference node installed in the lift

(g) Fixed reference nodes installed at the entrance

Figure 27: Overview of test-bed area

To investigate the impact of the NNA method, a ZigBee network was implemented in a test-bed area. The difference between the NNA method and the default approach is investigated in section 4.1.1. The static and movement scenarios for the PCA method and the EMA method were analysed and compared in sections 4.1.2 and 4.1.3, respectively. To simplify the analysis, the 3D model of test-bed is designed as Figure 28.

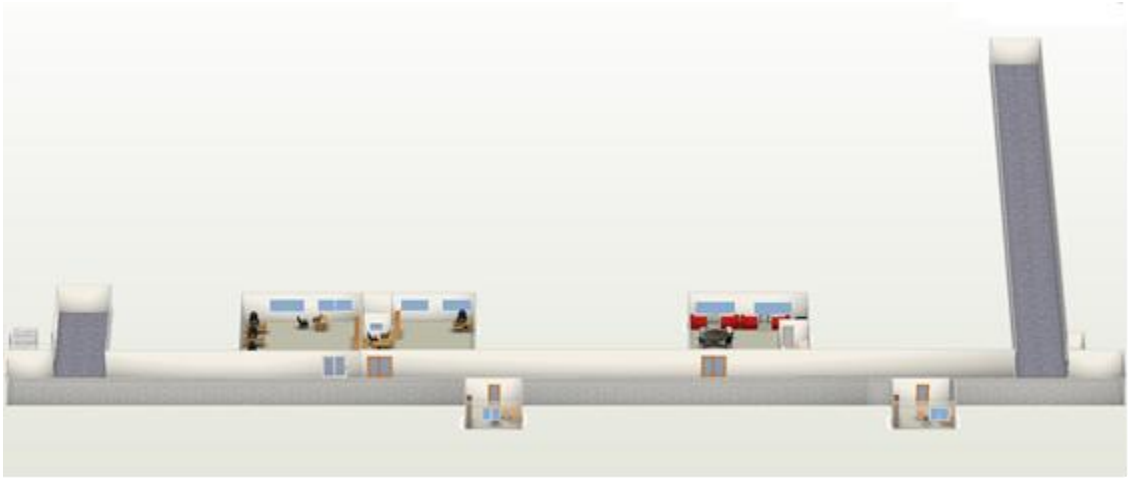

(a) Whole test-bed area

(b) Coffee room **(c) Office room**

Figure 28: 3D model of test-bed area

4.1.1 Testing of NNA

Rooms EB575, EB577 and EB575A on the fifth floor were selected to be the test bed, represented. For the first scenario, a mobile node (red star) was associated with a particular person present in room EB575. In this situation, the communication was triggered between the target and two reference nodes from room EB577, four nodes from room EB575A, and three nodes for

EB575, as shown in Figure 29 (b). The location of the target was estimated as the blue square in room EB575A, as shown in Figure 29 (b). This may result in wasting energy when expected to control HVAC systems and lighting systems based on occupants' location. Therefore, the NNA method was applied to the same situation, and it was found that the communication information from the reference nodes in room EB575A was disregarded and the location of the target was estimated instead as the green circle, as shown in Figure 29 (c).

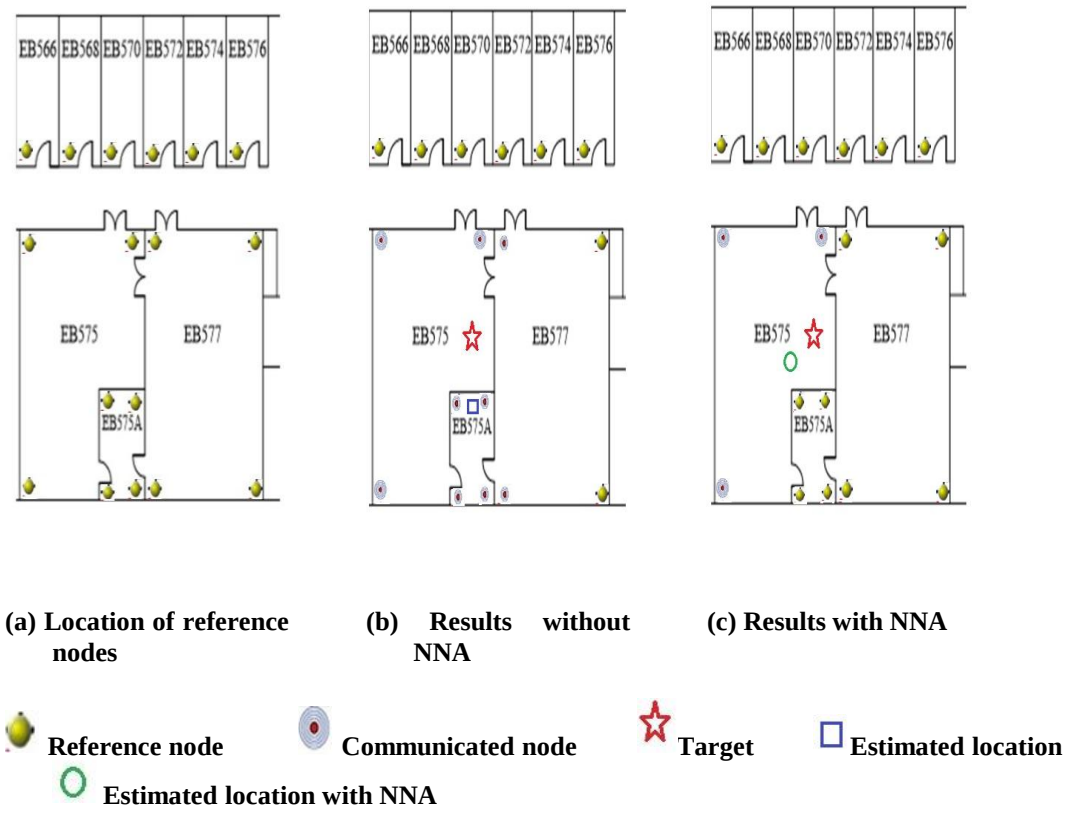

Figure 29: Near Neighbor Area analysis

Several tests are implemented in different positions of the fifth floor based on the NNA method and the CC2431 positioning engine which results are indicated in Table 4. It is obvious that places where the occupants have a fix position for longer period, the results of both systems are more accurate than places where the occupants have to move. For example, for corridor test, the CC2431

and NNA show the correct positions by 55% and 70%, respectively. However, for the meeting room, the results increase by 75% and 95% for CC2431 and NNA method, respectively. NNA method shows an enhancement of 95% for the office room compare with 60% of the CC2431 positioning engine. For the lift, where the installed sensor is far from the other sensors, both systems show an accurate result by 95%. For the coffee room where occupants may have a short-term stay, results of NNA method are significantly more accurate than the CC2431 positioning engine.

To sum up, the implementation results show the improvement of the indoor localization accuracy while using NNA.

Table 4: Comparison of NNA and CC2431 positioning engine

	Number of tests for each method	Correct CC2431 position	Correct NNA position	Percentage of correct position for CC2431	Percentage of correct position for NNA
Corridor	20	11	14	55 %	70%
Office room	20	13	19	60%	95%
Lift	20	19	19	95%	95%
Meeting room	20	15	19	75%	95%
Coffee room	20	10	18	50%	90%

4.1.2 Testing of PCA algorithm

Figure 30**Error! Reference source not found.** illustrates a sample of RSSI data collected from ne node at different locations during a period of 100 seconds. The RSSI packets were divided into 10 groups and a PCA was implemented on group one to choose a representative value as the best value for that group. Therefore, the calculated position is based on the best representative value. Figure 31 illustrates the modified RSSI values after applying the PCA algorithm. As an example,

Zone 5 includes a noise level of -35 dBm. By comparing with other signal values in the zone, this noise was isolated and filtered. Figure 32 and Figure 33 show the comparison of the coordinates with and without the PCA algorithm. Figure 32 represents the x-coordinate values for the actual position of x = 15 during a period of 400 seconds. Initially, both methods faced a delay in calculating the estimated location. The CC2431 positioning engine shows the estimated position after 20 seconds. This is faster than the PCA method, which shows the estimated position after 75 seconds. However, after the transient situation, the PCA method calculated the exact position 15 times while the CC2431 engine could not show the real position more than 3 times. Furthermore, the mean error for PCA algorithm is about 1.5 meters for a duration of 400 seconds for the x-axis. This error for the positioning engine of CC2431 is about 2.25 meter for the same coordinates. Figure 33 displays the y-coordinate values for y = 10 during 400 seconds. Same as the x-coordinate, the CC2431 engine reached the estimated value earlier than the PCA method. However, in stable situations, the mean error for PCA and CC2431 are 1.75 and 2.5 meters, respectively. Therefore, the y-axis data show that the PCA performs noticeably better than the CC2431.

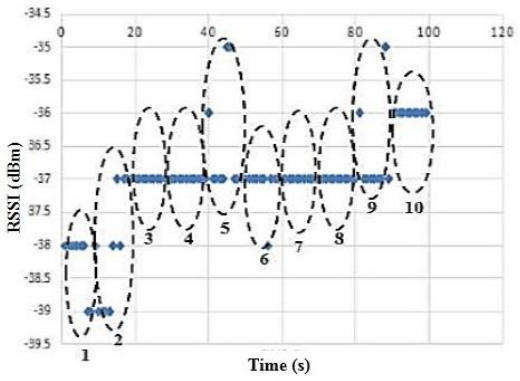

Figure 30: Raw RSSI data from one node in different distances

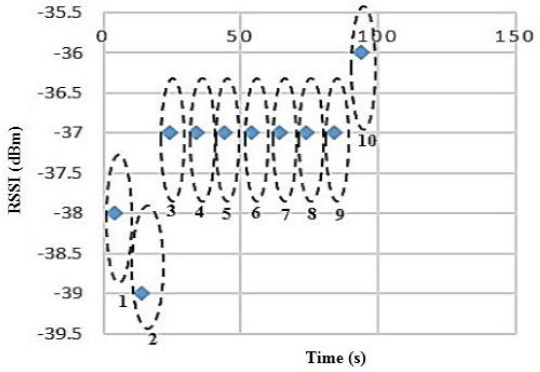

Figure 31: Output RSSI data by utilizing PCA filter

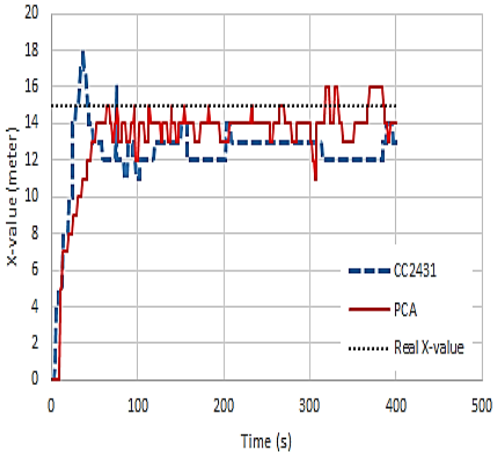

Figure 32: Comparison of X-coordinates for different methods

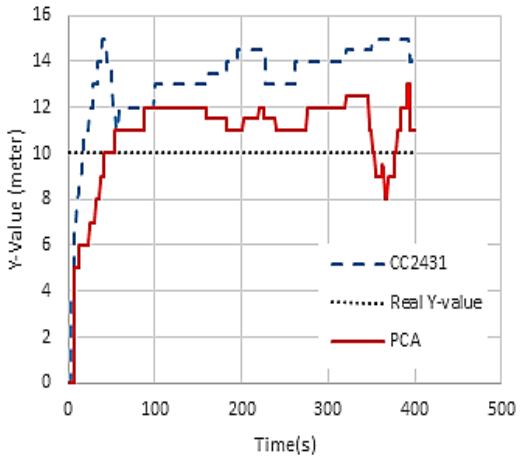

Figure 33: Comparison of Y-coordinates for different methods

Comparing the PCA with the CC2431 positioning engine, the PCA has a large delay when it begins. However, the estimated position is more accurate than CC2431 during the stable situations. The results represent improvement in terms of real distance in the fixed position. Figure 34 and Figure 35 represent the experiment platform with 2D and 3D plans of the test-bed area. The yellow circles illustrate the reference node and green circles show the position of the mobile target during the test.

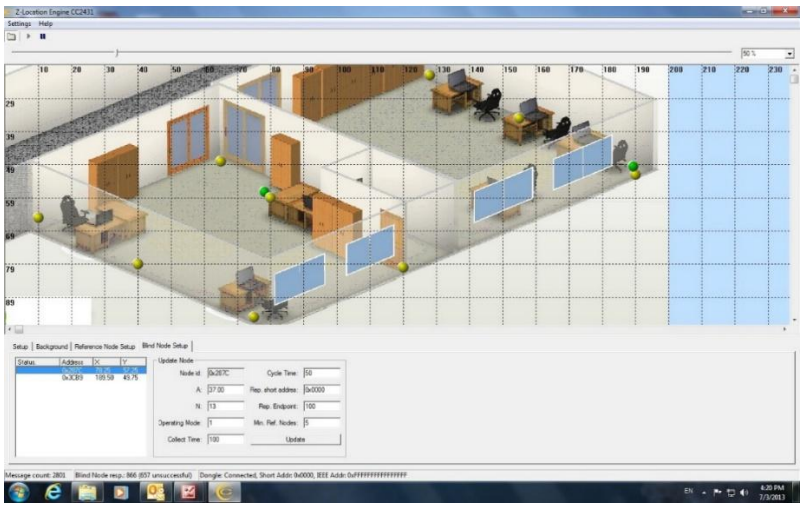

Figure 34: 3D model of office room

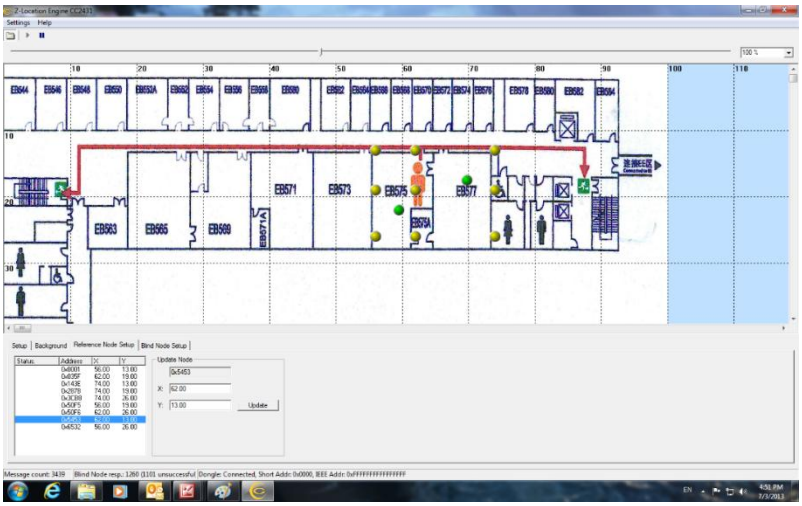

Figure 35: 2D model of test-bed area

The above mentioned tests are for static locations only. However, the dynamic location of occupants are also important for this research. The preferred walking speed is defined as the speed at which humans choose to walk. Many people prefer to walk at about 1.4 m/s (5.0 km/h). However, particularly for short distances, people are capable of walking at speeds upwards of 2.5 m/s (9.0 km/h). The Nike + iPod Sport Kit is utilized for measuring the speed of walking as the shoes includes a pedometer sensor that can communicate with iPhone wirelessly using 3G and 4G networks. The mobile node moved along the path with five different speeds (0.5, 1, 1.5, 2 and 2.4 m/s). The estimated positions using the CC2431 positioning engine and the PCA method were calculated based on their corresponding RSSI value.

Figure 36 illustrates the error distribution in a spider chart. The PCA method leads to high degree of accuracy in slow and regular motion. There is a trend in which an increase in speed leads to an increase in the error. However, even at maximum speed, the error in the PCA method remains lower than that of the CC2431 method. For CC2431, an increase in speed leads to an increase of the distance error, but the slope of the curve is much steeper than that of the PCA method. This

implies that as the speed is increased, the error has a dramatic upward trend for CC2431. The chart showed the fact that higher speed leads to lower accuracy in both CC2431 and the PCA algorithm. However, for speeds below 1.5 m/s, the error is lower than 1.5 meters, which is accurate enough for positioning mobile targets.

To sum up, when the target is fixed or moving with a speed less than 1.5 m/s, the results of PCA are more accurate than CC2431. However, the error increases with speed. Therefore, the PCA algorithm may not be suitable for high-speed movements such as emergency navigation, but it is good for estimating the location of occupants inside buildings.

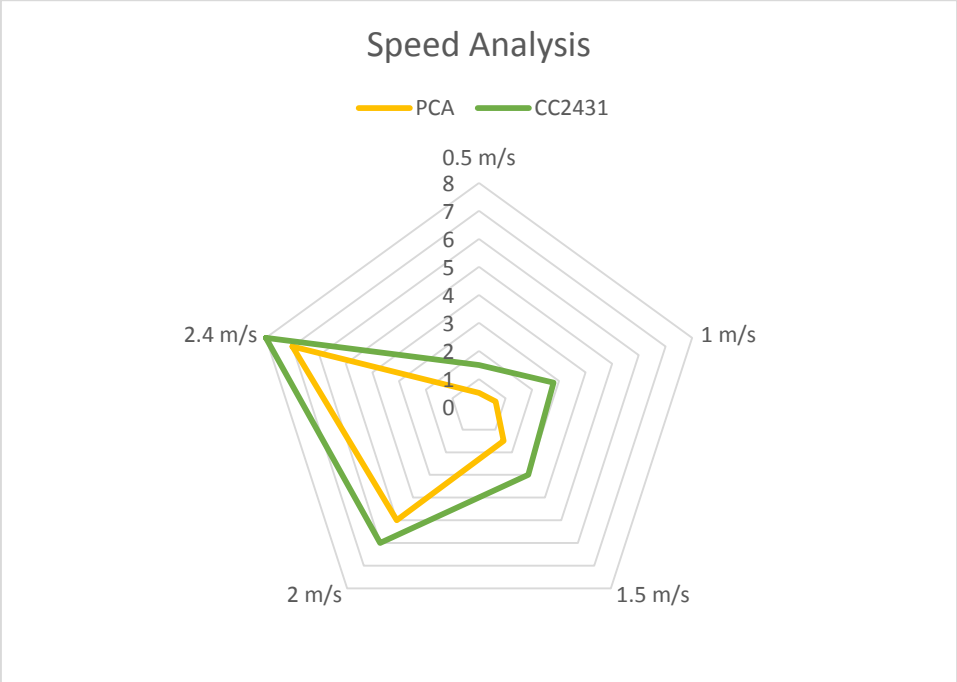

Figure 36: Error distribution of two systems in different speeds

4.1.3 EMA testing

As proposed in the methodology, to cope with the lower accuracy of the localization system during movement, the mobile target transferred the raw signals to the server, and the moving average algorithm was applied on the received signals. Based on the number of packets, two groups, consisting of five packets and ten packets, received signal data are considered for the evaluation. Figure 37 shows the results of the two scenarios. The red line shows the smoothed noise based on the behaviour of past packets. It shows that the unwanted signals are smoothed well in both scenarios. For instance, at time stamps 65s and 85s significant noise is detected. Both five and ten moving average smoothed the noise which results in higher accuracy of position estimation. It should be noted that in this method we need to manually input a number for P_0 (16), when the estimation starts. A significant distance between the real and smoothed RSSI can be recognized in Figure 37.

The smoothed signal should be at a reasonable range. If the signal smooth too much, small changes cannot be distinguished. Therefore, the value of 10 packets is considered in this research for the implementation parts.

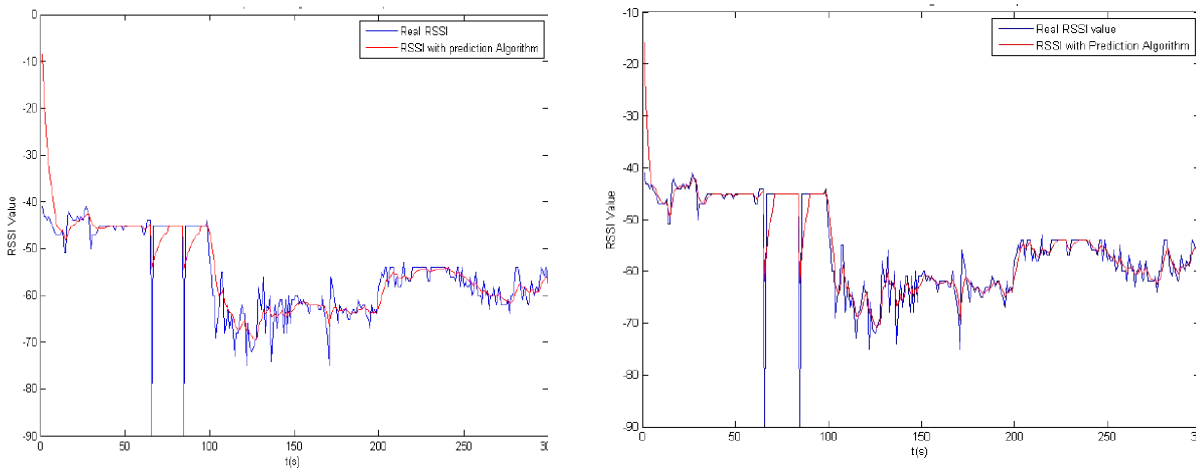

(a) Moving Average for 10 Packets **(b) Moving average for 5 packets**

Figure 37: Moving average and RSSI values

The concept of moving average is extended from RSSI value to the estimated positions as well. Based on the fact that there is a relationship between present positions with past locations, it is possible to estimate the near future position of the users. If the estimated and recorded positions are far from each other, the system will consider the value as a noise and try to smooth these differences.

To investigate the impact of a moving average on the calculated position, another experiment is conducted. The EMA filter is implemented on both RSSI and the estimated locations, separately. The average time to receive one signal is about 100 ms. Therefore, smoothing based on 10 signals gives the result within one second which is sufficient for a real-time estimation purpose in order to calculate the position in real-time.

Figure 38 depicts the errors for 300 seconds, based on Equation 18 in Section 3.1.2. When the filter was implemented on RSSI values (Figure 38(a)), the maximum error is less than 3 meters,

which is about 2 meters smaller than what was based on the estimated position values. The average error is less than 0.85 meter when the filter is applied to RSSI values, which is a good performance in terms of accuracy and capability. Therefore, to save processing time, the EMA filter was applied to RSSI values in this research.

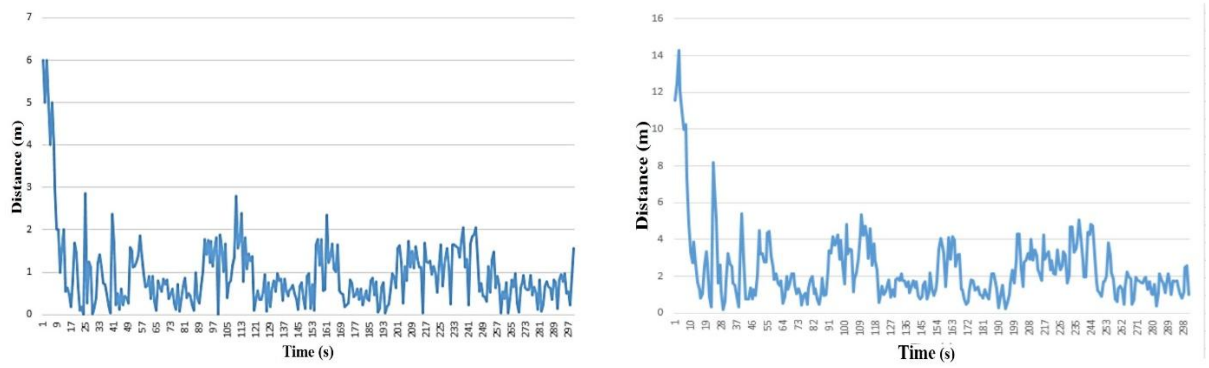

(a)Error Analysis for MA applied on RSSI values

(b) Error Analysis for MA applied on distance values

Figure 38: Moving Average filter implemented on both RSSI and distance values

A moving test was also carried out to evaluate the EMA method, the mobile target moved from the location A (0, 0) to location B (70, 70). Figure 39 presents the comparison of estimated coordinate X , computed by using the EMA filter, and the embedded position engine in CC2431. Two remarkable noises are illustrated at 44s and 47s in the case of CC2431 engine. However, they are well smoothed in the EMA method.

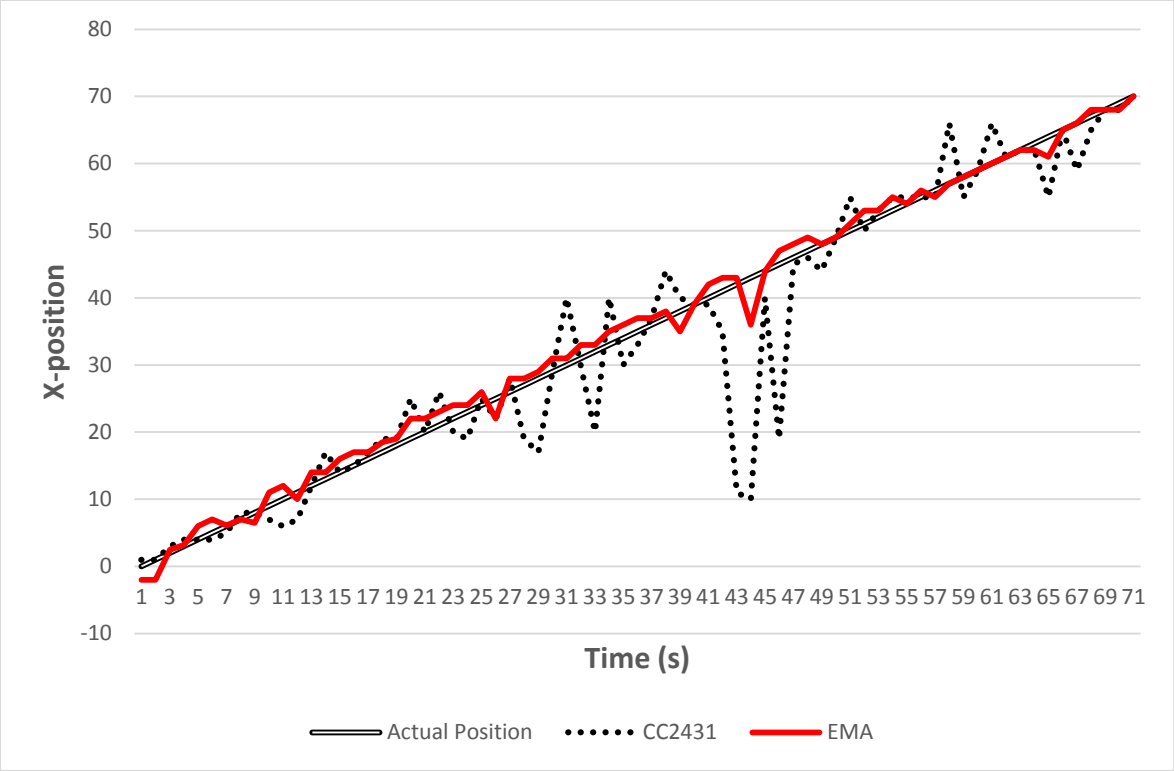

Figure 39: Comparison of X coordinate for different methods

Two remarkable noises are illustrated at 44s and 47s in the case of CC2431 engine. However, they are well smoothed in the EMA method. Comparison showed that at the beginning, the CC2431 positioning engine provide better accuracy than the EMA method. However, after the transient situation, the EMA method provides more accurate results than the CC2431. The explanation is that the EMA algorithm smoothed and estimated new values based on the last 10 packets which takes few seconds to receive packets and calculate the estimated result. It is clear that the distribution from EMA

To compare the EMA, PCA and CC2431 positioning engine together, another test is implemented. The user has to distribute the mobile node over interested tracking area, and then

record the data at several points which is called as reference points. A total number of 25 measurement points are identified for each method. The experimental test-bed was defined as room EB547 in the 5th floor of the building. Its area has dimension of (24.5×12.5m).

As shown in Figure 40, 25 measurement points are the target of estimating the errors.

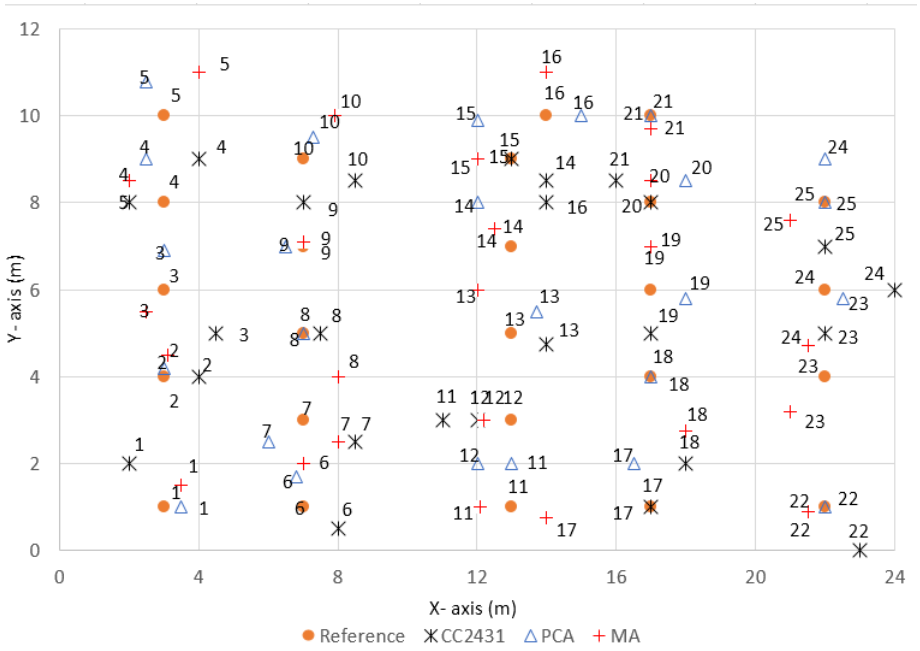

Figure 40: The localization error using CC2431, PCA and EMA methods

Figure 41 shows the localization error for all three methods. The maximum error were 3.5, 2 and 2 meters for CC2431, PCA and EMA, respectively.

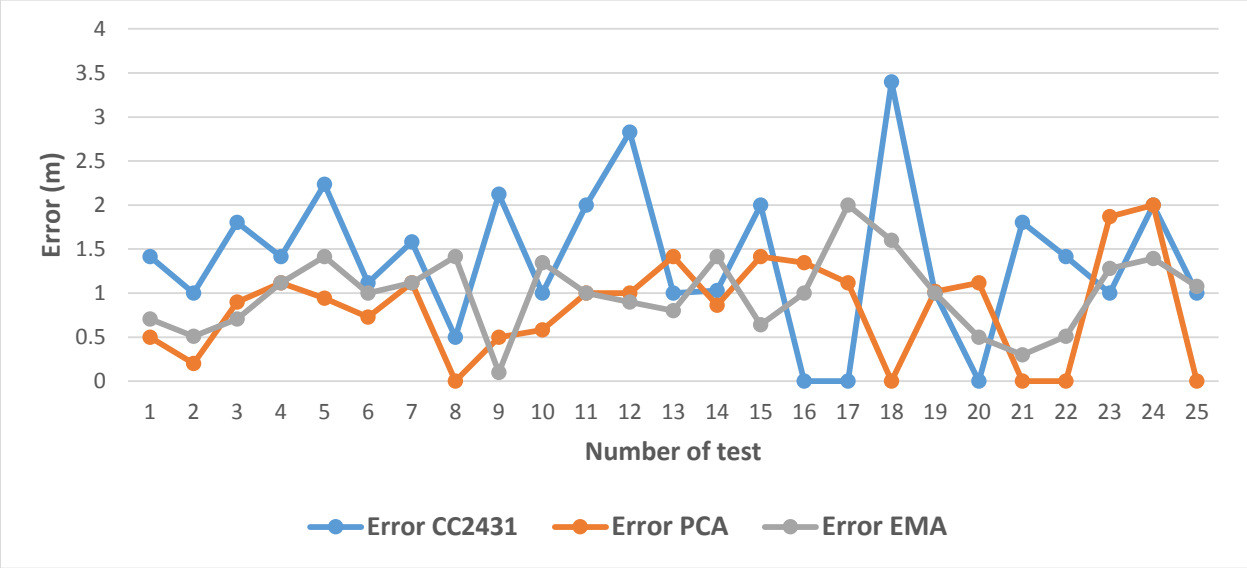

Figure 41: The distance error based on the number of tests

Table 5 compares the error of different methods. The PCA achieved the lowest error by the mean error of 0.83 meter and the CC2431 positioning engine showed the highest mean error by 1.39 meter. The standard error and standard deviation of each method are depicted in the table.

Table 5: Evaluation the CC2431, PCA and EMA methods

	Mean of Error (m)	**STANDARD ERROR (STANDARD DEVIATION OF THE MEAN)**	**STANDARD DEVIATION**
CC2431	1.39	±0.16	±0.83
PCA	0.83	±0.11	±0.58
EMA	0.99	± 0.08	±0.44

As mentioned before, the EMA method is based on the historical data of signals. In the case that the received signals change dramatically, the previous signal patterns can be helpful to smooth outlier signals. This situation may occur when the mobile target changes its location at a high speed. To investigate the effect of speed on the accuracy of the system, tests were implemented with five different speeds (0.5, 1, 1.5, 2 and 2.4 m/s). The estimated locations for the CC2431 and EMA method are calculated based on their RSSI value. Figure 42 represents the test bed area and path and Figure 43 illustrates the distribution error of all methods in the form of a spider chart.

This figure shows that in the case of moving speeds lower than 1.5 m/s the PCA method is the most accurate one, which has a maximum error of 1.4 m. in the case of speeds higher than 1.5 m/s, the EMA method is the most accurate one with the maximum error of 3.5 m.

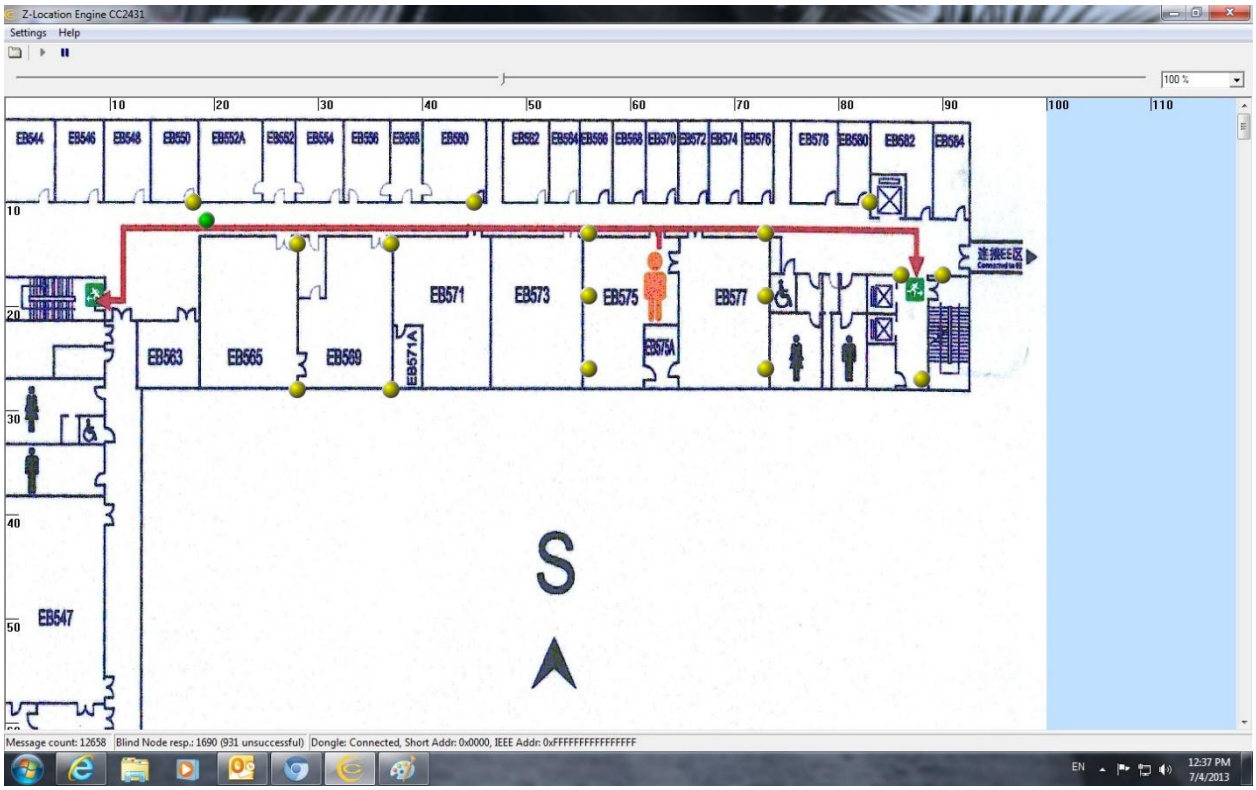

Figure 42: The architecture of sensors and test-path

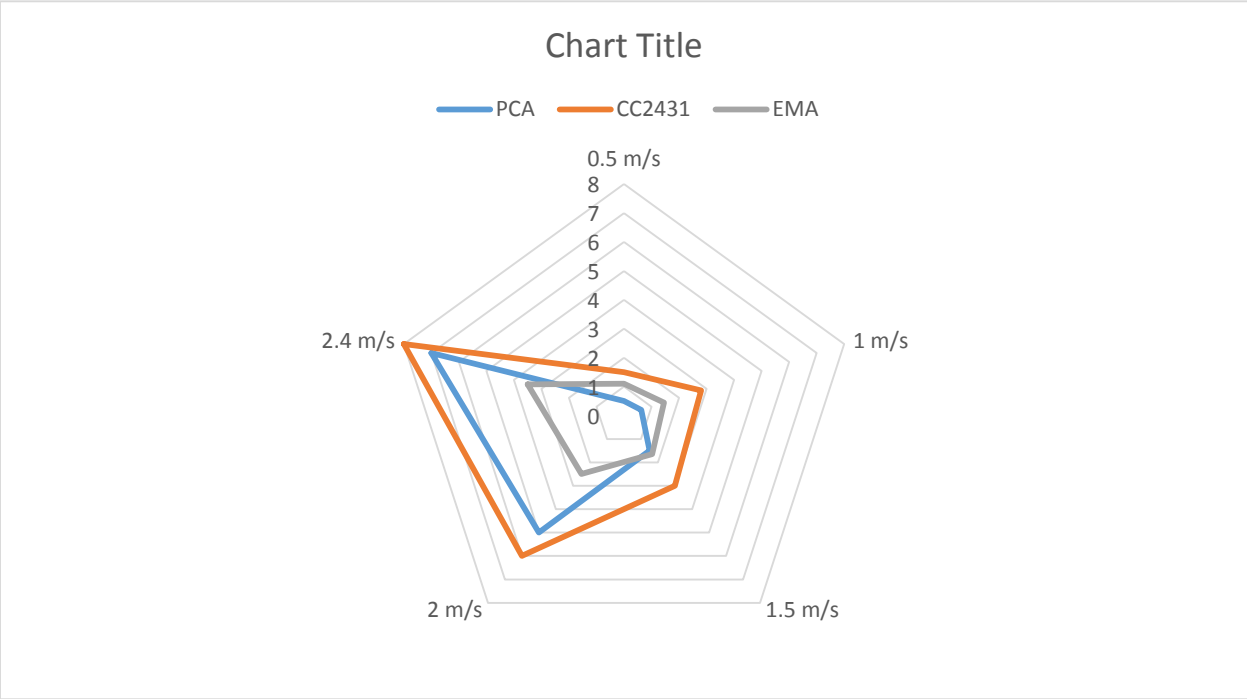

Figure 43: Errors for all methods at different speeds

As shown in Figure 43, concluded that higher speeds result in less accurate position estimation for all methods. However, the EMA method recovers from this situation better than other methods. For low and normal speeds, PCA method shows a more accurate estimation.

To examine the influence of antenna orientation, the received signal strengths were checked by rotating the antenna of the mobile nodes. No specific changes were observed on the performance.

4.1.4 Summary

In this research, the Indoor localization system is customized for the objective of the research by applying three algorithms: NNA, PCA and EMA based on RSSI values in a ZigBee-based sensor network. First, the drifting phenomenon which causes estimating the position in another

room is removed by utilizing NNA method. Second, the PCA trilateration approach in a non-offline phase analysis localization method is implemented. The filter has the capability of eliminating unwanted signals and noise. In this technique, each 10 signals were grouped together to extract a representative signal for computing the positions of the target. From the results, there is an indication of accuracy improvement. In a case whereby the user is placed in a specific location the error is noted to reduce. However, there is still need for more improvement as per the observations made from experiments conducted using high speeds. However, all experiments resulted in more accuracy compared with CC2431. Finally, the historical data of RSSI are considered as a guideline to predict the future data. For moving targets with different speeds, the proposed method showed more accurate results than the positioning engine embedded in CC2431.

To sum up, The NNA algorithm is an essential method while the location of mobile target is required to be considered as a zone area (one room). Both PCA and EMA methods showed the potential of more accurate result than CC2431 position engine. However, PCA is suitable for moving targets with speed lower than normal walking speed. EMA showed better results for moving targets with higher speeds such as fast robots or running situation.

In this research, for evaluation of the position of occupants inside the building, the combination of EMA and NNA method is used as it is important to estimate the location in the exact room of the building for energy saving purpose. However, an application of PCA method is presented in Appendix D.

4.2 Intelligent control based on thermal comfort and occupancy-driven

4.2.1 Thermal comfort modelling

There are several platforms of CFD, such as Fluent, Airpak, and Phonics. In this research, Airpak is selected due to its simplicity and capacity to model temperature, air velocity, PMV and PPD. The physical model of this research for analysis is a public office at a university building with two individual ceiling HVAC outlets, as shown in Figure 44. The parameters of the model are described as follows:

(1) Local coordinate system: starting point coordinates (0,0,0) and ending points (8.5,3,10.4);

(2) Room dimension: $8.5\ m\ \times 10.4\ m$;

(3) Two external windows facing south with dimensions: $1.6m \times 3m$;

(4) Dimension of office door: $2m \times 1.3m$;

(5) Two ceiling HVAC air supply outlets: Dimensions: Each outlet is considered as four squares with the dimension of $0.9m\ \times 0.09\ m$; air velocity: 2.5 *m/s*; air temperature: 18 ℃;

(6) Vent: The direction is along the Y axis with the dimension of $0.3m \times 0.3m$ .The air velocity is 2.5 m/s and air temperature has an ambient value.

(7) Indoor heating sources: seven sitting men (persons 1 to 7) with a calorific value of 75 w; two sitting women (persons 8 and 9) with calorific value of 60 w; nine LCDs with calorific value of 19.5 w; nine computer cases with calorific value of 220 w; and nine florescent lamp sets with total power of 100 w for each set, depicted as 0.4 m × 1.2 m0.4 m × 1.2 m squares

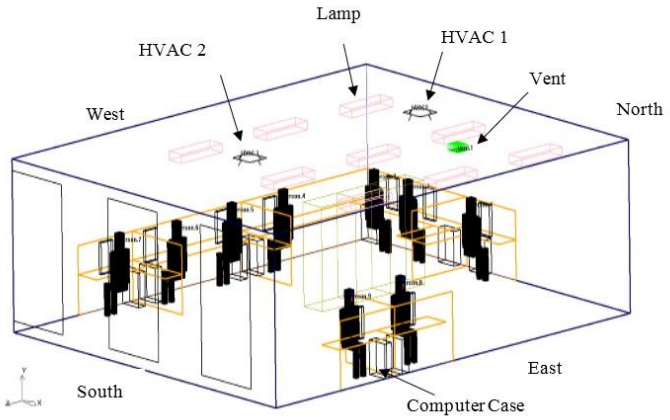

Figure 44: The geometry of office room with nine occupants

Setting boundary conditions

The temperature buoyancy condition for the CFD simulation was provided by thermal camera images which is shown in Figure 45. Indoor and outdoor temperatures are gathered by a group of DHT11 Arduino temperature and humidity sensors. As it was mentioned in the methodology section, seasonal based modelling are used in this research. The winter modelling are provided in Appendix B. The data for the CFD model were collected during the field measurements of a typical summer day as follows:

a) North wall

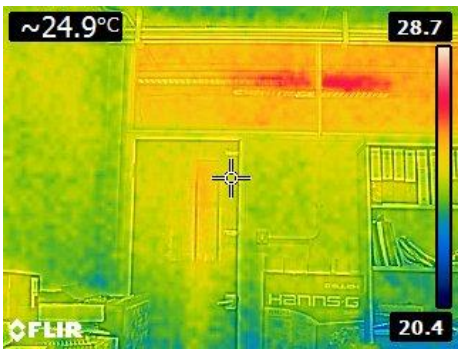

b) South wall

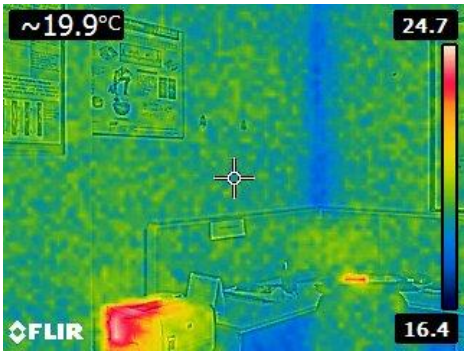

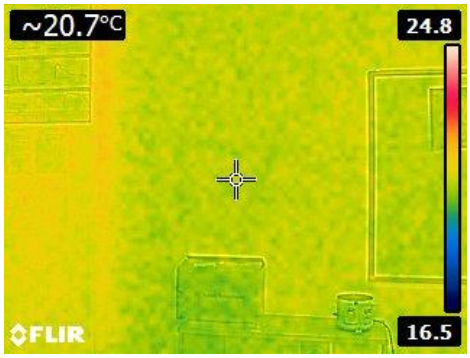

c) East wall **d) West wall**

Figure 45: Sample thermal images from different walls of the office

Table 6: CFD Boundary Conditions

Input	**Value**
Indoor measured parameters	
Relative humidity	40%
Dry-bulb temperature	21℃
External wall inside surface temperature Front wall (South)	24.9 ℃
Internal wall inside surface temperature East wall	19.9℃
Internal wall inside surface temperature West wall	20.7℃
Internal wall inside surface temperature Back wall (North)	21℃,
Floor	19 ℃
Ceiling	21.2 ℃
Air Supply	
Buoyancy density(1)	1.173 kg/m^3

Airflow supply rate	2.5 *m/s*
Outdoor measured parameters	
Dry-bulb temperature	33 ℃
Wet-bulb temperature	30 ℃

(1)The air was considered as an ideal gas

In this research two models of radiation are considered, which are the surface-to-surface radiation model and the solar load model [74]. The surface-to-surface model allows us to specify all or any objects which exchange radiative energy with other objects or with a specified remote temperature. The heat transfer rate of objects is defined as

$$Q=\boldsymbol{\varepsilon\sigma F}(\boldsymbol{T_{surface}^4-T_{remote}^4}) \quad \textbf{(42)}$$

where $T_{surface}$ represents the surface temperature of object, T_{remote} is the surface temperature to which the object radiates heat, σ is the Stefan-Boltzmann constant, F represents the view factor and ε shows the emissivity of the surface of the object of a given material. To model the radiation objects, Airpak calculates the view factors and computes the radiative heat flux based on calculated object temperatures. In this research, the calculation of radiation is specified in heat sources to account for radiation from objects such as computers, lightings and human bodies.

To include the effects of direct solar illumination as well as diffuse solar radiation, a solar load model is utilized. The model performs a ray tracing and shading for all boundary surfaces by providing the geometry and terrestrial location, date, and time. The following information is used as the input for Suzhou, China, where the building is located:

Table 7: Solar load model input

Input	Value
height	10 m above sea
Latitude	31º 18’ 14” N
Longitude	120º 35’ 43” E
Time	14:00
Date	June 15th, 2015
Sunshine fraction	1
Ground reflectance	0.23

Illumination parameters are specified as Sunshine fraction and Ground reflectance. Sunshine fraction is affected by clouds, which may reduce the direct solar irradiation. This fraction is a number between 0 and 1, where 1 is clear sky and 0 is complete cloud cover. Ground reflectance values are associated with the ground surface materials such as concrete, grass, rock, gravel, or asphalt. All objects in the solar radiation model are defined by their properties and specific material compositions.

Mathematical model

To calculate momentum conservation, mass conservation and energy conservation equations, a low Reynolds number turbulence model (RNG k-ε model) is implemented [75]. A grid model is generated to design the mathematical model of the room, depicted in Figure 46.

Turbulence is displayed through the use of different levels of two-equation k-ε models, i.e. the Standard k-ε, the RNG k-ε and the Realizable k-ε model. Further explanation for the mathematical formula of the k-ε models can be found in [76].

The standard k-ε model is widely utilized because it has a lower computation requirement and it is easier to converge. In the ε-equation, the RNG varies from the standard k-ε model introduced which displays a parameter that is the ratio between turbulence time scales and the mean flow. Hence, it results in predominant RNG model responses for the fast strain and a streamlined curvature in comparison with the standard k-ε model. For the standard k-ε model, it fulfils certain numerical requirements on the Reynolds stresses, which is based on the physics of turbulent flows.

Simultaneously, the influence of the heat radiation from each heat source is also considered. In addition, three assumptions are taken into consideration for the physical model. First, indoor air flow is estimated as steady turbulent flow. Second, to confirm the Boussinesq theory which says that the buoyancy lift is only influenced when changing the fluid density, it is assumed that there is good air tightness in the room. Therefore, the leakage effect is not considered in the simulated room. Finally, to simplify the model, the door of the office is ignored from the calculation and it is assumed that all windows are closed.

The modified mesh for simulation is set as the normal type and the coordinates of x, y, and z were set to 0.21, 0.1 and 0.07m, respectively.

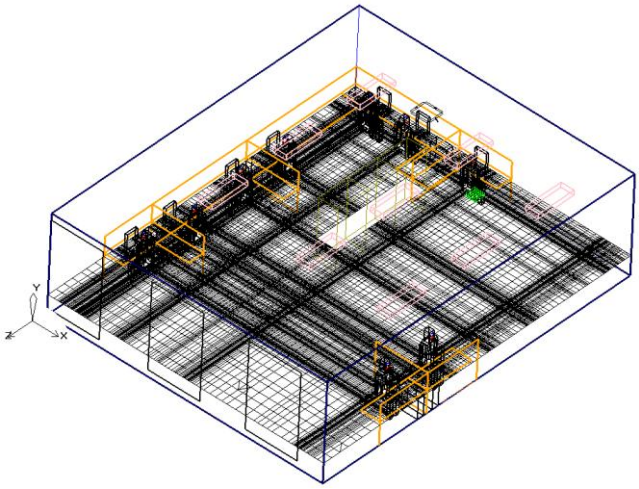

Figure 46: Grid generation in Airpak

Comfort and discomfort areas

The PPD and PMV identify cold and warm discomfort ranges for occupants. The PMV is expressed by the thermal sensation scale which is indicated in Table 8 [77]. The PPD refers to occupants who would vote according to the thermal sensation scale on which 0% represents totally satisfied and 100% represents completely dissatisfied. CFD has the capability to model these parameters using color-coding which can be seen in Section 4.3.

In order to analyse the thermal comfort level of occupants and identify the corresponding thermal zone they belong to, three location-based scenarios (with respect to the thermal zones and location of the occupants) are developed. Based on the simulation of comfort and discomfort areas, corresponding thermal zones are introduced in the office room. Details of selected thermal zones are explained in the following Sections.

Table 8: Thermal sensation grades and corresponding objective response

PMV	Thermal sensation
+3	Hot
+2	Warm
+1	Slight Warm
0	Normal
-1	Slight cool
-2	Cool
-3	Cold

4.2.2 Thermal Zone identification

Scenario 1

In this scenario, the room is occupied with nine individuals and both HVAC outlets are kept on, which is a typical situation in the room. Therefore, a comprehensive analysis is done for this scenario. To analyse all occupied areas of the room, four planes are considered in the CFD model, as shown in Figure 47. Vertical planes A, B and C are depicted through the occupant's position. A horizontal plane D covers the whole room at Y=0.6 m, which is approximately the height of the occupants when sitting in the office. It should be noted that the locations of occupants are separated by partitions in this office.

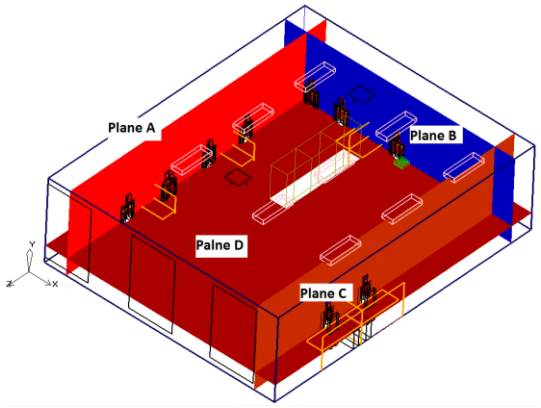

Figure 47: The location of four planes for analysis in the CFD

Figure 48 illustrates the airflow distribution and the air temperature stratification inside the modelled room. The results demonstrate that the air flow inside the room is wind-driven. Figure 48(a) does not show any discomfort condition for persons 4, 5, 6 and 7. However, the air velocity between occupants 6 and 7 is relatively high. Also, as shown in the air velocity of Figure 48(b), it is found that airflow is extremely high for person 1 which may result in local discomfort for this person. Figure 48(c) shows that the heat plume above person 8 are relatively high which might cause a local discomfort for this person. The air velocity between occupants 8 and 9 is relatively high. Figure 48(d) shows a good distribution of heat in the office. The red boxes shown in Figure 48(d) represent the heat surfaces of computers. From those figure, it is found that the average air velocity at the height of 0.6 meter is less than 2 m/s, which is considered as comfortable. There are two high speed airflow areas in the middle and north-eastern parts of the room. Fortunately, no occupants are located in those areas.

(a)

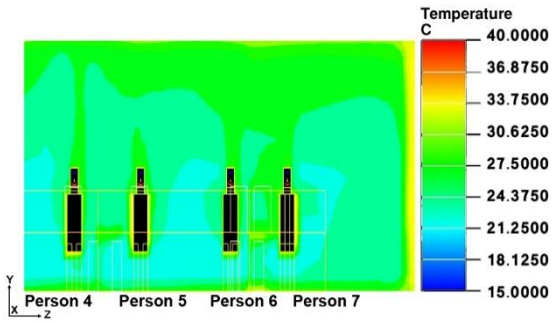
Temperature
C
40.0000
36.8750
33.7500
30.6250
27.5000
24.3750
21.2500
18.1250
15.0000
Person 4
Person 5
Person 6
Person 7

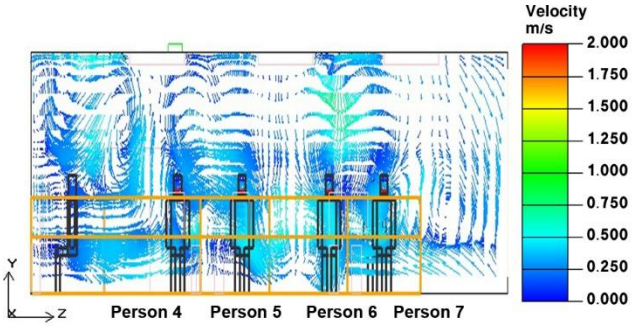
Velocity
m/s
2.000
1.750
1.500
1.250
1.000
0.750
0.500
0.250
0.000
Person 4
Person 5
Person 6
Person 7

(b)

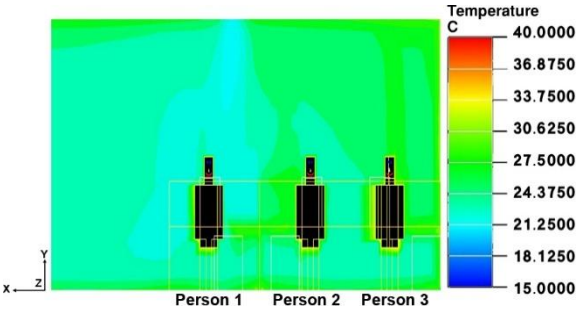
Temperature
C
40.0000
36.8750
33.7500
30.6250
27.5000
24.3750
21.2500
18.1250
15.0000
Person 1
Person 2
Person 3

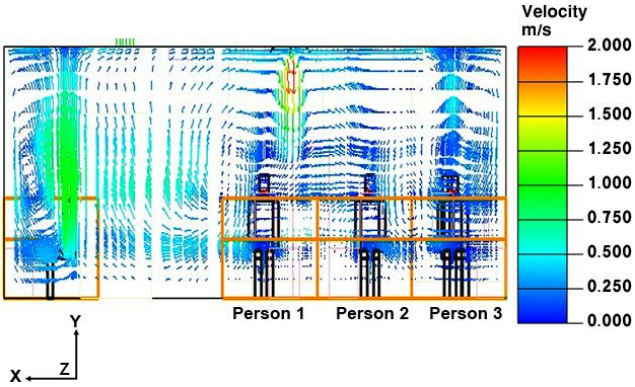
Velocity
m/s
2.000
1.750
1.500
1.250
1.000
0.750
0.500
0.250
0.000
Person 1
Person 2
Person 3

(c)

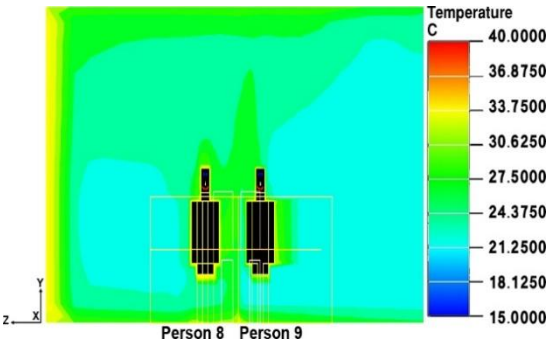
Temperature
C
40.0000
36.8750
33.7500
30.6250
27.5000
24.3750
21.2500
18.1250
15.0000
Person 8
Person 9

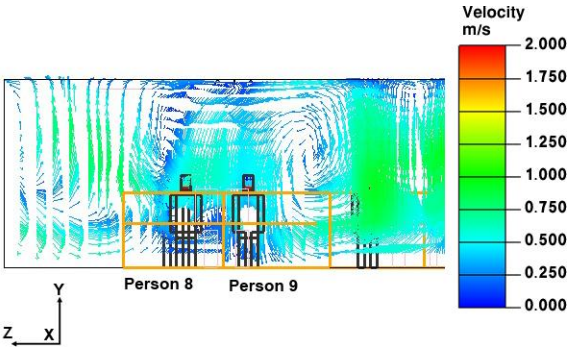
Velocity
m/s
2.000
1.750
1.500
1.250
1.000
0.750
0.500
0.250
0.000
Person 8
Person 9

(d)

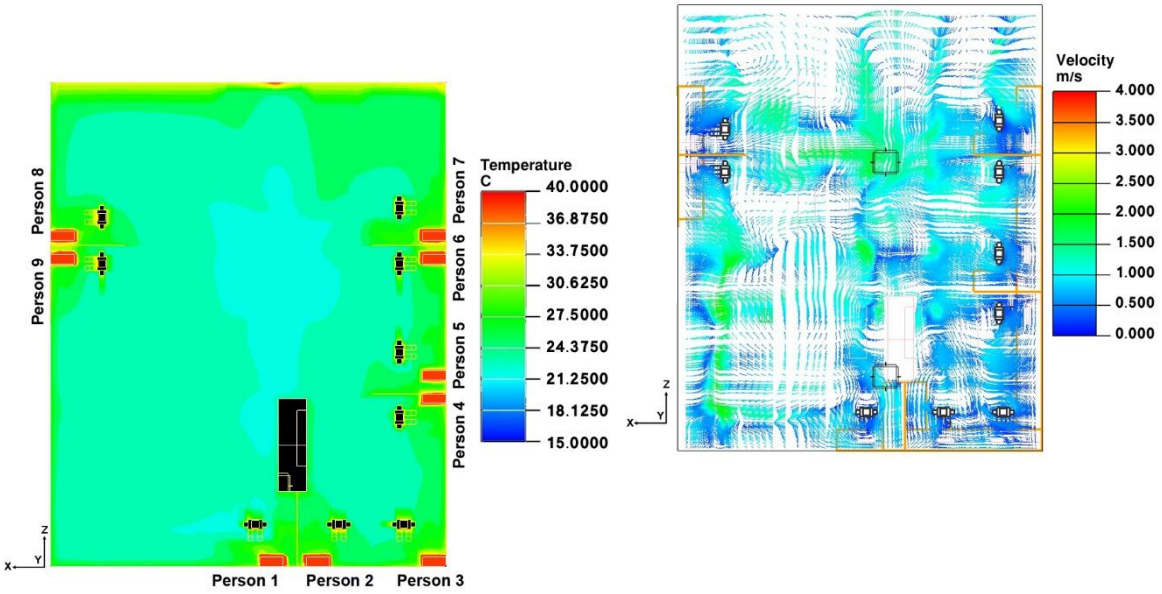

Figure 48: Verified model results based on temperature and air-velocity

To investigate the comfort and discomfort areas in terms of air speed, further analysis is applied using an iso-surface. And iso-surface is a three-dimensional surface which shows points of a constant value (e.g. temperature, velocity, pressure) within a volume of space. Airflow speed of 0.25 m/s or lower does not affect occupants' thermal acceptability at preferred temperatures. The airflow streamlines exit the HVAC through four separate channels at an angle of 45 degrees, as depicted in Figure 49. The iso-surface result of indoor airflow, for air speeds higher than 0.25 m/s, has been illustrated in Figure 50. The airflow jet omitted most occupants except persons 1, 2, and 3 which may result in a local discomfort for them. Most of the areas with an airflow speed higher than 0.25 m/s are located in upper part of the room due to their proximity to the HVAC outlets. Person 7 may also feel discomfort as he is close to the iso-surface result. According to the model, the middle and northern parts of the room have a higher sensitivity to discomfort level.

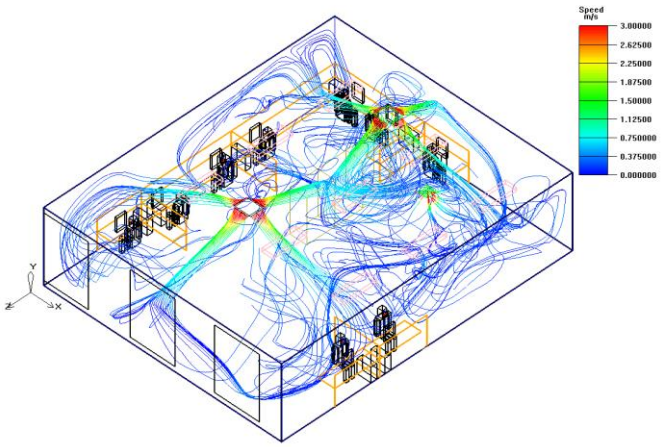

Figure 49: Indoor airflow streamlines from the air conditioning to outlet window

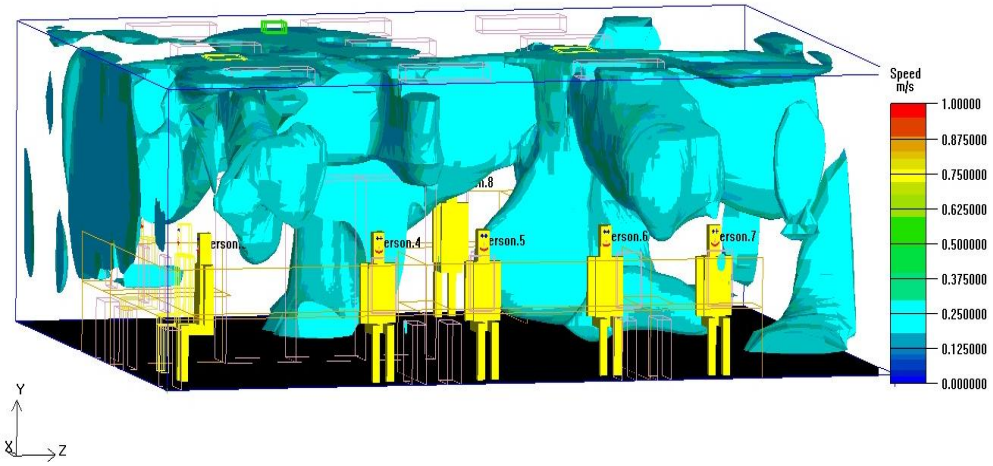

(a)

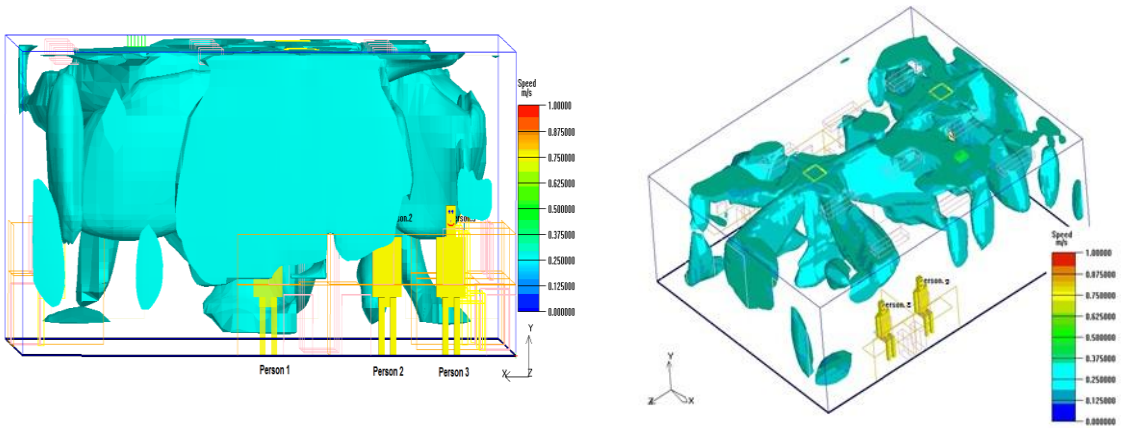

(b) (c)

Figure 50: Iso-surface result of indoor airflow with speeds higher than 0.25 m/s

Figure 51 and Figure 52 illustrate the PMV and PPD results, respectively. Both images confirm that locations near windows are not suitable for occupants. Persons 3, 7 and 8 are located close to the 25% dissatisfaction area, which can be identified from the PPD results. The PMV model confirms the possibility for discomfort for person 8 as this user is located in a warm area; however, it does not confirm any dissatisfaction issues for persons 3 and 7. The simulation does not show any discomfort issue for other persons in the room. Results of the survey for this scenario showed that persons 3 and 7 didn't feel any discomfort, but person 8 did feel discomfort. Most of the dissatisfaction areas are identified to be close to the windows.

In summary, when the room is fully occupied with all persons and both HVAC outlets are turned on, areas close to the windows are identified as discomfort areas. Persons 3, 7 and 8 are close to the 25% dissatisfaction areas. However, survey results showed that only person 8 felt discomfort. Other occupants felt comfort in this scenario based on simulations and survey results.

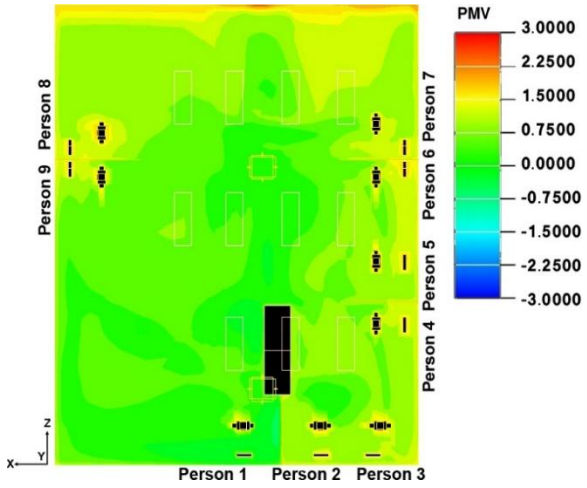

Figure 51: Predicted Mean Vote (PMV) model

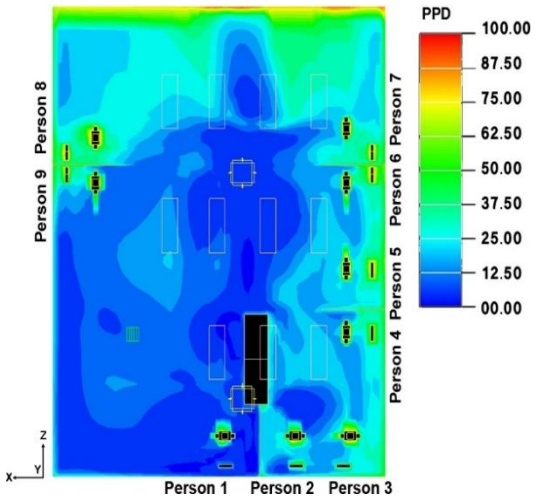

Figure 52: Predicted Percentage Dissatisfied (PPD) model

Scenario 2

In this scenario, while the room is considered fully occupied, the HVAC-1 is kept on and HVAC-2 is off. The corresponding airflow streamlines are depicted in Figure 53. It is deduced that the south-western area has worse air distribution than other areas. The air-velocity is depicted in Figure 53(b), which shows that the southern area (near the off HVAC outlet) has lower airflow. The PMV and PPD analyses are illustrated in Figure 53(c) and (d), respectively. From PMV illustration, it is obvious that persons 1, 2, and 3 are located in the comfort areas. The PDD figure illustrates that persons 1, 2, and 3 are placed in the reasonable area in terms of lower dissatisfaction percentage. Modelling shows that persons 5, 6, 7 and 8 are located in the dissatisfaction areas. In addition, person 9 is located on the boundary of comfort and discomfort areas, which may result in discomfort. However, the survey results for this scenario show that person 9 feels comfortable in this condition.

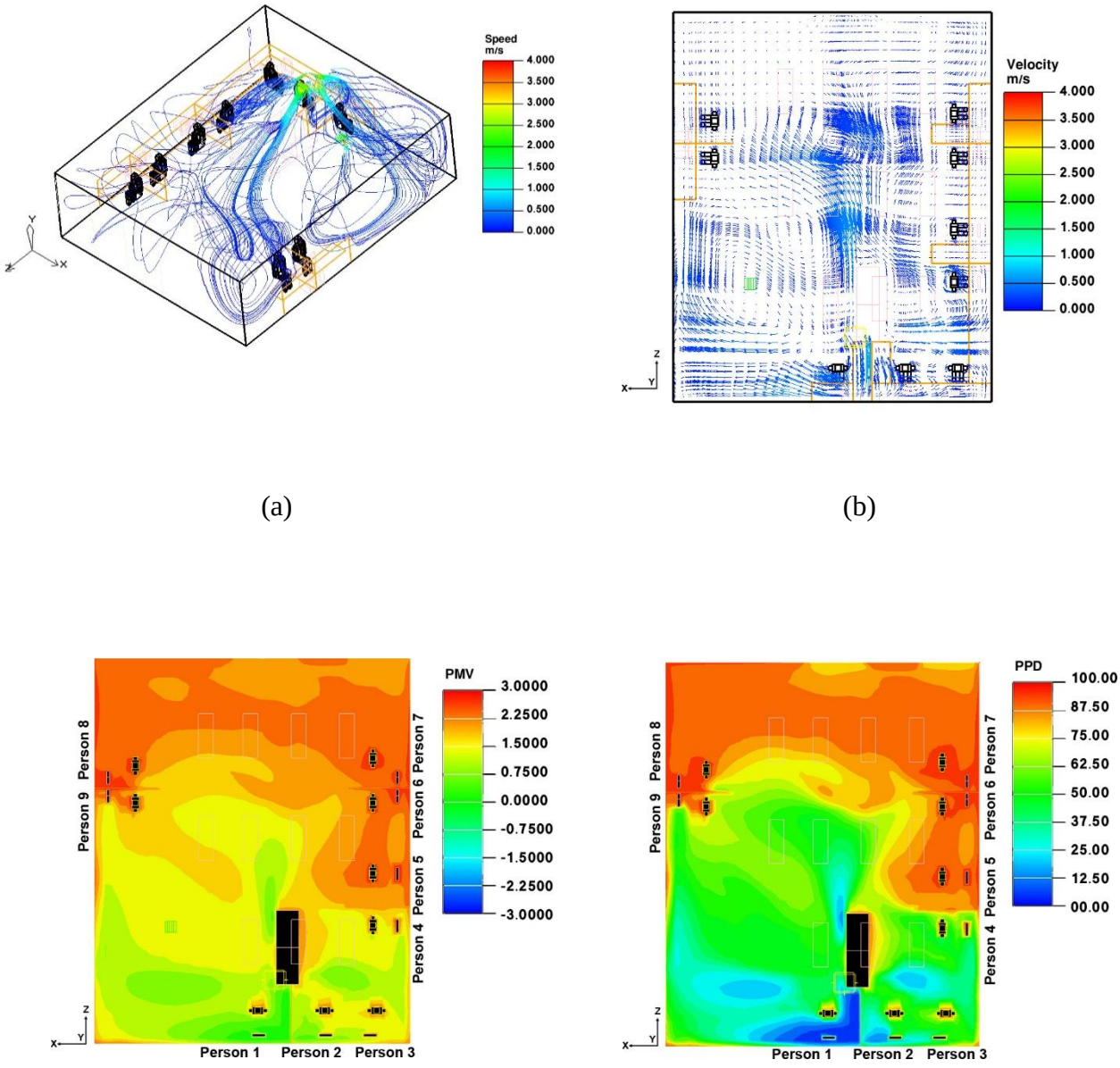

Figure 53: Analysis of the room with four occupants and HVAC-1

In summary, persons 1, 2, 3, 4 and 9 are located in the comfort areas and it is possible to consider them as in the same thermal zone. In addition, same as scenario 1, the location of person 8 was also identified as a dissatisfaction area.

Scenario 3

For the third scenario, it is assumed that the HVAC-2 is turned on while HVAC-1 is off. Figure 54(a) presents the airflow streamlines. The north-eastern region receives less air distribution than other regions. As shown in Figure 54(b), this region does not show any significant points for the airflow. Figure 54(c) and (d) show the comfort and discomfort areas for this scenario. From PMV model, it is seen that persons 1, 5, 6, 7, and 9 are located in a comfort area. Persons 2, 3, 4, and 8 may feel discomfort in this scenario. The PDD results show that persons 1, 5, 6, 7, and 9 are placed in the satisfaction area, while Persons 2, 3, 4 and 8 are placed in the dissatisfaction areas, which is confirmed by their thermal sensation vote.

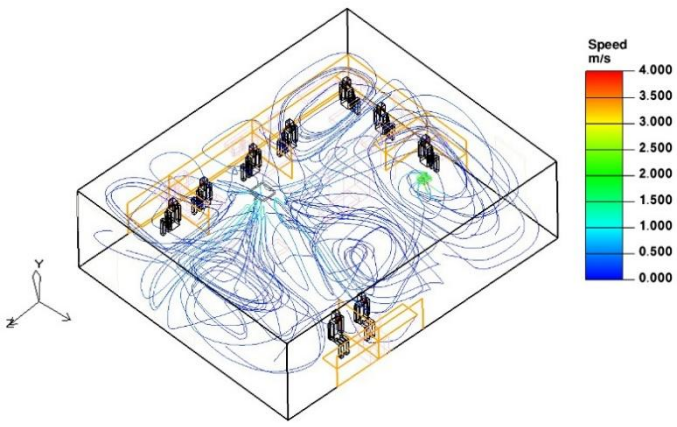

(a)

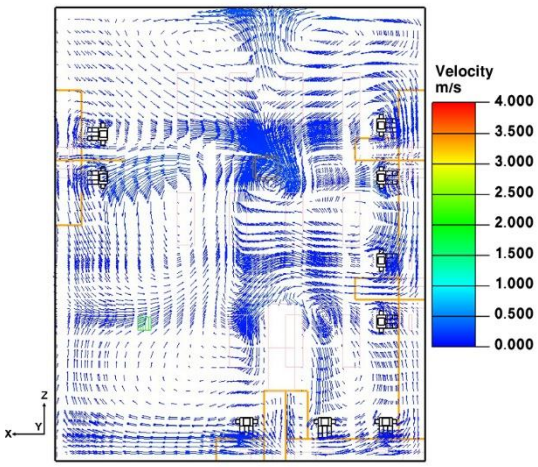

(b)

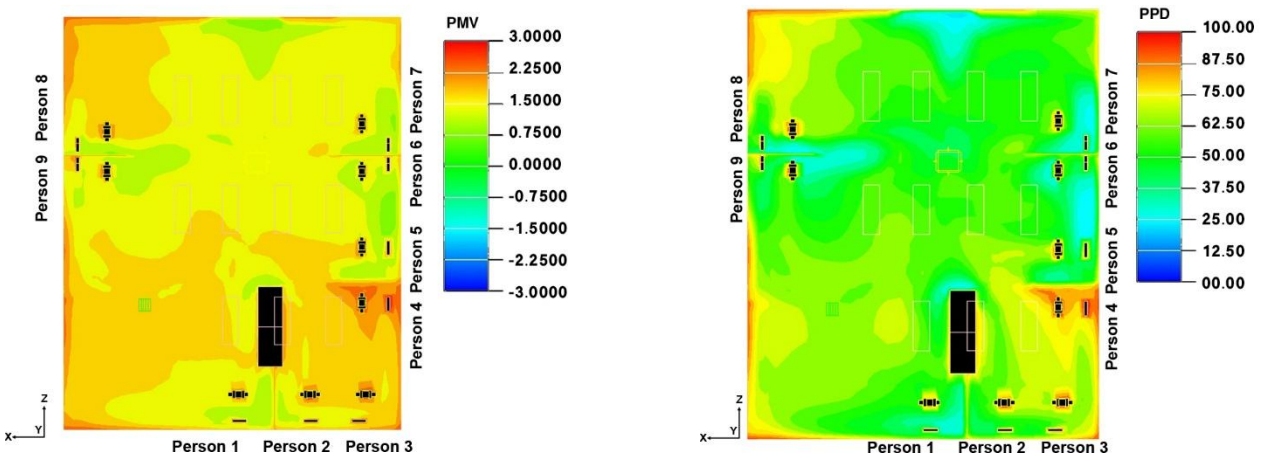

(c) (d)

Figure 54: Analysis of the room with five occupants and HVAC-2

Table 9: Thermal Zones for persons

Zone #	Person	Person	Person	Person	Person	Person
Zone 1		2	3	4	8*	9*
Zone 2	1	5	6	7		

To sum up, based on all scenarios that have been analysed, person 8 is located in a discomfort area in all scenarios and this person should be allocated to a better place. In addition, two thermal comfort zones are identified based on the analysis to relate the occupants' location with the control of HVAC outlets. This is shown in Table 9.

Zone 1 is considered for persons 2, 3, 4, 8 and 9 while Zone 2 is considered for persons 1, 5, 6, 7, 8, and 9. Persons 8 and 9 can be considered in either Zone 1 or Zone 2, depending on the presence of other persons in those two zones. However, the location of person 8 is not confirmed as a satisfied place and should be re-allocated.

4.2.3 Thermal preference profile

Figure 55 shows the room temperature measured for the period of December 3rd, 2016 to January 16th, 2017, counted as 1080 hours in total. This room was occupied by PhD students whose working hours were counted from 8:00 AM to 8:00 PM. This is about 540 hours during the 45 days.

Based on the survey results, it was found that in the most of the situations, occupants felt discomfort when the temperature was above 25 ºC or below 20 ºC. Temperatures between 21 ºC with 23 ºC recorded as the neutral feeling temperature which most of the people felt comfort. Temperatures in the range of 23 ºC with 25 ºC and 20 ºC with 21 ºC were the critical temperature ranges which means the temperature depends on the occupant's preference. This range of temperature can be considered as a comfort or discomfort temperature range. Therefore analysis of temperatures are grouped based on these ranges.

Table 10 shows the number of hours at a specific temperature range. From the table, it can be observed that there are 211 hours, around 21% of the whole time period, during which the room temperature is above 25 ºC. Among the 211 hours, 58% of the time occurred during the working hours and 42% occurred during non-working hours. Temperatures between 23 ºC and 25 ºC contributed to 28% of the total hours. 56% of this occurred during working hours and 44% occurred during non-working hours.

To sum up, during working and non-working hours, the room was heated by HVAC systems without considering the demand. There was a huge amount of energy wasted during non-working hours which could otherwise be saved by considering the occupancy of the room. In addition, There was no need to heat the room to reach the range of discomfort temperatures (above 25 ºC)

and consequently can be saved if this is avoided. Moreover, the range of temperatures between 20 ºC with 21 ºC and 23 ºC with 25 ºC are the boundaries where by considering the individual thermal preferences of occupants, it may be possible to save energy between these temperatures. Therefore, data are collected from occupants to predict their thermal preference and implement the results for HVAC controlling phase. Fuzzy set is used to organized the data and develop such profiles.

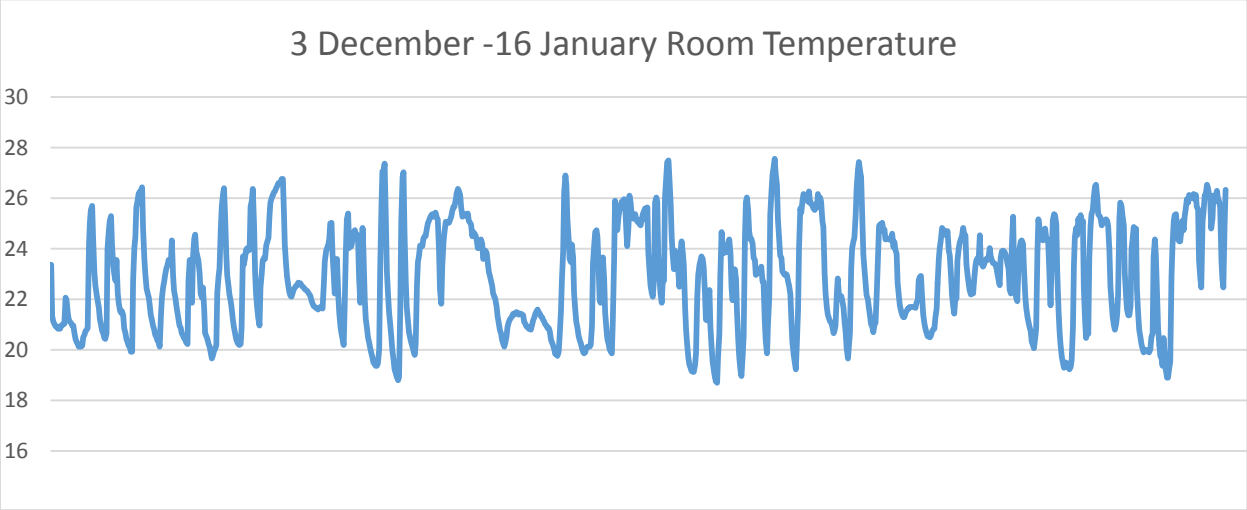

Figure 55: Room temperature from 3 Dec. to 16 Jan.

Table 10: Hourly room temperature range from 3 Dec. to 16 Jan. 2017

Hours	Temperature over 25ºC	Temperature between 23-25ºC	Temperature Between 21 -23 ºC	Temperature between 20-21ºC	Temperature below 20ºC
Total(1080 h)	211 h	301 h	297 h	176 h	76 h
Working(540 h) 8:00AM-8:00PM	124 h	169 h	107 h	80 h	53 h

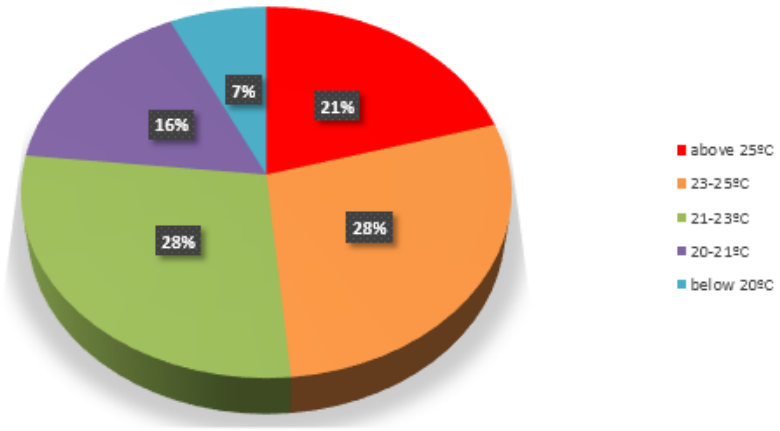

Figure 56: Temperaure distribution 3 Dec. to 16 Jan.

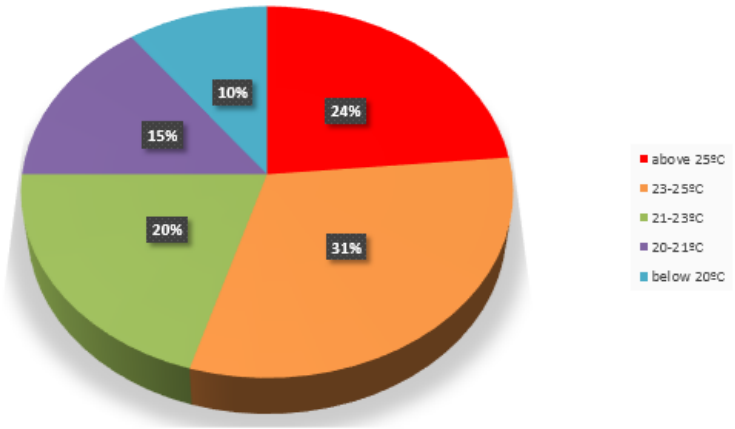

Figure 57: Temperature distribution 3 Dec. to 16 Jan. for working hours

Figure 58 represents the scatter plots collected from two users and the calculated comfort profile fuzzy sets. Figure 58 (a) and (b) show the scatter plots of comfort preference indices and the corresponding ambient temperature. Figure 58 (c) and (d) indicate the fuzzy sets of comfort profile for each user. The temperature associated with neutral feeling (Zero) is considered as the preferred temperature for each user. The blue area represents the region where occupants felt cool and the red areas show the region where occupants felt warm. Based on the present occupants in the office, the minimum and maximum preferred thermal boundaries for all the users are calculated. For

instance, Figure 58(c) shows that the middle preference temperature for user 1 is 23.6ºC with the minimum and maximum preference temperatures of 22.9 ºC and 24 ºC, respectively. From Figure 58 (d) it can be observed that middle preference temperature for user 2 is 22.4 ºC with the minimum of 21.9 ºC and maximum of 22.7 ºC.

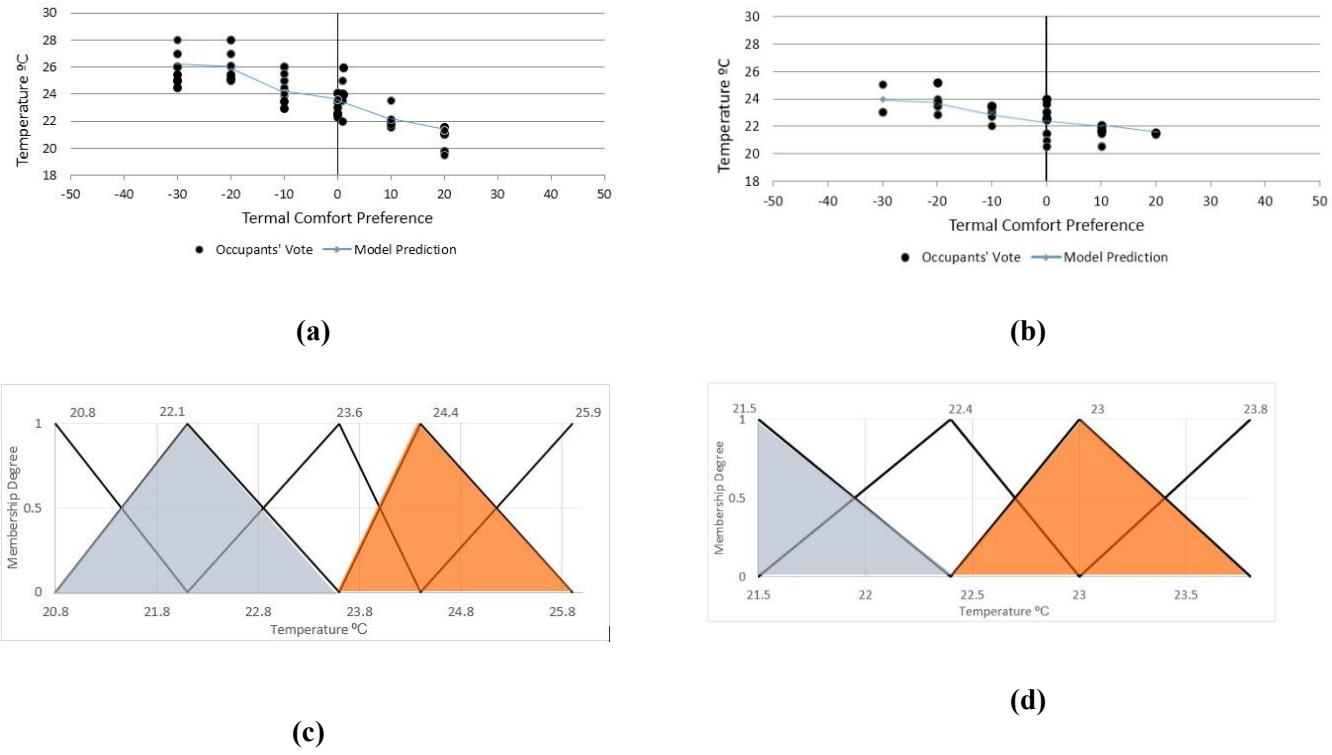

Figure 58: Thermal comfort preference and the calculated comfort profile fuzzy sets for each user: (a) data set and comfort profile for user 1 (b) data set and comfort profile for user 2

Figure 59 illustrates the room temperature and estimated thermal boundary for one working day based on the real occupancy data without considering the unoccupied time. It can be discovered that for most of the day, the room was heated above the preferred thermal boundary, which lead to uncomfortable and energy waste as well. Alternatively, keeping the room temperature between the thermal preference boundaries may increase the thermal comfort level of

the occupants. Adding thermal comfort zones based on modelling, occupancy data, and individual occupants' behaviour, may increase the potential of saving energy while maintaining comfort level. This is investigated in the Section 4.4.3.

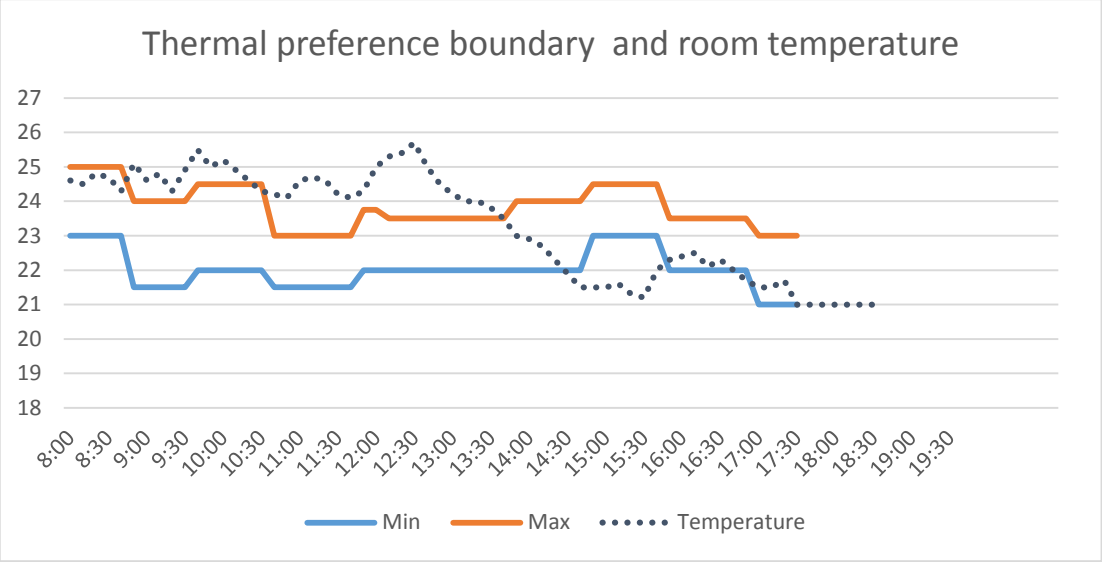

Figure 59: Room temperature and average preference boundary

4.2.4 Occupancy pattern

Occupant location data are for collected a period of six months by a real-time location system using ZigBee nodes, which are installed inside the room of the office. Figure 60 illustrates the occupancy distribution of the office with the nine persons during a typical working day. The recorded data for one week occupancy behaviour of persons are presented in Appendix C. The red colour shows absent periods while green colour shows present periods. Each column represents data of one of the room's occupants.

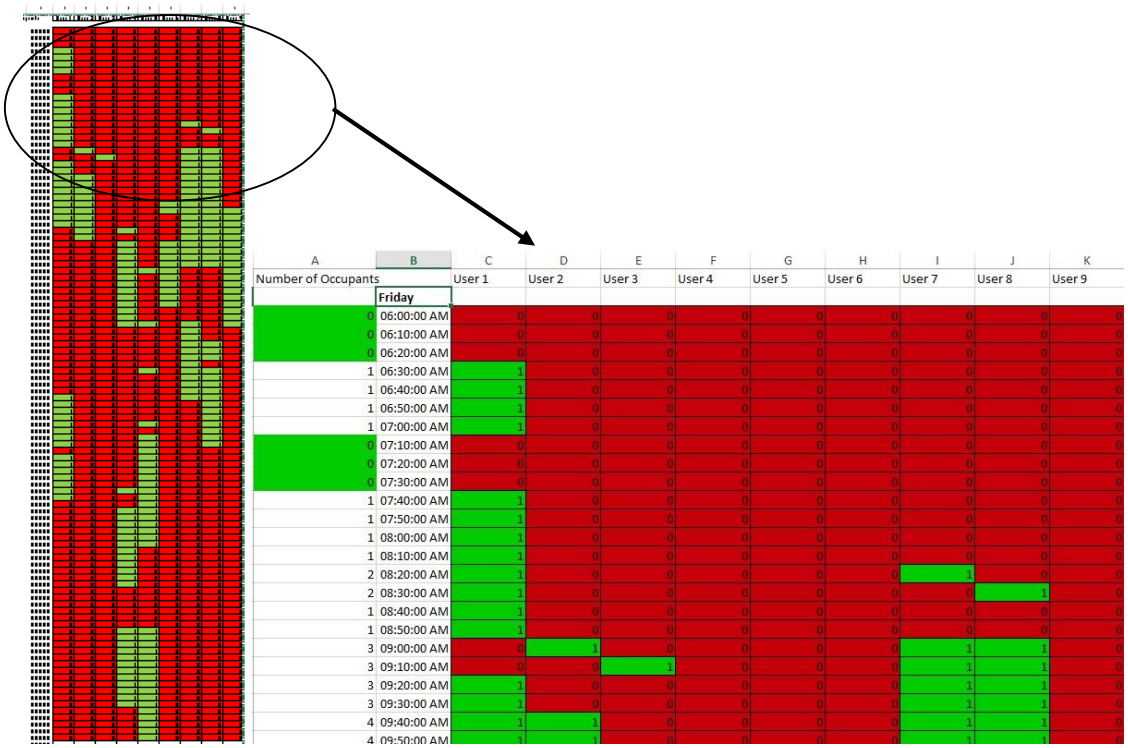

Number of Occupants	Friday	User 1	User 2	User 3	User 4	User 5	User 6	User 7	User 8	User 9
0	06:00:00 AM	0	0	0	0	0	0	0	0	0
0	06:10:00 AM	0	0	0	0	0	0	0	0	0
0	06:20:00 AM	0	0	0	0	0	0	0	0	0
1	06:30:00 AM	1	0	0	0	0	0	0	0	0
1	06:40:00 AM	1	0	0	0	0	0	0	0	0
1	06:50:00 AM	1	0	0	0	0	0	0	0	0
1	07:00:00 AM	1	0	0	0	0	0	0	0	0
0	07:10:00 AM	0	0	0	0	0	0	0	0	0
0	07:20:00 AM	0	0	0	0	0	0	0	0	0
0	07:30:00 AM	0	0	0	0	0	0	0	0	0
1	07:40:00 AM	1	0	0	0	0	0	0	0	0
1	07:50:00 AM	1	0	0	0	0	0	0	0	0
1	08:00:00 AM	1	0	0	0	0	0	0	0	0
1	08:10:00 AM	1	0	0	0	0	0	0	0	0
2	08:20:00 AM	1	0	0	0	0	0	1	0	0
2	08:30:00 AM	1	0	0	0	0	0	0	1	0
1	08:40:00 AM	1	0	0	0	0	0	0	0	0
1	08:50:00 AM	1	0	0	0	0	0	0	0	0
3	09:00:00 AM	0	1	0	0	0	0	1	1	0
3	09:10:00 AM	0	0	1	0	0	0	1	1	0
3	09:20:00 AM	1	0	0	0	0	0	1	1	0
3	09:30:00 AM	1	0	0	0	0	0	1	1	0
4	09:40:00 AM	1	1	0	0	0	0	1	1	0
4	09:50:00 AM	1	1	0	0	0	0	1	1	0

Figure 60: One day occupancy monitoring of the office for nine persons

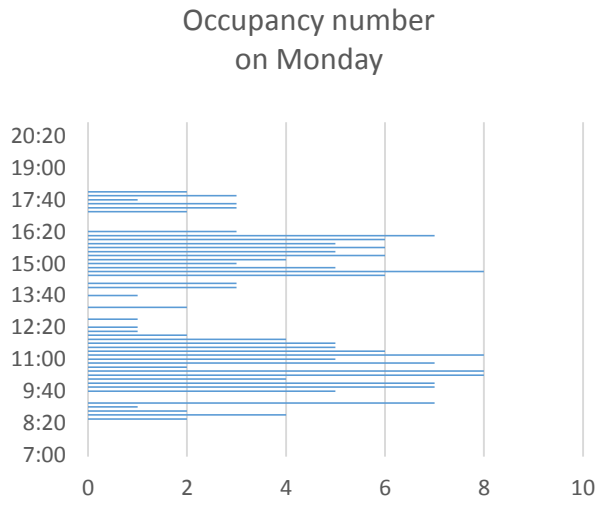

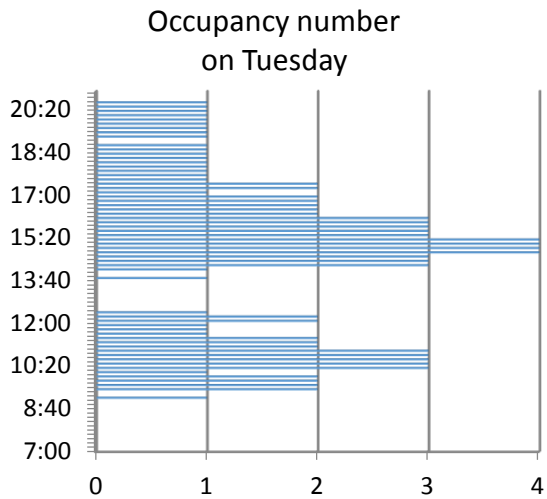

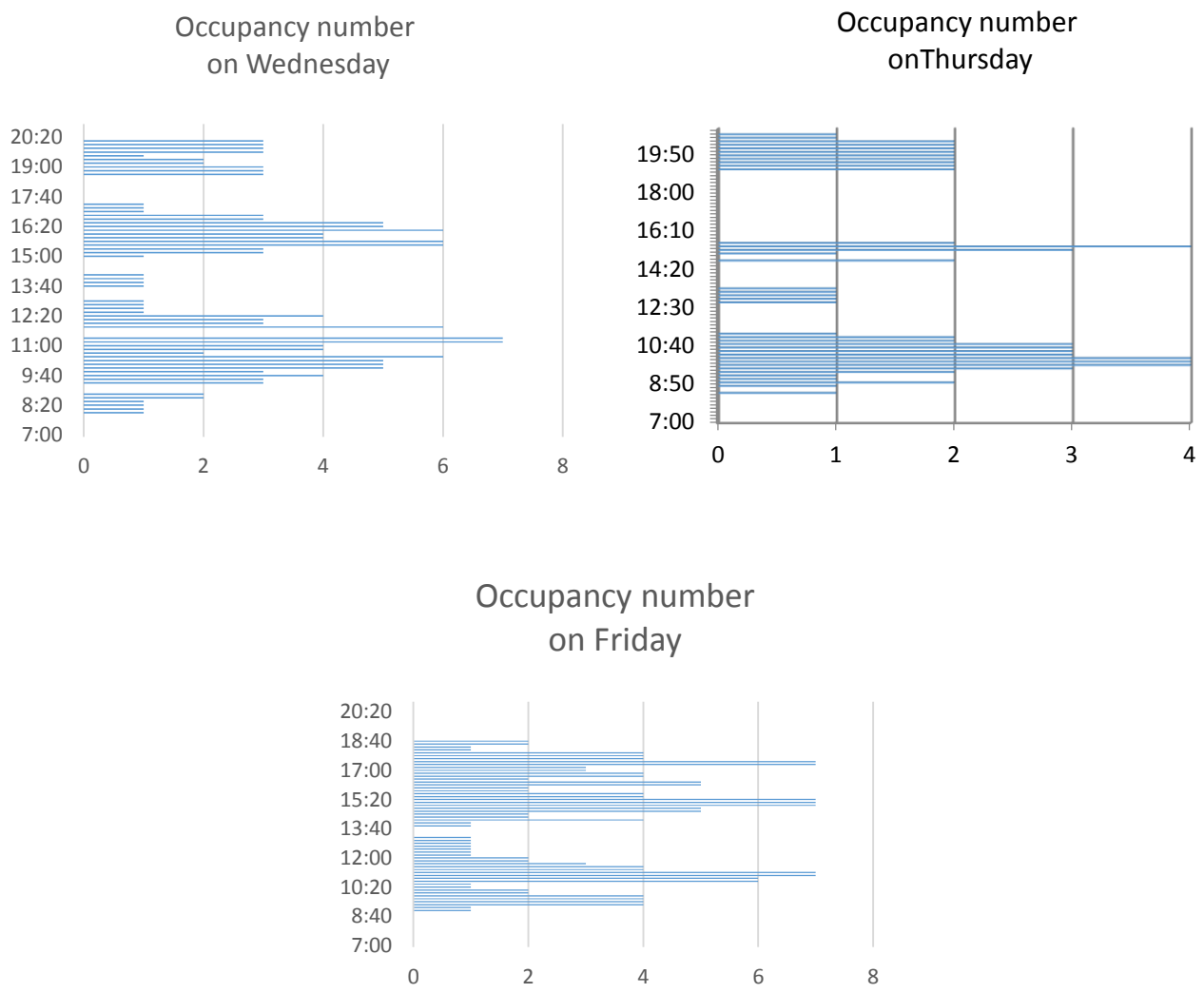

Figure 61: Occupancy number of office during one week

Figure 61 represents the number of persons in the office during one week. From data extracted by these figures there were no days where the office was fully occupied by all 9 occupants. Monday had the maximum occupied period with eight individuals. The maximum occupancy number for both Wednesday and Friday is seven individuals. The maximum occupancy number for Tuesday and Thursday is four throughout the entire day. The recorded data shows that the office is rarely

occupied as much as 80%. The average occupancy for the five working days of the week from 8:00 AM to 7:00 PM is less than four persons.

Moreover, in that week, there were about 17.16 hours during the working period in which the room was unoccupied, indicating that for about 31% of the total working hours during a given week, the room was empty. These data show the capability of saving energy while considering occupancy information.

In addition, Figure 62 shows the extracted data of one-month occupancy graph of the office with nine persons from 6 AM to 8 PM from the period of six months. For example, each Monday, all occupants were absent from the office for two hours (e.g., for lunch) and left the office before 6 PM.

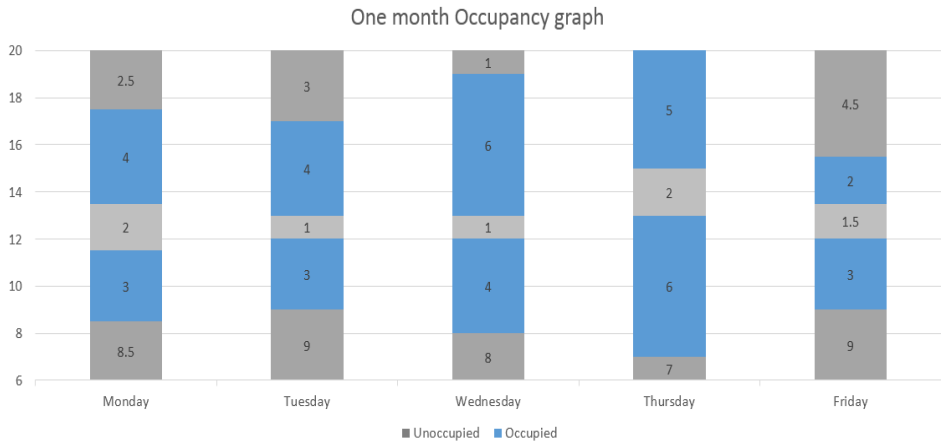

Figure 62: One month occupancy recorded in the office

Figure 63 depicts an individual's working schedule in the room during one week. Such information provides data to calculate the possibility of key behaviours that allow the development of the behavioural pattern of that person's presence for a specific time and day.

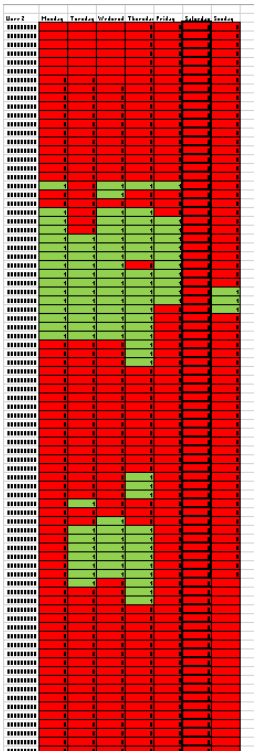

Figure 63: One week occupancy pattern for person 3

Results of semi-Markov model

In the university buildings, the probability that occupants have the same schedule during each day of a week is higher than for other types of buildings. For example, a lecturer may have a class at 11:00 AM each Monday. Therefore, the individual occupants' data based on the day of the week, is considered for behavioural pattern recognition process. For each season, two months occupancy data are recorded and the important patterns for each individual are extracted.

Considering the defined events code from Table 3 in Methodology section, a summary of important patterns for all occupants and a summary of important patterns for one occupant based on the day of the week in the winter season are shown in Table 11 and Table 12. It is noted here that some very long patterns are discarded due to a highly infrequent occurrence (once a week or

month). If a pattern repeated for more than one day of the week, then it is weighted as higher probability or being considered as a behavioural habit. For example “acde” is repeated three different days of the week for a single person, and is therefore assumed to be a regular behaviour of this person. However, a movement such as “cfgde” is only repeated on Mondays, suggesting that this can be based on the schedule of or regular Monday behaviour for that person.

Table 11: Resulting of patterns

	Shortest Pattern	**Longest Pattern**	**Most repeated pattern**
	hi	acdeabcde	cdeabc
# of Patterns	114	54	400

Table 12: Pattern of one occupant based on days of week

Day of Week	**Most repeated pattern**
Mon	deabc
	cfgde
	fghi
Tue	acde
Wed	acde
Thu	achi
	acde
Fri	deabc
	cdehi

Figure 64 shows the resulting Markov chain model for important patterns from historical behaviour data. Transitions are represented as solid arrows with numbers indicating the transition probability between states. The dashed arrow shows the automatic transitions, which is always made when the source node is reached. The transitions with probabilities less than 10% are discarded from the model. As shown in Figure 64, state "*a*" has a 40% transition probability to state "*c*" and a 60% probability to state "*bc*" during the month.

In Figure 65, the duration of the model is also included. The significant duration distributions are denoted as X~(*time*), where *time* is the expected duration of the model. For instance,"*bc*" has a minimum expected duration of 48 minutes before it transitions to the next state. State "*de*" has an expected duration of 19 minutes when it comes from state "bc". The red-arc and blue-arc indicates typical scenarios for specific days of a week.

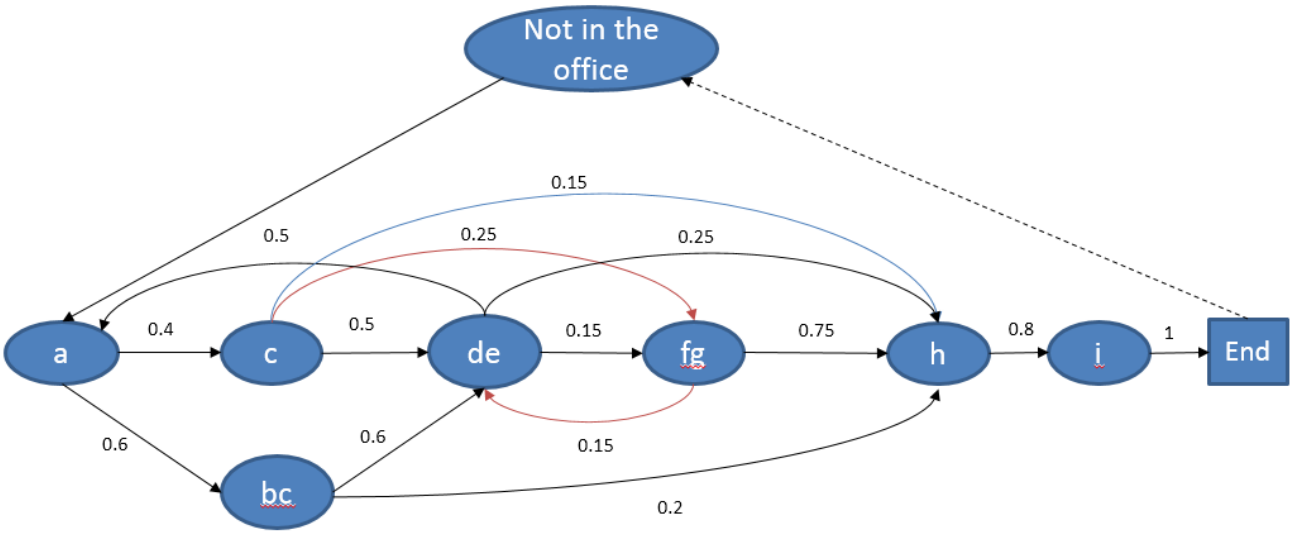

Figure 64: Markov model of behavioural patterns

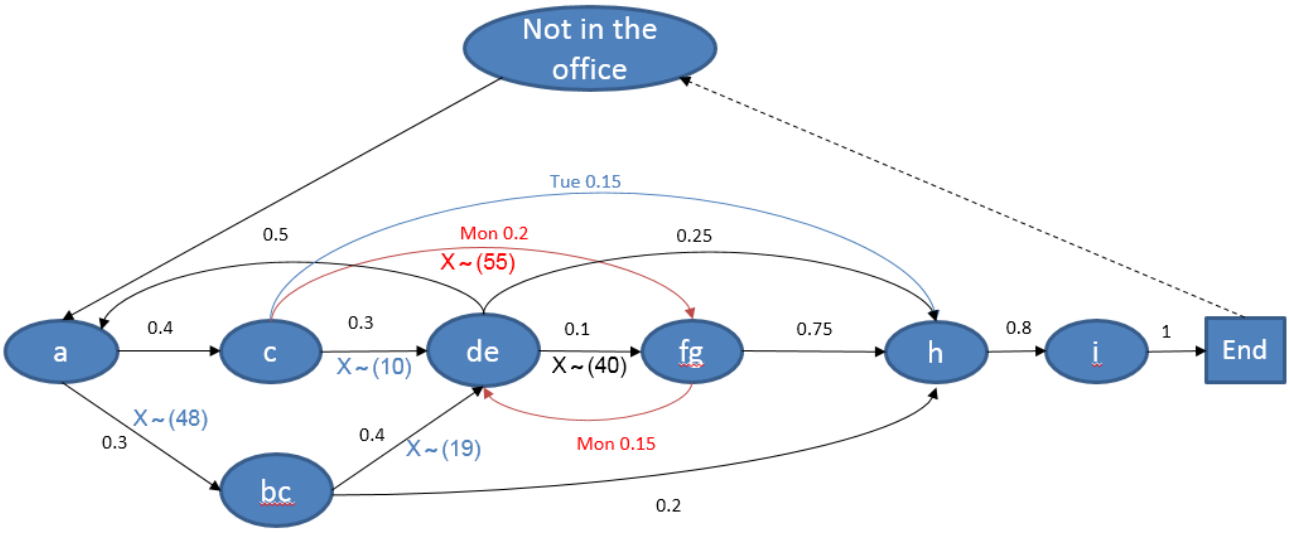

Figure 65: Semi-Markov model of behavioural patterns

4.2.5 Intelligent Control

A prototype system is developed based on previously mentioned methods and technologies. A ZigBee network is developed to collect data about temperature, occupancy, and energy consumption, and send the data to the server. These data are saved in a log file for further computations. The general process of intelligent control system for winter season is depicted in Figure 66.

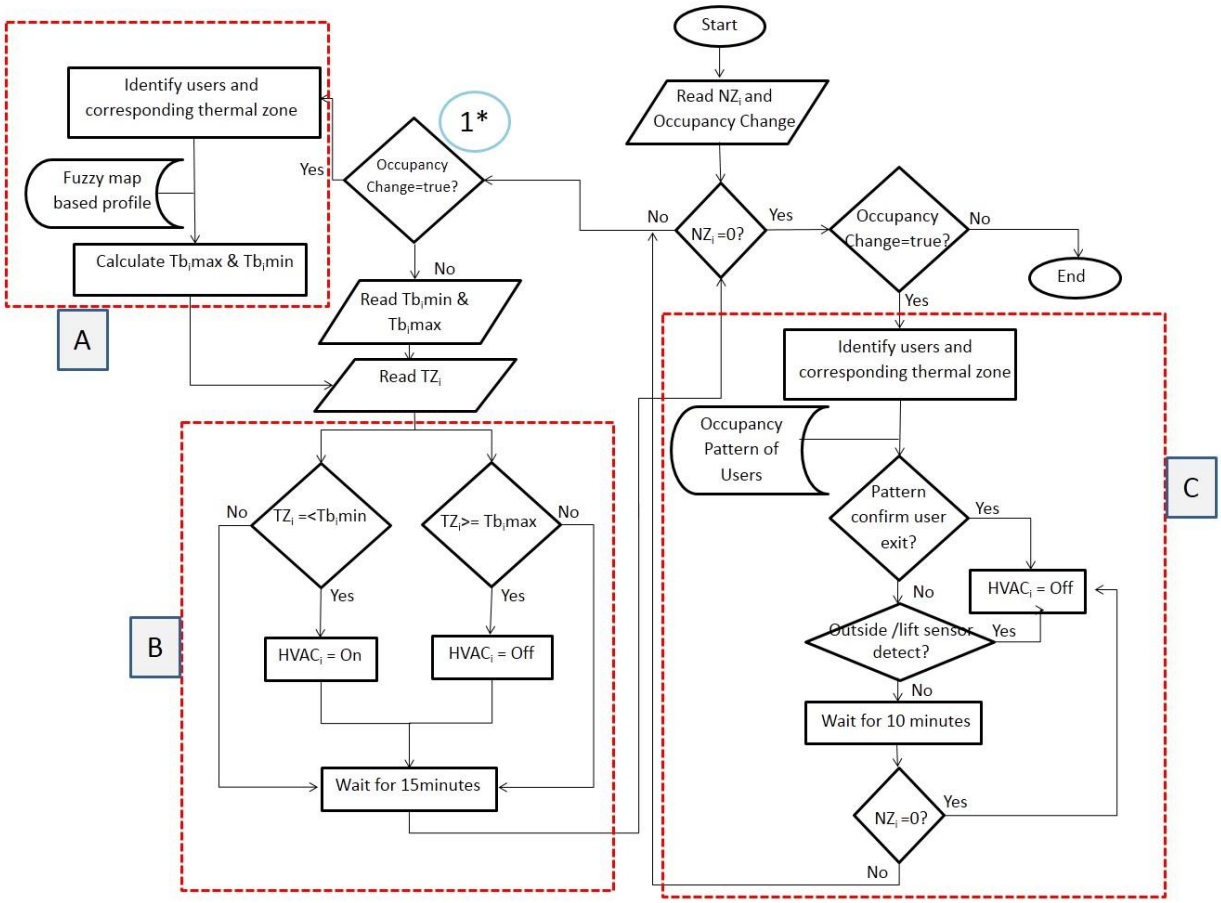

Figure 66: The process of intelligent control

The abbreviations in this algorithm are defined as:

NZi : number of occupants in the thermal zone i

Tbimin & Tbimax: The minimum and maximum preference temperature of occupants in zone i

TZi : The temperature of zone i

HVACi : The air conditioner in zone i

To explain the algorithm of intelligent control, three main parts are labeled.

Part A: in this subsection, the new person who just came to the office with his/her known corresponding thermal zone will be identified. Subsequently, his/her fuzzy map based thermal preference profile will be used to calculate the best range of temperature for this person if he/she is alone in the zone. For the case that other persons attended before him/her in the same thermal zone, the new fuzzy map of all persons will be computed and the range of Tbimin & Tbimax for presence persons will be calculated.

Part B: the zone temperature will be compared with the minimum and maximum preference temperature of persons in a specific zone. If the temperature is below or equal the Tbimin , the corresponding HVAC will be turned ON.

However, this subsection will be triggered each 15 min to turn OFF the HVAC if the zone temperature is equal or more than Tbimax .

Part C: this subsection is developed to turn OFF HVACs based on the occupancy pattern of persons or based on the "Leave the building" signals from the lift and/or outside sensors.

To clarify the process of the intelligent algorithm, different scenarios will be disscussed.

Scenario I: The first person (i.e. user 1 from thermal zone 1), comes to the office at 8:00 am.

As soon as detecting the person in the office, the value of NZi is changed to 1. Since the previous occupancy number was zero, occupancy change is confirmed as "true" in part (1*). Therefore, part A would be activated and the Tbimin & Tbimax will be extracted from the

person's profile. After reading the temperature of zone 1, the zone temperature will be controlled by HVAC1. As the room is occupied and NZ1 is more than zero, the zone temperature will be checked and controlled each 15 min.

Scenario II: The second person (i.e. user 4 from thermal zone 1), comes to the office at 9:00 am.

As soon as detecting the change in the occupancy number and confirmation from the occupancy changes (number 1→ 2), Part A will be activated and the new Tbimin & Tbimax will be computed based on the combination of thermal preference of users 1 and 2. After reading the zone 1 temperature, Part B will be applied.

Scenario III: The third person (i.e. user 8 from thermal zone 1 and 2) comes two the office.

From CFD analysis, it was found that this user can be allocated to both zones. At the current time, zone 2 is empty. Therefore in the identification of thermal zone at the moment, this person will be considered in zone 1 and consequently the new Tbimin & Tbimax will be computed based on three users in the same thermal zone.

Scenario IV: At 10:00 am, TZ1 shows the temperature above Tbimax but still NZ1 =3.

Part B of the algorithm will turn OFF the HVAC1 to keep the zone temperature between the preference ranges.

Scenario V: At 12:30 pm, last person in zone 2 leaves the office (i.e. user 6) and HVAC2 is ON.

NZ2 =0 and the occupancy change is "true". Therefore, the occupancy pattern of user 6 will be checked but the probability does not confirm that this leaving is a long-term condition. In

addition, lift and outside sensors did not detect this person. The HVAC2 still keeps ON for 10 minutes. If there is no change in the NZ2 value during this period, HVAC 2 will be turned OFF after 10 minutes.

In addition to the general intelligent process, some specific rules are defined to increase the efficiency of the control and reduce the frequency of temperature change. The following shows two sample rules of the intelligent control.

Check Tz1 and Tz2 % 15 min

If Nz1>1

And

If Tz1 <= Tbmin, and HVAC z1=OFF, Then ON HVAC1

Or

IF Tz1 >= Tbmax, and HVAC z1=ON, Then OFF HVAC 1

If Nz2>1

And

If Tz2 <= Tbmin, and HVAC z2=off, Then ON HVAC 2

or

IF Tz2 >= Tbmax, and HVAC z2=ON, Then OFF HVAC 2

Algorithm 2: Control of Zones' temperature

Tz1 and Tz2 represent the zone temperatures which will be recorded each 15 minutes.

Tbmin and Tbmax show the minimum and maximum thermal preference boundary which are calculated based on the presence of occupants. For instance, when a zone is occupied, the zone temperature will be checked. If it is below the Tbmin then the corresponding HVAC will be activated.

The second rule is implemented to reduce the duration of period for heating the zone. After the identification of occupancy changes, the probability of that change will be checked and if the value is above 10%, it can be considered as the possible long-term situation for occupants and consequently the related zone will be identified. Then, the new temperature boundary will be calculated based on the current presence occupants in the room. Next, the zone temperatures will be checked. If the differences between current temperature and the minimum or maximum computed boundaries, is more than 1.5 degree, both HVACs will be activated if they are in the "OFF" mode to reduce the period that the zone temperature reach between the boundaries.

If Nz1>1 And Occupancy change=true
If P>0.1 Then
Calculate Tbmax and Tbmin
Check Tz_i
If Tz_i<= Tbmin, and HVACi=off,
If $(tp_{imin} - t_{zi}) > 1.5$ Then On HVAC 1 and 2
Else
ON HVACi

Algorithm 3: Speed up heating the room when it is too cold

For instance, for a winter case, if the difference of zone temperature and preference temperature boundary of the present users was higher than 1.5 degree($(tp_{imin} - t_{zi}) > 1.5℃$) , both HVACs are activated without considering the occupancy of the other thermal zone until the next occupancy change is identified or the room temperature exceeded the maximum boundary. Alternatively, when ($t_{zi} - tp_{imax} > 1.5℃$), then both HVACs are deactivated to reduce the time spent in heating the room.

However, simple ON/OFF HVAC activation based on occupancy may not be cost effective for large HVAC systems. This is because starting up large fan motors require large current draw, potentially offsetting the money saved during the OFF period. Hence, a reasonable period (at least 10 minutes) [52] should be considered for changing the condition of HVAC systems. In addition, while saving energy using occupancy information, some comfort may be compromised and a complementary strategy to overcome this issue may be needed. Therefore, individual occupants' behavioural data are considered in order to create a historical prediction pattern and increase the possibility of having a cost effective controlling HVAC system.

4.3 Performance evaluation

Different methods can be applied to measure and assess the energy usage and savings, such as whole-building meter data, sub-metered data, and model-based data from the compliances and the facilities. Whole-building metering can give an overview to energy efficiency when comparing the energy consumption pattern to a baseline but investigating the impact of small changes regarding the individual behaviour of occupants can easily be overshadowed. On the other hand, Sub-metered data have the potential to provide more accurate measurements of individual impact.

For energy assessment based on modelling, different strategies can be applied in the simulation model to investigate the impact on energy saving. However, the real situation should be investigated by collecting energy consumption data and user behaviour data so as to be compared with the simulation results

In this research, as the individual behavioural pattern played an important role, data regarding the occupancy and thermal preference patterns from the occupants' regular behaviour were

collected. Additionally, sub-metered data were collected to compare the energy savings under different scenarios to the simulation model. Implementing different strategies simultaneously may not be possible and consequently limited the research to provide much comparative analysis. Hence, the combination of real and static data was utilized to evaluate and compare different conditions.

For the analysis of changes in energy consumption regarding ceiling mounted splits, four methods are applied in this section: Measure 1: Baseline HVAC method (BL) (measured), Measure 2: Duty cycle strategy (DC) (measured), Measure 3: Purely Occupancy-driven control (POD) (estimated) and Measure 4: Intelligent control (IC) (measured).

According to the Facility management office's schedules, all HVAC systems are programmed to turn on at 6:00 AM and turn off at 8:30 PM. However, users can manually control the HVAC systems if needed. This condition is referred to as the BL. The energy consumption data of each individual air-conditioning system in the room is recorded by using two ZigBee-based smart plug-ins, which wirelessly transmit this data to the server. Measure 2 is independent of the occupants' behaviour and room temperature. Therefore, this method is applied on a separate day of the week, considered to be the First Day test. It is difficult to compare energy consumption for HVAC across multiple days. On the other hand, it was not possible to track Measures 1 and 4 simultaneously due to the temperature dependency of Measure 4. As the HVAC loads are influenced by the temperature and solar radiation and different days have different weather patterns, three Mondays in the month with the same approximate temperature range are selected for the test. Therefore, Measures 1 and 4 are applied each Mondays of a month. Second and the third days test are considered for measure 1 and measure 4, respectively.

Measure 3 is only based on the occupants' behaviour but the users' behaviour could vary during different days. Hence, Measure 3 was created using information from real-time occupancy data and (I/O) HVAC control of third day test to make it comparable with measure 4. The source code of Measure 3 is provided in Appendix H.

Table 13 shows the outside temperature range for three days test.

Table 13: Outside temperature

Days	**Day test1 (DC)**	**Day test2 (BL)**	**Day test3 (IC and POC)**
Outside temperature	2ºC -7ºC	4ºC-9ºC	3ºC-8ºC

Aside from these differences, it is still possible to make a reasonable comparison. As the second day was warmer, the energy consumption was somewhat conservative and would have been higher than the recorded results for the first and third day Energy consumption based on different control strategies

Baseline method

The BL energy consumption (Figure 67) is obtained by considering the combination of prescheduled working hours and manual user control of HVAC systems. The maximum load is recorded as 17kW for both HVACs. In addition, the energy consumption for this typical day is not exactly the same as for the other days due to the different behaviour of occupants for manual control of the HVACs. Therefore, the energy consumption for this day is considered to be an

approximate energy consumption for comparison with other methods. The total power consumption for the baseline was 142.83 kW-H.

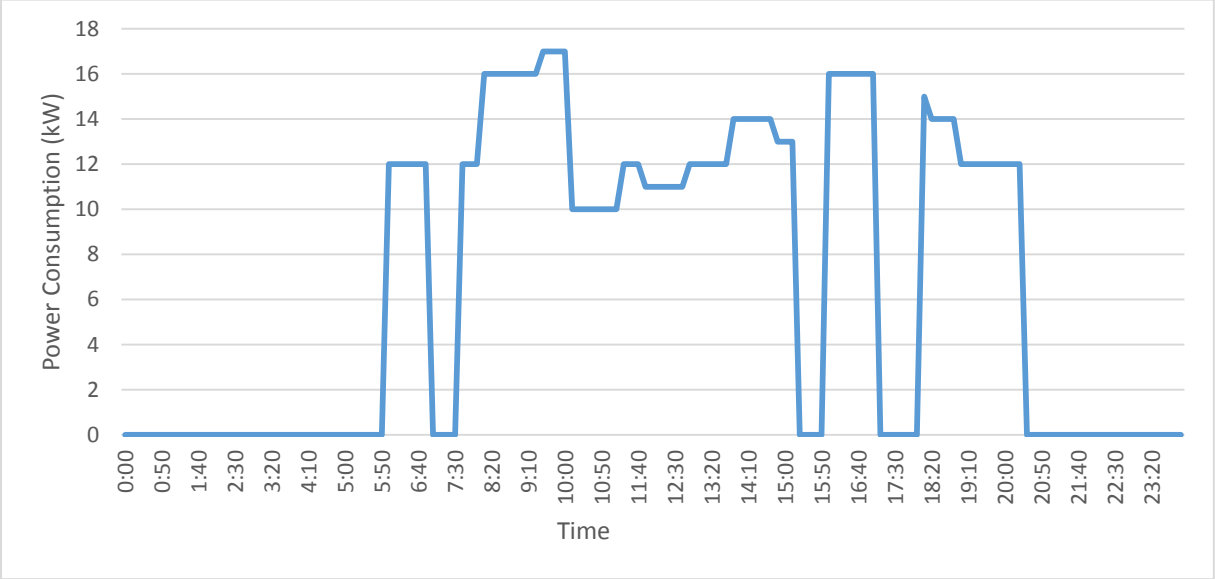

Figure 67: Energy consumption based on Baseline strategy

Table 14 summarizes the accumulated number of hours based on the indoor temperature. The office with BL stood out with nearly 180 minutes of the hours above 25 ºC, and 240 minutes between 23 ºC to 25 ºC and only 300 minutes of 21 to 23 ºC and zero minutes below 15 ºC.

Table 14: Accumulated number of hours based on the indoor temperature for baseline

Hours	Temperature over 25ºC	Temperature between 23-25ºC	Between 21 -23 ºC	Temperature below 21ºC
Working 8:00 AM-8:00PM (720 min)	180 min	240min	300 min	0min

Duty cycle strategy

Figure 68 shows the hourly plan for the DC method that was implemented. As this method for each season has approximately the same energy consumption due to the fixed set point of 26 ºC and same schedule, it is not necessary to trace the power consumption within a single day. Therefore, this strategy is implemented on the first day without considering the temperature. The blue columns show the Off period and the brown columns show the On period of HVACs during a day. The total power consumption for the DC method was 132 kW-H.

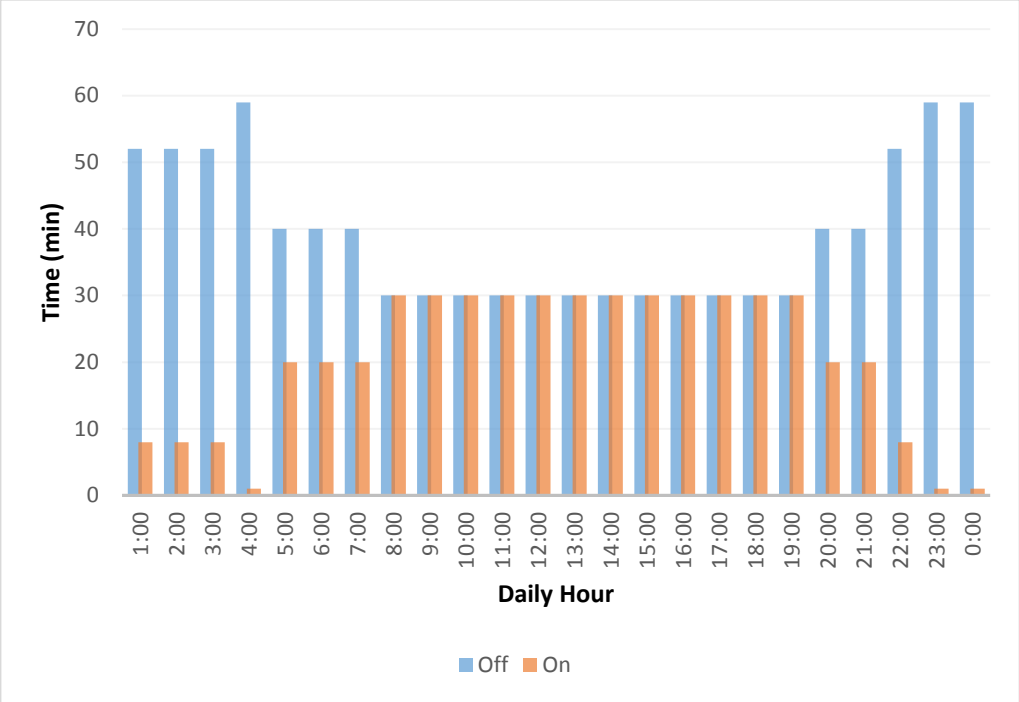

Figure 68: Energy consumption based on Duty cycle strategy

Intelligent control strategy

On the third day test, the IC method was applied. The HAVCs were controlled based on the historical and real-time occupancy, and the thermal preferences of occupants in the room that had

been recorded for two months. Figure 69 shows the temperature and the occupancy data. The mean temperature boundary for all occupants is depicted as two boxes at bottom and top of the graph. The maximum number of occupants was recorded as six persons, illustrated as bar charts. When the system recognized any occupancy number or boundary temperature changes, the control will respond and necessary rules will be applied to them.

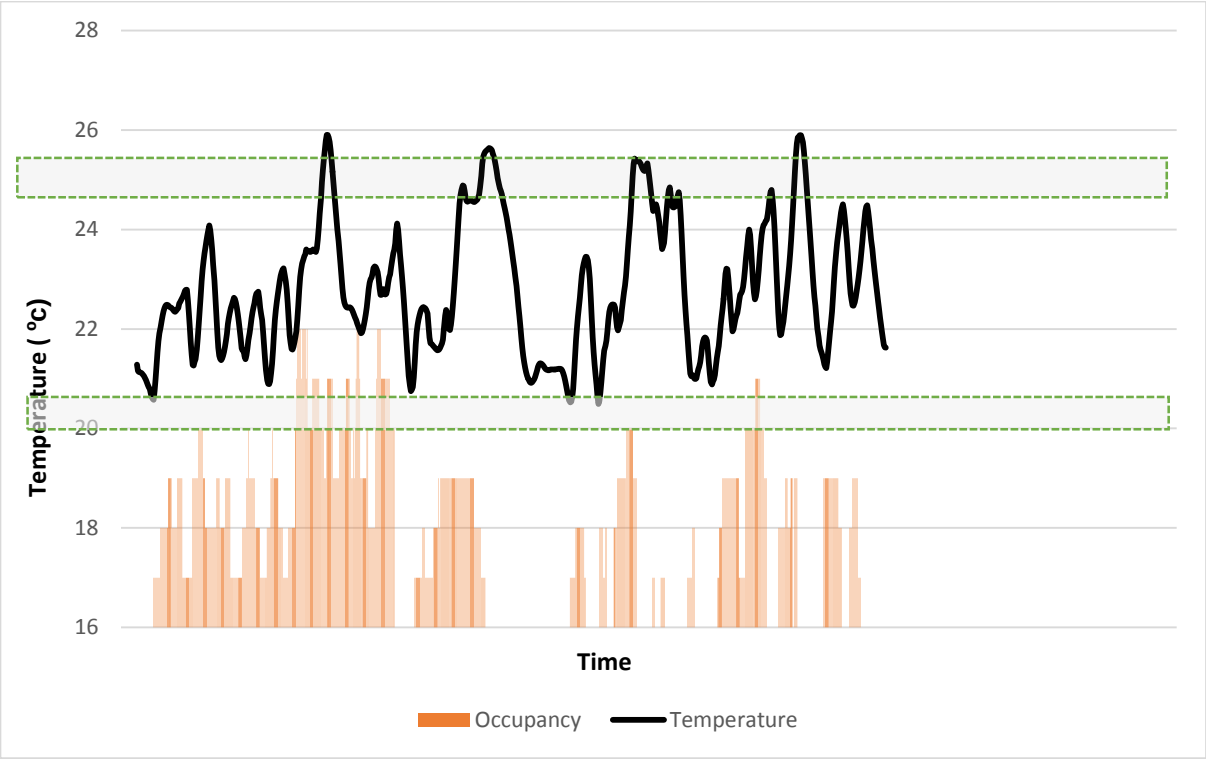

Figure 69: Hourly temperature and occupancy

Table 15 shows the duration of working hours in terms of temperature range. Implementing the IC method leads to keeping temperatures between 23 ºC and 25 ºC most of the time. Temperatures above 25 ºC and below 20 ºC were recorded as the shortest periods.

Table 15: Accumulated number of hours based on the indoor temperature for intelligent system

Hours	Temperature over 25ºC	Temperature between 23-25ºC	Temperature between 21 -23 ºC	Temperature between 20-21ºC	Temperature below 20ºC
Working 8:00 AM-8:00PM (720 min)	41 min	129 min	520 min	30min	0

Figure 70 shows the HVAC power consumption traces for the IC method. The first occupant presented at 8:00AM and the program reacted by turning on both HVACs. During the day when the system distinguished the possibility of a long term vacancy, it deactivated both HVACs. For instance, from 12:40 to 13:40 the HVACs were turned off. The maximum power consumption for that day recorded as 17kW and the total HVAC loads were calculated to be 84.16 kW-H.

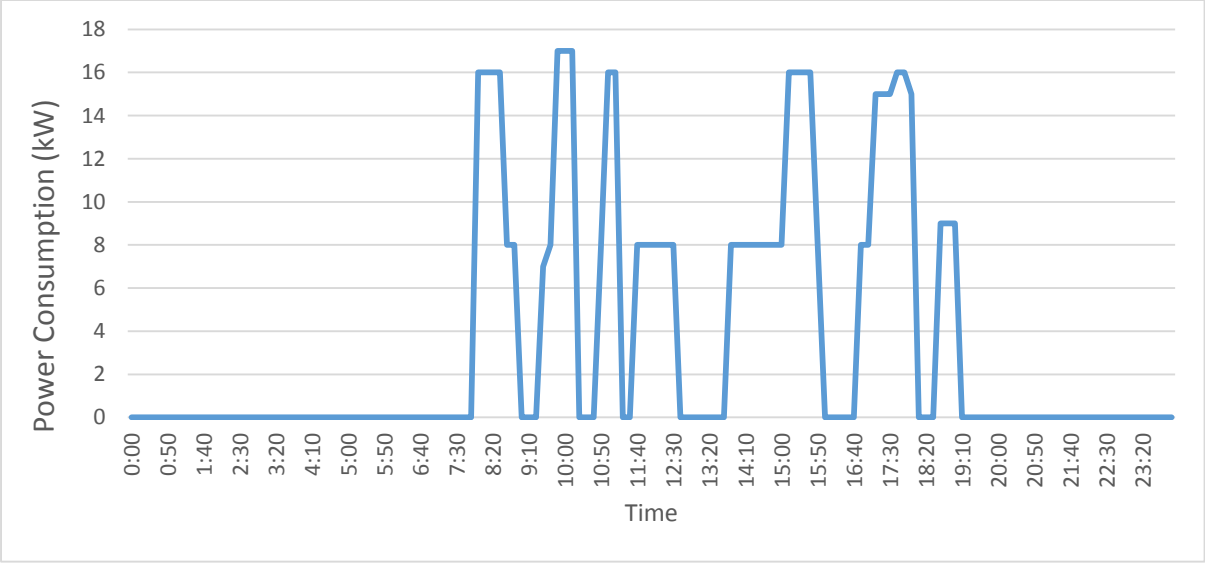

Figure 70: HVAC power consumption for IC

Purely occupancy-driven control

To investigate the differences in terms of power consumption between the POC and IC methods, the estimated power consumption of HVACs was computed based solely on occupancy data recorded from the third day test. Figure 71 illustrates the response activity of HVACs while only considering occupancy data. The total HVAC power consumption was computed to be 100.66 kW-H for that typical day. Although energy consumption from POC method is lower than that of the BL method, it should be considered that energy savings may not necessarily lead to the satisfaction and comfort of the occupants. Moreover, turning HVAC systems on or off in a short period will increase maintenance costs.

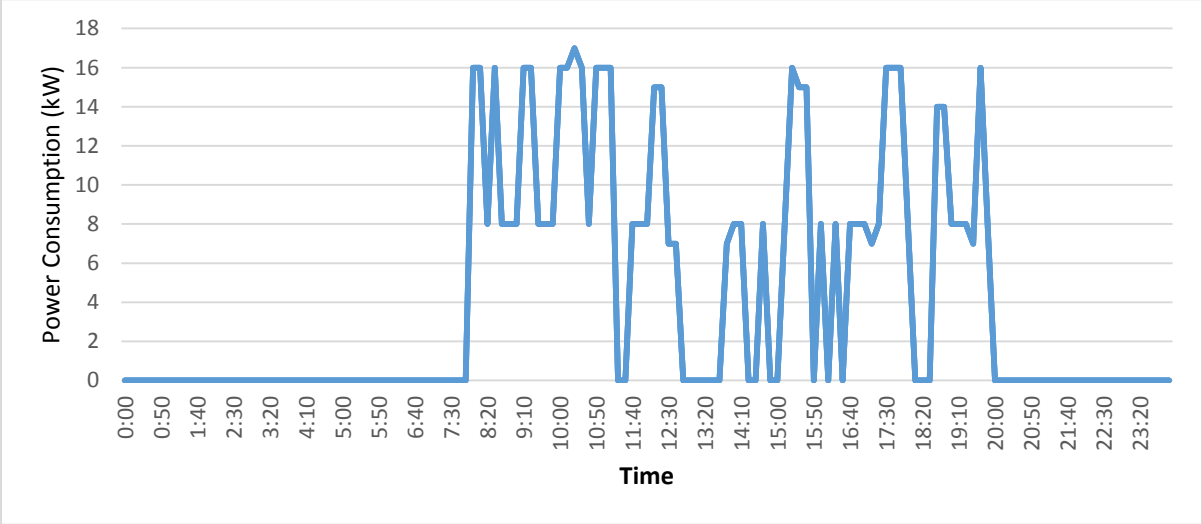

Figure 71: HVAC power consumption for purely occupancy strategy

4.3.1 Comparison and Discussions

The comparison of accumulated number of hours based on the indoor temperature for BL and IC is depicted in the form of a bar chart in Figure 72. For the temperatures above 25ºC, the BL method shows higher values than the IC method. This implies that the IC method reduced the period of time during which the temperature was above 25 ºC. On the other hand, the period during which the temperature was kept between 21 ºC to 23 ºC was increased for the systemic method. This shows the potential of achieving higher comfort levels for the IC method. In addition, for the BL method, room temperature did not decrease below 21 ºC even during unoccupied time which indicates a waste of energy. This is because while the room is unoccupied, there is no need to keep the room temperature above 21 degrees.

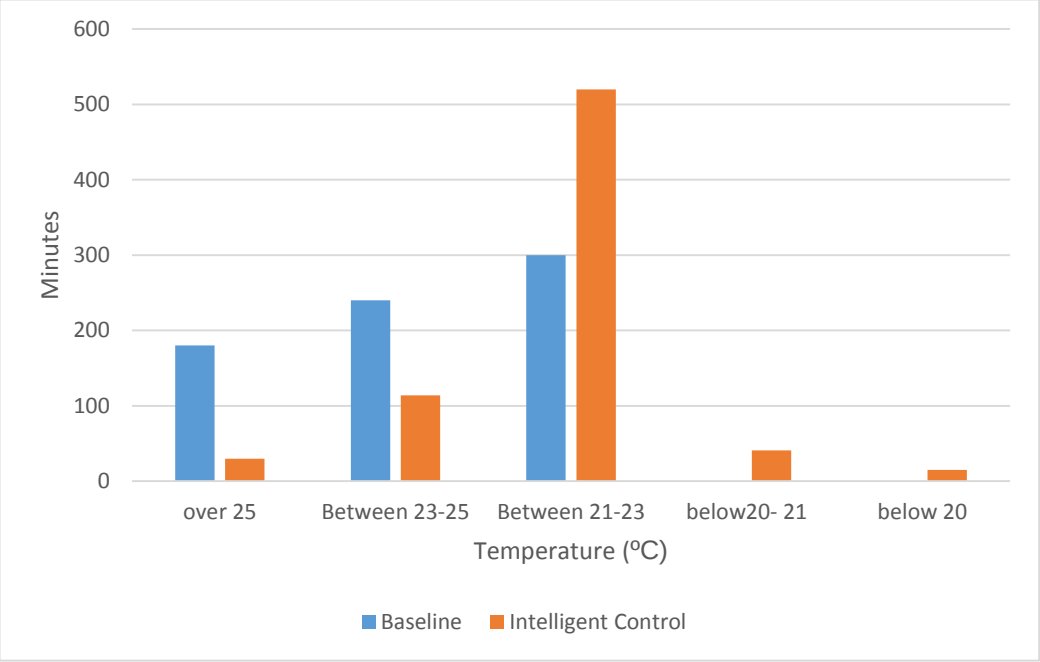

Figure 72: Comparison of accumulated number of hours based on the indoor temperature for baseline and intelligent cotrol

A comparison of power consumption for both the BL and IC methods during the day is illustrated in Figure 73. The area that is covered by both graphs indicates equal power consumption

for both methods. The BL started from 6:30 AM based on the prescheduled program but the IC started from 8:00AM when the first occupant presented into the room. The same situation happened at the end of the day. The HVAC continues working based on BL strategy until 20:30, but intelligent control turned off the HVACs after 19:00. At the start of the day, it may be better to activate HVACs in order to maintain temperature at the comfort level before the occupants enter the room. However, there are many days that the room may be unoccupied for the entire morning. Therefore, it is better to predict the room's occupancy probability during the weekdays, and add a passive heating/cooling schedule. This can be considered in the future work. While the power consumption of the IC method was higher than that of the BL method during some periods, the overall energy consumption shows a significant reduction by using the intelligent control strategy.

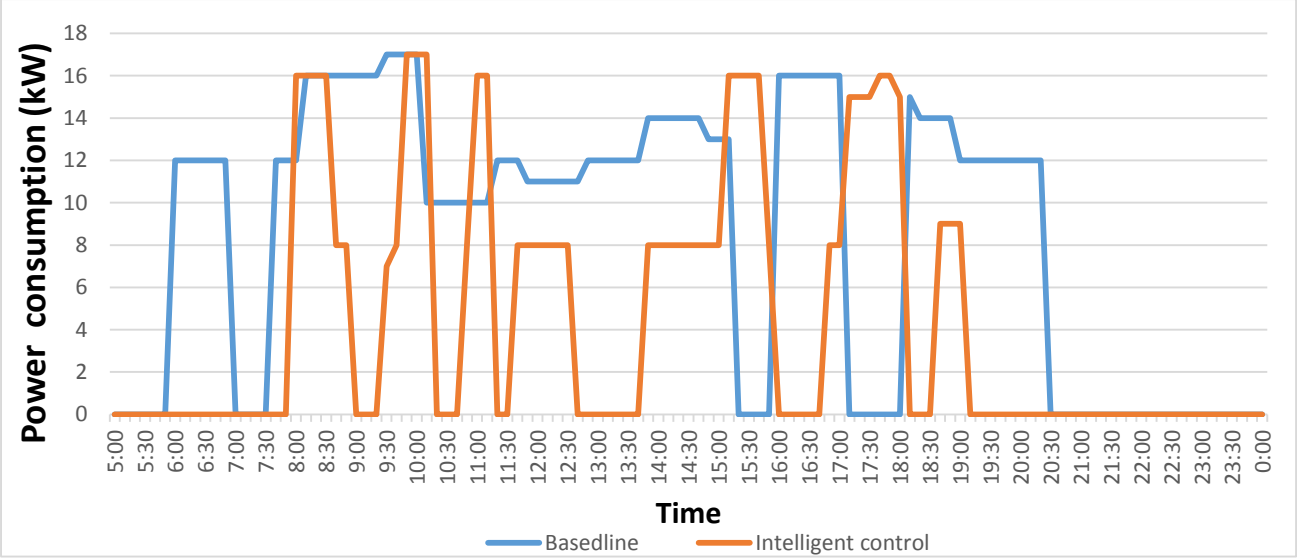

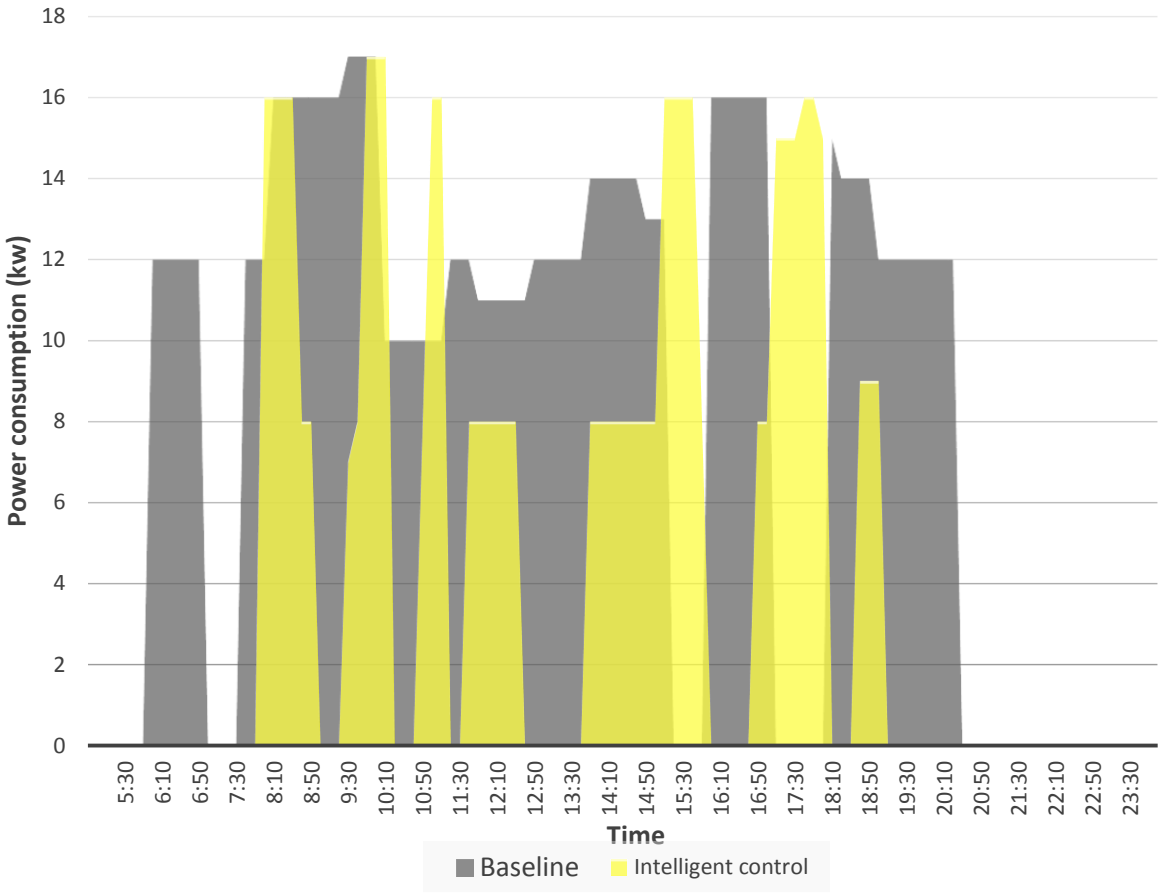

Figure 73: HVAC power consumption for baseline and intelligent control

Figure 74 shows the comparison of HVAC loads for the IC and POC where there are occupancy-driven based. Based on the experimental tests, there is an approximate duration of 7 minutes to change the room temperature. Moreover, the short-time occupancy behaviour of occupants caused a high fluctuation. However, It can be seen that the blue line, indicating the IC, has a significantly smooth behaviour, and the POC fluctuation is higher than the IC fluctuation. In addition, turn on and off HVAC systems regularly at intervals of less than five minutes will increase the maintenance costs. Therefore, the IC is more efficient than POC in terms of both comfort and cost.

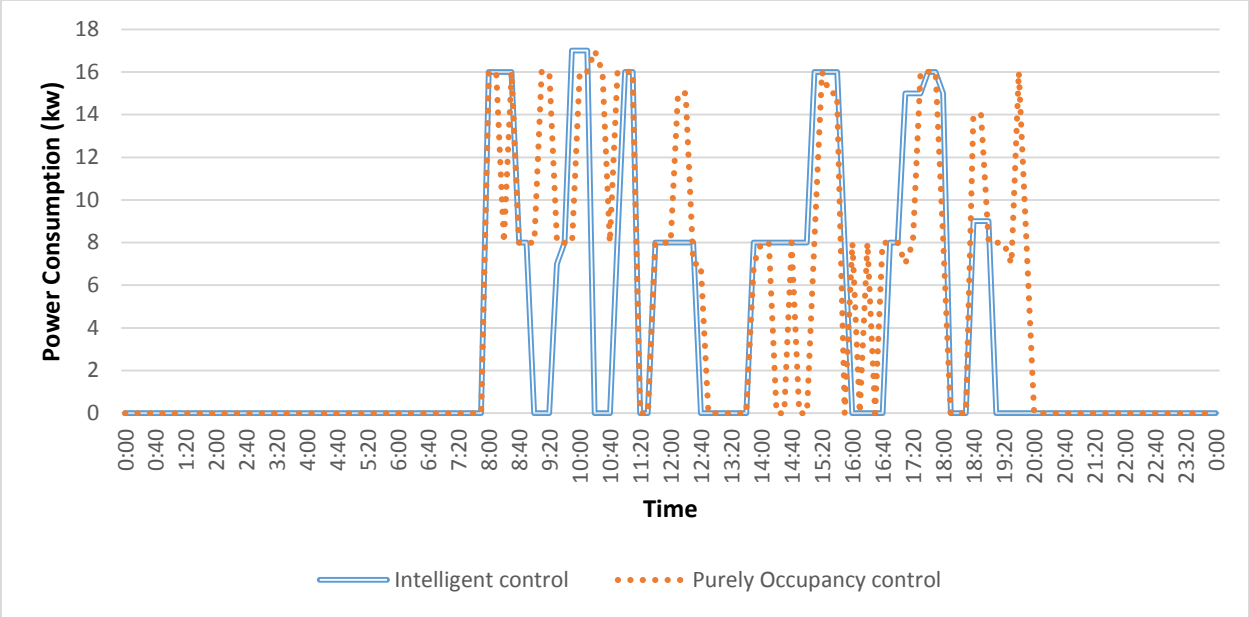

Figure 74: HVAC loads for POC and IC

Table 16 shows the energy saving potential for different strategies comparing to the BL method.

The total observed electricity savings for IC are higher than for DC and POC. In addition, POC has the potential to be implemented based on the offline data based on occupants' positions and historical behaviours. Moreover, the energy savings percentage from POC is close to that of IC. Therefore, for a longer period of energy savings analysis and a more accurate comparison, it is possible to utilize the combination of BL data and occupancy pattern, which is explained in validation section 4.4.3.

Table 16: Energy consumption and potential saving for different strategies

Method	Baseline (BL)	Duty cycle (DC)	Purely Occupancy (POC)	Intelligent Control (IC)
Energy Consumption (kW-H)	142.83	132	100.66	84.16

Saving Energy	5.25%	29.5%	41%

4.3.2 Validation

It is not possible to implement the BL and IC method simultaneously in the same room. In addition, different days test results may not be a good comparison for these two methods due to the different weather conditions and varying occupants' behaviours. Therefore, the comparison of IC and BL energy consumptions may not provide an accurate result. On the other hand, POC method has the capability to be implemented in the offline mode which means it can be applied on the same day that BL was tested. Therefore, same occupants' behaviour and same weather condition can provide more accurate comparison.

In addition, if we show that the energy saving from IC and POC is in the same range or even better results collects for IC, it is possible to compare the BL and POC for a longer period of time and achieve more accurate results. Therefore, in the first part of this section, IC and POC will be compared and if the results show similar saving achievement, the POC will be used instead of IC for comparison with BL.

To evaluate the accuracy of fuzzy map approach in predicting the satisfied temperature range, another survey based on occupants' feeling in different temperatures is conducted. For the second survey, different voting scale is designed to avoid the similarities and psychological impacts.

During another survey which is considered as the third survey, the performance of whole intelligent system, will be analysed. In this stage, the survey is done by the occupants during different predefined strategies and the results are compared.

Energy optimization

To evaluate the performance of IC in details, data from a typical day are selected. Figure 75 represents the results of IC. The mean temperature of the room and ambient temperature are depicted. The mean lower and mean upper thermal preference of all users are calculated. The working duration of the HVACs are depicted at the top of the graph.

Figure 75: Intelligent HVAC controller results

At the beginning of the day, user 2 arrived at the office at about 7:00 AM while outdoor temperature and indoor temperatures were recorded as 15℃ and 18.3℃, respectively. The zone 1 temperature also was recorded as 19.2℃.The calculated thermal preference for this user is in the range of [21.3-24℃]. The intelligent controller decided to turn on HVAC 1 at 7:15 AM as this person is identified in zone 1 for a long-term stay with the probability of 0.35. Although there was no person in zone 2, the intelligent controller system turned on HVAC 2 because the difference of zone temperature and preference temperature of user 2 was bigger than 1.5 degrees ($tp_{imin} - t_{zID} > 1.5℃$) (21.3℃-19.2℃ $>$ 1.5℃), which was defined as a rule for the intelligent controller. After the time that temperature reached the lower boundary of the user's thermal preference, HVAC 2 was turned off. This happened around 8:00 AM while that time the temperature was recorded as 21.8℃.

We have a fluctuation of temperature between 8:30 AM to 9:30 AM when other users arrived at the room and the door is opened frequently. This is the normal period of user attendance. The Intelligent system reacted by turning on both HVAC 1 and 2 based on the occupancy data. However, the system turned off HVAC 2 at about 9:20 AM to hold the temperature between the boundaries of present users in zone 2. Zone 2 was unoccupied from 11:00 AM until 2:00 PM. The system evaluated this situation as a long-term condition. Consequently, HVAC 2 was inactive. All persons left the room before 12:30 PM. The intelligent controller kept both HVACs off until about 2:00 PM due to the real-time occupancy data. Around 2:10 PM two users from different zones came back to the office. The system activated both HVAC systems. There are some dramatic changes in the temperature. For example, at 16:10 when the last user left the building, the temperature reduced sharply. The reason could be explained as the transfer of outdoor air into the room from open door or windows in the office. Although both HVACs were off from 11:20 to

14:10, the temperature maintained approximately constant. This is due to heat transferred from computers.

User 6 from zone 2 came back to the office around 16:55 but the system did not react at that time and considered that case as a short-stay based on the probability. However, after 10 minutes the system turned on both HVACs to compensate for the difference between zone temperature and preference temperature of the user based on the 1.5 degree rule ($|t_{zID} - tp_{imin}| > 1.5$℃). If the user could control the HVACs manually, he would turn them on in less than 10 minutes. In other words, 10 minutes is a long period for the user to stay in the office with low temperature, which is the drawback of decision-making systems. These systems can make predictions based on the previous data and react based on new data patterns, but require enough time to be confirmed.

To investigate the difference of energy consumption, IC is compared with POC. After confirming that saving energy for IC is in a reasonable range compared with POC, it is possible to implement the POC on the offline data to estimate energy savings. Hence, it is more accurate to be compared with the same time and day of that when BL is implemented.

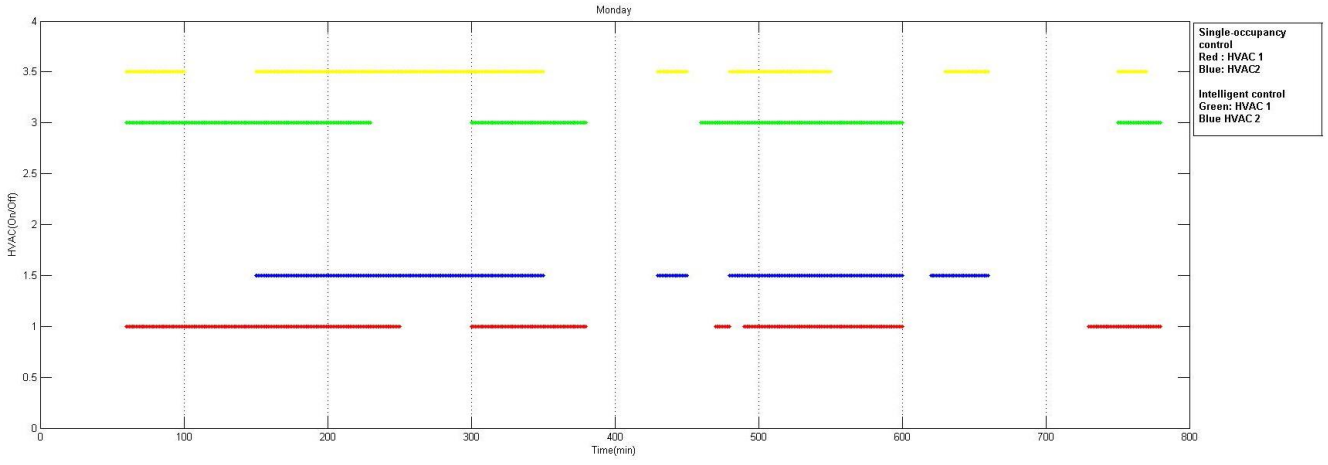

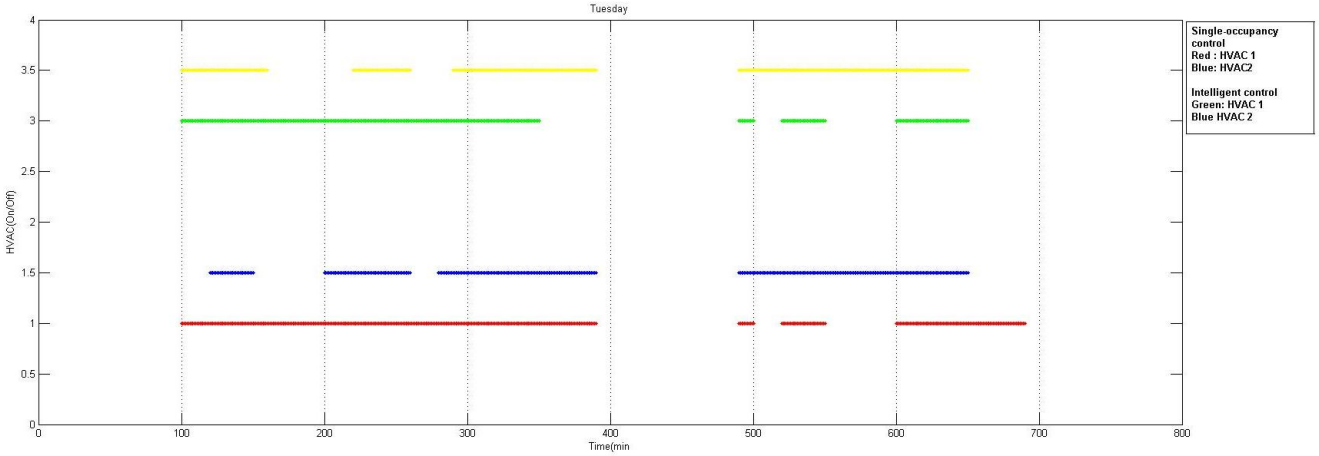
Tuesday
HVAC(On/Off)
Time(min
Single-occupancy control
Red : HVAC 1
Blue: HVAC2
Intelligent control
Green: HVAC 1
Blue HVAC 2

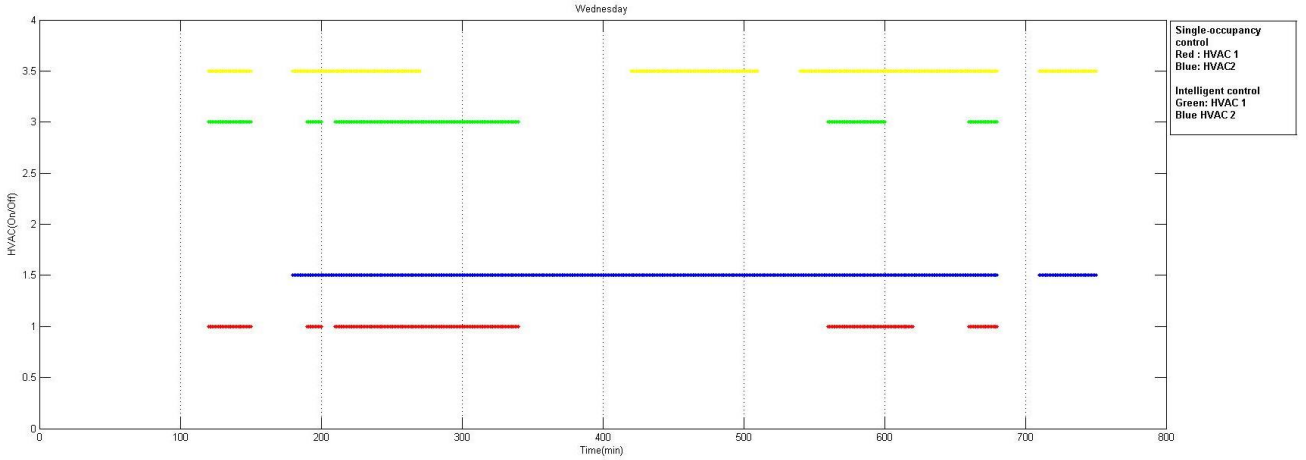
Wednesday
HVAC(On/Off)
Time(min)
Single-occupancy control
Red : HVAC 1
Blue: HVAC2
Intelligent control
Green: HVAC 1
Blue HVAC 2

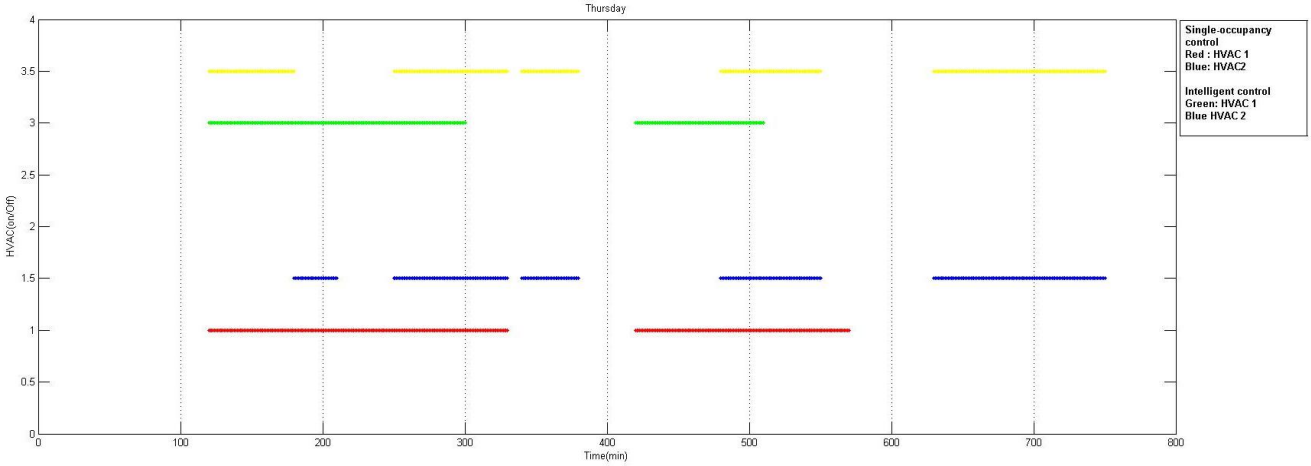
Thursday
HVAC(on/Off)
Time(min)
Single-occupancy control
Red : HVAC 1
Blue: HVAC2
Intelligent control
Green: HVAC 1
Blue HVAC 2

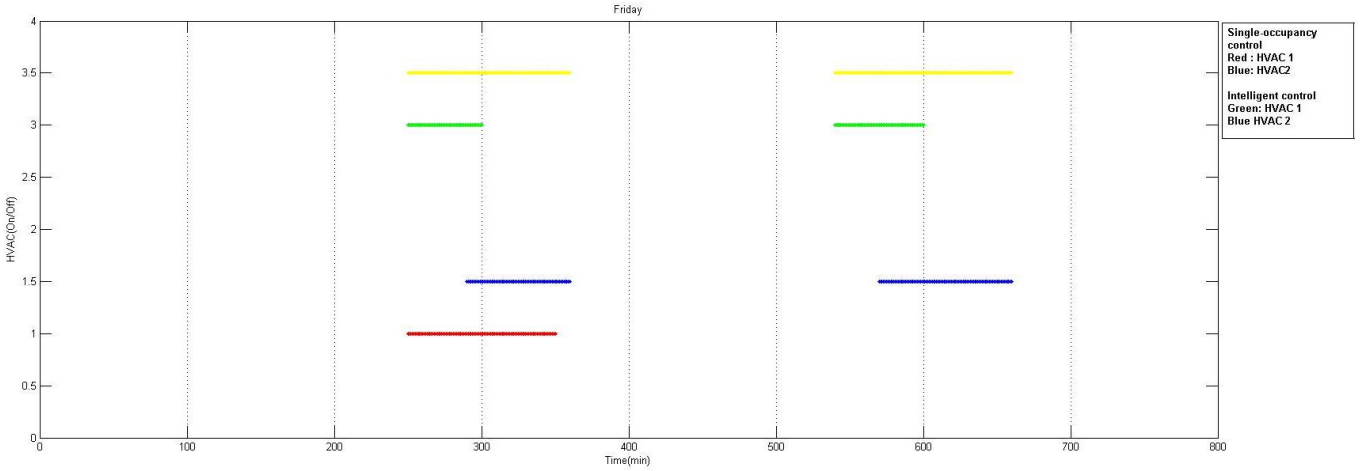

Figure 76: Comparison of IC and POC

Figure 76 illustrates a five working days' performance of an HVAC system based on IC and POC. It can be observed that the IC method consumed about 4.5% less energy than the POC method during the same test period, based on the same occupancy behaviour but provide more comfort to the occupants.

Table 17 shows the detailed daily energy savings percentage.

Table 17: Comparison of Intelligent control and Purely occupancy control

	Mon	**Tue**	**Wed**	**Thu**	**Fri**
Saving IC compare with POC	6.59%	5.68%	8.64%	0%	-1.6%

The maximum energy savings occurred on Wednesday which is 8.64% less energy used. On Friday, the POC used 1.6% less energy compared with that of IC. On Thursday, the approximate energy consumption for both strategies were same. Considering the data from Table 16, it is

concluded that the average energy savings for IC is about 4.5% to 6% higher than for the POC method. Therefore, the POC method can be applied on the BL data, allowing a comparison of results.

Figure 77 shows the comparison between the BL and POC methods for five working days. The summary of extracted data is shown in Table 18. On day 5, the energy savings from POC was extremely high which was 68.97%. On that day, the last occupants forgot to turn off HVACs. Therefore, a huge amount of power was wasted. However, in the POC, the HVACs were turned off them based on real occupancy data, resulting in large energy savings. Although, day 3 shows the lowest energy savings with a value of 28.19%, this is still considered as a significant amount of savings. The average energy savings for the whole testing period shows the potential of 40% energy savings while utilizing the POC strategy. However, ignoring day 5, the average energy savings was calculated as 32.76%, which remains a considerable value.

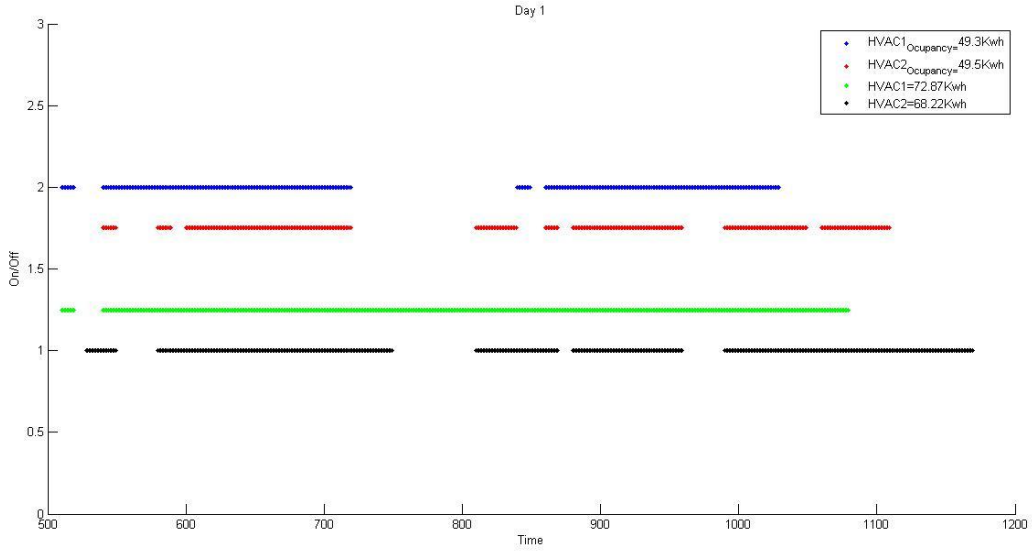

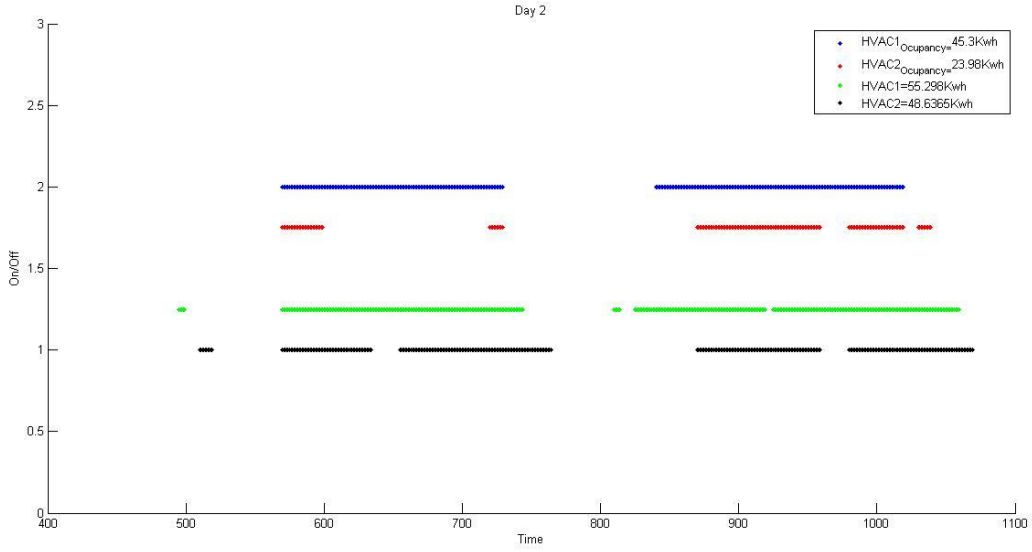
Day 2
HVAC1Ocupancy=45.3Kwh
HVAC2Ocupancy=23.98Kwh
HVAC1=55.298Kwh
HVAC2=48.6365Kwh
On/Off
Time

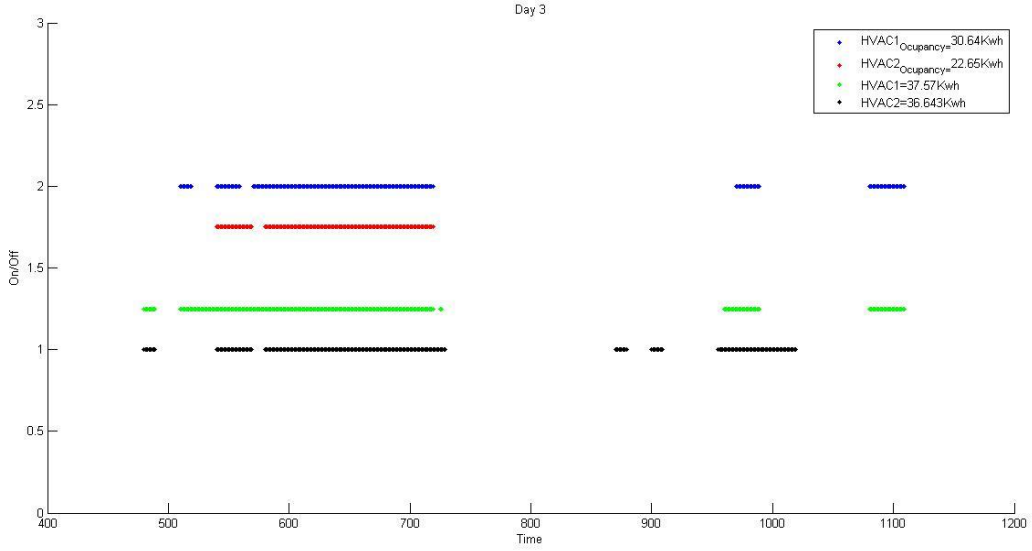
Day 3
HVAC1Ocupancy=30.64Kwh
HVAC2Ocupancy=22.65Kwh
HVAC1=37.57Kwh
HVAC2=36.643Kwh
On/Off
Time

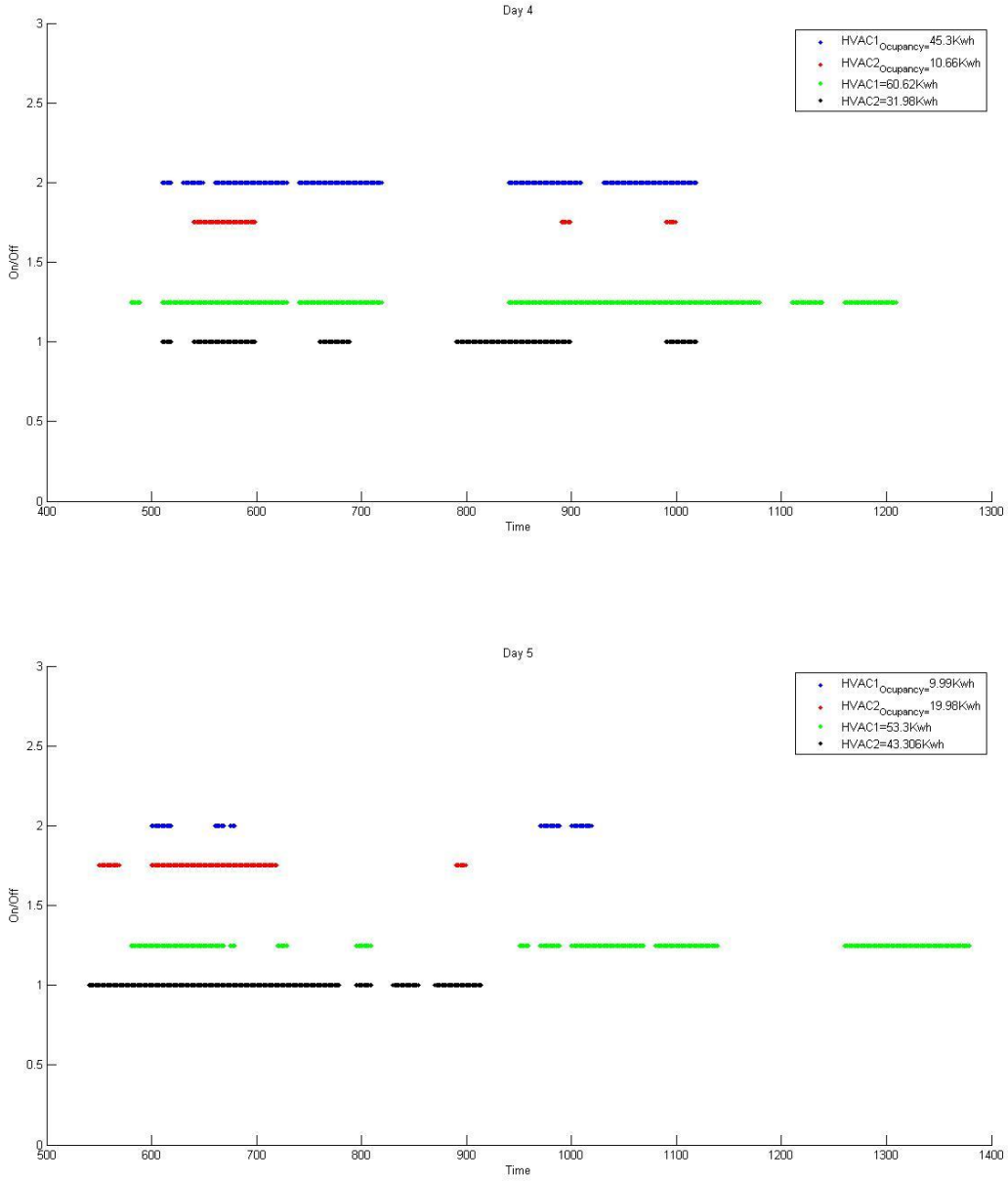

Figure 77: Comparison of BL and POC

Table 18: Comparison between BL and POC

	Day 1	Day 2	Day 3	Day 4	Day 5
POC Energy Consumption	98.8 (kW-H)	69.28 (kW-H)	53.29 (kW-H)	55.96 (kW-H)	29.97 (kW-H)
BL Energy Consumption	141.09 (kW-H)	103.93 (kW-H)	74.21 (kW-H)	92.6 (kW-H)	96.606 (kW-H)
Savings for POC strategy	29.97%	33.33%	28.19%	39.56%	68.97%

Figure 78 shows the energy consumption comparison of POC, IC and BL for five working days. The yellow areas represent the energy savings by using the POC strategy. The green line depicts the BL strategy's energy savings. The estimated energy savings for the IC method are illustrated as a dash line. It is clear that day 5 contains the maximum difference in savings between the BL and POC methods, and that day 3 contains the minimum energy savings.

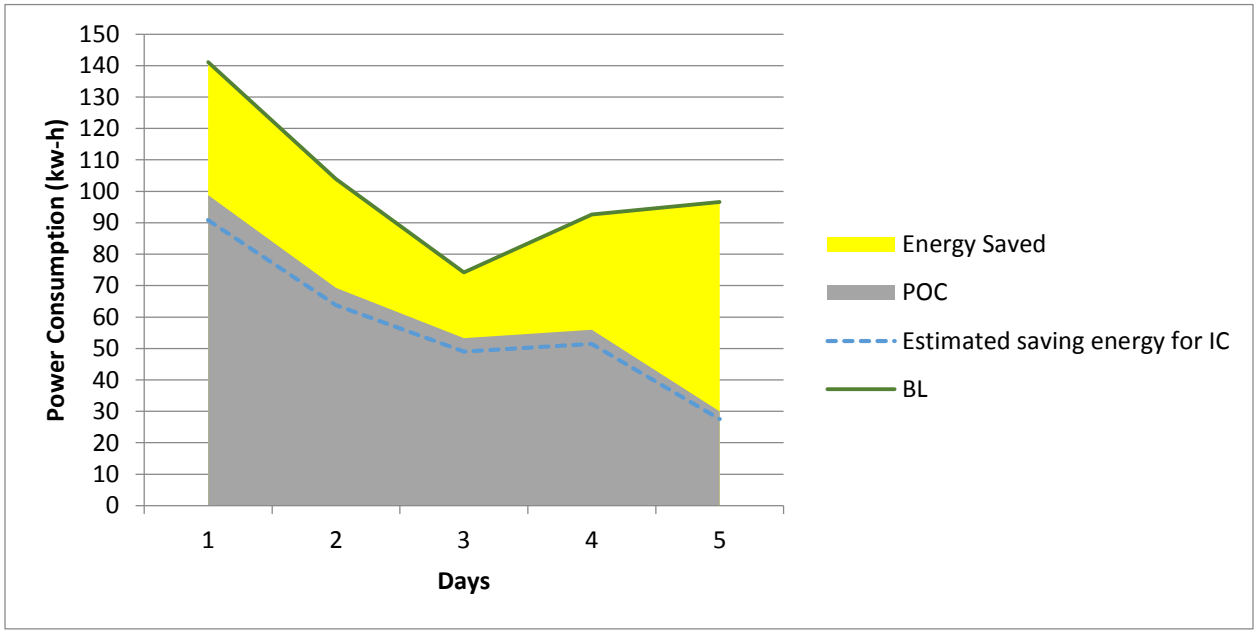

Figure 78: Estimated and measured saving energy

Figure 79 shows one month of the HVACs operation when kept on due to the POC method. According to the BL data, the HVACs operated from 6:00AM to 8:30 PM with the manual control of occupants. The total operational hours for HVAC1 and HVAC2 are recorded as 201 and 163 hours, respectively. In the case of POC strategy, it is showed that HVAC 1 worked for 131.96 hours, equalling about 5.5 days, and HVAC 2 operated for 97.81 hours, equalling about 4.07 days.

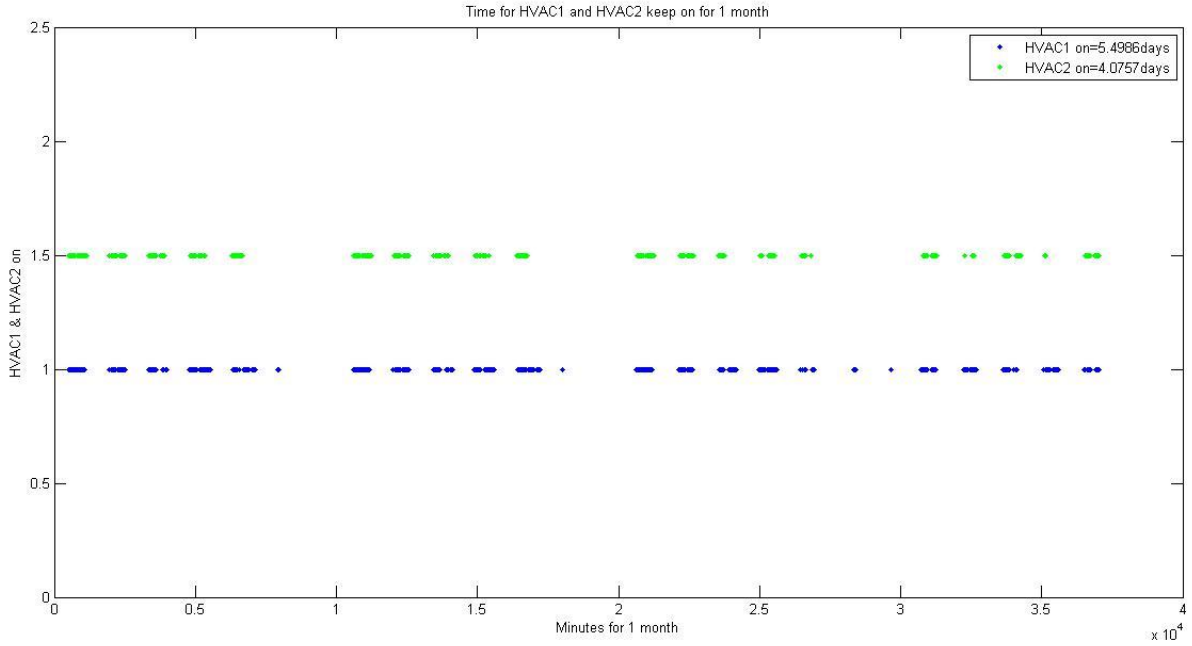

Figure 79: HVACs keep on for one month based on POC

The results for monthly analysis indicate an approximate savings of 34.38% during working hours for HVAC1 and 39.99% for the operation of HVAC 2. Considering the results of Table 16, analysis shows the potential to save about 30-40% energy for the POC approach and 35-48% for the IC approach. However, the thermal comfort and occupant satisfaction level need to be evaluated for the IC, which are examined in the following section.

Thermal comfort and fuzzy map evaluation

To verify the extracted data from fuzzy maps, another survey was conducted. During a 5-day period, the room temperature is manually changed by the operator to one of the randomly selected temperatures. Afterward, a survey is conducted to collect the thermal votes of occupants. At the end, the pattern of thermal comfort areas extracted from fuzzy maps is compared with the second survey.

As an example, Figure 80 illustrates the comparison of fuzzy map comfort areas and the specific thermal comfort evaluation for user 3. The blue curve indicates the neutral area from the fuzzy graphs. The two-dash line shows the minimum and maximum of the neutral areas. The minimum, maximum, and middle of the neutral areas are extracted from the fuzzy map as 20.7, 21.5 and 22.8ºC, respectively. The vertical axis shows the range of votes by 8 ranges. The range [0 1] is considered as the natural range, indicated by the oval in the graph. From the 40 votes recorded at different temperatures, 19 votes fall in this range with the minimum and maximum temperatures of 20 ºC and 23.5 ºC. Comparing with the minimum and maximum computed range, extracted from the fuzzy map, a reasonable range of thermal preference is validated. For user 7, the same test has been done and results are depicted in Figure 81. The minimum, maximum, and middle of the neutral areas are computed as 22, 24.5 and 23.5ºC, respectively. From the 40 votes cast at different temperatures, 26 votes fall in the range of [0 1], with minimum and maximum temperatures of 20.7 ºC and 25 ºC. The computed and the current test both confirm that this person prefers a wide range of temperatures not exceeding 25ºC.

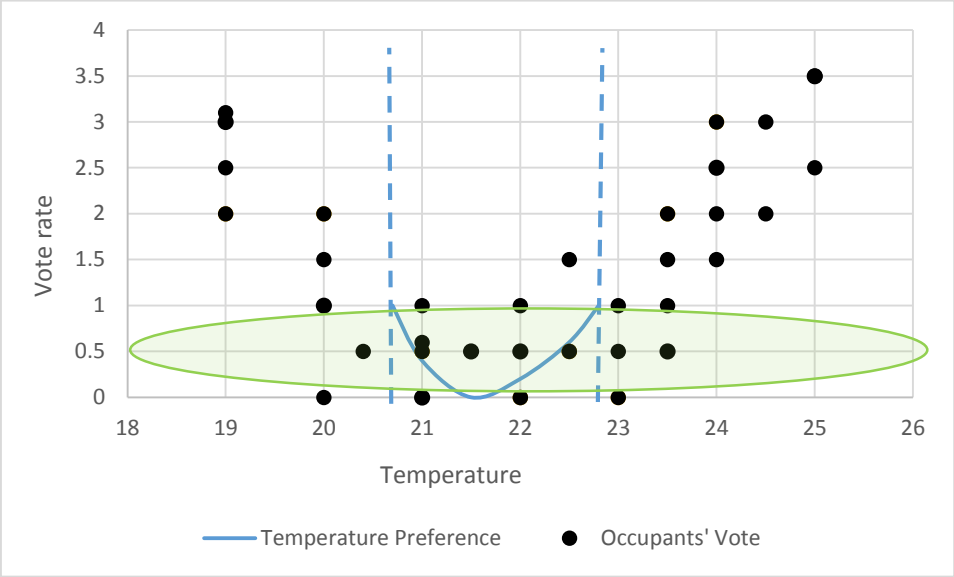

Figure 80: Thermal comfort preference test for user 3

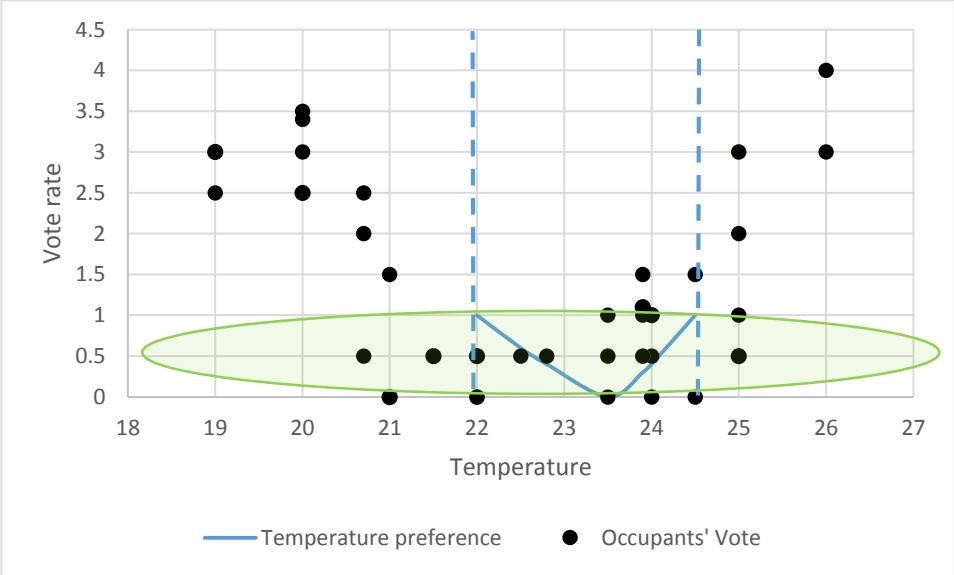

Figure 81: Thermal comfort preference test for user 7

The results of test for all nine occupants are presented in Table 19. Details of each person's survey can be found in Appendix A. It can be seen that the results extracted from the survey cover the computed thermal preference range of occupants as shown in Figure 82. In another word, the

results confirm that fuzzy map method provide a reliable range for the occupants' thermal preferences to be utilized as one of the input parameters in our intelligent control.

Table 19: Comparison of actual feeling and thermal preference profiles

Users	Number of total satisfied votes (between [0 1])	Range of Temperature for total satisfied votes (between [0 1]) ºC	Number of votes between [0 1] and inside thermal preference range	Range of thermal preference ºC
1	22	21-24.5	19	21.3-24
2	20	20 -23.6	15	21-22.5
3	19	20 -23.5	12	20.7 -22.8
4	28	21-25	17	23-25
5	18	20.6-24.5	8	21.7-23.5
6	20	20-24.5	12	20-23.5
7	26	20.7-25	17	22 -23.5
8	15	21-24	10	22.1-24.2
9	19	21-25	11	21.5-23.5

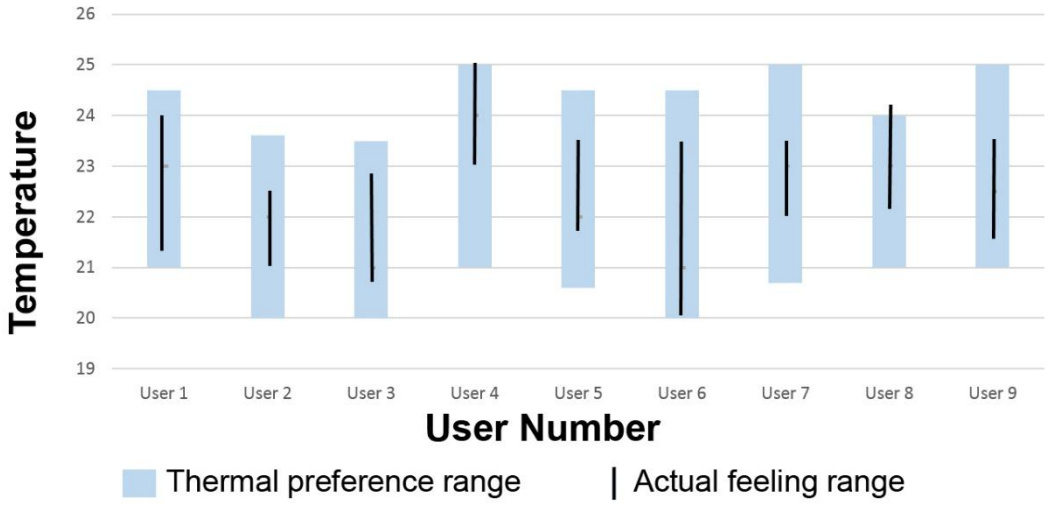

Figure 82: Comparison of actual feeling and thermal preference profiles

To evaluate how the system calculate the situation when all users in the same thermal zone present in the office, zone 1 is selected.

The related fuzzy map of all four users extracted from fuzzy survey is depicted in Figure 83.

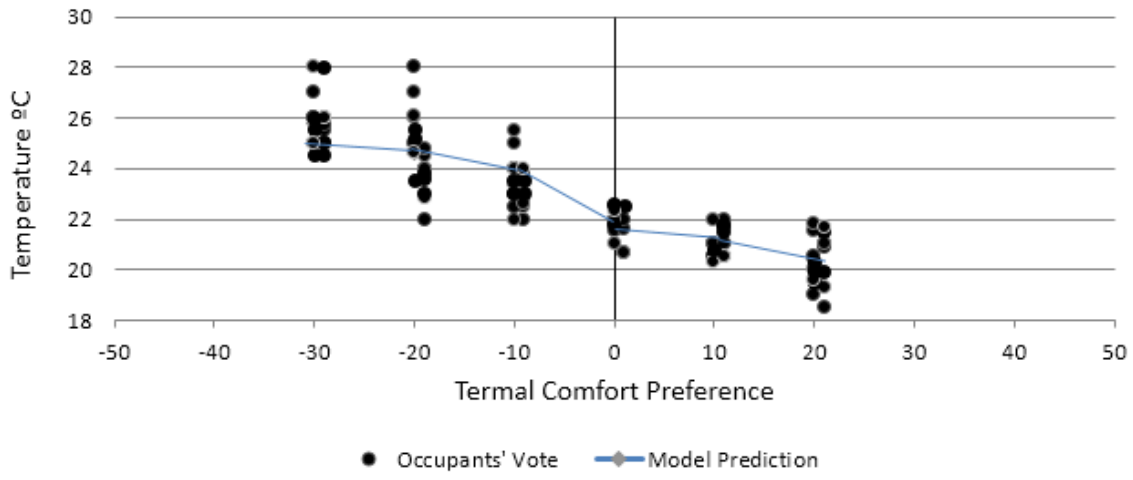

(a) Scatter graph when zone 1 is fully occupied

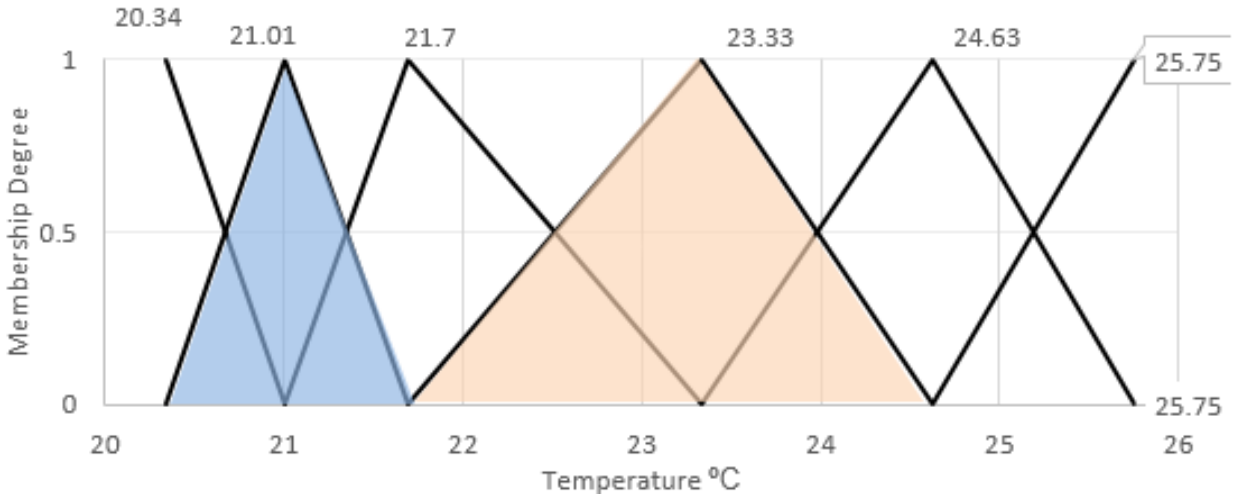

(b) Fuzzy pattern

Figure 83: Thremal preference range when one 1 is fully occupied

The fuzzy map shows the minimum, neutral and maximum range of temperatures as 21 ºC , 21.7 ºC and 23.4 ºC respectively.

To evaluate the accuracy of the fuzzy map approach, data extracted from the second survey are depicted in the form of a scatter graph as Figure 84.

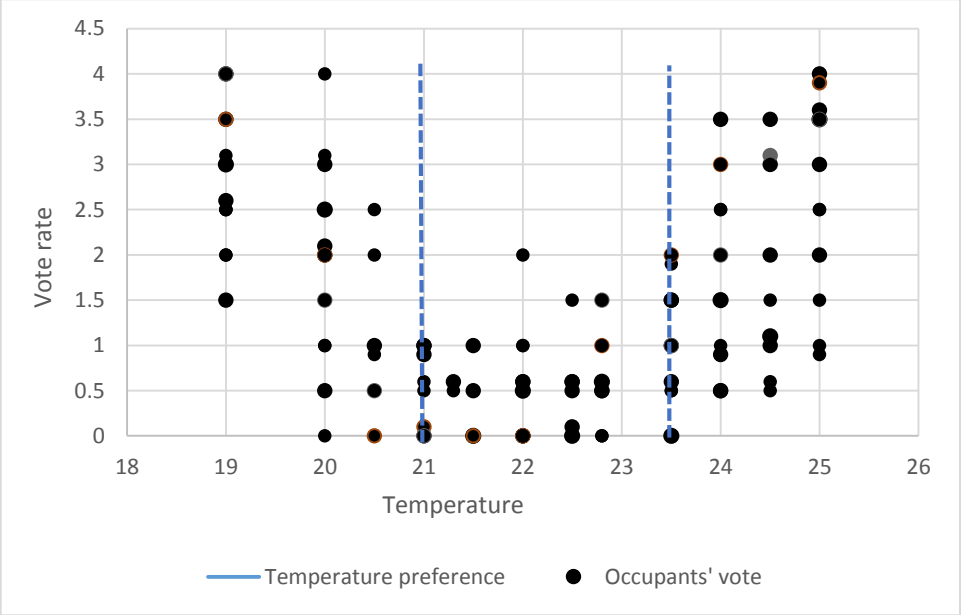

Figure 84: The second survey votes from four occupants in the same thermal zone

The total 178 votes are collected from four occupants located in the same thermal zone. Table 111 summarised the extracted results. 45 percent of total votes (81 votes) are collected in the range between 0 and 1 which represents the satisfied thermal feeling. The range of satisfied temperatures are 21 ºC and 22.8 ºC. However, in terms of percentage, 72 percent of the satisfied votes are located in the area between 21 ºC and 23.5 ºC.

Table 20: Comparison of actual feeling and thermal comfort profiles

Number of total satisfied votes (between [0 1])	Percentage	Number of votes between [0 1] and inside thermal preference range 21-23.5°C	Percentage
81	45%	59	72%

Comparing the results of fuzzy maps and the second survey shows that the fuzzy map could calculate the satisfied range of temperature while four occupants located in their thermal zones.

In the next stage of experiment, the performance of intelligent system will be analysed.

To evaluate whether occupants feel comfortable or not utilizing different HVAC strategies, the thermal sensation votes were recorded via another survey (third survey) for a period of five working days for each method. The rate of 1 to 7 corresponding to very cold to very hot should be considered. The number 4 represents the neutral point; neither hot nor cold.

Figure 85 illustrates the daily thermal sensation vote of nine occupants for the BL method during the measuring period. From the figure 85, the thermal sensation vote at the arrival time was mainly around neutral (number 4), indicating occupants feel neither hot nor cold when they arrive. The votes in the morning were gradually increased because of the rise of indoor air temperature and showed the thermal sensation vote to be very hot in the afternoon, which may be a result of direct sunlight in the afternoon and longer working period of HVACs.

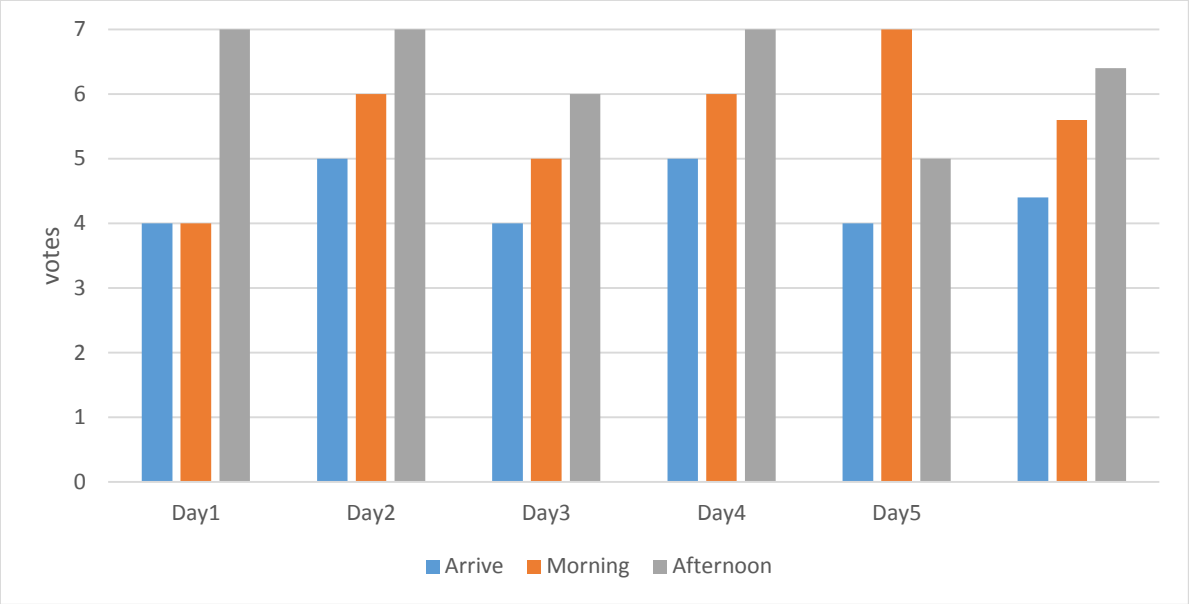

Figure 85: Daily thermal sensation vote for baseline method

Figure 86 shows the daily thermal sensation vote for duty cycle strategy. It can be observed that at the arrival time, except day 5, occupants vote as slightly cold or cold. While the morning and afternoon votes show a slight increase in the thermal sensation vote, the average remains in the cold regime. Days 3 and 4 recorded the lowest vote rate, which is likely due to the fact that these days were the coldest days during the test period.

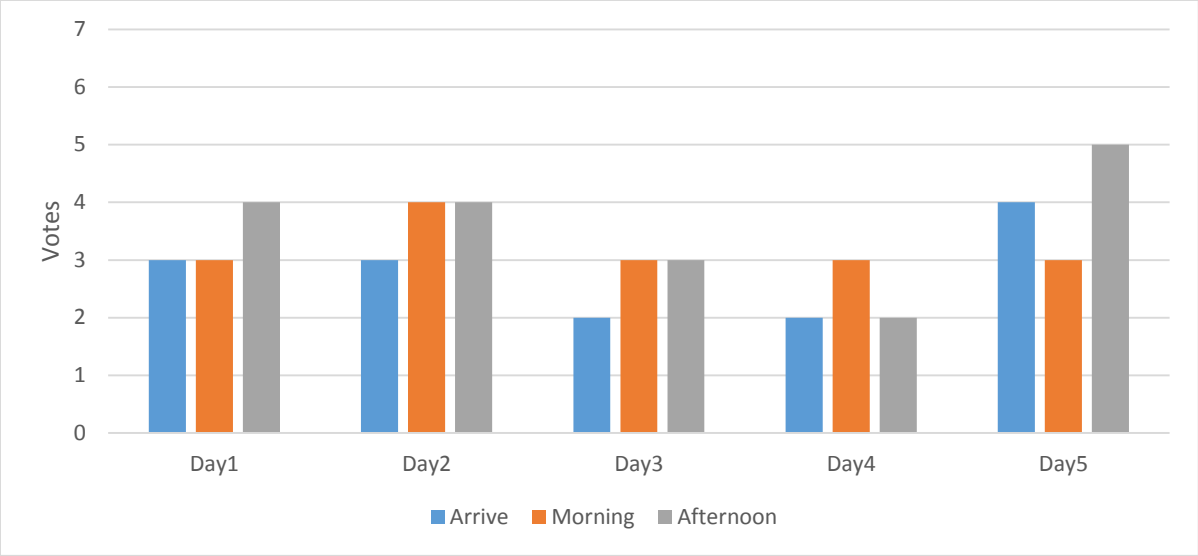

Figure 86: Daily thermal sensation vote for duty cycle method

The thermal sensation vote for the POC method is depicted in Figure 87. This figure shows a clear cold feeling at the arrival time. However, a significant increase was recorded in the morning. Even in the afternoons of the test period, occupants felt hot. The trend shows an improvement of the comfort feeling. However, occupants experienced a wide range of temperatures from *cold* to *hot* during the day, as this method was only based on occupancy data, ignoring room temperature.

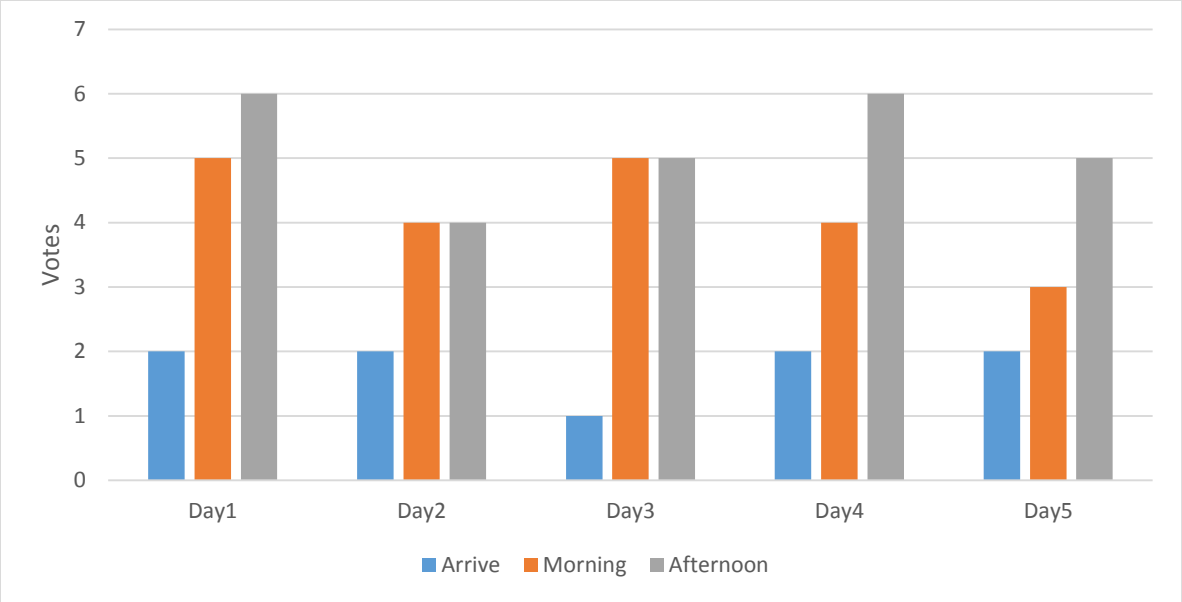

Figure 87: Thermal sensation vote for the POC method

Figure 88 shows the thermal sensation vote for the intelligent control method. At the arrival time, occupants vote for a slightly colder temperature. However, in the morning and afternoon time, the thermal sensation vote shows a significant enhancement with an average around the neutral point. In this method, there were no votes for *warm* and *hot*, showing the capability of control the temperature around the occupants' preference temperature.

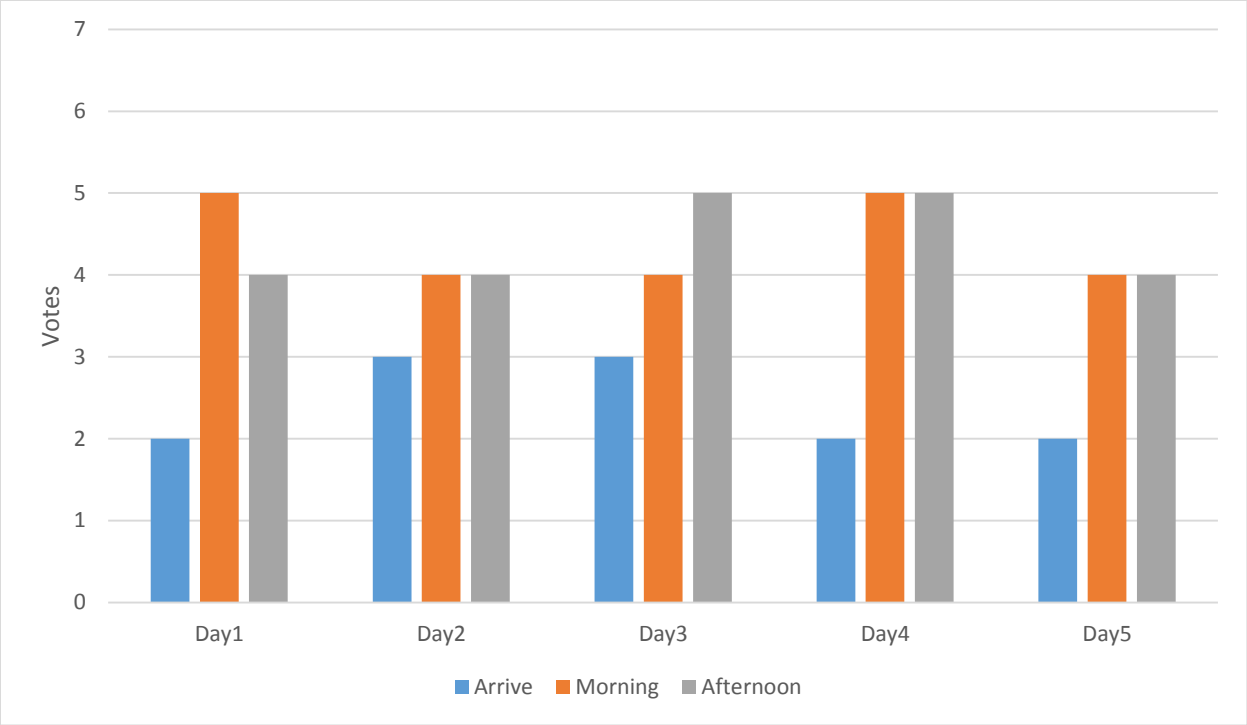

Figure 88: Thermal sensation vote for the IC strategy

The average thermal sensation vote for all methods is depicted in Figure 89. At the arrival time, the baseline strategy shows the best method to provide occupant satisfaction. The POC and IC strategies show the weakest results as these strategies were performed when the first occupant entered the room. Therefore, to achieve better thermal comfort level results for these approaches, a passive HVAC schedule is required to keep the temperature within the satisfied area before the occupants' attendance. The DC shows the cold feeling at arrival time as well. In the morning vote, all votes were improved slightly. However, the duty cycle still remains in the cold area and the BL shows a feeling from *slightly warm* to *hot.* The POC and IC strategies keep the temperature around the neutral point of neither *hot* nor *cold*.

In the afternoon records, occupants clearly felt hot in the BL method. The DC strategy shows a smooth increase, but still remains in the *cold* area. The thermal sensation for the single occupancy

method was recorded as *warm* but the IC strategy accurately kept the thermal sensation in the neutral zone.

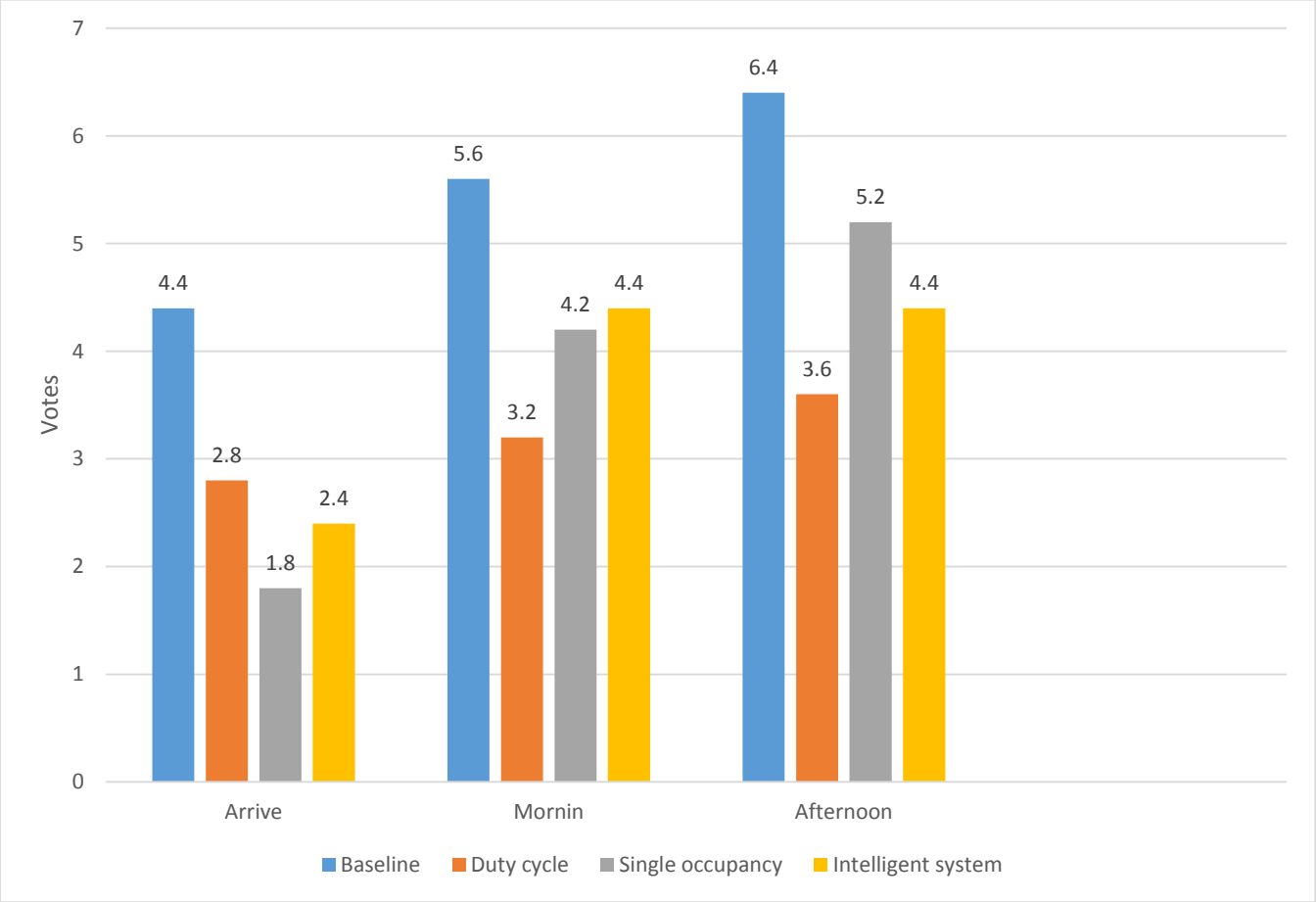

Figure 89: Thermal sensation vote for all methods

To sum up, the BL strategy provided a better comfort feeling at the arrival time. On the other hand, The IC strategy provided a good satisfaction during the morning and afternoon. By considering the energy consumption of four strategies, the IC strategy shows the highest potential of saving energy while maintaining comfort for occupants.

4.3.3 Additional Observations from users' study

During the experimental tests, the general occupants' information are collected from users who are participated in this research. The data are provided through the interview and survey from the users. Table 21 shows the information.

Table 21: User General Information

User #	Gender	Age	Type of Work/Research	Activity Level	Weight	acoustic quality	Average Temperature preference range for winter (min-Max) °C
1	M	26	Computer work	A	65	1	21.3-24
2	M	28	Research	C	66	1	21-22.5
3	M	31	Research/Lab	D	69	2	20.7-22.8
4	M	30	Research/Lab	A	64	3	23-25
5	M	32	Research	C	65	2	22.5-23.5
6	M	29	Research/Lab	C	61	3	20.5-23.5
7	M	34	Research	A	77	2	22-24.5
8	F	29	Research	B	59	1	22.1-24.2
9	F	24	Research/Lab	B	79	1	21.5-23.5

The activity level of occupants collected based on the following scales:

Activity Level:

(A) Not very Active: Spend most of the day time sitting

(B) Lightly Active: Spend good part of the day on your feet

(C) Active: Spend good part of the day doing some physical activity

(D) Very Active: Heavy physical activity

The acoustic quality scales are formed as (1) noisy (2)Normal (3)Silent

Analyzing these data can provide some assumptions and patterns which can be a guideline for future research. However, due to the small size of population, verification of findings need more investigations and a bigger population size.

1) Users 4, 7 and 8 are assigned for the highest temperatures in the maximum preference range. The age of these users are above 29 year old. In addition, users 4 and 7 rated for the activity level as "Not very active" and user 8 answered as "Lightly Active". Although, the age of users 3,5 and 6 are above 29 year old but their activity levels are "Very Active" , "Active" and "Active".
   It can be concluded that higher ages with lower activity level may lead to the higher preference temperature during the winter. Particularly, for user 4, the minimum and maximum preference temperatures are 23 ºC and 25 ºC which are the highest minimum and maximum preference temperatures compared with other users.

2) Users 2 and 3 prefer the lowest maximum temperatures by 22.5 ºC and 22.8 ºC. Their activates rate show the "Very Active" level. Therefore, the higher activity level may result in lower preference temperature. They also prefer the mostly lowest minimum temperatures by 21 ºC for user 2 and 20.7 ºC for user 3. This can be explained as their higher metabolism rate due to the activity level of them.

3) User 1 as the youngest person in the office has the maximum flexibility to the temperature changes with satisfaction range between 21.3 ºC to 24 ºC. Also this

user introduced his activity as computer work which is different with the other users in the office.

4) Users 1,2,8 and 9 are placed in the areas beside and in front of the office's door which can be a reason for their "noisy" votes.

5) Users 3,4,6 and 9 are introduced their works as research /Lab . Comparing their minimum temperature preferences show that except user 4, the minimum temperature preferences for the other ones are computed below 21.5 ºC.

Chapter 5: Conclusions, limitations and future work

In the present research a novel method is proposed to provide occupancy-driven intelligent control of HVAC based on thermal comfort. Air conditioners consume a significant part of energy consumption in buildings. An automated occupancy-driven HVAC system lead to reduction in energy usage in buildings. However, it is essential to consider the occupants' comfort level for such systems.

Occupancy information is a significant factor that influences the energy efficiency of HVAC systems. Real-time monitoring of occupants' positions provides information to avoid heating or cooling unoccupied areas in buildings. Therefore, a localization system based on ZigBee technology is utilized to collect such data. Three algorithms were used to further improve the

accuracy of the data. The near neighbour area (NNA) method was used to identify occupants in the exact room in real-time by filtering the communication signals from nodes which were not installed in the same room. Using the principle component analysis (PCA) method as a filter allowed us to remove unwanted signals and consequently achieved higher precision in monitoring results for low speed mobile targets. In static situations, the mean error after applying the PCA method was 0.83 meters, which is less than that of the original CC2431 positioning engine (1.39 meters). However, for the moving targets with high speed, PCA could not achieve the expected accuracy. Hence, the Exponential Moving Average (EMA) method was used for the moving targets in higher speed, which predict the next position based on the 10 last signals. By applying EMA filter, the significant noises from signals were removed which lead to more accurate estimating of the position.

The PCA, EMA and the default position engine in the CC2431 were compared in different speeds. The collected data indicate that a higher speeds, result in less accurate position estimation for all methods. However, the EMA method recovers from this situation better than other methods. For low and normal speeds, PCA method shows a more accurate estimation.

Based on the actual geometry of the building, a Computational Fluid Dynamics (CFD) model was built for the test bed area. The air distribution and flow, the Predicted Mean Vote (PMV) and the Predicted Percentage Dissatisfied (PPD) were calculated. Areas with a higher potential of discomfort and comfort were then identified. To verify the simulation results, surveys were carried out to investigate the real feelings of the occupants under different conditions. Consequently, different thermal zones with associated occupants were identified for the test bed area.

In addition, a personalized thermal profile was created for individuals by analysing the feedback from persons in the room about their perception of the environment in different

temperatures. Based on the presence occupants in the room, the minimum and maximum preferred temperatures are estimated and the current room temperature was checked to see if any actions were needed.

To avoid frequently turning ON and OFF HVAC systems, an occupancy pattern was created for each individual based on historical data. Semi-hidden Markov chain was used to develop the pattern and forecast the short-term or long-term of leave the office condition for each occupants.

An intelligent control was developed based on the real-time locations of the persons, occupancy pattern of individuals, thermal preference profile of occupants and the current zone temperatures.

To evaluate the proposed methodology, four control strategies were applied to a shared office occupied by nine users and equipped with two individual air conditioners: Baseline, duty cycle, purely occupancy-driven and intelligent control. The comparison of the energy consumption resulted from the baseline and IC showed that intelligent control achieved a high percentage of saving energy by 41% while maintaining the thermal comfort level. The purely occupancy-driven and duty cycle strategies showed a reduction of 29.5% and 5.25% energy usage, respectively. However, different days have different weather condition with various occupants' behaviour, which make it difficult to compare intelligent control by the baseline, accurately. Therefore, offline data were used to do further comparisons among BL, POC and IC. The results showed that the intelligent control strategy saved more energy than purely occupancy-driven strategy for about 6% based on one week data. Consequently, the purely occupancy-driven strategy was applied on the offline data extracted from the baseline strategy and showed the average reduction of about 38% from one month evaluation.

The thermal comfort level corresponding to different strategies has been evaluated as well. The results indicated that, at the arrival time, the baseline strategy provided the highest occupants satisfaction while the purely occupancy-driven and intelligent control strategies had the weakest results. Therefore, a passive heating/cooling schedule was required for these two methods to keep the temperature within the satisfied area before the occupants' attendance. From the occupants' vote, duty cycle strategy achieved a low level of satisfaction as well. In the morning, all four strategies slightly improved based on occupants' vote. The purely occupancy-driven and intelligent control strategies kept the thermal comfort around the neutral point of neither hot nor cold. However, the duty cycle strategy achieved slightly cold votes. In the afternoon records, baseline strategy showed a clear feeling hot votes. The duty cycle strategy showed a smooth increase but still remained in the cold votes. The thermal sensation for purely occupancy-driven was recorded as warm but intelligent control strategy kept the thermal sensation in the satisfied votes.

To sum up, the intelligent control strategy showed a significant energy saving while maintaining the thermal comfort level. However, in large scale buildings, developing thermal comfort model to investigate thermal zones could be a challenging task, which requires huge amount of computation. Based on the experience of the author, it is possible to categorize different rooms based on their functionality and apply the same analysis method. For example, to group rooms based on individual, shared offices and common rooms. Common rooms can be considered as classrooms, meeting rooms, coffee rooms and laboratories, which have lots of temporary occupants. The approach to control HVAC systems for such rooms is to focus on schedules and real-time occupancy detection of areas and CO2 aggregations, which can be considered as our future work. In addition, to reduce modelling work load of individual and shared offices, it is

possible to group rooms with approximately same solar illumination based on their orientations. If there is not a big difference in terms of decoration and occupants' location, it is possible to use the same model for similar office rooms.

The methodology for the study has following limitations:

i. The prototype tracking sensor which is used for positioning the occupants inside the building in this research had an inconvenient size. Therefore, it was difficult for occupants to carry it for the whole day which could affect the occupancy data and the behavioural pattern.

ii. Two patterns were needed to be extracted through the occupancy data and thermal sensation votes. In addition, those patterns are seasonal based and collecting such data require enough time. However, due to the limitation of time, adequate data may not be collected to develop accurate patterns and analyse the system in different seasons.

iii. Accurate assessment of thermal comfort level requires other parameters such as humidity and air flow rate. However, in this research, only temperature is considered for assessment purpose.

iv. Applying the proposed approach in a larger scale test area can provide more accurate comparison with existence control strategies but can also increase the cost. In this research, the test bed area with corresponding occupants are selected based on the availability and budget limitations.

In view of research work and conclusions, the following aspects provide the directions of future work for further enhancement of the proposed methodology.

i. Develop different layer for fuzzy map to consider the humidity and air flow rate

ii. Extend the investigation of the intelligent control for proportional control of HVAC systems and not only “ON” and “OFF” method.

iii. Individual user study can provide valuable information which needs more investigations.

References

[1] "INTERNATIONAL ENERGY STATISTICS," US. Energy Information Administration, [Online]. Available: https://www.eia.gov/totalenergy/data/browser/?tbl=T01.01#/?f=M. [Accessed 2 09 2017].

[2] "European Environment Agency," 2014. [Online]. Available: http://www.eea.europa.eu/data-and-maps/indicators/final-energy-consumption-by-sector-9/assessment-1. [Accessed 19 3 2017].

[3] U.S. Energy Information Administration (EIA), 2016. [Online]. Available: https://www.eia.gov/totalenergy/data/browser/?tbl=T01.01#/?f=M. [Accessed 19 3 2017].

[4] Energy Information Administration (EIA), "International Energy Outlook 2011," Washington, 2012.

[5] B. P. I. E. (BPIE), "Europe's buildings under the microscope, a country-by-country review of the energy performance of buildings, 2011," Brussels, 2011.

[6] M. Ellis and E. Mathews, "Needs and trends in building and HVAC system design tools," *Building and Environment,* vol. 37, no. 5, pp. 461-470, 2002.

[7] U. D. o. Energy, "Buildings Energy Data Book," Washington, 2012.

[8] P. Bertoldi and B. Atanasiu, "Electricity consumption and efficiency trends in the enlarged European Union," in *ES--JRC*, European Union, 2007.

[9] E. Hitchin and C. Pout, "Local cooling, global warming? UK carbon emissions from air conditioning in the next two decades," in *CIBSE*, Dublin, 2000.

[10] P. Lajoie, D. Aubin, V. Gingras, P. Daigneault, F. Ducharme, D. Gauvin, D. Fugler, J. Leclerc, D. Won, M. Courteau, S. Gingras, M. Héroux, W. Yang and H. Schleibinger, "The IVAIRE project – a randomized controlled study of the impact of ventilation on indoor air quality and the respiratory symptoms of asthmatic children in single family homes," *Indoor Air,* 2015.

[11] N. Nasrollahi, I. Knight and P. Jones, "Workplace satisfaction and thermal comfort in air conditioned office buildings: Findings from a summer survey and field experiments in Iran," *Indoor Built Environ.,* vol. 17, pp. 69-79, 2008.

[12] ASHRAE, ASHRAE handbook, Fundamentals, Atlanta, GA.: American Society of Heating, 2009.

[13] E. M. Kan, K. Yadanar, N. H. Ling, Y. Soh and N. Lin, "Multi-agent Control System with Intelligent Optimization for Building Energy Management," Singapore, 2014.

[14] A. Wagner, E. Gossauer, C. Moosmann, T. Gropp and R. Leonhart, "Thermal comfort and workplace occupant satisfaction-results of field studies in German low energy office buildings," *Energy Buil.,* vol. 39, pp. 758-769, 2007.

[15] K. Cena and R. Dear, Field study of occupant comfort and office thermal environment in a hot, arid climate, Perth,Western Australia: Murdoch University, 1999.

[16] C. Huizenga, S. Abbaszadeh, L. Zagreus and E. Arens, " Air quality and thermal comfort in office buildings: results of a large indoor environmental quality survey,," in *Proceedings of Healthy buildings*, Lisbon, 2006.

[17] H. Magdalena, G. Marco and M. Marcus, "Calibrated CFD simulation to evaluate thermal comfort in a highly-glazed naturally ventilated room," *Building and Environment,* vol. 70, pp. 73-89, 2013.

[18] L. Yang, M. Ye and B.-J. he, "CFD simulation research on residential indoor air quality," *Science of the Total Environment,* vol. 472, p. 1137–1144, 2014.

[19] C. Redlich, J. Sparer and M. Cullen, Sick-building syndrome, Lancet, 1997, pp. 1013-1016.

[20] C. Lin, M. J. Chiu, C. Hsiao, R. Lee and Y. Tsai, "Wireless Health Care Service System for Elderly With Dementia," *IEEE Transactions on Information Technology in Biomedicine,* vol. 10, no. 4, pp. 696-704, 2006.

[21] C. Jihong, "Patient Positioning System in Hospital Based on Zigbee," in *2011 International Conference on Intelligent Computation and Bio-Medical Instrumentation*, Wuhan, Hubei, 2011.

[22] J. Deshmukh and U. Shinde, "A low cost environment monitoring system using raspberry Pi and arduino with Zigbee," in *2016 International Conference on Inventive Computation Technologies (ICICT)*, Coimbatore, 2016.

[23] C. Yuan, L. Fei, C. Jianxin and J. Wei, "A smart parking system using WiFi and wireless sensor network," in *2016 IEEE International Conference on Consumer Electronics-Taiwan (ICCE-TW)*, Nantou, 2016.

[24] M. Pazhoohesh and C. Zhang, "AUTOMATED CONSTRUCTION PROGRESS MONITORING USING THERMAL IMAGES AND WIRELESS SENSOR NETWORKS," in *CSCE 2015, Building on Our Growth Opportunities*, Regina, Canada, 2015.

[25] W. Roozing and A. Göktoğan, "Low-cost vision-based 6-DOF MAV localization using IR beacons," in *2013 IEEE/ASME International Conference on Advanced Intelligent Mechatronics*, Wollongong, NSW, 2013.

[26] T. Fujisawa and K. Saitoh, "Material Gain Analysis of GeSn/SiGeSn Quantum Wells for Mid-Infrared Si-Based Light Sources Based on Many-Body Theory," *IEEE Journal of Quantum Electronics,* vol. 51, no. 5, pp. 1-8, 2015.

[27] K. Khoshelham, "Automated Localization of a Laser Scanner in Indoor Environments Using Planar Objects," in *Proceedings of the 2010 International Conference on Indoor Positioning and Indoor Navigation (IPIN)*, Campus Science City, ETH Zurich, Switzerland, 2010.

[28] J. Larrañaga, L. Muguira, J. Lopez-Garde and J. Vazquez, "An Environment Adaptive ZigBee-Based Indoor Positioning Algorithm," in *Proceedings of the 2010 International Conference on Indoor Positioning and Indoor Navigation (IPIN)*, Campus Science City, ETH Zurich, Switzerland, 2010.

[29] J. Zhou and J. Shi, "RFID localization algorithms and applications-a review," *Journal of Intelligent Manufacturing,* vol. 20, no. 6, pp. 695-707, 2009.

[30] A. Danjo, Y. Watase and S. Hara, "A Theoretical Error Analysis on Indoor TOA Localization Scheme Using Unmanned Aerial Vehicles," in *2015 IEEE 81st Vehicular Technology Conference (VTC Spring)*, Glasgow, 2015.

[31] Y. Ma, K. Pahlavan and Y. Geng, "Comparison of POA and TOA based ranging behavior for RFID application," in *2014 IEEE 25th Annual International Symposium on Personal, Indoor, and Mobile Radio Communication (PIMRC)*, Washington, DC, 2014.

[32] M. Pelka and H. Hellbrück, "S-TDoA — Sequential time difference of arrival — A scalable and synchronization free approach forl Positioning," in *2016 IEEE Wireless Communications and Networking Conference*, Doha, 2016.

[33] S. Bohidar, S. Behera and C. Tripathy, "A comparative view on received signal strength (RSS) based location estimation in WSN," in *2015 IEEE International Conference on Engineering and Technology (ICETECH)*, Coimbatore, 2015.

[34] R. Zheng Sun, R. Farley, T. Kaleas, J. Ellis and K. Chikkappa, "Cortina: Collaborative context-aware indoor positioning employing RSS and RToF techniques," in *2011 IEEE International Conference on Pervasive Computing and Communications Workshops (PERCOM Workshops)*, Seattle, WA, 2011.

[35] S. Roy and M. Nene, "Prevention of node replication in Wireless Sensor Network using Received Signal Strength Indicator, Link Quality Indicator and Packet Sequence Number," in *2016 Online International Conference on Green Engineering and Technologies (IC-GET)*, Coimbatore, 2016.

[36] S. Tomic, M. Beko and R. Dinis, "Distributed RSS-AoA Based Localization With Unknown Transmit Powers," *IEEE Wireless Communications Letters,* vol. 5, no. 4, pp. 392-395, 2016.

[37] T. Rappaport, Wireless Comminations-Principles and Practice Prentice Hall communications engineering and emerging technologies series, Dorling Kindersley, 2009.

[38] A. Aswani, M. Master, J. Taneja, D. Culler and C. Tomlin, "Reducing Transient and Steady State Electricity Consumption in HVAC Using Learning-Based Model-Predictive Control," in *in Proceedings of the IEEE*, 2012.

[39] Y. Agarwal, B. Balaji, S. Dutta, R. Gupta and T. Weng, "Duty-cycling buildings aggressively: The next frontier in HVAC control," in *Proceedings of the 10th ACM/IEEE International Conference on Information Processing in Sensor Networks*, Chicago, IL, 2011.

[40] H. Jo, J. Lee and S. Joo, "Scheduling of air-conditioner using occupancy prediction in a smart home/building environment," in *2014 IEEE International Conference on Consumer Electronics (ICCE)*, Las Vegas, NV, 2014.

[41] N. Nassif and S. Moujaes, "A cost-effective operating strategy to reduce energy consumption in a HVAC system," *International Journal of Energy Research,* vol. 32, pp. 543-558, 2008.

[42] L. Ciabattoni, G. Cimini, F. Ferracuti, M. Grisostomi, G. Ippoliti and M. Pirro, "Indoor thermal comfort control through fuzzy logic PMV optimization," in *International Joint Conference on Neural Networks (IJCNN)*, Killarney, 2015.

[43] N. Nassif, S. Kajl and R. Sabourin, "Two-objective on-line optimization of supervisory control strategy," *Building Services Engineering Research and Technology,* vol. 25, p. 241–251, 2004.

[44] S. Papadopoulos and E. Azar, "Optimizing HVAC operation in commercial buildings: A genetic algorithm multi-objective optimization framework," in *Winter Simulation Conference (WSC)*, Washington, DC, 2016.

[45] T. Songuppakarn, W. Wongsuwan and W. San-um, "Artificial neural networks based prediction for thermal comfort in an academic classroom," in *International Conference and Utility Exhibition on Green Energy for Sustainable Development (ICUE)*, Pattaya, 2014.

[46] T. Yu and C. Lin, "An Intelligent Wireless Sensing and Control System to Improve Indoor Air Quality: Monitoring, Prediction, and Preaction," *International Journal of Distributed Sensor Networks,* vol. 11, no. 8, 2015.

[47] M. Nowak and A. Urbaniak, "Utilization of intelligent control algorithms for thermal comfort optimization and energy saving," in *12th International Carpathian Control Conference (ICCC)*, Velke Karlovice, 2011.

[48] R. Freire, G. Oliveira and N. Mendes, "Predictive controllers for thermal comfort optimization and energy savings," *Energy and Buildings,* vol. 40, p. 1353–1365, 2008.

[49] P. Ferreira, A. Ruano, S. Silva and E. Conceição, "Neural networks based predictive control for thermal comfort and energy savings in public buildings," *Energy and Buildings,* vol. 55, p. 238–251, 2012.

[50] G. Brager and R. de Dear, "Thermal adaptation in the built environment: a literature review," *Energy and Buildings,* vol. 27, p. 83–96, 1998.

[51] W. Guo and M. Zhou, "Technologies toward thermal comfort-based and energy-efficient HVAC systems: A review," in *IEEE International Conference on Systems, Man and Cybernetics*, San Antonio, TX, 2009.

[52] F. Jazizadeh, A. Ghahramani, B. Becerik-Gerber, T. Kichkaylo and M. Orosz, "User-led decentralized thermal comfort driven HVAC operations for improved efficiency in office buildings.," *Energy and Buildings,* vol. 70, pp. 398-410, 2014.

[53] D. Daum, F. Haldi and N. Morel, "A personalized measure of thermal comfort for building controls," *Building and Environment,* vol. 46, no. 1, pp. 3-11, 2011.

[54] M. Feldmeier and J. Paradiso, "Personalized HVAC control system," in *2010 Internet of Things (IOT), IEEE*, Tokyo, 2010.

[55] V. Erickson and A. Cerpa, "Thermovote: participatory sensing for efficient building hvac conditioning," in *In Proceedings of the Fourth ACM Workshop on Embedded Sensing Systems for Energy-Efficiency in Buildings*, 2012.

[56] Y. Murakami, M. Terano, K. Mizutani, M. Harada and S. Kuno, "Field experiments on energy consumption and thermal comfort in the office environment controlled by occupants' requirements from PC terminal," *Building and Environment,* vol. 42, pp. 4022-4027, 2007.

[57] V. Erickson, M. Carreira-Perpiñán and A. Cerpa, "OBSERVE: Occupancy-based system for efficient reduction of HVAC energy," in *Proceedings of the 10th ACM/IEEE International Conference on Information Processing in Sensor Networks*, Chicago, 2011.

[58] E. Marshall, J. Steinberger, T. Foxon and V. Dupont, "Modelling the Delivery of Residential Thermal Comfort and Energy Savings: Comparing How Occupancy Type Affects the Success of Energy Efficiency Measures," *Sustainable Ecological Engineering Design,* pp. 327-339, 2016.

[59] L. Klein, J. Kwak, G. Kavulya, F. Jazizadeh, B. Becerik-Gerber and M. Tambe, "Coordinating occupant behavior for building energy and comfort management using multi-agent system," *Automation in Construction,* vol. 22, p. 525–536, 2012.

[60] L. Jolliffe, Principal Component Analysis, Springer Series in Statistics, 2002.

[61] M. Pazhoohesh and C. Zhang, "A Practical Localization System Based on principal component analysis," in *2nd World Congress on Computer Applications and Information Systems*, Hammamet, Tunisia, 2015.

[62] G. Arce, Nonlinear Signal Processing: A Statistical Approach, New Jersey, USA: Wiley, 2005.

[63] S. Kay, Fundamental of Statistical Signal Processing, Prentice Hall, 1993.

[64] M. Pazhoohesh, R. Shahmir Nizam and C. Zhang, "Investigating thermal comfort and occupants position impacts on building sustainability using CFD and BIM," in *49th International Conference of the Architectural Science Association*, Australia, 2015.

[65] H. Heierman, G. Youngblood and D. Cook, "Mining Temporal Sequences to Discovery Interesting Patterns," KDD Workshop on Mining Temporal and Sequential Data, 2004.

[66] R. Bathoorn, A. Koopman and A. Siebes, "Frequent Patterns that Compress, Technical Report," Utrecht University, 2006.

[67] T. Duong, D. Phung, H. Bui and S. Venkatesh, "Efficient duration and hierarchical modeling for human activity recognition," *Artificial Intelligence,* vol. 173, no. 7, pp. 830-856, 2009.

[68] S. Yu and H. Kobayashi, "An Efficient Forward-Backward Algorithm for an Explicitduration HMM," *IEEE Signal Processing,* 2003.

[69] S. P. Meyn and R. L. Tweedie, Markov Chains and Stochastic Stability, Cambridge University Press, 2009.

[70] J. Nicol, A Handbook of Adaptive Thermal Comfort: Towards a Dynamic Model Low Energy Architecture Research Unit, London: London Metropolitan University, 2008.

[71] S. Guillaume, "Designing fuzzy inference systems from data: An interpretability oriented," *IEEE Transactions on Fuzzy Systems,* vol. 9, no. 3, pp. 426-443, 2001.

[72] L. Wang and J. Mendel, "Generating fuzzy rules by learning from examples," *IEEE Transactions on systems, man, and cybernetics,* vol. 22, no. 6, pp. 1414-1427, 1991.

[73] L. Wang, "The WM method completed: A flexible fuzzy system approach to data mining," *IEEE Trans. Fuzzy Syst.,* vol. 11, no. 6, pp. 768-782, 2003.

[74] M. Kaviany, Principles of Heat Transfer, New York: John Wiley & Sons, 2002.

[75] N. Koutsourakis, J. Bartzis and N. Markatos, "Evaluation of Reynolds stress, k-ε and RNG k-ε turbulence models in street canyon flows using various experimental datasets," *Environmental fluid mechanics,* pp. 1-25, 2012.

[76] B. Moshfegh and R. Nyiredy, "Comparing RANS models for flow and thermal analysis of pin fin heat sinks," in *15th Australasian Fluid Mechanics Conference*, Sydney, Australia, 2004.

[77] E. I. 7730, "Moderate thermal environments—analytical determination and interpretation of thermal comfort using calculation of the PMV and PPD indices and local thermal comfort," 2005.

[78] B. Akinic, F. Boukamp, C. Gordon, D. Huber, C. Lyons and K. Park, "A formalism for utilization of sensor systems and integrated project models for active construction quality control," *Automation in Construction,* vol. 15, no. 2, pp. 124-138, 2006.

[79] C. Gordon, F. Boukamp, D. Huber, E. Latimer, K. Park and B. Akinci, "Combining reality capture technologies for construction defect detection: A case study," Istanbul, Turkey, 2003.

[80] H. Park, H. Lee, H. Adeli and I. Lee, "A new approach for health monitoring of structures: terrestrial laser scanning," *Comput. Aided Civ. Infrastruct. Eng.,* vol. 22, no. 1, pp. 19-30, 2007.

[81] F. Bosche, "Automated recognition of 3D CAD model objects in laser scans and calculation of as-built dimentions for dimensional compliance control in construction," *Adv. Eng. Inf.,* vol. 24, no. 1, pp. 107-118, 2010.

[82] F. Bosche, C. Hass and B. Akinci, "Automated Recognition of 3D CAD objects in site laser scan for project 3D status visualization and performance control," *ASCE J.COMPUTING CIVIL Eng.,* vol. 23, no. 6, pp. 391-404, 2009.

[83] Y. Turkan, F. Bosche, C. T. Haas and R. Haas, "Automated progress tracking using 4D schedule and 3D sensing technologies," *Automation in Construction,* vol. 22, p. 414–421, 2012.

[84] S. Kiziltas, B. Akinci, E. Ergen and P. Tang, "Technological assessment and process implications and field data capture technologies for construction and facility/infrastructure management," *J. Inf. Technol. Constr.,* vol. 13, pp. 134-154, 2008.

[85] J. Neto, D. Arditi and M. Evens, "Using colors to detect structural components in digital pictures," *Comp. Aided Civ. Infrastruct. Eng.,* vol. 17, no. 1, pp. 61-67, 2002.

[86] J. Zou and H. Kim, "Using HSV color based space for construction equipment idle time analysis," *J. Comput. Civ. Eng.,* vol. 21, no. 4, pp. 238-246, 2007.

[87] M. Golparvar-Fard, F. Pena-Mora, C. Alboleda and S. Lee, "Visualization of construction progress monitoring with 4D simulation model overlaid on time-lapsed photographs," *J. Comput. Civ. Eng.,* vol. 23, no. 6, pp. 391-404, 2009.

[88] A. Braun, S. Tuttas, A. Borrmann and U. Stilla, "Automated progress monitoring based on photogrammetric point clouds and precedence relationship graphs," in *The 32nd International Symposium on Automation and Robotics in Construction and Mining (ISARC 2015)*, Oulu, Finnland, 2015.

[89] X. a. Zhang,, "Automating progress measurement of construction projects," *Automation in Construction,* vol. 18, no. 3, pp. 294-301, 2009.

[90] T. Lukins and E. Trucco, "Towards automatted visual assessment of progress in construction projects," Warwick,UK, 2007.

[91] S. Ocaña, I. Guerrero and I. Requena, "Thermographic survey of two rural buildings in Spain," *Energy and Buildings,* vol. 36, no. 6, pp. 515-523, 2004.

[92] Y. Ham and M. Golparvar-Fard, "An automated vision-based method for rapid 3D energy performance modeling of existing buildings using thermal and digital imagery," *Advanced Engineering Informatics,* vol. 27, no. 3, pp. 395-409, 2013.

[93] C. Wang, Y. Cho and M. Gai, "As-is 3D thermal modeling for existing building envelopes using a hybrid LIDAR system," *Journal of Computing in Civil Engineering,* vol. 27, no. 6, pp. 645-656, 2012.

[94] S. Lagüela, L. Díaz-Vilariño, J. Martínez and J. Armesto, "Automatic thermographic and RGB texture of as-built BIM for energy rehabilitation purposes," *Automation in Construction,* vol. 31, pp. 230-240, 2013.

[95] S. Lagüela, L. Diaz-Vilarino, D. Roca and J. Armesto, "Aerial oblique thermographic imagery for the generation of building 3D models to complement Geographic Information Systems," in *Proc. of QIRT'14.*, 2014.

[96] a. Dimitrov and M. Golparvar-Fard, "Vision-based material recognition for automated monitoring of construction progress and generating building information modeling from unordered site image collections," *Advanced Engineering Informatics,* vol. 28, no. 1, pp. 37-49, 2014.

[97] H. González-Jorge, S. Lagüela, P. Krelling, J. Armesto and J. Martínez-Sánchez, "Single image rectification of thermal images for geometric studies in façade inspections," *Infrared Physics & Technology,* vol. 55, no. 3, pp. 421-426, 2012.

[98] D. González-Aguilera, S. Lagüela, P. Rodríguez-Gonzálvez and D. Hernández-López, "Image-based thermographic modeling for assessing energy efficiency of buildings façades," *Energy and Buildings,* vol. 65, pp. 29-36, 2013.

[99] P. Bison, A. Bortolin, G. Cadelano, G. Ferrarini, K. Furlan and E. Grinzato, "Geometrical correction and photogrammetric approach in thermographic inspection of buildings," in *In 11th International Conference on Quantitative InfraRed Thermography*, 2012.

[100] M. Pazhoohesh and C. Zhang, "Automated construction progress monitoring using thermal images and wireless sensor networks," in *CSCE 2015, Building on Our Growth Opportunities*, Regina, Canada, 2015.

[101] M. Zeiler, Modeling Our World: The ESRI Guide to Geodatabase Design, ESRI, Inc., 1999.

[102] M. Golparvar-Fard, F. Peña-Mora and S. Savarese, "Automated Progress Monitoring Using Unordered Daily Construction Photographs and IFC-Based Building Information Models," *Journal of Computing in Civil Engineering*, vol. 29, no. 1, 2015.

[103] M. Elfeky and A. Lemagarmid, "Periodicity Detection in Time Series Databases," *IEEE Trans. on Knowl. and Data Eng.*, vol. 17, pp. 875-887, 2005.

[104] M. Pazhoohesh and C. Zhang, "Building Energy Management based on occupant location," in *Sustainable Buildings and Structures: Proceedings of the 1st International Conference on Sustainable Buildings and Structures*, Suzhou, P.R. China, 2015.

Appendix A

Comparison of thermal preference profile and actual feeling of nine occupants

User 1

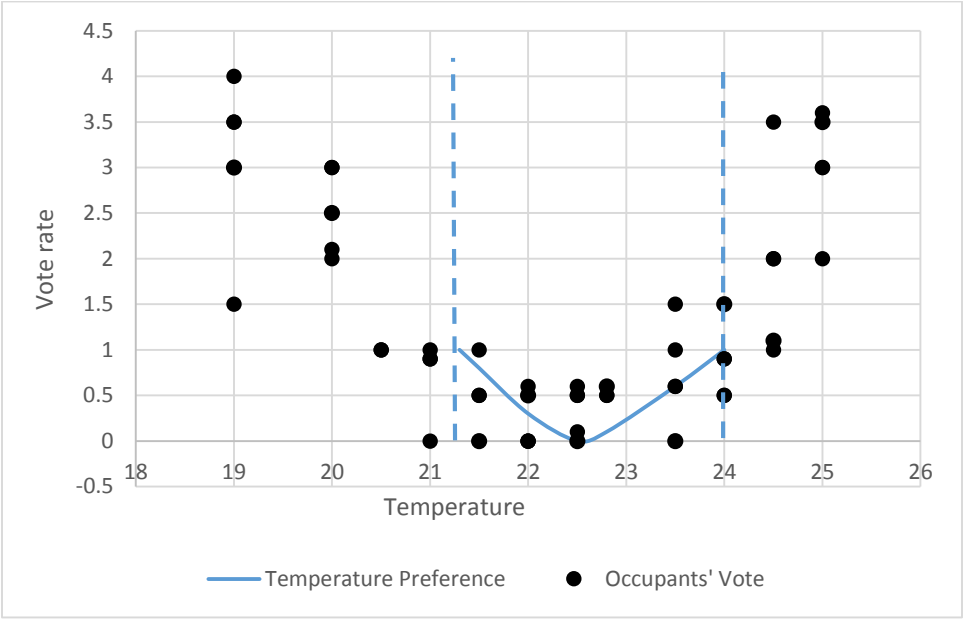

User 2

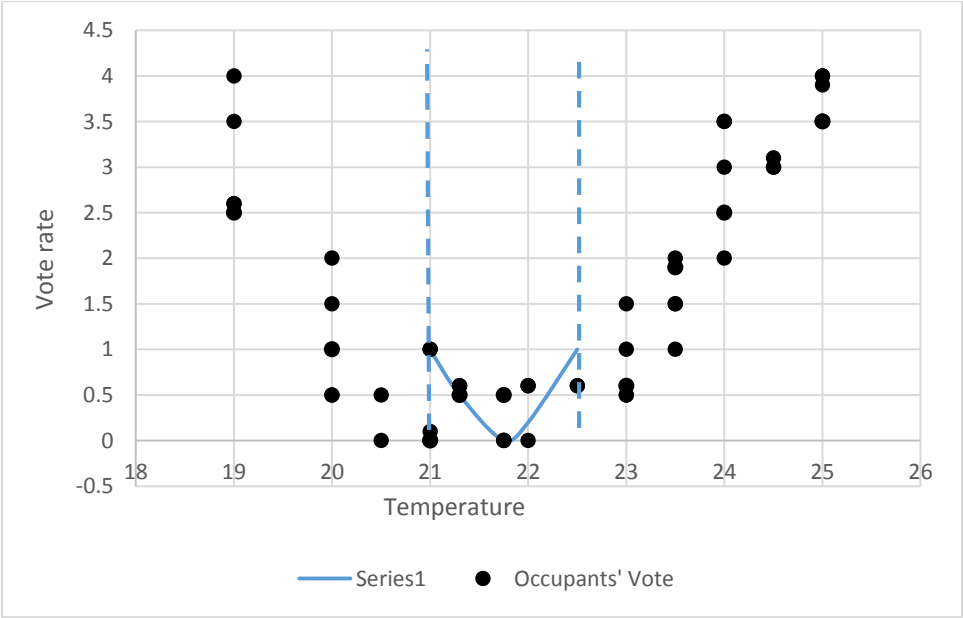

User 4

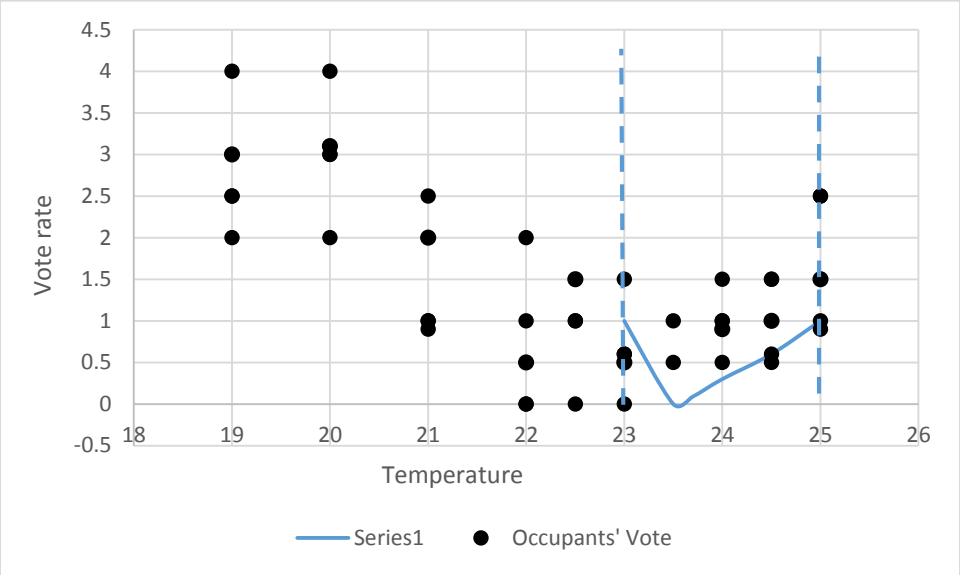
4.5
4
3.5
3
2.5
2
1.5
1
0.5
0
-0.5
18
19
20
21
22
23
24
25
26
Vote rate
Temperature
Series1
Occupants' Vote

User 5

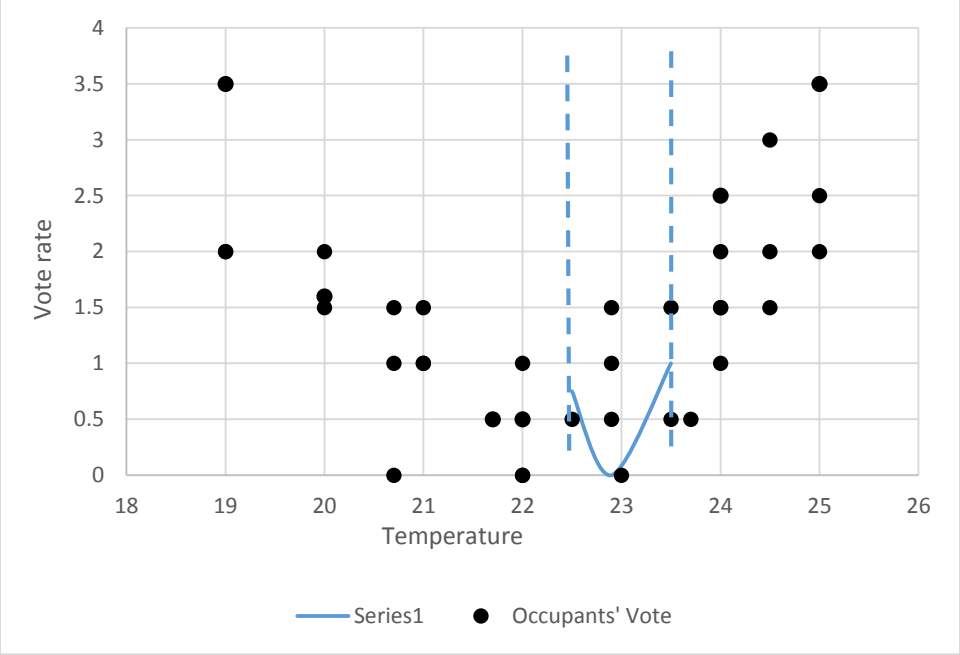
4
3.5
3
2.5
2
1.5
1
0.5
0
18
19
20
21
22
23
24
25
26
Vote rate
Temperature
Series1
Occupants' Vote

User 6

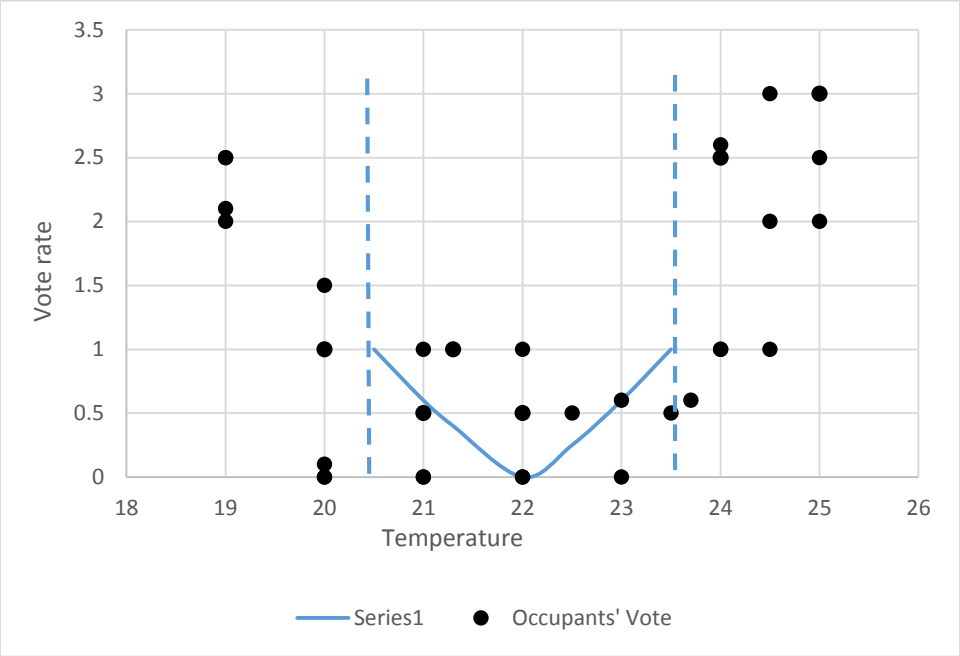
3.5
3
2.5
2
1.5
1
0.5
0
Vote rate
18
19
20
21
22
23
24
25
26
Temperature
Series1
Occupants' Vote

User 8

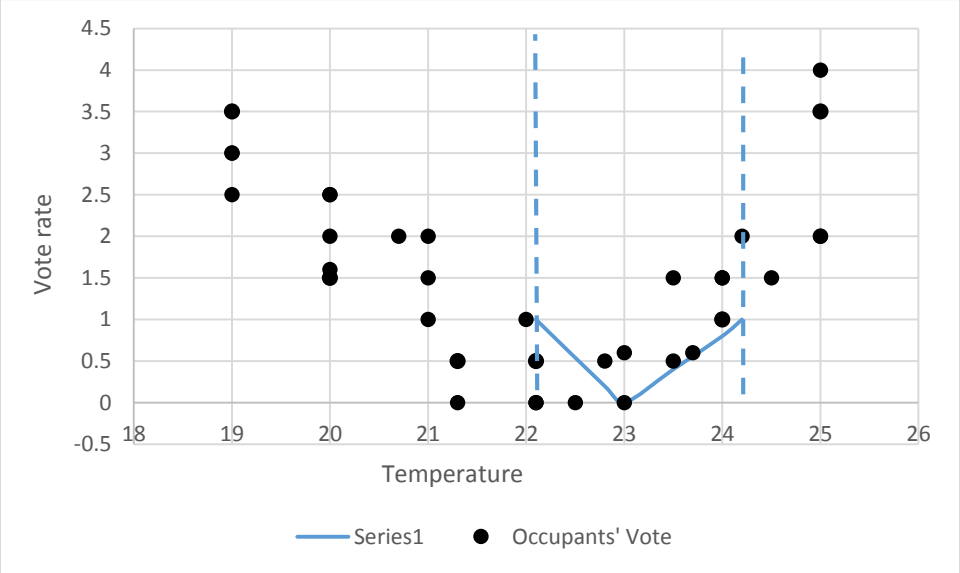
4.5
4
3.5
3
2.5
2
1.5
1
0.5
0
-0.5
Vote rate
18
19
20
21
22
23
24
25
26
Temperature
Series1
Occupants' Vote

User 9

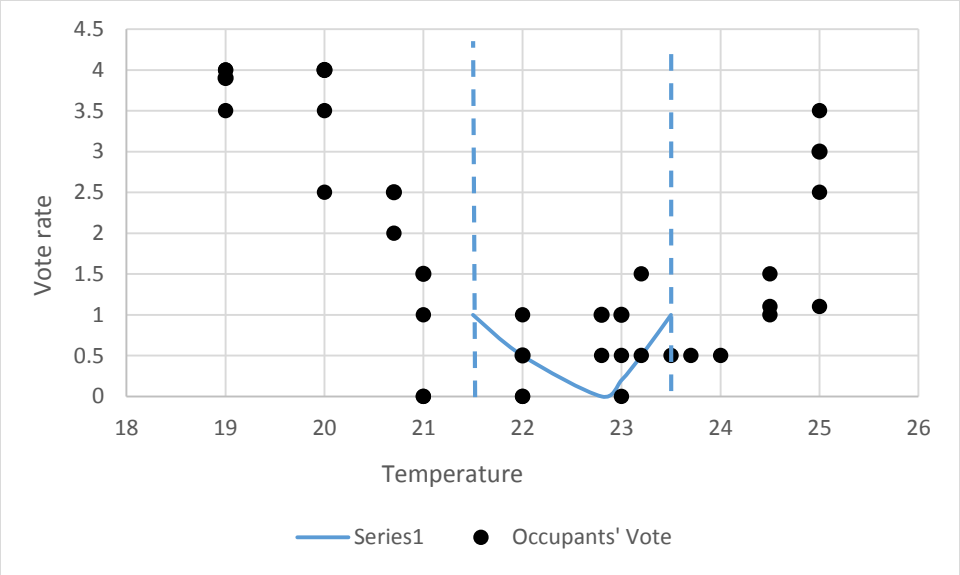
4.5
4
3.5
3
2.5
2
1.5
1
0.5
0
Vote rate
18
19
20
21
22
23
24
25
26
Temperature
Series1
Occupants' Vote

Appendix B

Winter room CFD modelling:

Scenario 1: Both HVACs are turned ON

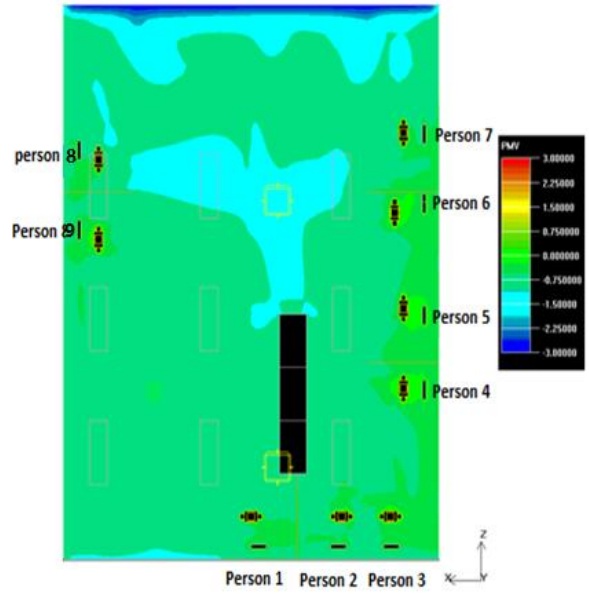

Predicted Mean Vote (PMV) model

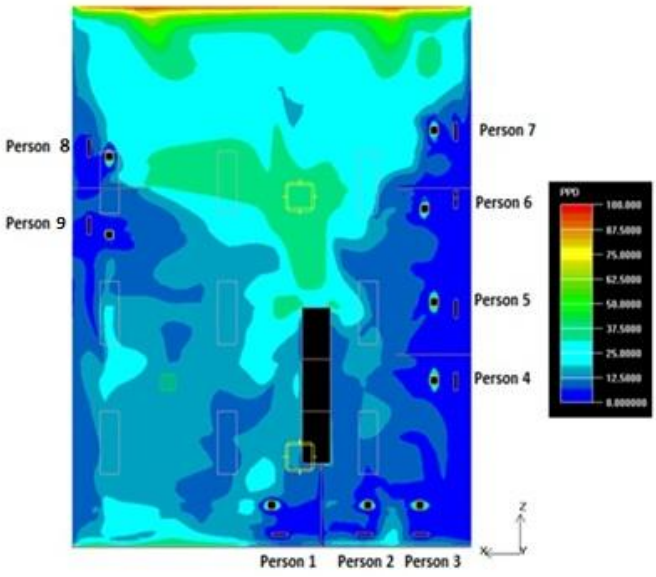

Predicted Percentage Dissatisfied (PPD) model

Scenario 2: HVAC 1 is turned ON

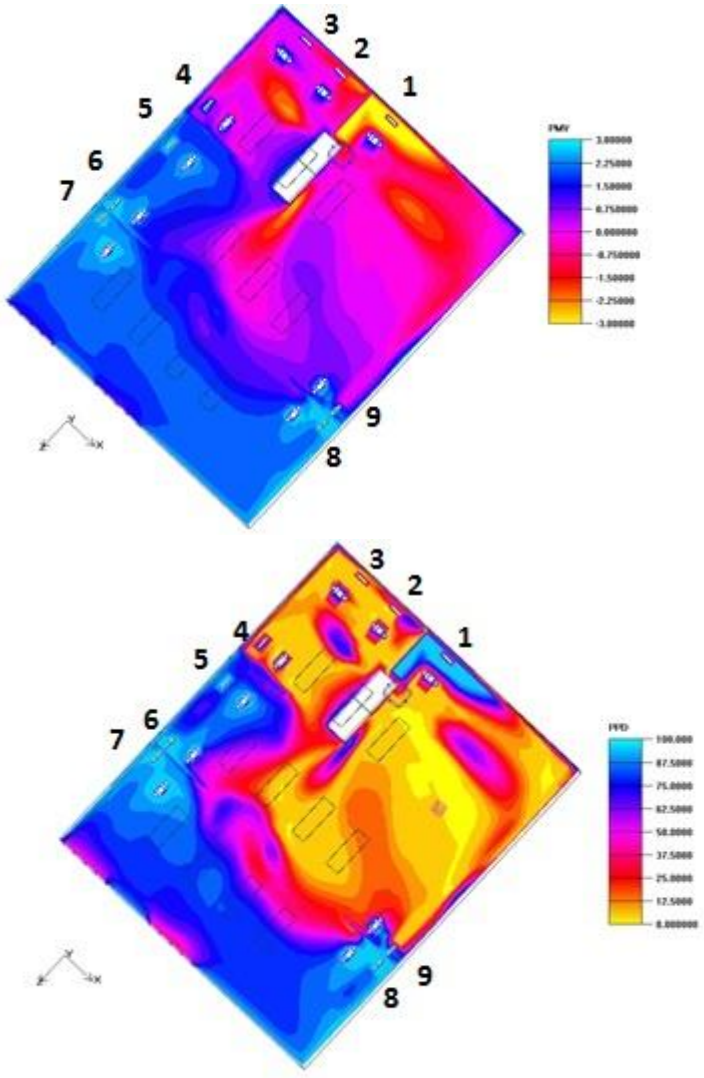

Modelling of the room when HVAC-1 is ON

Scenario 3: HVAC 2 is turned ON

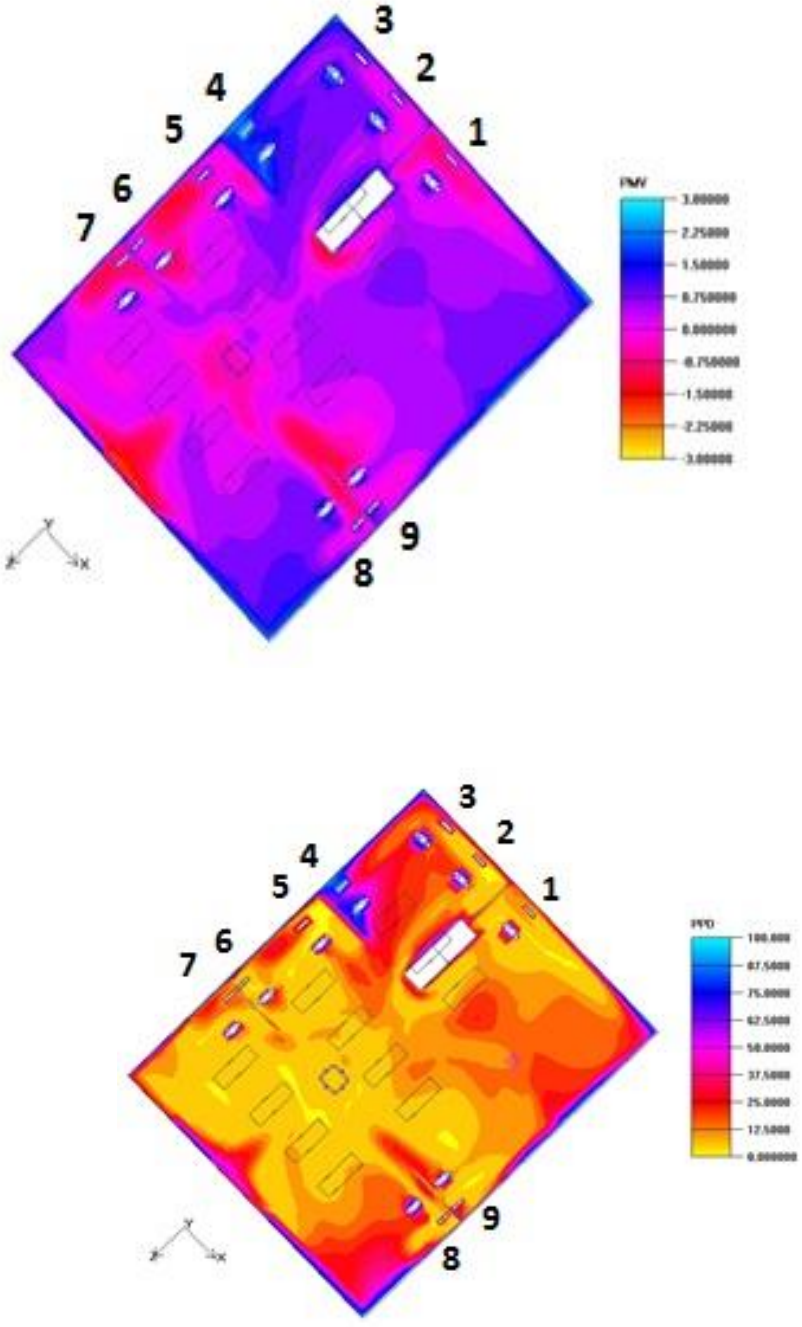

Modelling of the room when HVAC-2 is ON

Appendix C

One week occupancy data based on individuals:

User 1:

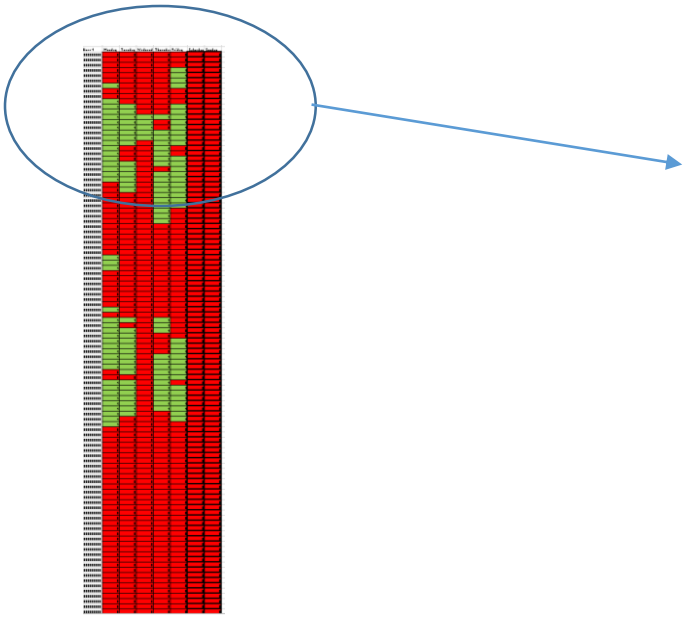

User 1	Monday	Tuesday	Wednesd	Thursday	Friday	Saturday	Sunday
06:00:00 AM	0	0	0	0	0	0	0
06:10:00 AM	0	0	0	0	0	0	0
06:20:00 AM	0	0	0	0	0	0	0
06:30:00 AM	0	0	0	0	1	0	0
06:40:00 AM	0	0	0	0	1	0	0
06:50:00 AM	0	0	0	0	1	0	0
07:00:00 AM	1	0	0	0	1	0	0
07:10:00 AM	0	0	0	0	0	0	0
07:20:00 AM	0	0	0	0	0	0	0
07:30:00 AM	1	0	0	0	0	0	0
07:40:00 AM	1	1	0	0	1	0	0
07:50:00 AM	1	1	0	0	1	0	0
08:00:00 AM	1	1	1	1	1	0	0
08:10:00 AM	1	1	1	0	1	0	0
08:20:00 AM	1	1	1	0	1	0	0
08:30:00 AM	1	1	1	1	1	0	0
08:40:00 AM	1	1	1	1	1	0	0
08:50:00 AM	1	1	0	1	1	0	0
09:00:00 AM	1	0	0	1	0	0	0
09:10:00 AM	1	0	0	1	0	0	0
09:20:00 AM	1	0	0	1	1	0	0
09:30:00 AM	1	1	0	1	1	0	0
09:40:00 AM	1	1	0	0	1	0	0
09:50:00 AM	1	1	0	1	1	0	0
10:00:00 AM	1	1	0	1	1	0	0
10:10:00 AM	0	1	0	1	1	0	0
10:20:00 AM	0	1	0	1	1	0	0
10:30:00 AM	0	0	0	1	1	0	0
10:40:00 AM	0	0	0	1	1	0	0
10:50:00 AM	0	0	0	1	1	0	0
11:00:00 AM	0	0	0	1	0	0	0
11:10:00 AM	0	0	0	1	0	0	0
11:20:00 AM	0	0	0	1	0	0	0
11:30:00 AM	0	0	0	0	0	0	0
11:40:00 AM	0	0	0	0	0	0	0
11:50:00 AM	0	0	0	0	0	0	0
12:00:00 PM	0	0	0	0	0	0	0
12:10:00 PM	0	0	0	0	0	0	0
12:20:00 PM	0	0	0	0	0	0	0

User 2:

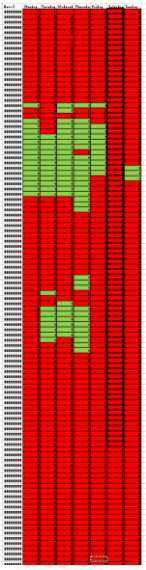

User 3:

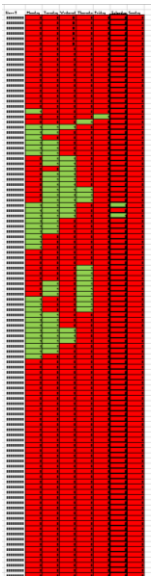

User 4:

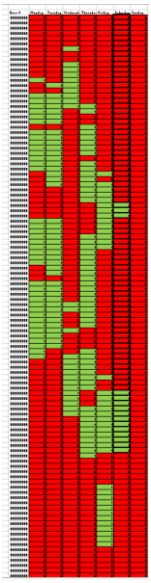

User 5:

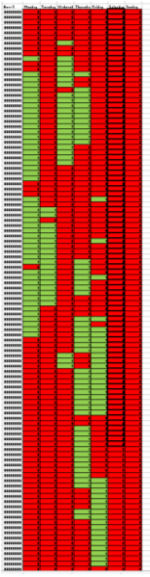

User 6:

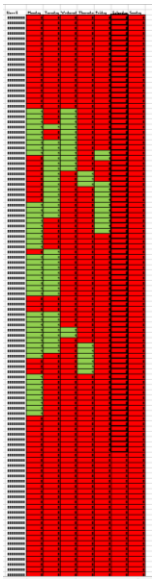

User 7:

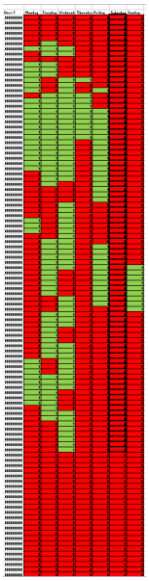

User 8:

User 9:

One week office room occupancy data:

Monday:

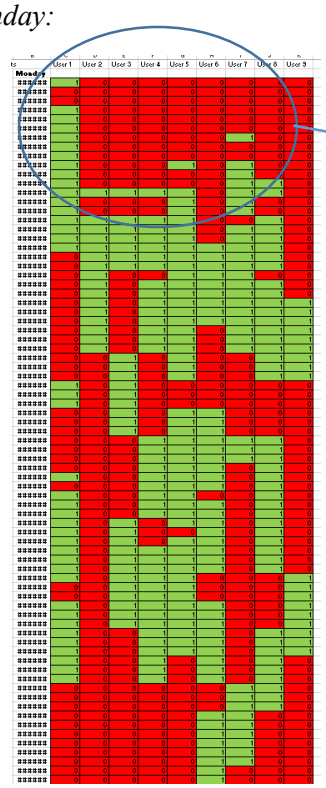

	User 1	User 2	User 3	User 4	User 5	User 6	User 7	User 8	User 9
Monday									
07:00:00 AM	1	0	0	0	0	0	0	0	0
07:10:00 AM	0	0	0	0	0	0	0	0	0
07:20:00 AM	0	0	0	0	0	0	0	0	0
07:30:00 AM	1	0	0	0	0	0	0	0	0
07:40:00 AM	1	0	0	0	0	0	0	0	0
07:50:00 AM	1	0	0	0	0	0	0	0	0
08:00:00 AM	1	0	0	0	0	0	1	0	0
08:10:00 AM	1	0	0	0	0	0	0	0	0
08:20:00 AM	1	0	0	0	0	0	0	0	0
08:30:00 AM	1	0	0	0	1	0	1	0	0
08:40:00 AM	1	0	0	0	0	0	1	0	0
08:50:00 AM	1	0	0	0	0	0	1	1	0
09:00:00 AM	1	1	1	1	1	0	1	1	0
09:10:00 AM	1	0	0	0	1	0	1	0	0
09:20:00 AM	1	0	0	0	1	0	1	0	0
09:30:00 AM	1	1	1	1	1	0	0	1	0
09:40:00 AM	1	1	1	1	1	0	1	1	0
09:50:00 AM	1	1	1	1	1	0	1	1	0
10:00:00 AM	1	1	1	1	1	1	1	1	0
10:10:00 AM	0	1	1	1	1	1	1	1	0
10:20:00 AM	0	1	1	1	1	1	1	1	0
10:30:00 AM	0	1	0	0	1	1	1	0	0
10:40:00 AM	0	1	0	1	1	1	1	1	0
10:50:00 AM	0	1	0	1	1	1	1	1	0
11:00:00 AM	0	1	0	1	1	1	1	1	1
11:10:00 AM	0	1	0	1	1	1	1	1	1
11:20:00 AM	0	1	0	1	1	1	1	1	1
11:30:00 AM	0	1	0	1	1	0	1	1	1
11:40:00 AM	0	1	0	1	1	0	1	1	1
11:50:00 AM	0	1	0	1	1	0	1	1	1
12:00:00 PM	0	0	1	0	1	0	0	1	1
12:10:00 PM	0	0	1	0	1	0	0	1	1
12:20:00 PM	0	0	1	0	1	0	0	1	1
12:30:00 PM	1	0	1	0	0	0	0	0	0
12:40:00 PM	1	0	1	0	0	0	0	0	0
12:50:00 PM	1	0	1	0	0	0	0	0	0
01:00:00 PM	0	0	1	0	1	1	0	0	0
01:10:00 PM	0	0	1	0	1	1	0	0	0
01:20:00 PM	0	0	1	0	1	1	0	0	0
01:30:00 PM	0	0	0	1	1	1	1	1	0
01:40:00 PM	0	0	0	1	1	1	1	1	0

Tuesday:

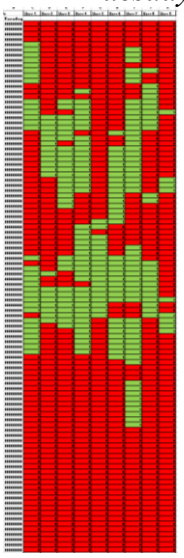

Wednesday

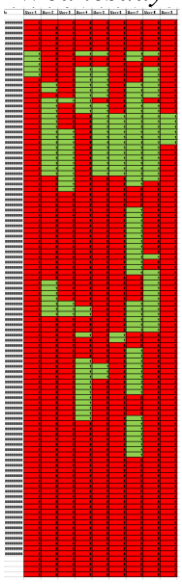

Thursday

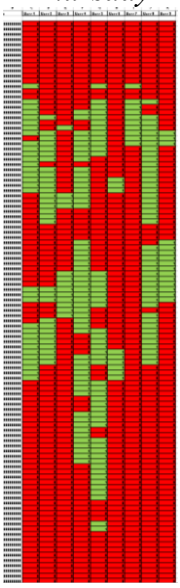

Friday

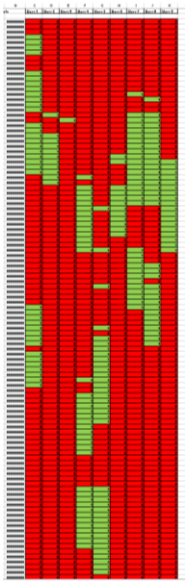

Saturday

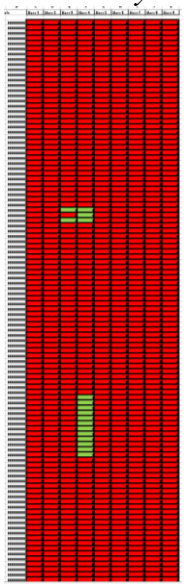

Sunday

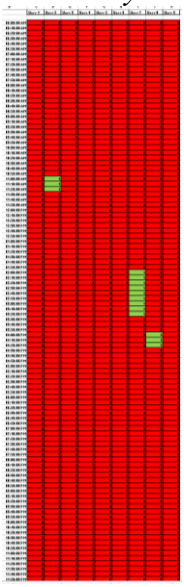

Appendix D

Quick construction progress monitoring for concrete structure using thermal imaging techniques

Abstract:

Construction progress monitoring ensures the construction project is consistent with the schedule and enables the detection of any deviations in the geometry and/or any variation in the schedule. The traditional progress monitoring requires specialized personnel to walk around on the construction site to manually collect data and verify the progress of activities, which is time consuming, costly and/or error prone. Image-based technology is effective for recording on-site data geospatially and chronologically. It has gained increasing attention in the construction field for progress monitoring, work space analysis and quality assurance. However, a notable downside of image processing is the light condition, particularly for noisy environments such as construction sites. Poor or undesirable ambient light conditions produce low quality images which significantly affect the accuracy of data extracted from related images and lead to a high level of errors. Much research strives to reduce the level of errors in image-based monitoring methods but it still has remained a challenging technique. This paper presents an innovative approach based on thermal image analysis to overcome problems related to the image quality. This method includes acquiring the thermal and optical images by utilizing an infrared-camera, estimating the location of captured images with wireless sensor networks, analyzing the image for progress identification and finally updating a building information model. Numerous tests have been implemented to show the feasibility of inferring the actual state of progress by the use of thermal images. It is finally concluded that the proposed method has a great potential to overcome the limitation of image-based monitoring and can be used to automate construction progress monitoring.

Introduction

Indoor spatial description

There are two major systems being used to model the actual state of construction progress and consequently model the building: laser-scanning-based and image-based. Both systems conduct the process of collecting data from the site, identifying existing components, and generating 3D models to be integrated into existing models.

Laser scanning-based system

In a laser scanning-based system, a laser range scanner is utilized to collect point clouds and merge them into a 3D model. Recent applications of this method can be construction quality control [78], conditions assessment [79], health monitoring [80] and component tracking [81]. For progress monitoring purposes, Bosche et al [82], for example, have presented a semi-automated registration method for aligning the as-built and as-planned models, in which the point cloud is generated based on manually selecting at least three pairs of corresponding points in the two data sets. Laser scanning is also integrated with other data such as schedules. Turkan et al. [83] have proposed a progress tracking system which fuses 3D laser scans with 4D models to automate construction progress monitoring. Their system is tested for a concrete building construction project and the results indicate the importance of the planning of scan. However, temporary occlusions lead to low level object identification. Despite the accuracy of laser-scanning-based techniques, costs, resolutions, the mixed-pixel issues, regular sensor calibrations and slow warm-up times are noted as the main drawbacks of this method [81] [84].

Image-based system

Image-based systems are considered an affordable method for many construction companies to collect data. Numerous studies have been conducted to utilize and improve the image data for construction project monitoring and management purposes. Neto et al. [85] have proposed a colour-edge-detector algorithm to identify the construction components, in which a predefined library based on the RGB ranges for different materials is created. Zou and Kim [86] have developed a method based on HSV (hue, saturation, and value) and colour to compute the idle time of hydraulic excavators automatically. Golparvar-Fard et al. [87] have proposed an image-based approach to estimate project status information using daily photographs captured from a construction site. In their research, time-lapsed images have been created with all building components to specify whether or not specific areas have expected appearances and the construction progress can therefore be monitored.

Braun et al. [88] have introduced photogrammetric point clouds to facilitate the as-planned versus as-built comparison. In this method, a dense point cloud is reconstructed from the images, which is compared to an existing 4D building model. However, due to the numerous obstructions found on a construction site, only a small subset of building elements are successfully detected. Zhang et al, [89] and Lukins & Trucco, [90] have presented a similar automated method with a different recognition stage. In their method, a comparison is made between pre-calibrated images and previous photos. Specific areas of interest are analysed by focusing on pixel changes to detect any differences from past photos, creating a time-lapsed image. The time-lapsed images method has the highest level of automation reported so far. However, it has many limitations: (1) The fixed camera has limited the analysis to only the closest structural frame to the camera. (2) Lighting conditions and shadow issues significantly affect the image processing. (3) Dynamic occlusions

make it difficult to analyse the components, and (4) Static occlusion may result in false detection [87].

Infrared thermography is the technique of measuring infrared radiation emitted by bodies, proportionally dependent on their superficial temperature [91]. The use of this technique has been usually limited to three types of applications in the construction related research. The first includes obtaining the thermographs of an existing building for analysing the heating or cooling energy requirement of the building envelop taking into account the local climate [92] [93]. The second relates to the real-time defect detection (air infiltrations, thermal bridges and moisture areas) in retrofitting existing building system in terms of energy efficiency for heating or cooling loads [94] [95]. The third use is associated with material detection of the existing [96]. However, very few studies have indicated its utility in the application of photogrammetric principles for the measurement of geometry directly from thermographs [97] [98], or from a combination of visible and thermographic images looking for an improvement in the geometric resolution [99]. Lagüela [95] investigated the extent of thermographic images to represent the as-built geometry and successfully extracted height, width and openings of the structure.

The traditional progress monitoring requires specialized personnel to walk around on the construction site to manually collect data and verify the progress of activities, which is time consuming, costly and/or error prone. Image-based technology is effective for recording on-site data geospatially and chronologically. It has gained increasing attention in the construction field for progress monitoring, work space analysis and quality assurance. However, a notable downside of image processing is the light condition, particularly for noisy environments such as construction sites. Poor or undesirable ambient light conditions produce low quality images which significantly affect the accuracy of data extracted from related images and lead to a high level of errors. Much

research strives to reduce the level of errors in image-based monitoring methods but it still has remained a challenging technique.

Methodology

As-built plan

The real geometry data is a significant parameter for creating a simulation within a building. As mentioned in the literature review, the as-built plan does not always follow the exact as-planned form. Hence, it is important to utilize a method to monitor the construction progress and provide an as-built model after the building is constructed. A novel approach is proposed in this research to create an as-built plan specifically for concrete structures by integrating thermal image processing and localization [100]. The kernel point of this stage is to take thermal pictures of the construction site at designated locations, identify elements with different construction stages, and update the 4D Building Information Modelling (BIM) model. The process is based on the following assumptions: (1) The 3D BIM model and the construction schedule are available; (2) The structure is composed of reinforced concrete components; and (3) The location and orientation of the IR-camera can be tracked accurately in real time. As shown in Figure 90**Error! Reference ource not found.**, the overall procedure for thermal image-based automated progress monitoring is divided into four major steps, which are: 4D BIM acquisition, onsite data collection, image processing, and model updating.

First, daily photos are taken from the construction site. Simultaneously, the location and orientation of the camera are identified by using a wireless sensor network installed on the site

(Figure 90(a)). As the image should be taken while the camera is fixed, the PCA method, which has a higher accuracy for low speed targets, can be used. By using the same location and orientation, the images of the as-planned model are extracted from the 4D BIM model (Figure 90 (b)). The purpose of the image-processing step is to identify whether the scheduled components have been constructed or not. By applying a colour-based filter on the thermal images, environment noise such as occlusion can be removed. However, there may be some other dynamic occlusions (e.g. workers, moving vehicles), but these will be removed in the next step.

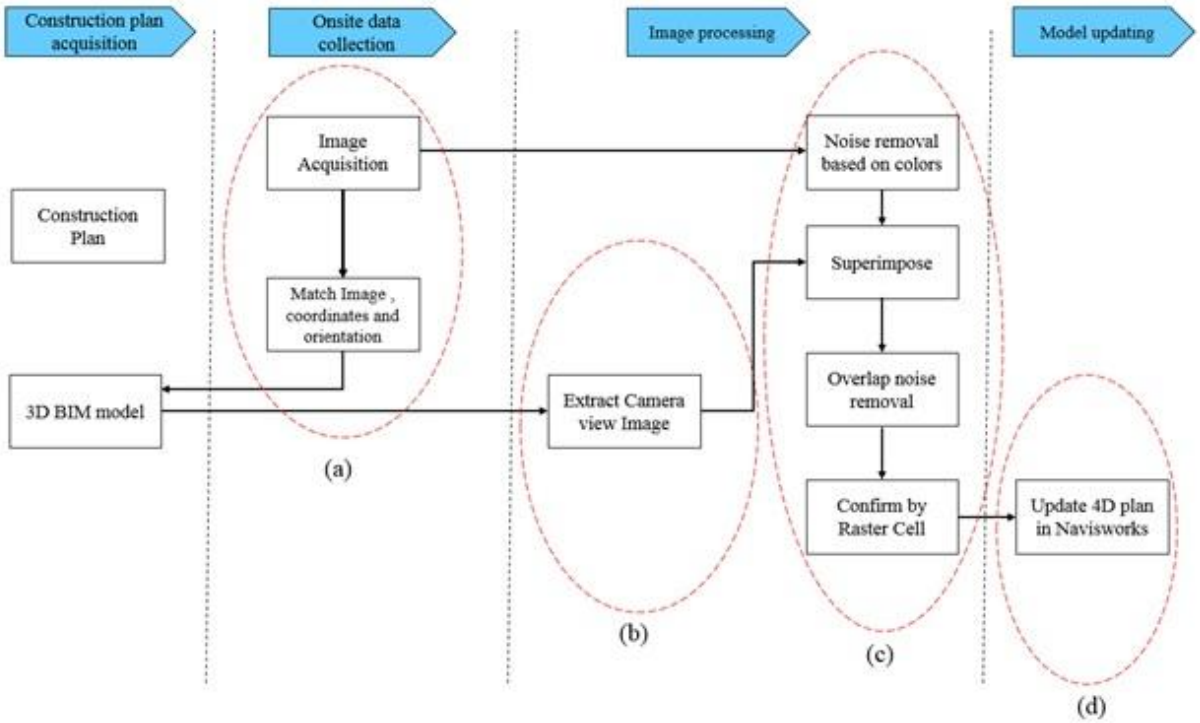

Figure 90: Thermal image-based automated progress monitoring procedure

The edge detection filter and superimpose method are both utilized to remove further noises. Next, the raster cell method is applied on the output to confirm the presence of newly built components (Figure 90 (c)). Finally, the confirmation obtained through the image processing is

used to update the 4D BIM model using the date recorded in the thermal images and the constructed components (Figure 90(d)).

Onsite data collection

In the proposed method, it is assumed that the construction schedule and 3D BIM model are available. The ideal location and orientation of the camera is based on consideration of the effectiveness of capturing appropriate progress details. A plug-in is developed to retrieve the coordinates of the target components in the model and create a bounding box for that area, then identify the four corners as suggested locations for the camera. Preliminary camera-view images are obtained from those locations to determine which locations should be used. A location system based on the ZigBee wireless sensor network is used in this research to capture the location of the IR-Camera while capturing images on site. In Section 3.1.1, the principal component analysis (PCA) approach was used to smooth the unwanted signals in a noisy environment, which lead to a more accurate position estimation for lower speed targets. By utilizing the same methodology, X and Y coordinates are recorded for the IR-camera when pictures are taken. The orientation data are manually recorded while taking each image on site, and will be used together with the coordinates to extract the corresponding 3D camera-view image from the BIM model. Based on the image captured, three types of images need to be processed for progress monitoring: optical, thermal, and camera-view images. Optical and thermal images are taken simultaneously from the construction site by using IR-Cameras. Camera-view images are extracted from the 4D BIM model based on the location and orientation of the camera.

Image processing

The details of the thermal-image-processing are shown in Figure 91. The difference in surface temperature between elements (e.g., concrete elements and scaffoldings) leads to different colours in thermal images. These differences are considered a valuable point to remove unnecessary objects from thermal images. However, some objects may have the same temperature as concrete elements. Hence, camera view images and the superimpose method are used to recognize the area of interest.

The occlusions are removed by applying a colour-based filter on the thermal image for removing unnecessary areas. Afterwards, the edges of components in the camera view image are identified. In addition, the superimpose method is applied on both images to recognize the areas of interest. Non-overlap areas are removed from the superimposed image using what is called the final noise removal filter. Next, the raster cell method has been utilized to confirm the object's existence.

At the same time, the same image processing method is applied to the optical image, as shown in the right-hand side part of Figure 91, and a grayscale image is generated to detect the edges of the components. The non-overlap areas are removed from the superimposed image based on optical pictures and camera view images. After that, the raster cell method is applied to recognize the newly constructed components. The combination of the results from both thermal and optical image processing will lead to more accurate results for the identification of components.

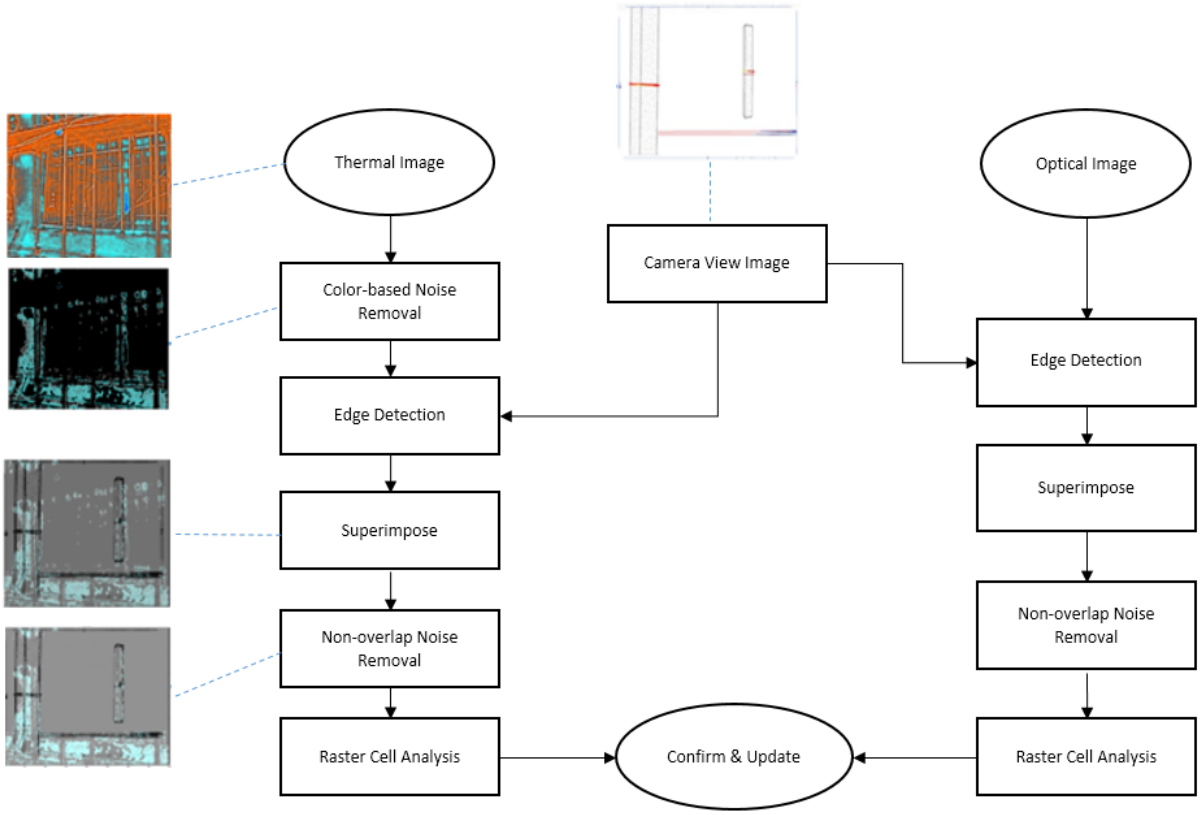

Figure 91: Image processing method

Raster cell analysis

Raster cell analysis is utilized to identify the percent match between two images. A raster comprises a matrix of cells or pixels composed into rows and columns where each cell possesses a state representing information. In our case, the state of a cell represents the existence of the concrete components. The images are rasterized with proper cell size for further processing. The cell size, or spatial resolution, of the raster depends on the level of detail (or number of features). The cell must be sufficiently small to show the required detail. However, smaller cells are not necessarily better because they require greater storage space, which often results in longer processing times.

Two states are considered for each cell: occupied and free. For instance, a cell can be defined as free when there are no points in it, which means that part does not exist. When it is not possible to make a statement or few points are detected in the cell, it can be marked as *potentially exists*.

For encoding raster data from scratch, a cell-by-cell raster encoding method is utilized (Figure 92), also referred as Exhaustive Enumeration [101]. This technique encodes a raster by making records for every cell magnitude by row and column. This strategy could be considered as an extensive spreadsheet wherein every cell of the spreadsheet represents a pixel in the raster picture. By doing so, an overlapped region can be identified between two images and existing components can be confirmed if the overlapped percentage exceeds a certain threshold.

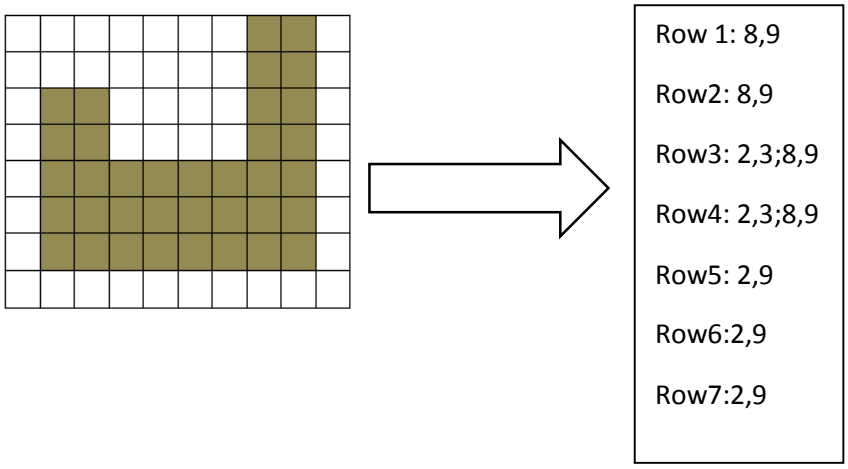

Figure 92: Cell-by-Cell Encoding of raster cell

BIM model updating

Once the image-processing step is finished, the results are interpreted by the plug-in in the form of binary variables associated with the completion (or absence) of respective building elements. These variables correspond to the schedule in the form of an as-built schedule and thus

the 4D model is updated. However, if any deviations are present in the as-planned and as-built model, these will not be incorporated in the updated model but may instead result in reporting an absence of the as-planned element. When the newly constructed element is confirmed by the raster cell method, the date is updated on the elements' descriptions in the 4D BIM model.

Thermal Image based spatial modelling

As mentioned in the literature review, the as-built plan may not be exactly as same as the as-planned form in the construction phase. Therefore, the thermal image-based approach introduced in the methodology section will be examined in this section. First, the feasibility of utilizing thermal images for modelling the real geometry of the building is discussed. Next, several case studies based on the new approach are conducted.

Feasibility analysis and experimental measurement

Infrared-camera, which is also known as IR-camera, is acting as a non-contact sensor absorbing the heat energy from surfaces of objects and giving an illustration in the form of thermal images. This device allows users not only to measure temperature, but also to detect and evaluate any heat-related parameters such as humidity. Due to the existence of blackbody radiation, objects produce electromagnetic wave radiation to the external environment [102]. Wavelength that is between 2~1000 micron is called thermal infrared. Thermal infrared images are based on thermal infrared sensitive Charge-Coupled Device (CCD) imaging of objects. These images reflect the temperature

field of the object surface. Different colours will be presented based on the surface temperature of the objects.

Concrete is the most widely used material in construction projects. As the key constituents of concrete, cement releases heat when in contact with water, which is known as cement hydration. Three stages are involved in the hydration process. The first stage is a dormant period, where at the initial moment of reaction, water contacts cement particles, and the heat starts to be released. However, due to the existence of gypsum in cement, a thin film is produced and covers around cement particles. The reaction rate decreases due to the filming and heat release rate decreases correspondingly. The second stage is phase-boundary reaction stage, which is characterized by the highest heat release rate. Cement particles are continuously produced by reaction and the production rate increases quickly. Therefore, the heat produced by the hydration is the highest among the three stages. The third stage is diffusion control stage, where the cement particles are incessantly accumulated from previous stages and the reaction rate decreases; therefore, the heat released decreases gradually because the hydration is complete.

Based on the significant temperature changes during the hydration process of concrete, IR-camera is used to take thermal pictures of the concrete components on construction sites so as to investigate the feasibility of using the proposed method. Figure 93**Error! Reference source not ound.** shows the optical and thermal images taken by using an IR-Camera. The relative environmental temperature and humidity are 26.5℃ and 44%, respectively. The elements shown in the pictures are concrete beams precast manually. Beams in Zone 1 were casted 7 days prior to the photo being taken, while beams in zone 2 were casted 5 days prior to the photo being taken. The beams in zone 3 were casted in the morning and beams in zone 4 were casted 10 minutes before the photo being taken. The beams in Zone 4 can be regarded as fresh concrete. It is obvious

from the thermal image that temperatures of these beams were different based on the colours and the shape of the beams can be easily identified by colours. In general, without considering the weather conditions, the surface temperatures of fresh and short term concrete are higher than that of more aged concrete due to the hydration reaction. The surface temperature of the 7-day concrete is similar to that of the surrounding environment. Heat is absorbed by water evaporation so that the surface temperature of 5 days concrete is lower than that of fresh concrete. According to temperature differences and varied colour shown in the thermal images, the casting sequence of the beams can be estimated.

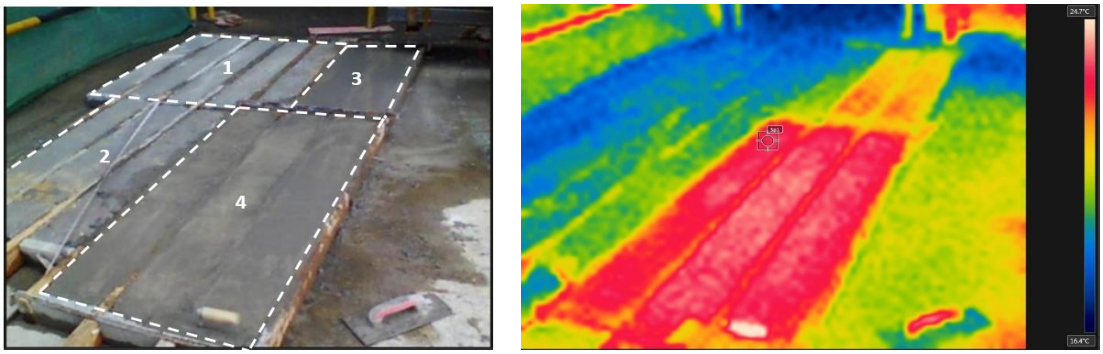

(a) (b)

Figure 93: Optical (a) and thermal (b) images of concrete beams

Further analysis has been done to evaluate the feasibility of using IR-camera for construction progress monitoring. Images of a selected concrete beam were taken for 6 consecutive days with time intervals of 0min, 30min, 60min, 120min and 240 min for each day. Images were taken at 9:00 AM, 9:30 AM, 10 AM, 11 AM and 1 PM. Environmental temperature and humidity were recorded by using a thermometer at the moment when the thermal images were captured and the surface temperatures of concretes are extracted from thermal images. Figure 94 shows the temperature variation tendency of concrete along time. The relationship between environmental temperature and concrete surface also can be observed from these figures.

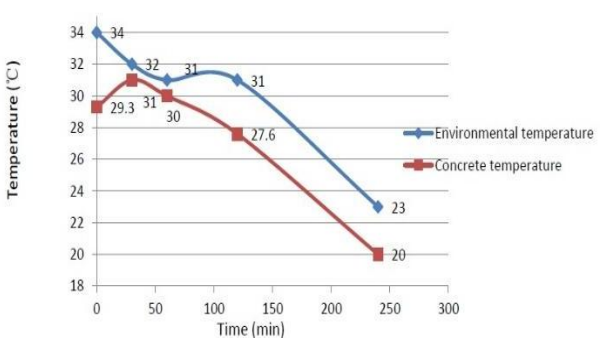

(a) Fresh concrete (Day 1)

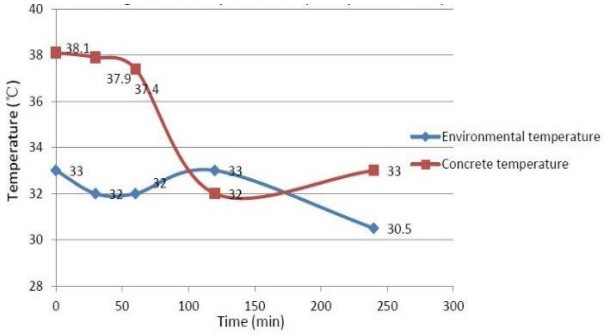

(b) One-day old concrete (Day 2)

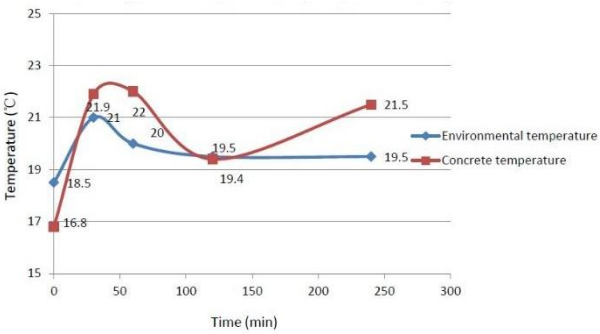

(c) Two-day old concrete (Day 3)

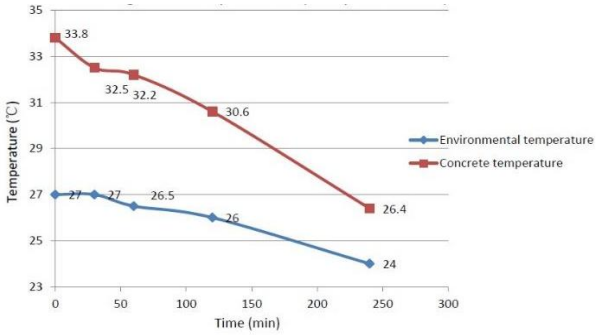

(d) Three-day old concrete (Day 4)

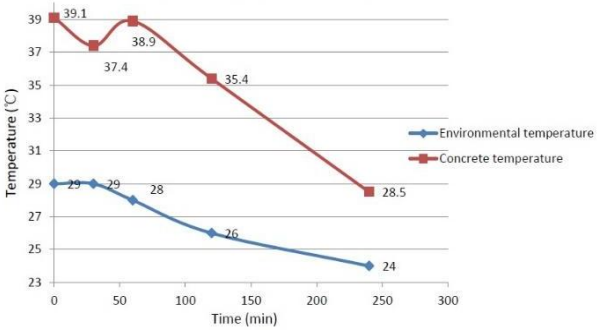

(e) Four-day old concrete (Day 5)

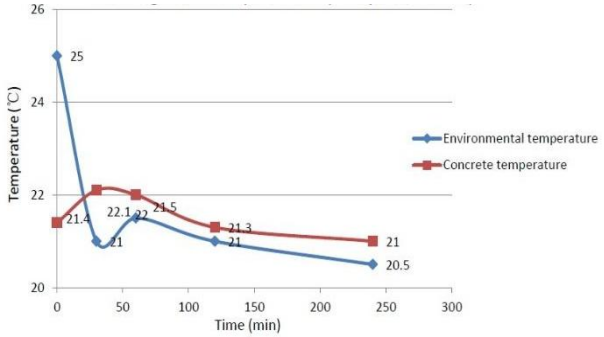

(f) Five-day old concrete (Day 6)

Figure 94: Temperature variation of concrete and environment for six consecutive days

For fresh concrete, the maximum environmental and element temperatures are 34℃ and 31℃, respectively, as shown in Figure 94(a). Environmental temperature is a bit higher than concrete temperature for fresh concrete. The reason can be that IR-Camera only measures the surface temperature of concrete, where water evaporation on the surface of concrete absorbs a large amount of heat. This process results in the lower surface temperature of concrete compared with environmental temperature. Water is a significant reactant for cement hydration. Water evaporation restrains hydration reaction and thus decreases the amount of heat generation from hydration reaction.

As shown in Figure 94 (b), surface temperature of one-day concrete is higher than environmental temperature because the water has been evaporated after one day curing. Cement hydration continuously proceeds and heat is produced, therefore, the surface temperature of concrete is higher than environmental temperature. In addition, solar radiation also influences the surface temperature of concrete. The longer time of solar radiation, the higher surface temperature of the concrete compared with environmental temperature. When solar radiation is screened, the surface temperature of concrete will decrease.

Surface temperature variations of two, three, four and five days concrete are depicted in **Error! eference source not found.**(c), (d), (e) and (f), respectively, showing that the surface temperature mostly remains above the environmental temperature, which supports the hypothesis that the temperature differences can be captured in the thermal image obviously. In some cases, as shown in Figure 94 (c) and (f), the temperature differences between the surface and environment are small due to the rainfall that occurred the day before. The evaporation process of water particles covering the surface of the concrete absorbed the heat, which led to the surface temperature decrease and close to the environmental temperature.

Figure 95 presents the variation of temperature differences between concrete surface and environment within the 6 consecutive days. The positive temperature variation increases continuously in the six days because of the heat generated continuously from the hydration reaction. Two peaks occurred on day two and day five with two sags appeared on day three and day six, which can be explained by the rainfall.

The important finding from Figures 2 and 3 is that surface temperature of concrete is significantly higher than the environment, especially in sunny days. While in rainy days, the difference is not so obvious.

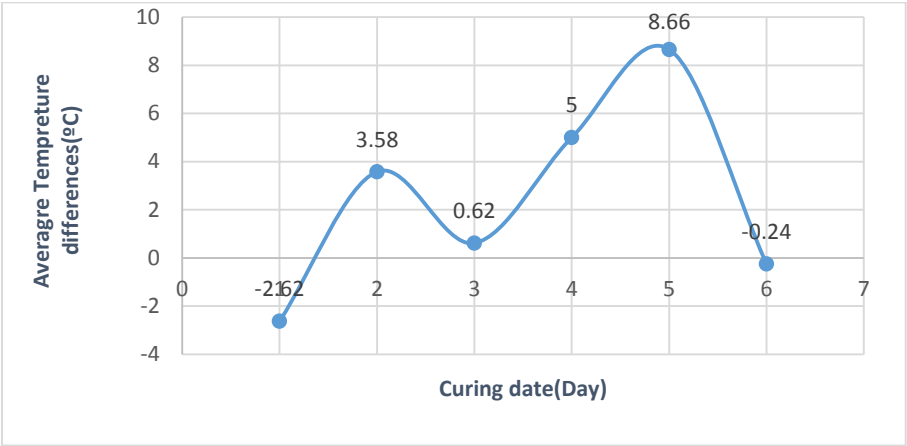

Figure 95: Temperature differences of concrete and environment within 6 consecutive days

To further investigate the feasibility of using thermal images, more pictures were taken on site in complex situations for structures under construction. Figure 96 and Figure 97 illustrate the temperatures on the surface of concrete columns, stairs and scaffoldings. The areas with different temperatures can be identified clearly; even concrete components inside a formwork are detectable, as shown in Figure 96

(a) Optical image **(b) Thermal Image**

Figure 96: Different temperature areas on the surface of concrete columns and stairs

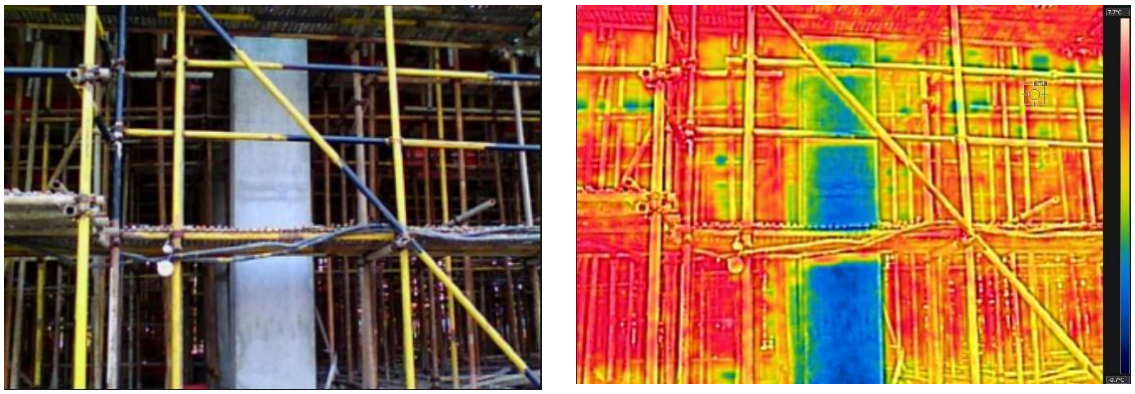

(a) Optical image **(b) Thermal Image**

Figure 97: Different temperature areas on the surface of concrete columns

Besides temperature, humidity is another parameter which should be taken into account since the temperature differences are not so obvious in rainy days. Using the *Humidity* filter available in the IR-camera, images taken show extra information besides the temperature. As shown in Figure 98 zones with different humidity can be identified in different colours, which can be used as supplementary information to identify different elements on construction site.

As mentioned in the literature review section, lighting conditions are known as a big challenge in photometric image processing. To show how good that the thermal-images-based method can solve such problems, pictures were taken under a poor lighting condition, as shown in Figure 99 It is nearly impossible to detect columns from the optical pictures (Figure 99 (a) and (c)). However, in the thermal images, they are easily detected, as shown in Figure 99(b) and (d).

In some cases, due to the high congestion of scaffoldings or other occlusions, it is very difficult to identify the existence of elements from the images taken. Thermal images can be really useful in such cases. A messy construction environment is shown in Figure 100(a) with a thermal image shown in Figure 100 (b), which shows how significant the thermal images can be used for identifying the existence of elements in such a noisy environment.

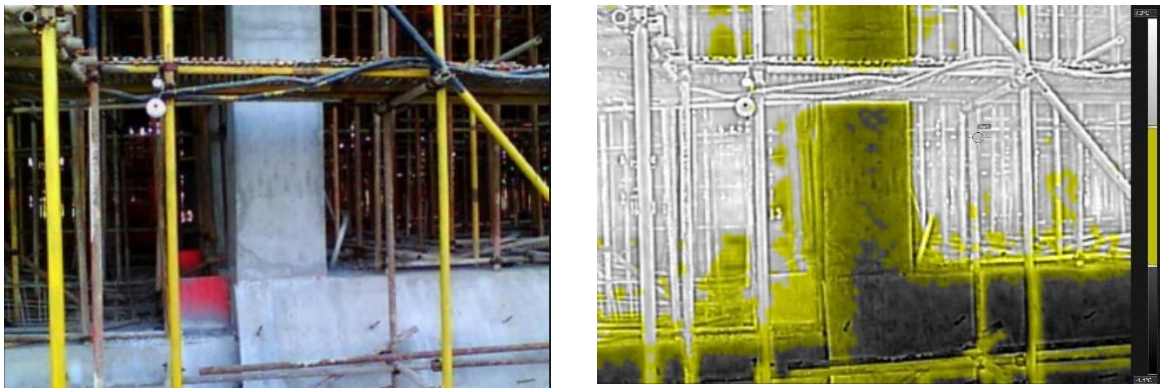

(a) Optical image **(b) Thermal Image with humidity filter**

Figure 98: Different humidity areas on the surface of concrete columns

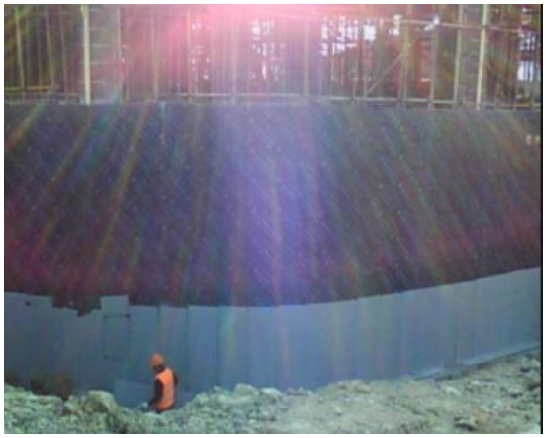

(a) Optical image with poor lighting condition

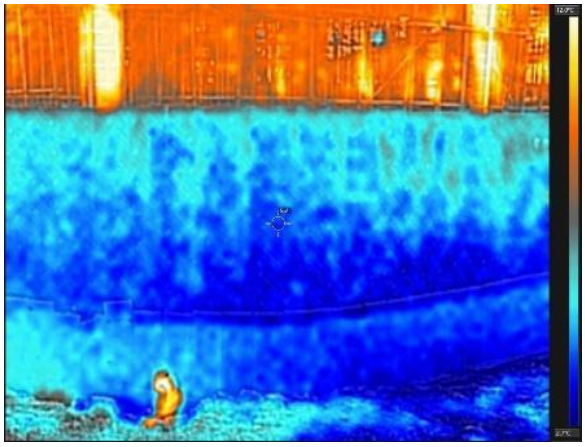

(b) Thermal image from with poor lighting condition

(c) Optical image with poor lighting condition

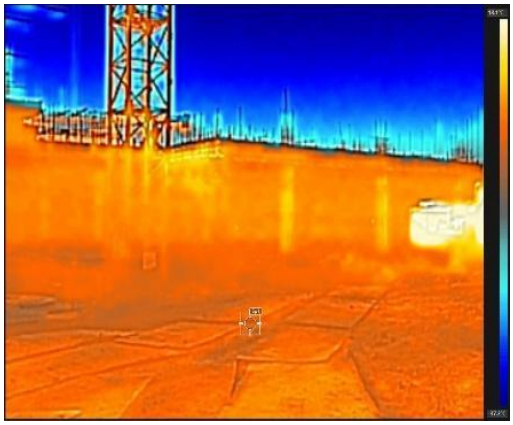

(d) Thermal image with poor lighting condition

Figure 99: Identify areas from poor lighting condition image

(a) Optical image from a noisy environment

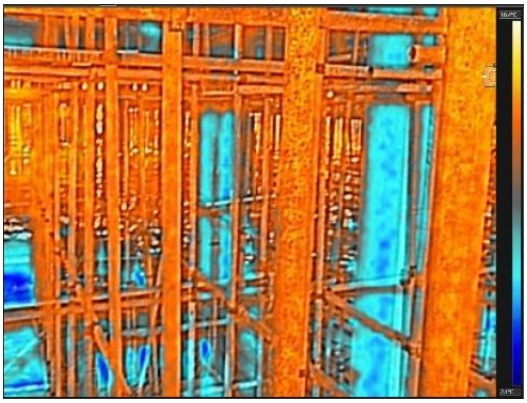

(b) Thermal Image from a noisy environment

Figure 100: Identify objects from a noisy environment

To sum up, based on the feasibility analysis and experimental measurements, it is applicable to identify newly built concrete components on construction site based on thermal images taken by IR-Camera and develop an automated progress monitoring system. Hence, the proposed methodology is explained in the next section.

Case study

A construction site, located in Suzhou, China, was chosen to investigate the proposed method (Figure 101). An IR-camera, NEC TH7102, was used to take pictures on site. The camera had a resolution of 320 × 240 with 76,800 pixels. The thermal sensitivity of the camera was less than 0.07 °C with the accuracy of ±2°C. Utilizing a data cable, captured images were saved to the server in the JPEG image format for further processing. The time of image capturing was used as the file name. For instance when the image was captured at 14:23:29 on October, 24, 2015, the file name of thermal and optical images would be "T2015101124142329.jpg" and "O2015101124142329.jpg", respectively. This information was used to identify the location data

when connected to the location system mentioned previously. The coordinates of the camera were extracted from the tracking data recorded. It should be noted that a time boundary of 5 seconds is considered for each image and its correspondence location. This boundary reduced the error of mismatching images and positions. The orientation of the camera was added to the image data manually. A more accurate method, such as using a total station, could be applied in the future to improve the accuracy. These location data were utilized to extract the camera view image for the corresponding position in the 3D BIM model. Two test areas were selected to conduct the case studies, as shown in Figure 101. Zone 1 was a typical area with two columns and a wall in between. Zone 2 was an area with noisy environment where scaffoldings are around the columns.

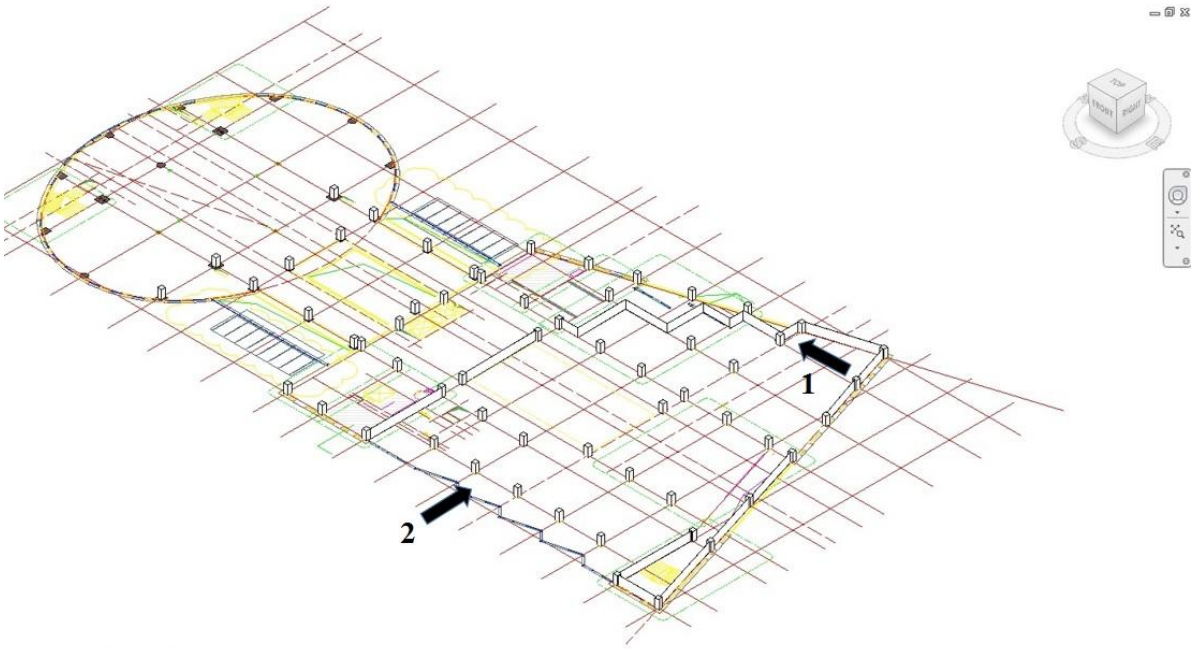

Figure 101: A partial BIM model of the construction site

Case I, Zone 1

The optical and thermal images are depicted in Figure 102(a) and (b), Figure 102(c) presents the camera-view image extracted from the BIM model based on coordinates and orientation of the IR-camera. Matlab R2010 is used for developing the image processing method. The applied edge detection on the camera-view image is depicted in Figure 102(d).

An initial noise removal was implemented on the thermal image to remove the orange areas, as shown in Figure 102 (e). The superimposed image Figure 102 (f) shows the overlapping of thermal and camera-view images. After final removing the useless areas which are shown as the black areas in the figure, raster cell method was implemented on the superimpose image and the results are shown in Table 22. Part 2 has a rate of 97% while part 1 has the minimum confirmed raster cells by 79% as it is occupied by occlusions. Parts 3 and 4 have the confirmed raster cells by 90% and 82%, respectively. It is clear that both images do not fully cover each other which can be explained by the slight differences of coordinates between real and estimated position due to accuracy. However, the percentage of objects confirmation for all parts has a successful range.

Table 22: Percentage of confirmed raster cell per object for Case I, Zone 1

Part	Percentage confirmation
1	79%
2	97%
3	90%
4	82%

(a) Optical Image

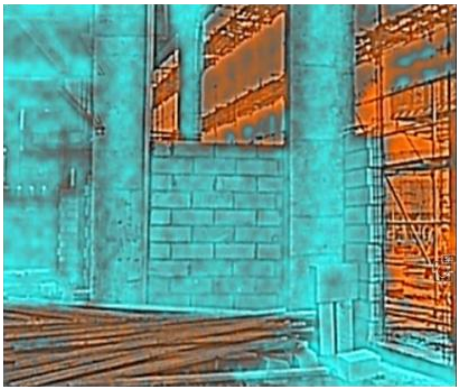

(b) Thermal Image

(c) Camera View Image in BIM

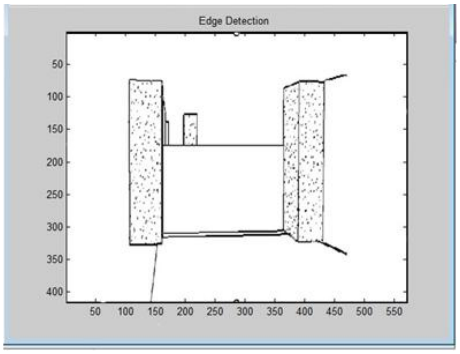

(d) Edge Detection Result from Camera View Image

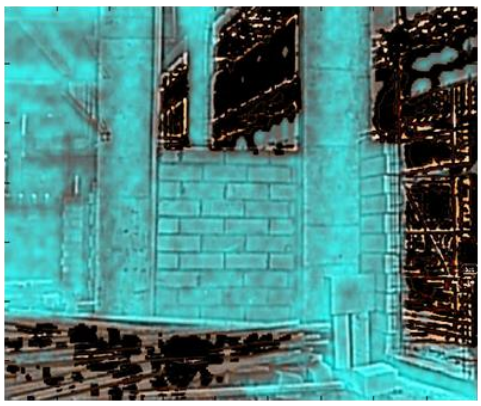

(e) Initial Noise Removal

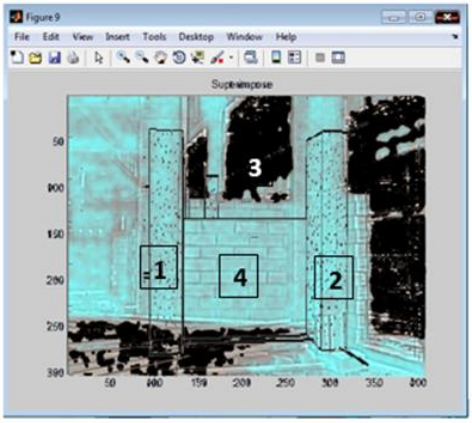

(f) Superimposed Image and final Noise Removal

Figure 102: Case study for zone 1

Case II, Zone 2

Figure 103(a) and (b) show the thermal image and initial noise removal image, respectively. The camera-view image extracted from the BIM model based on the related position and orientation is shown in Figure 103(c). The result of edge detection is illustrated in Figure 103 (d). Figure 103**Error! Reference source not found.**(e) and (f) show the superimpose and the final oise removal stages.

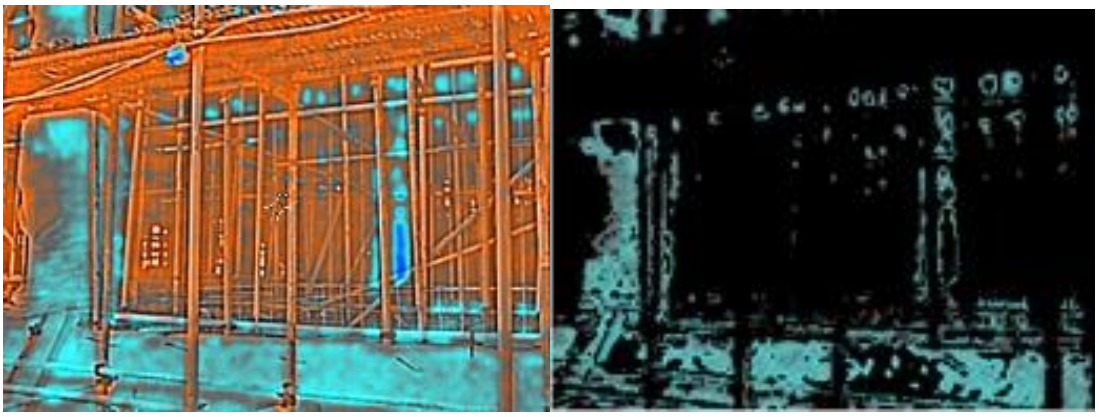

a) Thermal image **b) Initial noise removal**

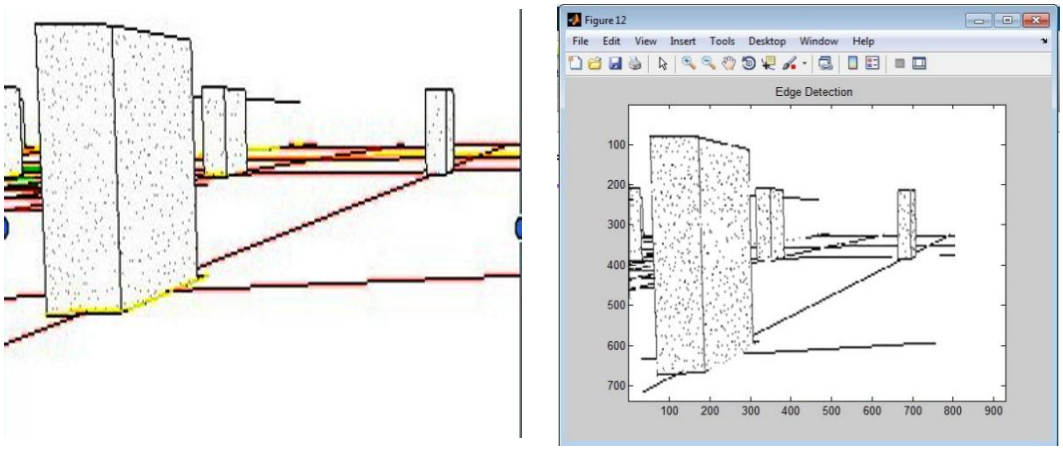

c) Camera-view image in BIM **d) Edge-detection result from camera-view image**

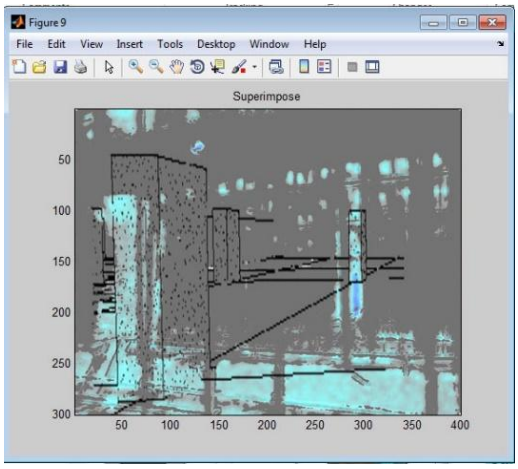

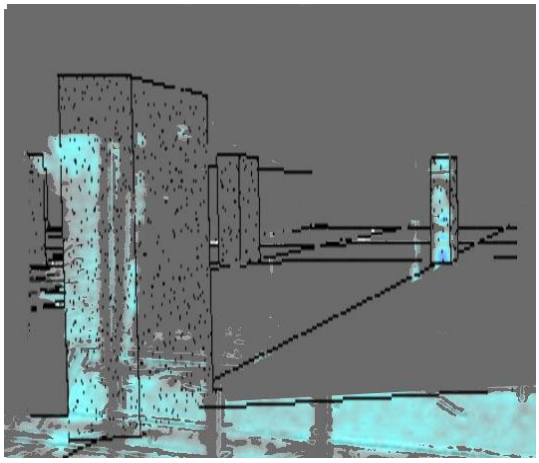

e) Superimposed image **f) Final noise removal**

Figure 103: Case study for zone 2 in a noisy environment

Table 23: Percentage of confirmed raster cell per object for Case II, Zone 2

Part	Percentage confirmation
Left Column	57%
Right Column	80%
Left behind column	0%

Since the depth of two columns in the back side are the same, the camera-view image shows three columns in this position. However, only two columns are distinguished from thermal image. The depth of camera view image is another factor which is needed to investigate further in our future research. The left column has a raster confirmation of 57% and right column is confirmed

by 80%. The results of raster cell method shows that thermal image-based technique has the potential to identify new constructed components even in a noisy environment.

Case III

In the previous two case studies, *Rainbow* filter was used to take thermal images. However, elements of the building built several months ago would not show significant temperature difference from the environment. In that case, *Rainbow* filter which only focuses on surface temperature may not be suitable or detecting existing elements. Therefore, other filters available in the IR-camera were investigated to further demonstrate the feasibility of applying the proposed method. For example, *Humidity* filter can be used to capture images showing the humidity of objects. A third case study was carried out by using the combined information captured using both *Rainbow* and *Humidity* filters in the IR-camera.

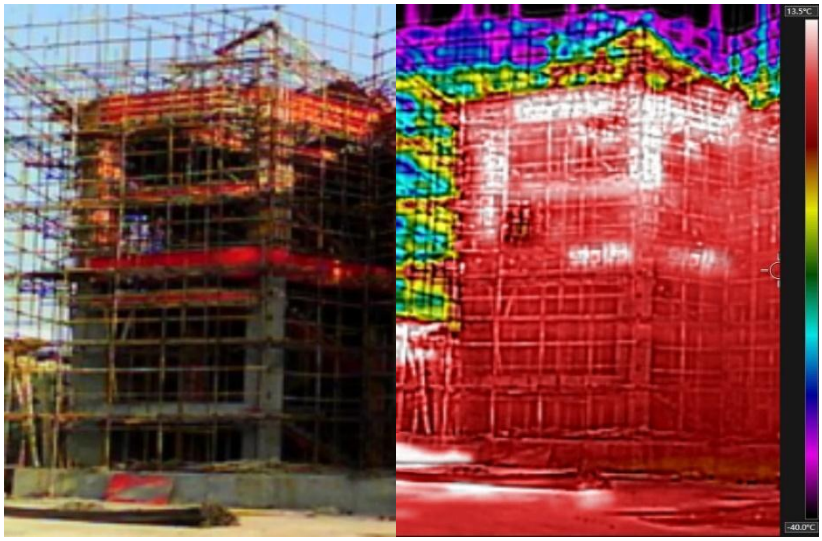

(a) Optical image **(b) Thermal image**

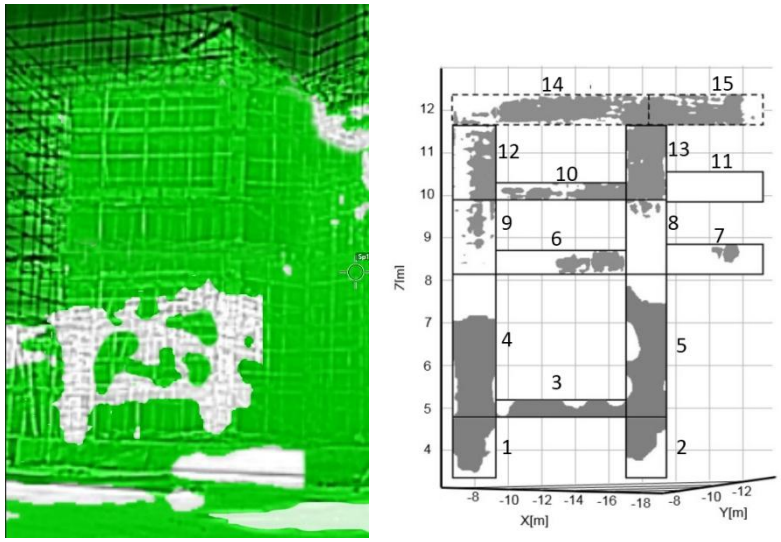

(c) Humidity image **(d) Raster cells on elements surface**

Figure 104: Image processing for optical, thermal and humidity images

Figure 104 (a), (b) and (c) illustrate the optical, thermal and humidity images taken for the concrete frame structure. The same image processing method introduced before was implemented in this case study to identify existing building elements. Figure 104(d) illustrates the results based on the combination of optical, thermal and humidity images. Fifteen parts of the building were identified manually based on the structure in the raster cell plot. The grey areas represent the confirmed raster cells. As shown in Table 23, Part 13 has a rate of 95% of confirmed raster cell, while part 11 has not any confirmed raster cells as it is still under construction. Parts 14 and 15 can be identified by 66% and 72%, respectively. Parts 3, 4 and 5 could be detected easily from the humidity image as there are not covered by formworks. Parts 6, 7, 8 and 9 have few confirm raster cells and Part 10 is confirmed by a high percentage.

Table 24: Percentage of confirmed raster cell per object for case III

Part number	Existing elements	Part number	Non-existing element
13	95%	15	72%
3	79%	14	66%
5	75%	11	0%
10	71%		
4	68%		
1	67%		
2	56%		
12	55%		
6	24%		
9	20%		
7	13%		
8	8%		

Conclusion and limitations

This section presents an innovative approach to monitor construction progress projects using infrared camera and thermal image analysis. In the proposed approach, images can be of low quality or taken in a noisy environment. Characterized by concrete surface temperature, thermal image filter, colour-based noise removal, and the location calculation, image processing played an essential role in providing the necessary information for 4D BIM model updating. Thermal images offer more data than traditional digital photos. Temperature and humidity differences are the main parameters that are utilized to improve the quality of images for image processing. To identify the orientation and location of taken photos, a ZigBee wireless sensor network based on PCA method is utilized.

The main contribution of this study is that the proposed methodology succeeded in automating almost the entire process of 4D BIM updating using image processing. This methodology included site images acquisition, image analysis for progress identification, and 4D BIM model

development. To the best of the author's knowledge, this study is one of the first comprehensive efforts to use IR-Camera for progress identification of construction sites.

Several case studies involving a construction site showed that there is a greater accuracy can be achieved than in traditional methods of progress identification and updating project schedule automatically. However, all existing elements could not be verified ambiguously with collected data.

Future studies are required to further analysis of different filters of IR-Camera to evaluate the potential of concrete properties for progress monitoring. There is another filter which is called iron filter which may be suitable for steel components which requires more investigation.

Moreover, there are some other filters which can be applied on thermal images such as Iron, Lava and so on. Numerous empirical experiments showed that humidity and temperature filters are adequate to gain reasonable results in image processing.

To sum up, in the first case study, all columns and walls could be identified by the use of thermal image. However, the slight differences of coordinates between real and estimated position, may result in not fully cover images in superimpose image which leads to lower confirmation in raster cells. The second case study observes the potential of thermal image as well. Although, non-adjusted depth in the camera view image could result in less accuracy and confirmation which needs more investigations. For components which their temperature adhere closely to the environment temperature, it is possible to use other filters in IR-Camera such as humidity filter. This filter can be implemented for old constructed parts or parts that stay in the shadow area. It can be concluded that image processing only on the optical photo, cannot identify all the building elements due to the low quality of image, poor lighting conditions and messy environment.

However, the combination of optical, thermal and humidity images resulted in a high range of object detections which still needs more investigation.

Appendix E

PCA method

```
% consider the clustered RSSI data set of 10 variables
   Load data.mat

% remove the mean variable-wise (row-wise)
    data=data-repmat(mean(data,2),1,size(data,2));

% calculate eigenvectors (loadings) W, and eigenvalues of the covariance
matrix
    [W, EvalueMatrix] = eig(cov(data'));
    Evalues = diag(EvalueMatrix);

% order by largest eigenvalue
    Evalues = Evalues(end:-1:1);
    W = W(:,end:-1:1); W=W';

% generate PCA component space (PCA scores)
    pc = W * data;

% plot PCA space of the first two PCs: PC1 and PC2
    plot(pc(1,:),pc(2,:),'*')
```

Appendix F

Trilateration algorithm

```
% usage: [N1 N2] = Trilateration(P,S,W)
% P = [P1 P2 P3 P4 ..] Reference points matrix
% S = [s1 s2 s3 s4 ..] distance matrix.
% W : Weights Matrix (Statistics).
% N : calculated solution


function [N1 N2] = Trilateration(P,S,W)
[mp,np] = size(P);
ns = length(S);
if (ns~=np)
    error('Number of reference points and distances are different');
end
A=[]; b=[];
for i1=1:np
    x = P(1,i1); y = P(2,i1); z = P(3,i1);
    s = S(i1);
    A = [A ; 1 -2*x  -2*y  -2*z];
    b= [b ; s^2-x^2-y^2-z^2 ];
end
if (np==3)
    warning off;
    Xp= A\b;  % Gaussian elimination
   % or Xp=pinv(A)*b;
   % the matrix  inv(A'*A)*A' or inv(A'*C*A)*A'*C or pinv(A)
   % depend only on the reference points
   % it could be computed only once
    xp = Xp(2:4,:);
    Z = null(A,'r');
    z = Z(2:4,:);
    if rank (A)==3
        %Polynom coeff.
        a2 = z(1)^2 + z(2)^2 + z(3)^2 ;
        a1 = 2*(z(1)*xp(1) + z(2)*xp(2) + z(3)*xp(3))-Z(1);
        a0 = xp(1)^2 +  xp(2)^2+  xp(3)^2-Xp(1);
        p = [a2 a1 a0];
        t = roots(p);

        %Solutions
        N1 = Xp + t(1)*Z;
        N2 = Xp + t(2)*Z;
    end
end
```

```
if  (np>3)
%Particular solution

    if W~=diag(ones(1,length(W)))
        C = W'*W;
        Xpdw =inv(A'*C*A)*A'*C*b; % Solution with Weights Matrix
    else
        Xpdw=pinv(A)*b; % Solution without Weights Matrix
    end

    % the matrix  inv(A'*A)*A' or inv(A'*C*A)*A'*C or pinv(A)
    % depend only on the reference points
    % it could be computed only once
    N1 = Xpdw;
    N2 = N1;
end
```

Appendix G

Wang-Mendel Method used for fuzzy modeling

```
clear all
clc

%% Load data, allocate training test dataset
disp('loading data......')
load votes.mat
y = c0;
y1 = [];
y2 = [];
[PNum, D] = size(y);
for i  =  1 : PNum
    if   mod(i, 3) == 0
         y2 = [y2; y(i, :)];
    else y1 = [y1; y(i, :)];
    end
end

%%

%% Initializes the fuzzy system (domain division, membership center, and
width
disp('Initializing Fuzzy Systems......')
Partition = [5,  5,  5,  5,  5];
center = cell(D,1);
sigma = cell(D,1);
for i = 1 : D
    center1 = [];
    sigma1 = [];
    for j = 1 : Partition(i)-2
        center1 = [center1 j*(1/(Partition(i)-1))];
        sigma1 = [sigma1 1/(Partition(i)-1)];
    end
    center{i} = [0 center1 1];
    sigma{i} = [1/(Partition(i)-1) sigma1 1/(Partition(i)-1)];
end
%%

%% draw out the initial membership function curve
disp('draw out the initial membership function curve......')
x = (0:0.001:1)';
figure
for i = 1 : D
    temp1 = [];
    for j = 1: Partition(i)
        temp1 = [temp1 SymTri(x, center{i}(j), sigma{i}(j))];
    end
    subplot(2, 3, i)
    plot(x, temp1,'LineWidth', 2)
```

```
end
%%



%% create ideal fuzzy rules part1
disp('Automatic generation of complete rule......')
DreamRuleLength = 1;  % The number of rules in an ideal rule base

for i = 1 : D-1
    DreamRuleLength = DreamRuleLength*Partition(i);
end
DreamRule = zeros(DreamRuleLength, D+2);
for i = 1 : D-1
    if i == 1
            interval = DreamRuleLength/Partition(i);
            for j = 1 : DreamRuleLength/interval
                DreamRule((j-1)*interval+1:j*interval, i) = j;
            end
    else    newinterval = interval/Partition(i);
            temp = [];
            for  j = 1 : interval
                 temp = [temp; ceil(j/(newinterval))];
            end
            temp1 = [];
            for  j = 1 : DreamRuleLength/interval
                 temp1 = [temp1; temp];
            end
            interval = newinterval;
            DreamRule(:, i) = temp1;
    end
end
%%




%% Learn to get the rules
disp('Learn to get the rule Library......')
LearnRule = [];
for i = 1 : length(y1)
    newrule = RuleLearner_case1(y1(i,:), center, sigma);
    LearnRule = [LearnRule; newrule];
end
%%


%% merge rules and fuzzy center and width parameter after the new member
disp('Merge rule Library......')
CompressRule = [];
EmptyRule = [];   % Initialize an area that does not generate a rule
for i = 1 : DreamRuleLength
    tempruleset = [];
    for j = 1 : size(LearnRule, 1)
```

```
        if   LearnRule(j, 1:D-1) == DreamRule(i, 1:D-1)
             tempruleset = [tempruleset; LearnRule(j, :)];
        end
    end
    if   isempty(tempruleset)
         EmptyRule = [EmptyRule; DreamRule(i, :)];

    else EmergeRule = tempruleset(1,:);
         tempcenter = 0;
         for  k = 1 : size(tempruleset,1)
              tempcenter = tempcenter + tempruleset(k, D)*tempruleset(k,
D+1);
         end
         newcenter = tempcenter/sum(tempruleset(:,D+1));
         tempsigma = 0;
         for   k = 1 : size(tempruleset)
               tempsigma = tempsigma + abs(newcenter - tempruleset(k,
D))*tempruleset(k, D+1);
         end
         newsigma = tempsigma/sum(tempruleset(:,D+1));
         EmergeRule (D) = newcenter;        % D dimension, put center
parameter first
         EmergeRule (D+1) = newsigma;       % Dimension D+1 place width
parameter
         EmergeRule (D+2) = 1 - ( newsigma/abs(max(tempruleset(:,D)) -
min(tempruleset(:,D))) );       % Confidence degree of d+2 dimension
placement rules
         CompressRule = [CompressRule; EmergeRule];
    end

end

%% completion rules, EmptyRule rules are formulated in the center and width
of output
disp('Complete rules......')
iteration = 0;
while ~isempty(EmptyRule)
       iteration = iteration + 1;
       disp(iteration)
       NeighborNum = [];
       for i = 1 : size(EmptyRule)
           tempNeighborNum = 0;
           for j = 1 : size(CompressRule)
               if  sum(abs(EmptyRule(i, 1:D-1) - CompressRule(j,1:D-1))) == 1
                   tempNeighborNum = tempNeighborNum + 1;
               end
           end
           NeighborNum = [NeighborNum; tempNeighborNum];
       end
       [maxNeighborNum,maxNeighborNumIndex] = max(NeighborNum);
       NeighborRule = [];
       for i = 1 : size(CompressRule)
           if  sum(abs(EmptyRule(maxNeighborNumIndex, 1:D-1) -
CompressRule(i,1:D-1))) == 1
               tempNeighborNum = tempNeighborNum + 1;
               NeighborRule = [NeighborRule; CompressRule(i,:)];
```

```
            end
        end
        SpecaluRule = EmptyRule(maxNeighborNumIndex, :) ;
        if ~isempty(NeighborRule)
           Specalucenter = sum((NeighborRule(:,D)).*
(NeighborRule(:,D+2)))/(sum((NeighborRule(:,D+2))));
           Specalusigma = sum(abs((NeighborRule(:,D))-Specalucenter).*
(NeighborRule(:,D+2)))/(sum((NeighborRule(:,D+2))));
           Specaludoc = 1 - Specalusigma/abs(max(NeighborRule(:,D)) -
min(NeighborRule(:,D)));
           SpecaluRule  (D)   =     Specalucenter;
           SpecaluRule  (D+1) =     Specalusigma;
           SpecaluRule  (D+2) =     Specaludoc;
        end
        EmptyRule(maxNeighborNumIndex, :) = [];
%         if Specalusigma ~= 0 && ~isnan(Specalusigma)
%            CompressRule = [CompressRule; SpecaluRule];
%         end
end
%%


%% To assign a label to a given rule and translate it into a regular form
disp('Label the resulting rules and translate them into regular forms ')
RuleBase = CompressRule;
outputpara = CompressRule(:, D:D+1);
outputpara = sortrows(outputpara,1);
center{D} = outputpara(:,1)';
sigma{D} = outputpara(:,2)';
for i = 1 : size(outputpara,1)
    for j = 1 : size(RuleBase,1)
        if center{D}(i) == RuleBase(j, D)
           RuleBase(j, D) = i;
        end
    end
end
RuleBase = RuleBase(:, 1:D);
Partition(D) = size(outputpara,1);
%%

%% In order to obtain the rules of Fu% label, and transformed into a regular
form
disp('Draw the membership function curve of the complete rule base......')
x = (0:0.001:1)';
figure
for i = 1 : D
    temp1 = [];
    for j = 1: Partition(i)
        temp1 = [temp1 SymTri(x, center{i}(j), sigma{i}(j))];
    end
    subplot(2, 3, i)
    plot(x, temp1,'LineWidth', 2)
end
%%

%% test model output performance
```

```
TsOutput = [];
for  i = 1 : size(y2, 1)
     output = WM_fuzzyprocessor( y2(i, 1:D-2), RuleBase, center, sigma);
     TsOutput = [TsOutput; output];
end
MSE = 10000*(abs(TsOutput - y2(:,D)))'*(abs(TsOutput - y2(:,D)))/(size(y2,
1));
figure
plot(y2(:,2))
hold on
plot(TsOutput,'r')
title(strcat('the testing MSE is ', num2str(MSE)))
```

Appendix H

Purely occupancy-driven control of HVACs

```
%day
%hour
%minute
%state:leaving-0/office-1/coffee-2/restroom-3/class-4/lab-5/meeting-6 %(
%Coffee and restroom are considered as Short temporary locations and Class
%and lab and meeting are considered as Long-stay locations

userNumber=9;
dayNumber=26;

%%
%data read - 1 month---this page is data reading from the excel
[~,timeData]=xlsread('C:\Users\Mehdi\Downloads\fuzzy logic-all\fuzzy
logic\Files\locationRecord.xlsx','Sheet1','D2:D1453');
save timeData


%%
clear;clc

%Creat a new diary file.
C=clock;
eval(['diary ', sprintf( '%02d.', C(1:5) ), 'txt']);
clear C

load('timeData.mat');
timeHourMinute=zeros(size(timeData,1),2);
for i=1:size(timeData,1)
    tmpFind1=find(timeData{i}==':');
    tmpFind2=find(timeData{i}=='M');
    if isempty(tmpFind2)
        disp('Impossible Error!');
    else
        if isempty(tmpFind1)
            disp(['Warning0: Line=' int2str(i)]);
            timeHourMinute(i,1)=str2double(timeData{i}(1:tmpFind2(1)-2));
        elseif size(tmpFind1,2)==1
            timeHourMinute(i,1)=str2double(timeData{i}(1:(tmpFind1(1)-1)));

timeHourMinute(i,2)=str2double(timeData{i}((tmpFind1(1)+1):(tmpFind2(1)-2)));
        elseif size(tmpFind1,2)==2
            timeHourMinute(i,1)=str2double(timeData{i}(1:(tmpFind1(1)-1)));

timeHourMinute(i,2)=str2double(timeData{i}((tmpFind1(1)+1):(tmpFind1(2)-1)));
        else
            disp(['Error: > 2, Line=' int2str(i)]);
        end
    end
```

```
end

diary off

clear i timeData tmpFind1 tmpFind2
save timeHourMinute
%             user           day         hour     minute      state
primData=[zeros(size(timeHourMinute,1),2) timeHourMinute
zeros(size(timeHourMinute,1),1)];
clear timeHourMinute
%%
%(day-1).*24.*60+hour.*60+minute
tmpData=(primData(:,2)-1).*24.*60+primData(:,3).*60+primData(:,4);
primData=[primData tmpData];
% save primData2
clear tmpData

%%
clear;clc

userNumber=9;
dayNumber=26;

load('primData.mat');
%    day         hour     minute      state
for i=userNumber:-1:1
    usersData{i}=primData((primData(:,1)==i),2:end);
end

clear i primData

%delete wrong data
for iUser=1:userNumber
    t1=usersData{iUser}(2:end,5)-usersData{iUser}(1:end-1,5);
    usersData{iUser}([find(t1<0)+1 find(t1==0)],:)=[];
end
save usersData
clear iUser

%%
%states by one minute.(leaving-0/office-1/coffee-2/restroom-3/class-4/lab-
5/meeting-6)
clear;clc
load('usersData.mat');
userNumber=9;
dayNumber=26;

timeTable=zeros(60*24*dayNumber,userNumber);
for iUser=1:userNumber
    for iLine=1:size(usersData{iUser},1)-1
        timeTable(usersData{iUser}(iLine,5):usersData{iUser}(iLine+1,5)-
1,iUser)=usersData{iUser}(iLine,4);
    end
end
```

```
clear dayNumber   iUser       userNumber
clear iLine       usersData
save timeTable

%%
load('timeTable.mat')

%canculate hvacs on(number of users(1~5) in Zone 1--> hvac1 on / (6~9) -->
hvac2 on) or off
timeTable(timeTable>1)=0;
nUser1=sum(timeTable(:,1:5),2); % Zone 1
nUser2=sum(timeTable(:,6:end),2); %Zone 2
nUser1(nUser1==1)=0;
nUser2(nUser2==1)=0;
nUser1(nUser1>1)=1;
nUser2(nUser2>1)=1;
time1=1:size(nUser1,1);
time1(nUser1==0)=[];
nUser1(nUser1==0)=[];
time2=1:size(nUser2,1);
time2(nUser2==0)=[];
nUser2(nUser2==0)=[];
plot(time1,nUser1,'b.');
hold on
plot(time2,nUser2+0.5,'g.');
ylim([0 2.5]);
openTime1=sum(nUser1);
openTime2=sum(nUser2);
legend(['HVAC1 on=' num2str(openTime1/(24*60)) 'days'],['HVAC2 on='
num2str(openTime2/(24*60)) 'days']);
xlabel('Minutes for 1 month');
ylabel('HVAC1 & HVAC2 on');
title('Time for HVAC1 and HVAC2 keep on for 1 month');

save fig1
clear nUser1     openTime1  time1      timeTable
clear nUser2     openTime2  time2

%%
% pattarn
load('timeTable.mat');

timeTable(timeTable>1)=0;
iMinute=60*24*7;
userNumber=9;
tmpData=zeros(iMinute,userNumber);

for i=1:iMinute:size(timeTable,1)
    if i+iMinute-1>size(timeTable,1)
        tmpData(1:size(timeTable,1)-i+1,:)=tmpData(1:size(timeTable,1)-
i+1,:)+timeTable(i:size(timeTable,1),:);
    else
        tmpData=tmpData+timeTable(i:(i+iMinute-1),:);
    end
end
```

```
clear i    iMinute     timeTable     userNumber

%possibility
tmpData=tmpData./max(max(tmpData));

nUser1=sum(tmpData(:,1:5),2);
nUser2=sum(tmpData(:,6:end),2);

clear tmpData
save nUser12

nUser1(nUser1<2)=0;
nUser2(nUser2<2)=0;
nUser1(nUser1>=2)=1;
nUser2(nUser2>=2)=1;
time1=1:size(nUser1,1);
time1(nUser1==0)=[];
nUser1(nUser1==0)=[];
time2=1:size(nUser2,1);
time2(nUser2==0)=[];
nUser2(nUser2==0)=[];
%%
plot(time1,nUser1,'b.');
hold on
plot(time2,nUser2+0.5,'g.');
ylim([0 2.5]);
openTime1=sum(nUser1);
openTime2=sum(nUser2);

legend(['HVAC1 on=' num2str(openTime1/(24*60)) 'days'],['HVAC2 on='
num2str(openTime2/(24*60)) 'days']);
xlabel('Minutes for 1 week');
ylabel('HVAC1 & HVAC2 on');
title('Time for HVAC1 and HVAC2 keep on for 1 week');

save fig2
clear openTime1  openTime2  time1   time2    tmpData
clear nUser1     nUser2
```